VERLAG DER TECHNISCHEN UNIVERSITÄT GRAZ

Christopher Albert

Hamiltonian Theory of Resonant Transport Regimes in Tokamaks with Perturbed Axisymmetry

CES 38

MONOGRAPHIC SERIES TU GRAZ
COMPUTATION IN ENGINEERING AND SCIENCE

Christopher Albert

Hamiltonian Theory of Resonant Transport Regimes in Tokamaks with Perturbed Axisymmetry

Monographic Series TU Graz

Computation in Engineering and Science

Monographic Series TU Graz

Computation in Engineering and Science Volume 38

Christopher Albert

Hamiltonian Theory of Resonant Transport Regimes in Tokamaks with Perturbed Axisymmetry

This work is based on the dissertation *"Hamiltonian Approach to Resonant Transport Regimes due to Non-Axisymmetric Magnetic Perturbations in Tokamak Plasmas"*, presented at Graz University of Technology, Institute of Theoretical and Computational Physics in 2017.

Supervision / Assessment:

Martin Heyn (Graz University of Technology)

Per Helander (University of Greifswald)

Cover photo	Vier-Spezies-Rechenmaschine by courtesy of the Gottfried Wilhelm Leibniz Bibliothek – Niedersächsische Landesbibliothek Hannover
Cover layout	Christina Fraueneder, TU Graz Stefan Schleich, TU Graz
Print	DATAFORM Media Ges.m.b.H.

Print
ISBN 978-3-85125-746-5

E-Book
ISBN 978-3-85125-747-5
DOI 10.3217/978-3-85125-746-5

Preface

This book is a revised version of the author's dissertation (Albert, 2017). Resonant transport regimes in non-axisymmetrically perturbed tokamaks are treated by the application of Hamiltonian perturbation theory in action-angle variables. The main advantages of this method are the independence from assumptions on geometry such as the large-aspect-ratio limit and its extensibility to non-linear regimes. In the context of this problem, weakly non-linear theory is applied to go beyond the quasilinear limit and allow for a physically consistent transition between limiting cases.

Naturally, a significant portion of this text is dedicated to the review of well-known concepts found in the cited literature and aims to clarify some details, which may not be obvious to a graduate student studying the scientific literature, or not obvious at all. In that sense, the text is aimed to be useful for the reader to efficiently acquire knowledge on both, required basics and the specific topic.

The initial part introduces methods for studying resonant effects in a perturbed Hamiltonian system subject to collisional effects. To separate the essential points from additional requirements in the general case, the development starts with a bottom-up approach, where concepts are developed based on a one-dimensional example and then generalised to a wider class of systems. In the second part, the Hamiltonian description of guiding-centre motion in an axisymmetric magnetic field is reviewed together with some required aspects of plasma kinetic theory. Finally, the general form of the method from the first part is applied to the specific problem of resonant transport regimes in a non-axisymmetrically perturbed tokamak plasma.

Results from computations confirm the significance of contributions from those regimes to neoclassical toroidal viscous torque in medium-sized tokamaks with magnetic perturbations from coils installed for the control of edge-localized modes. The major features of this work appear to be relevant for quantitative evaluation of toroidal torque, namely complete geometry, consideration of magnetic drift, magnetic shear and the transition region between quasilinear and non-linear regimes under the assumption of well-separated resonances.

Acknowledgements

Working in the group of *Martin Heyn* and *Winfried Kernbichler* under the supervision of the former has been a very rewarding experience that allowed me to explore a field of research that I have learned to love during the past years. I am especially grateful to *Sergei Kasilov*, whose unique physical intuition and countless hours spent together in Graz and Kharkov have been of priceless value both professionally and personally. For continuous professional and personal support in the office, I would like to thank my colleagues *Gernot Kapper* and *Andreas Martitsch*. Furthermore, I would like to extend my gratitude to *Ker-Chung Shaing* and *Wolfgang Suttrop* for their continued interest in our group's work and valuable discussions. As one can learn a lot by teaching, I owe a great deal of insight to the students with whom I had the pleasure to work together, especially *Lukas Grabenwarter*, *Patrick Lainer*, *Katharina Rath* and *Florian Seeber*. To my parents *Brigitte* and *Hans Albert*, I am forever indebted for their guidance and the foundation that allowed me to pursue this path. My greatest thanks go to my beloved *Romana*, who makes it possible for me to keep my balance between physics and real life.

This work has been carried out within the framework of the EUROfusion Consortium and has received funding from the Euratom research and training programme 2014-2018 under grant agreement No 633053. The views and opinions expressed herein do not necessarily reflect those of the European Commission. The author gratefully acknowledges support from NAWI Graz and funding from the KKKÖ at ÖAW for the initial part of the work as well as the OeAD under the grant agreement "Wissenschaftlich-Technische Zusammenarbeit mit der Ukraine" No. UA 06/2015.

Contents

0 Introduction **7**

1 Hamiltonian mechanics **13**
1.1 Lagrangian, Hamiltonian and equations of motion 13
1.2 Action-angle variables 16
1.3 A one-dimensional example 17
1.4 Treatment of perturbations and resonances 23
1.5 Fourier harmonics in canonical angles 28
1.6 A numerical experiment for the pendulum 29

2 Kinetic description and resonant interaction **33**
2.1 Liouville's theorem 33
2.2 Collisions and the kinetic equation 35
2.3 Weakly non-linear kinetic theory 37
2.4 Quasilinear limit 40
2.5 Non-linear limit 43
2.6 Numerical solution for weakly non-linear kinetics 46

3 Hamiltonian theory of guiding-centre motion in a tokamak **51**
3.1 Guiding-centre Lagrangian 51
3.2 Canonical form of the guiding-centre Lagrangian 53
3.3 Transformation of radial dependencies 55
3.4 Action-angle variables in quasi-1D systems 57
3.5 Action-angle variables in a tokamak 63
3.6 Thin orbit approximation 67
3.7 Approximate transformation to canonical coordinates 74

4 Resonant transport regimes **77**
4.1 Basic kinetic theory 77
4.2 Kinetic equation and conservation laws 79
4.3 Toroidal torque density and flux-force relation 82

4.4 Hamiltonian perturbation 83
4.5 Quasilinear approximation 85
4.6 Non-axisymmetric magnetic perturbation 88
4.7 Quasilinear resonant transport regimes and NTV torque 89
4.8 Transport coefficients 91
4.9 Transition to non-linear transport regimes 93

5 Results and discussion **101**
5.1 Quasilinear resonant transport regimes 101
5.2 Non-linear resonant transport regimes 110
5.3 Treatment of finite orbit width 112
5.4 Summary and Outlook 116

A Construction of magnetic flux coordinates **119**
A.1 Clebsch Form 119
A.2 Magnetic flux 120
A.3 Transformation to flux coordinates 122

B Analytical comparison to existing results **123**
B.1 Toroidal drift frequencies 123
B.2 Bounce integrals in the large-aspect-ratio limit 124
B.3 Eulerian approach to drift-orbit resonances 126
B.4 Transport coefficients for bounce-drift resonances 131
B.5 Expressions for the transit-drift resonance 134

List of Figures **139**

Bibliography **141**

Introduction

Background

The general topic of this text is the behaviour of magnetically confined fusion plasmas in tokamaks with small non-axisymmetric perturbations. For readers not familiar with the issue this section will give a very short introduction together with references to relevant literature. A current overview can be found e.g. in the review articles of Boozer (2005) and Ongena et al. (2016). In the last paragraph, the purpose of the present work in this general context is outlined.

Magnetic confinement fusion is considered to be a potential technology for sustainable world-wide large-scale energy supply. In analogy to the natural processes heating the Sun, fusion reactions between small nuclei are used as a power source. To initiate this process, the nuclei have to be brought together sufficiently close, which is possible by gravitational pressure inside the Sun. Here on earth, we have to rely on other mechanisms, one of them being a magnetic trap for a sufficiently hot plasma of nuclei (usually deuterium and tritium) together with their electrons. To produce a significant amount of energy by fusion reactions that allow for the plasma to be mostly self-heated (or fully – ignited), the product of density, pressure and energy confinement time has to be sufficiently high (Lawson, 1957). Devices currently believed to be able to fulfil those requirements[1] are tokamak (Artsimovich, 1972; Wesson, 2011), and stellarator (Spitzer, 1958). Both of these devices have the topology of a torus and rely on magnetic coils to produce a toroidal magnetic field. In the stellarator, additional poloidal field components required for plasma stability are produced by a twisted coil geometry. The classical tokamak is an axisymmetric device, which means that toroidal currents are required to produce a poloidal magnetic field. Up to today, the best confinement properties have been reached in so-called H-mode plasmas in tokamaks (Wagner et al., 1984), which has made it possible to achieve fusion gains of the order of heating power already in the 1990s (Keilhacker et al., 1999). In this operational mode, a transport barrier is formed at

[1] Another possible candidate is inertial confinement fusion (Nuckolls and Wood, 1972), which relies on laser beams instead of magnetic fields, which is not the scope of the present text.

the plasma edge, which results in a substantial enhancement of energy confinement time. This improvement comes at a cost: the occurrence of *edge-localised modes* or *ELMs* (Zohm, 1996), small instabilities that lead to the continuous expulsion of heat towards the device wall, is still an issue of active research. While not dramatic for current devices, those modes will have to be reduced or suppressed in future devices of dimensions large enough for significant energy production, namely ITER (Loarte et al., 2003), to avoid damage to the wall. One way to achieve this purpose is to intentionally perturb the original axisymmetry by so-called *resonant magnetic perturbations* or *RMPs* (Evans et al., 2004) using additional coils.

The purpose of this work is the investigation of side-effects from such perturbations on toroidal plasma rotation. One reason for the importance of this question is the requirement of sufficiently high toroidal plasma rotation for magnetohydrodynamic stability (Ida and Rice, 2014). In a completely axisymmetric plasma, the toroidal rotation velocity can in principle take arbitrary values due to conservation of toroidal angular momentum linked to this symmetry. Breaking the symmetry by non-axisymmetric magnetic field perturbations, e.g. by toroidal field ripple, error fields or RMP fields, leads to non-ambipolar transport that results in toroidal rotation damping, an effect known as *neoclassical toroidal viscous* (*NTV*) *torque* (Shaing, 1986; Shaing et al., 2010). Accurate computation of this effect is possible and required for the distinction from turbulent effects not considered here (Kasilov et al., 2014; Martitsch et al., 2016).

It should be stressed that NTV torque is related to the part of the RMP field that is not in resonance with the equilibrium magnetic field, while the resonant part leads to additional *resonant* torque, which requires a different treatment (Heyn et al., 2008). In this sense, the term *resonant* used here is not related to the "R" of RMP but rather to orbital resonances, which can play a major role in NTV torque at low-collisionality conditions relevant for reactor applications (Martitsch et al., 2016). Although initial results from a fully numerical kinetic approach to the effect of RMPs in tokamaks (including resonant torque) have been published (Albert et al., 2016c), the scope of this text is intentionally limited to the self-contained topic of the Hamiltonian approach to resonant transport regimes of NTV torque.

The first task of this work is to formulate a method to treat the quasilinear limit (Romanov and Filippov, 1961; Vedenov et al., 1961) produced by infinitesimal perturbations without the limitations of bounce-averaging or expressions for large aspect-ratios. This is done by a Hamiltonian approach in action-angle coordinates introduced by Taylor (1964) first for magnetic traps, established in the context of quasilinear transport in tokamak plasmas by Kaufman (1972), and applied in particular by Hazeltine et al. (1981) and Mahajan et al. (1983). A notable application of the Hamiltonian approach is plasma heating by quasilinear wave-particle inter-

action (Osipenko and Shurygin, 1989, 1990; Bécoulet et al., 1991; Eriksson and Helander, 1994; Timofeev and Tokman, 1994; Kasilov et al., 1997). Since perturbation amplitudes can reach more than half a percent of the axisymmetric magnetic field module (Martitsch et al., 2016), the second task is to overcome the limitation of infinitesimal perturbations required for quasilinear theory. To achieve this, non-linear effects by orbital resonances are taken into account following secular perturbation theory (Chirikov 1960; 1979) in combination with a kinetic approach describing the transition between quasilinear and non-linear limit, where the limiting cases have originally been introduced in the context of plasma wave-particle interaction (Romanov and Filippov, 1961; Vedenov et al., 1961; Zakharov and Karpman, 1963).

Overview

The main features of this work are the following:

- Unified descriptions of low-collisional quasilinear and non-linear resonant transport regimes of neoclassical viscous torque in non-axisymmetrically perturbed tokamak plasmas without limitations on device geometry.
- Accurate transition between superbanana and superbanana plateau regimes and equivalent bounce resonance regimes.
- Review of the construction of action-angle coordinates and canonical frequencies in a tokamak.
- Natural appearance of a magnetic shear term that is absent in the standard local neoclassical ansatz.
- Extension to consider the full orbit width for computation of toroidal torque.
- Demonstration that a momentum-conserving collision operator is not required for quasilinear resonant transport regimes at sub-sonic rotation.
- Illustration of importance of the discovered features on a model tokamak and ASDEX Upgrade with resonant magnetic perturbations.
- Efficient implementation in the code NEO-RT (Albert and Kasilov, 2017) by interpolation of pre-computed frequencies and a non-linear attenuation parameter.

This first chapter on Hamiltonian mechanics should serve as a quick overview of well-known concepts and methods that are applied in the subsequent chapters. In particular, this includes the treatment of resonances in the context of Hamiltonian perturbation theory, which is demonstrated on the example of a one-dimensional pendulum. Moreover, a number of notations and conventions used in the remaining text will be defined here. In chapter 2 the basic concepts of kinetic theory are outlined and the general weakly non-linear perturbation theory in the low-collisionality limit is introduced.

Chapter 3 describes the transformation to action-angle variables for the guiding-centre motion of in the magnetic field of a tokamak. Though the use of actions and adiabatic invariants dates back to the beginning of research in the field of magnetic plasma confinement, some specific details needed for a consistent derivation are not completely clear from common literature. One of these peculiarities is the transformation of geometrical angles from magnetic coordinates in a way to obtain

a canonical form of the guiding-centre Lagrangian. This has been solved by an exact transformation closely related to the one of Li et al. (2016) and additionally by a modification of the approximate method of White (1990).

In chapter 4, general conservation laws for flux-surface averaged quantities are formulated with emphasis on particle density and toroidal momentum density. The toroidal torque at low collisionality due to a small non-axisymmetric Hamiltonian perturbation is derived based on the action-angle variables for the unperturbed system for the quasilinear case. The approach is then extended to the weakly non-linear case (lower collisionality and/or higher perturbation amplitudes), where new orbit classes (e.g. superbananas) become relevant.

In chapter 5 results from computations from the code NEO-RT (Albert and Kasilov, 2017) that has been developed based on the presented approach are presented, validated and analysed. Computations have been performed for test cases in a circular tokamak and equilibria from the experiment ASDEX Upgrade with ELM control coils (resonant magnetic perturbations or RMPs). In the end, an outlook on the possible treatment of finite orbit width is given. The chapter is mostly based on parts of the author's publications on the topic to which references are given.

Finally, the appendix includes details on the construction of magnetic flux coordinates, analytical comparisons to existing works and a list of formulas used in derivation and implementation of the method.

Some remarks on the notation

To balance clarity and readability, dependent variables of functions are given explicitly where needed, e.g. in the first occurrence of partial derivatives $\partial J_\parallel(J_\perp, H, p_\varphi)/\partial p_\varphi$ and omitted in subsequent lines as in $\partial J_\parallel/\partial p_\varphi$. Jacobians of variable transformations $(x_1, x_2, x_3) \to (y_1, y_2, y_3)$ are denoted by

$$\frac{\partial(x_1,x_2,x_3)}{\partial(y_1,y_2,y_3)} \equiv \det \begin{pmatrix} \frac{\partial x_1(y_1,y_2,y_3)}{\partial y_1} & \frac{\partial x_1(y_1,y_2,y_3)}{\partial y_2} & \frac{\partial x_1(y_1,y_2,y_3)}{\partial y_3} \\ \frac{\partial x_2(y_1,y_2,y_3)}{\partial y_1} & \frac{\partial x_2(y_1,y_2,y_3)}{\partial y_2} & \frac{\partial x_2(y_1,y_2,y_3)}{\partial y_3} \\ \frac{\partial x_3(y_1,y_2,y_3)}{\partial y_1} & \frac{\partial x_3(y_1,y_2,y_3)}{\partial y_2} & \frac{\partial x_3(y_1,y_2,y_3)}{\partial y_3} \end{pmatrix}. \tag{1}$$

N-tuples of quantities (this includes vectors) are denoted by bold-face letters, i.e. $\boldsymbol{J} = (J_1, J_2, J_3)$. In particular for vectors, the co- and contravariant notation with superscripts and subscripts (see, e.g. the book of D'haeseleer et al. (1991)) is chosen. The sum convention applies for repeated indices at opposite positions,

$$a^k b_k \equiv \sum_k a^k b_k. \tag{2}$$

There are a few ambiguities in the notation, most notably the use of letters m and n for both mass/density as well as harmonic indices, and the use of D_{ij} not only

as components of diffusivity but also as transport coefficients later. Normally, the choice should be clear from the context, and otherwise the notation is resolved by additional comments and/or by including subscript α for the particle species, i.e. m_α is the mass of species α.

Chapter 1

Hamiltonian mechanics

1.1 Lagrangian, Hamiltonian and equations of motion

A classical mechanical system (see e.g. the books of Goldstein (1980), Landau and Lifshitz (1960), Lichtenberg and Lieberman (1983) or Arnold (1989)) is fully characterised by its *Lagrangian* $L(\boldsymbol{q}, \dot{\boldsymbol{q}}, t)$, which is a function of N *generalised coordinates* q^i in *configuration space*, N *generalised velocities* $\dot{q}^i$ and time t. The solution of a mechanical problem is given by a *trajectory* in configuration space, i.e. a twice continuously differentiable curve $\boldsymbol{q}(t)$ for which $\dot{\boldsymbol{q}}(t) = \mathrm{d}\boldsymbol{q}(t)/\mathrm{d}t$, and the *action functional*

$$S = \int_{t_0}^{t_1} \mathrm{d}t\, L(\boldsymbol{q}(t), \dot{\boldsymbol{q}}(t), t) \tag{1.1}$$

takes an extremal value. Here, in contrast to many other texts, we did not identify dotted notation with a time derivative *a priori* – the three quantities $\dot{\boldsymbol{q}}$, $\dot{\boldsymbol{q}}(t)$ and $\mathrm{d}\boldsymbol{q}(t)/\mathrm{d}t$ are of different nature. Without argument, $\dot{\boldsymbol{q}}$ describes N independent velocity variables, $\dot{\boldsymbol{q}}(t)$ their evolution over time parameter t, and $\mathrm{d}\boldsymbol{q}(t)/\mathrm{d}t$ a tangent vector to the parameterized curve $\boldsymbol{q}(t)$ in configuration space. Only in Lagrangian mechanics one immediately identifies $\dot{\boldsymbol{q}}(t)$ with the curve velocity $\mathrm{d}\boldsymbol{q}(t)/\mathrm{d}t$ already at the level of the action law, thereby effectively dropping N velocity dimensions to work only in N-dimensional configuration space. In that case one can deduce that each component of $\boldsymbol{q}(t)$ must fulfil a set of N second-order ordinary differential equations – the *Euler-Lagrange equations*

$$\frac{\mathrm{d}}{\mathrm{d}t}\left(\frac{\partial L}{\partial \dot{q}^i}(\boldsymbol{q}(t), \dot{\boldsymbol{q}}(t), t)\right) - \frac{\partial L}{\partial q^i}(\boldsymbol{q}(t), \dot{\boldsymbol{q}}(t), t) = 0. \tag{1.2}$$

Here, at first, q^i and $\dot{q}^i$ are treated as independent variables in $2N$-dimensional *(velocity) phase-space* on which $L(\boldsymbol{q}, \dot{\boldsymbol{q}}, t)$ is defined. Only after taking partial derivatives, one may set $\boldsymbol{q} \equiv \boldsymbol{q}(t)$ and $\dot{\boldsymbol{q}} \equiv \dot{\boldsymbol{q}}(t) = \mathrm{d}\boldsymbol{q}(t)/\mathrm{d}t$ to their values along the trajectory and take a total time derivative.

Since the extremal path in Eq. (1.1) is not affected by a constant shift in S, adding a total time derivative inside the integral results in a new Lagrangian

$$\bar{L}(\boldsymbol{q}(t), \dot{\boldsymbol{q}}(t), t) = L(\boldsymbol{q}(t), \dot{\boldsymbol{q}}(t), t) + \frac{\mathrm{d}F(\boldsymbol{q}(t), \dot{\boldsymbol{q}}(t), t)}{\mathrm{d}t}, \tag{1.3}$$

that describes the same mechanical system as L. Here, F can be any *dynamical variable* (a function depending on position, velocity and time), for which the total time derivative is defined as

$$\begin{aligned}\frac{\mathrm{d}F(\boldsymbol{q}(t), \dot{\boldsymbol{q}}(t), t)}{\mathrm{d}t} &= \frac{\partial F}{\partial t} + \frac{\mathrm{d}q^i(t)}{\mathrm{d}t}\frac{\partial F}{\partial q^i} + \frac{\mathrm{d}\dot{q}^i(t)}{\mathrm{d}t}\frac{\partial F}{\partial \dot{q}^i} \\ &= \frac{\partial F}{\partial t} + \dot{q}^i(t)\frac{\partial F}{\partial q^i} + \frac{\mathrm{d}\dot{q}^i(t)}{\mathrm{d}t}\frac{\partial F}{\partial \dot{q}^i}\end{aligned} \tag{1.4}$$

along any trajectory. If all $\partial F/\partial \dot{q}^i$ vanish one may describe such a total time derivative as

$$\frac{\mathrm{d}F(\boldsymbol{q}(t), t)}{\mathrm{d}t} = \frac{\mathrm{D}F}{\mathrm{D}t}(\boldsymbol{q}(t), \dot{\boldsymbol{q}}(t), t), \tag{1.5}$$

where

$$\frac{\mathrm{D}F}{\mathrm{D}t}(\boldsymbol{q}, \dot{\boldsymbol{q}}, t) = \frac{\partial F(\boldsymbol{q}, t)}{\partial t} + \dot{\boldsymbol{q}} \cdot \frac{\partial F(\boldsymbol{q}, t)}{\partial \boldsymbol{q}}, \tag{1.6}$$

is an advective derivative being a function on positions, velocities and time, independent from the actual trajectory. The latter is only inserted in Eq. (1.5).

Derivatives of L with respect to $\dot{q}^i$ are called *generalised momenta*

$$p_i = \frac{\partial L(\boldsymbol{q}, \dot{\boldsymbol{q}}, t)}{\partial \dot{q}^i}, \tag{1.7}$$

which are conserved along any actual trajectory $\boldsymbol{q}(t)$ (short: *conserved*), in case L is independent of the respective coordinate q^i. Together with $\boldsymbol{q}$, canonical momenta $\boldsymbol{p}$ form a set of so-called *canonically conjugate coordinates* in $2N$-dimensional *phase space*. Introducing the *Hamiltonian* $H(\boldsymbol{q}, \boldsymbol{p}, t)$ by a Legendre transformation

$$H(\boldsymbol{q}, \boldsymbol{p}, t) = \boldsymbol{p} \cdot \dot{\boldsymbol{q}}(\boldsymbol{q}, \boldsymbol{p}) - L(\boldsymbol{q}, \dot{\boldsymbol{q}}(\boldsymbol{q}, \boldsymbol{p}), t),$$

we obtain the equivalent Hamiltonian description of Eq. (1.2). Here yet another use of the velocity symbol is introduced, with $\dot{\boldsymbol{q}}(\boldsymbol{q}, \boldsymbol{p})$ being velocity components of a coordinate transformation from canonical coordinates $(\boldsymbol{q}, \boldsymbol{p})$ to non-canonical phase-space coordinates $(\boldsymbol{q}, \dot{\boldsymbol{q}})$.[1] The resulting set of $2N$ first-order ordinary differential equations,

$$\begin{aligned}\frac{\mathrm{d}q^i(t)}{\mathrm{d}t} &= \frac{\partial H}{\partial p_i}(\boldsymbol{q}(t), \boldsymbol{p}(t), t), \\ \frac{\mathrm{d}p_i(t)}{\mathrm{d}t} &= -\frac{\partial H}{\partial q^i}(\boldsymbol{q}(t), \boldsymbol{p}(t), t),\end{aligned} \tag{1.8}$$

[1] This also clarifies that the term "velocity phase-space" is a result of (incorrectly) identifying coordinates with the actual space – there is only one phase-space where phase-points can be described by different systems of coordinate.

describes the temporal evolution of coordinates and momenta. They are called *Hamilton's equations of motion* or *canonical equations*. This formulation is a geometrical one, as the right-hand side of Eqs. (1.8) describes a so-called *Hamiltonian vector field*

$$\begin{pmatrix} \dot{\boldsymbol{q}} \\ \dot{\boldsymbol{p}} \end{pmatrix} = \begin{pmatrix} \partial H/\partial \boldsymbol{p} \\ -\partial H/\partial \boldsymbol{q} \end{pmatrix} = \begin{pmatrix} 0 & I \\ -I & 0 \end{pmatrix} \nabla_{\boldsymbol{q},\boldsymbol{p}} H, \tag{1.9}$$

and the left-hand side its integral curves. Similar to the Lagrangian formalism above, we will only identify the (global) vector field of phase-velocities $\dot{\boldsymbol{q}}$ and $\dot{\boldsymbol{p}}$ with the (local) tangent to a particular orbit $\boldsymbol{q}(t)$ and $\boldsymbol{p}(t)$ if explicitly stated as $\dot{\boldsymbol{q}}(t)$, $\dot{\boldsymbol{p}}(t)$.

Introducing the Poisson bracket

$$\{f, g\} \equiv \frac{\partial f}{\partial q^i}\frac{\partial g}{\partial p_i} - \frac{\partial f}{\partial p_i}\frac{\partial g}{\partial q^i}, \tag{1.10}$$

total time derivatives of dynamical variables $f(\boldsymbol{q}, \boldsymbol{p}, t)$ along a phase-trajectory is expressed by

$$\frac{\mathrm{d}f(\boldsymbol{q}(t), \boldsymbol{p}(t), t)}{\mathrm{d}t} = \frac{\partial f}{\partial t} + \frac{\mathrm{d}q^i(t)}{\mathrm{d}t}\frac{\partial f}{\partial q^i} + \frac{\mathrm{d}p_i(t)}{\mathrm{d}t}\frac{\partial f}{\partial p_i} = \frac{\partial f}{\partial t} + \{f, H\}, \tag{1.11}$$

with the right-hand side evaluated at $(\boldsymbol{q}(t), \boldsymbol{p}(t), t)$. In the Hamiltonian formalism, it becomes thus particularily easy to write an advective derivative of f along the Hamiltonian (phase-velocity) vector field (1.9) along phase-space trajectories. Namely,

$$\frac{\mathrm{D}f}{\mathrm{D}t}(\boldsymbol{q}, \boldsymbol{p}, t) = \frac{\partial f}{\partial t} + \frac{\partial H}{\partial p_i}\frac{\partial f}{\partial q^i} - \frac{\partial H}{\partial q^i}\frac{\partial f}{\partial p_i} = \frac{\partial f}{\partial t} + \{f, H\}, \tag{1.12}$$

and for a particular trajectory

$$\frac{\mathrm{d}f(\boldsymbol{q}(t), \boldsymbol{p}(t), t)}{\mathrm{d}t} = \frac{\mathrm{D}f}{\mathrm{D}t}(\boldsymbol{q}(t), \boldsymbol{p}(t), t). \tag{1.13}$$

This will allow us to use $\mathrm{d}f/\mathrm{d}t$ and $\mathrm{D}f/\mathrm{D}t$ synonymously, as long as a relation is valid for all trajectories defined by H. This is in contrast to Eq. (1.4) of the Lagrangian formalism, where $\mathrm{d}\boldsymbol{q}(t)/\mathrm{d}t$ would first have to be expressed via the Euler-Lagrange equations (1.2) to obtain an equivalent expression.

For $\boldsymbol{q}$ and $\boldsymbol{p}$, canonical equations (1.8) may also be written as

$$\begin{aligned} \frac{\mathrm{d}q^i(t)}{\mathrm{d}t} &= \{q^i, H\}, \\ \frac{\mathrm{d}p_i(t)}{\mathrm{d}t} &= \{p_i, H\}. \end{aligned} \tag{1.14}$$

For the Hamiltonian itself, it follows that

$$\frac{\mathrm{d}H}{\mathrm{d}t} = \frac{\partial H}{\partial t} = \frac{\partial L}{\partial t}. \tag{1.15}$$

Hence, if $L(\boldsymbol{q}, \dot{\boldsymbol{q}}, t) = L(\boldsymbol{q}, \dot{\boldsymbol{q}})$ does not explicitly depend on time, H is conserved along the trajectories defined via L. If there are no explicitly time-dependent constraints in addition, H is equal to the total energy. We call such systems *conservative*.

It is possible to switch to a new set of canonically conjugate variables $(\bar{\boldsymbol{q}}, \bar{\boldsymbol{p}})$ by *canonical transformations* that leave the Poisson brackets (1.10) invariant,

$$\{f, g\} = \frac{\partial f}{\partial \bar{q}^i}\frac{\partial g}{\partial \bar{p}_i} - \frac{\partial f}{\partial \bar{p}_i}\frac{\partial g}{\partial \bar{q}^i}. \tag{1.16}$$

This is usually performed via a *generating function*, for example $F_2 = F_2(\boldsymbol{q}, \bar{\boldsymbol{p}}, t)$ and

$$p_i = \frac{\partial F_2}{\partial q^i}, \qquad \bar{q}^i = \frac{\partial F_2}{\partial \bar{p}_i}. \tag{1.17}$$

If F_2 depends on time explicitly, H is transformed to a new Hamiltonian[2]

$$\bar{H}(\bar{\boldsymbol{q}}, \bar{\boldsymbol{p}}) = H + \frac{\partial F_2}{\partial t}\,. \tag{1.18}$$

1.2 Action-angle variables

A conservative system is called *integrable* if it is possible to find a set of N independent *first integrals of motion* $\boldsymbol{\alpha}$ with $\mathrm{d}\boldsymbol{\alpha}/\mathrm{d}t = 0$ and $\{\alpha_i, \alpha_j\} = 0$. A specific set of $\boldsymbol{\alpha}$ uniquely determines the trajectory in phase space together with N initial values. If the motion is bounded in phase space, it can then be shown (see e.g. Arnold (1989)) to be *conditionally periodic*, i.e., it is possible to choose *angle variables* $\boldsymbol{\theta}$ that evolve linearly in time for any trajectory, so

$$\boldsymbol{\theta}(t) = \boldsymbol{\Omega} t, \tag{1.19}$$

with conserved *canonical frequencies* $\boldsymbol{\Omega} = \boldsymbol{\Omega}(\boldsymbol{\alpha})$. The pairs $(\boldsymbol{\theta}, \boldsymbol{\alpha})$ do not generally form a set of canonically conjugate coordinates. It is however possible to perform a transformation $\boldsymbol{J}(\boldsymbol{\alpha})$ to a set of N *action variables* $\boldsymbol{J}$ that are canonically conjugate to the angles $\boldsymbol{\theta}$. One also says that $\boldsymbol{\alpha}$ are a set of coordinates in N-dimensional action space. Conversely, $\boldsymbol{\alpha} = \boldsymbol{\alpha}(\boldsymbol{J})$ can be written as functions of canonical actions. In particular, since $H = \alpha_1$ itself is conserved, it will depend only on $\boldsymbol{J}$ but not on $\boldsymbol{\theta}$. From Eq. (1.8) we obtain

$$\frac{\mathrm{d}J_i(t)}{\mathrm{d}t} = 0, \tag{1.20}$$

$$\frac{\mathrm{d}\theta^i(t)}{\mathrm{d}t} = \Omega^i = \frac{\partial H(\boldsymbol{J})}{\partial J_i}. \tag{1.21}$$

[2] Sometimes called the *Kamiltonian* due to its often used label K (Goldstein, 1980, p. 380)

To determine action-angle variables for a certain system, a canonical transformation $(\boldsymbol{q}, \boldsymbol{p}) \to (\boldsymbol{\theta}, \boldsymbol{J})$ is performed via the *abbreviated action* (also called *Hamilton's characteristic function*) written in terms of $\boldsymbol{q}$ and $\boldsymbol{\alpha}$,

$$W(\boldsymbol{q}, \boldsymbol{\alpha}) = \int_{\boldsymbol{q}_0}^{\boldsymbol{q}} \mathrm{d}\boldsymbol{q}' \cdot \boldsymbol{p}(\boldsymbol{q}', \boldsymbol{\alpha}) \tag{1.22}$$

$$= \int_{\zeta_0}^{\zeta_1} \mathrm{d}\zeta \, \frac{\mathrm{d}q^i(\zeta)}{\mathrm{d}\zeta} p_i(\boldsymbol{q}(\zeta), \boldsymbol{\alpha}), \tag{1.23}$$

where the integral is taken along a path of constant $\boldsymbol{\alpha}$, which also implies constant $\boldsymbol{J}$. This path is the actual trajectory in phase space for this specific set of $\boldsymbol{\alpha}$. Nevertheless, the curve parameter ζ used for integration can be different from time t.

The transformation reads

$$p_i(\boldsymbol{q}, \boldsymbol{J}) = \frac{\partial W(\boldsymbol{q}, \boldsymbol{\alpha}(\boldsymbol{J}))}{\partial q^i}, \tag{1.24}$$

$$\theta^i(\boldsymbol{q}, \boldsymbol{J}) = \frac{\partial W(\boldsymbol{q}, \boldsymbol{\alpha}(\boldsymbol{J}))}{\partial J_i} = \left(\frac{\partial \boldsymbol{J}}{\partial \boldsymbol{\alpha}}\right)^{-1} \frac{\partial W(\boldsymbol{q}, \boldsymbol{\alpha})}{\partial \boldsymbol{\alpha}}. \tag{1.25}$$

The actions can be easily computed explicitly in the case of a *separable* system, where for a certain set of $(\boldsymbol{q}, \boldsymbol{p})$, W can be written as a sum of terms depending only on one coordinate each,

$$W(\boldsymbol{q}, \boldsymbol{\alpha}) = \sum_i W_i(q^i, \boldsymbol{\alpha}) = \int \mathrm{d}q^i \, p_i(q^i, \boldsymbol{\alpha}) \,. \tag{1.26}$$

In a separable system, the actions are given by integrals

$$J_i(\boldsymbol{\alpha}) = \frac{1}{2\pi} \oint \mathrm{d}q^i \, p_i(q^i, \boldsymbol{\alpha}) = \frac{1}{2\pi} \oint \mathrm{d}q^i \, \frac{\partial W_i(q^i, \boldsymbol{\alpha})}{\partial q^i} \tag{1.27}$$

taken either over the range of motion of one round-trip (back and forth) if oscillatory (*libration*) or one period in q^i if periodic (*rotation*). We will keep this distinction in mind to maintain consistent sign conventions for canonical actions, angles and frequencies later.

Finally we note that in action-angle variables dynamical time derivatives in Eq. (1.11) take an especially simple form using Poisson brackets with the Hamiltonian,

$$\{f, H\} = \Omega^i \frac{\partial f}{\partial \theta^i}. \tag{1.28}$$

1.3 A one-dimensional example

To illustrate the methods that are defined in a general way, let us consider a conservative one-dimensional mechanical system of a particle with mass m_α, position x, momentum p in a potential $U(x)$. The Hamiltonian of such a system is given by

$$H = \frac{p^2}{2m_\alpha} + U(x) \tag{1.29}$$

and the equations of motion are

$$\frac{\mathrm{d}x}{\mathrm{d}t} = \frac{p}{m_\alpha}, \tag{1.30}$$

$$\frac{\mathrm{d}p}{\mathrm{d}t} = -\frac{\mathrm{d}U(x)}{\mathrm{d}x}. \tag{1.31}$$

Because H is conserved in this system, it can be used to write p as a function of position and integrals of motion,

$$p(x, H) = \sigma\sqrt{2m_\alpha(H - U(x))}, \tag{1.32}$$

$$\frac{\partial p(x, H)}{\partial H} = \sigma\sqrt{\frac{m_\alpha}{2}}\frac{1}{\sqrt{H - U(x)}} = \frac{m_\alpha}{p(x, H)}. \tag{1.33}$$

The constant $\sigma = \pm 1$ specifies whether the motion is directed towards the positive or negative x direction. Since the system is one-dimensional, the abbreviated action W in Eq. (1.26) is trivially separable, since it contains only one term

$$\begin{aligned} W = W_x &= \int_{x_0}^{x} \mathrm{d}x'\, p(x, H) \\ &= \int_{x_0}^{x} \mathrm{d}x'\, \sigma\sqrt{2m_\alpha(H - U(x))}. \end{aligned} \tag{1.34}$$

To be more specific, let us choose a cosine-shaped potential

$$\begin{aligned} U(x) &= U_0(1 - \cos(x)) \\ &= 2U_0 \sin^2(x/2), \end{aligned} \tag{1.35}$$

which results in the Hamiltonian

$$H = \frac{p^2}{2m_\alpha} + U_0(1 - \cos(x)). \tag{1.36}$$

The classical physical interpretation of this system is the pendulum of mass m_α on a rigid, massless rod in a homogeneous gravitational field. In this case, x takes the role of the angle of the pendulum towards the vertical axis. Alternatively, it can represent a particle in a 2π-periodic cosine-shaped potential well. In that case, x is interpreted as a Cartesian coordinate and the size of the system is infinite. In a more abstract sense, this Hamiltonian also appears in weakly non-linear approximations

within more complex systems, which will become clear in the subsequent section. Integrals of the type (1.34) for the pendulum Hamiltonian can be represented by elliptic integrals E and K depending on the parameter

$$\kappa = k^2 \equiv \frac{H}{2U_0},$$

defined e.g. in the book of Gradshtein and Ryzhik (1965) (see also the article of Brizard (2013), who uses the same notation for elliptic integrals as we do here).

One important feature of the pendulum Hamiltonian is the existence of two distinct types of motion. If the parameter κ is smaller than one, the libration kind of motion is bounded between two turning points given by

$$H = U(x^{\pm}) = U_0(1 - \cos(x^{\pm}))\,, \tag{1.37}$$

$$x^{\pm} = \pm \arccos(1 - 2\kappa) \tag{1.38}$$

$$= \pm 2 \arcsin(\sqrt{\kappa}). \tag{1.39}$$

The classical pendulum would oscillate between those two points. For $\kappa > 1$, the rotation kind of motion is unbounded, corresponding to a pendulum rotating over the top. This kind of behaviour leads to two regions in phase space that have to be treated separately. The boundary in-between defined by $\kappa = 1$ is called *separatrix*.

To be consistent with later terminology, we switch to the particle-in-well interpretation and call the librating orbits *trapped* and the rotating orbits *passing*.

For trapped orbits, the action associated to x is given by an integration forth and back between the turning points from Eq. (1.27),

$$\begin{aligned}
J(H) &= \frac{1}{2\pi}\int_{x^-}^{x^+} \mathrm{d}x\ p(x,H)|_{\sigma=1} + \frac{1}{2\pi}\int_{x^+}^{x^-} \mathrm{d}x\ p(x,H)|_{\sigma=-1} \\
&= \frac{1}{\pi}\int_{x^-}^{x^+} \mathrm{d}x\ p(x,H)|_{\sigma=1} \\
&= \frac{1}{\pi}\int_{x^-}^{x^+} \mathrm{d}x \sqrt{2m_\alpha(H - 2U_0\sin^2(x/2))} \\
&= \frac{\sqrt{2m_\alpha U_0}}{\pi}\int_{x^-}^{x^+} \mathrm{d}x \sqrt{\kappa - \sin^2(x/2)} \\
&= \sqrt{m_\alpha U_0}\frac{8}{\pi}\left(E(\kappa) - (1-\kappa)K(\kappa)\right)\,.
\end{aligned} \tag{1.40}$$

As mentioned at the end of section 1.2, the integration direction has been switched at the turning points to result in a non-zero J.

For passing orbits, integration over one period of the motion in x results in

$$\begin{aligned} J(H) &= \frac{1}{2\pi}\int_{-\pi}^{\pi} \mathrm{d}x\, p(x,H) \\ &= \sigma\frac{\sqrt{2m_\alpha U_0}}{2\pi}\int_{-\pi}^{\pi} \mathrm{d}x\, \sqrt{\kappa-\sin^2(x/2)} \\ &= \sigma\sqrt{m_\alpha U_0}\frac{4\sqrt{\kappa}}{\pi}E(\kappa^{-1})\,. \end{aligned} \tag{1.41}$$

In contrast to the trapped case, we have maintained the positive x-direction in the integration. The result are different signs in J distinguishing co-passing orbits with $\sigma = 1$ from counter-passing orbits with $\sigma = -1$. This detail of the sign convention for canonical actions is frequently neglected or taken for granted in the literature (it is for example clear that gyration of a positively charged particle in the negative sense results in negative magnetic moment). In any case we should keep it in mind for the later developments for axisymmetric plasmas, where it will be crucial for the correct expressions for canonical variables.

The associated canonical frequency for trapped orbits is computed according to Eq. (1.21). For reasons that will become clear in the following paragraphs, we call it the bounce frequency ω_b corresponding to the bounce time τ_b and write

$$\Omega = \left(\frac{\partial J(H)}{\partial H}\right)^{-1} \equiv \omega_b = \frac{2\pi}{\tau_b}. \tag{1.42}$$

Here, the derivative with respect to H in principle affects also the boundaries $x^\pm = x^\pm(H)$ by the Leibniz rule,

$$\begin{aligned} \frac{\partial}{\partial H}\int_{x^-(H)}^{x^+(H)} \mathrm{d}x\, p(x,H) = &\int_{x^-(H)}^{x^+(H)} \mathrm{d}x\, \frac{\partial p(x,H)}{\partial H} \\ &+ \frac{\mathrm{d}x^+(H)}{\mathrm{d}H}\, p(x^+,H) - \frac{\mathrm{d}x^-(H)}{\mathrm{d}H}\, p(x^-,H)\,. \end{aligned} \tag{1.43}$$

However, since $p(x^+,H) = p(x^-,H) = 0$, the latter two boundary terms vanish and we obtain

$$\begin{aligned} \tau_b = 2\pi\frac{\mathrm{d}J}{\mathrm{d}H} &= 2\int_{x^-}^{x^+} \mathrm{d}x\, \left.\frac{\partial p(x,H)}{\partial H}\right|_{\sigma=1} \\ &= \sqrt{2m_\alpha}\int_{x^-}^{x^+} \frac{\mathrm{d}x}{\sqrt{H-U(x)}} \\ &= \sqrt{\frac{m_\alpha}{U_0}}\int_{x^-}^{x^+} \frac{\mathrm{d}x}{\sqrt{\kappa-\sin^2(x/2)}}\,. \end{aligned} \tag{1.44}$$

If the analytical solution for J were not known, one could integrate the equations of motion ((1.30)-(1.30)) numerically and use the orbit time τ as an integrand to

substitute x, taking $x(\tau)$ from the orbit integration and

$$\mathrm{d}x = \frac{p}{m_\alpha}\mathrm{d}\tau = \sqrt{\frac{2}{m_\alpha}}\sqrt{H - U(x)}\,\mathrm{d}\tau\,. \tag{1.45}$$

The general bounce time integral (1.44) then becomes

$$\begin{aligned}\tau_b &= \sqrt{2m_\alpha}\int_{\tau^-}^{\tau^+}\frac{\mathrm{d}\tau}{\sqrt{H - U(x(\tau))}}\sqrt{\frac{2}{m_\alpha}}\sqrt{H - U(x(\tau))}\\ &= 2\int_{\tau^-}^{\tau^+}\mathrm{d}\tau\,,\end{aligned} \tag{1.46}$$

which is two times the time of one half-turn. As expected, this is indeed the bounce time of the one-dimensional oscillation.

For our cosine potential in particular, we can just take a derivative of the analytical solution for the action in Eq. (1.40) and obtain

$$\tau_b = \sqrt{\frac{m_\alpha}{U_0}}4K\left(\kappa\right)\,, \tag{1.47}$$

$$\Omega = \sqrt{\frac{U_0}{m_\alpha}}\frac{\pi}{2K\left(\kappa\right)} = \omega_b\,. \tag{1.48}$$

The canonical frequency Ω is the bounce frequency ω_b, which becomes the usual harmonic frequency

$$\omega_0 = \sqrt{\frac{U_0}{m_\alpha}} \tag{1.49}$$

for $\kappa \ll 1$ where the orbit remains close to $x = 2n\pi$ with integer n. Orbits at $\kappa \lesssim 1$ take longer and longer time to complete as the anharmonic contributions grow stronger at higher energy (Fig. 1.1). At the separatrix $\kappa = 1$ the system approaches one of the unstable equilibrium points $x = (2n+1)\pi$ to come arbitrarily close with time.

The bounce (transit) time for passing orbits can be computed by the same means. The analytical results for the cosine potential follow as

$$\tau_b = \sqrt{\frac{m_\alpha}{U_0}}\frac{2K\left(\kappa^{-1}\right)}{\sqrt{\kappa}}\,, \tag{1.50}$$

$$\Omega = \sigma\sqrt{\frac{U_0}{m_\alpha}}\frac{\pi\sqrt{\kappa}}{K\left(\kappa^{-1}\right)}\,. \tag{1.51}$$

This is already known as the canonical (bounce) frequency $\Omega = \omega_b$, which can now become negative for counter-passing particles, where $\sigma = -1$ over the whole

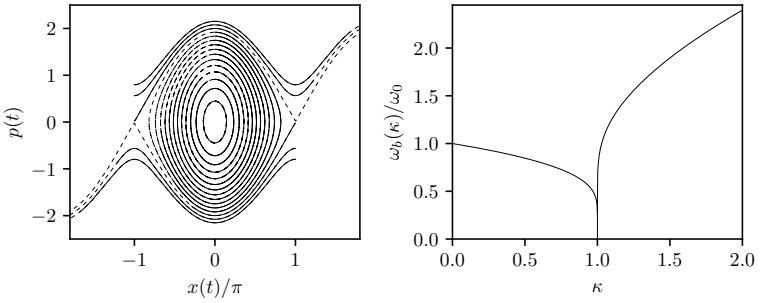

Figure 1.1: Left: pendulum orbits in phase-space with initial conditions equally spaced in $\kappa \in (0.05,\, 1.1585)$ traced until the bounce time $\tau_0 = 2\pi/\omega_0$ of the harmonic limit at $\kappa = 0$ (solid) and their full shape (dashed). Right: dependency of bounce frequency $|\omega_b|$ on κ with limit 0 at the separatrix $\kappa = 1$. The frequency ω_b of passing orbits becomes larger than ω_0 already close to the separatrix, tending towards the linear behaviour of free orbits further outside.

orbit. This follows from the sign convention when computing canonical angles for momenta from Eq. (1.25), which yields

$$\theta(x,J) = \left(\frac{\partial J}{\partial H}\right)^{-1} \frac{\partial W(x,H)}{\partial H} = \Omega \frac{\partial W(x,H)}{\partial H}\,. \tag{1.52}$$

Using Eqs. (1.33) and (1.45), the canonical angle follows as

$$\begin{aligned}\theta &= \Omega \frac{\partial}{\partial H} \int_{x_0}^{x} \mathrm{d}x'\, p(x,H) = \Omega \int_{x_0}^{x} \mathrm{d}x'\, \frac{\partial p(x,H)}{\partial H} \\ &= \Omega \int_0^{\tau} \mathrm{d}\tau'\, \frac{p}{m_\alpha} \frac{m_\alpha}{p} = \tau\Omega = 2\pi\sigma \frac{\tau}{\tau_b}\,,\end{aligned} \tag{1.53}$$

where the global $\sigma = -1$ is relevant for counter-passing orbits only. It is thus equal to the orbit time τ normalized to the bounce time τ_b (both always positive) spanning 2π in one full turn and is valid for both, trapped and passing orbits in general one-dimensional Hamiltonian systems. Here, the orbit time τ appears as a purely geometrical quantity in phase space – a rescaled canonical angle θ. For the cosine potential, it is given by the incomplete elliptic integral

$$\theta(x) = \frac{\pi F\left(\frac{x}{2}|\kappa^{-1}\right)}{K(\kappa^{-1})}, \tag{1.54}$$

in the passing region and by

$$\theta(x) = \frac{\pi F\left(\frac{x}{2}|\kappa\right)}{2K(\kappa)} \tag{1.55}$$

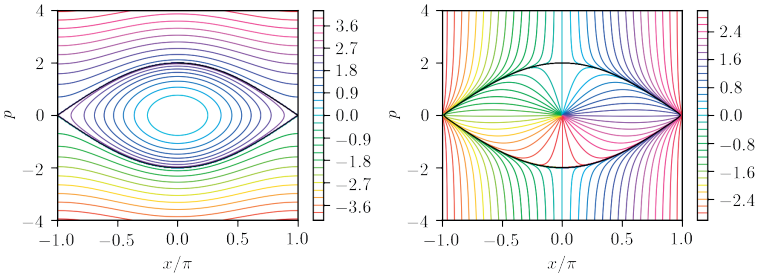

Figure 1.2: Evenly spaced contours of constant canonical actions J (left) and angles θ (right) for the pendulum. By convention, $J > 0$ in the trapped region and has sign σ of p in the respective passing region. Angle θ is zero at $x = 0$ (in the trapped region only for $\sigma = 1$) and grows with x in both passing regions specified by $\sigma = \pm 1$.

in the trapped region during the first half-oscillation $x^- < x < x^+$ with $\sigma = +1$, together with a phase-shifted variant of the expression for the other with $\sigma = -1$ (see Fig. 1.2).

For a general potential $U(x)$ with local minima, multiple classes of trapped particles with different turning points can arise, as long as their total energy H is below the respective local maximum that marks the boundary of the potential well. In that case, different starting positions x_0 lead to different classes of canonical frequencies and angles.

1.4 Treatment of perturbations and resonances

We are now going to introduce a time-harmonic perturbation $H_1(\boldsymbol{\theta}, \boldsymbol{J}, t)$ on an originally unperturbed Hamiltonian $H_0(\boldsymbol{J})$ with the new Hamiltonian being $H = H_0 + H_1$. The perturbation shall be of smaller order than H_0 and be represented by a Fourier series

$$H_1(\boldsymbol{\theta}, \boldsymbol{J}, t) = \sum_{\boldsymbol{m}} H_{\boldsymbol{m}}(\boldsymbol{J}) e^{\mathrm{i}(\boldsymbol{m}\cdot\boldsymbol{\theta} - \omega t)} \tag{1.56}$$

with complex coefficients $H_{\boldsymbol{m}}$. In case of a resonance

$$\boldsymbol{m} \cdot \boldsymbol{\Omega} - \omega = 0 \tag{1.57}$$

between canonical frequencies $\boldsymbol{\Omega}$ and perturbation frequency ω (which can also be zero), special treatment is required. The technique of choice is known as *secular perturbation theory* (Lichtenberg and Lieberman, 1983, p. 109) and can be applied in a number of systems involving resonant interaction of a perturbation with the

original system. A review of the method with emphasis on resonance overlap and resulting Arnol'd diffusion is given by Chirikov (1979), who introduced the concept of chaotic diffusion in his work on magnetic traps (Chirikov, 1960).

The applicability of the method relies on the resonances to be well separated, so we can treat each harmonic $\boldsymbol{m}$ in canonical angles individually similar to the case of a linear system. Still, the result is a 1-dimensional non-linear system for each harmonic. This way, some non-linear features of the overall system are captured, which is the reason why the method can be classified as weakly non-linear. As we will see, new orbit classes oscillating at a non-linear bounce frequency ω_{bN} around each resonance will emerge.

First, we introduce the resonant phase by a Galilean transformation

$$\bar{\theta} = \boldsymbol{m} \cdot \boldsymbol{\theta} - \omega t + \bar{\theta}_0, \tag{1.58}$$

where $\bar{\theta}_0$ is defined to shift the complex phase of $H_{\boldsymbol{m}}$ such that

$$H_{\boldsymbol{m}} e^{\mathrm{i}(\boldsymbol{m}\cdot\boldsymbol{\theta}-\omega t)} = -|H_{\boldsymbol{m}}| \cos\bar{\theta}\,. \tag{1.59}$$

In the one-dimensional case with only one pair (θ, J), where the canonical angle is the normalised bounce time of the unperturbed system, Eq. (1.58) can be written as

$$\bar{\theta} = m\omega_b \tau - \omega t + \bar{\theta}_0, \tag{1.60}$$

with a scalar harmonic index m. At the resonance condition (1.57) with $\omega = m\omega_b$, fulfiled only for a specific $J = J_{\mathrm{res}}$, the interpretation of $\bar{\theta}$ becomes clear from the modified expression

$$\bar{\theta} = \omega(\tau - t) + \bar{\theta}_0. \tag{1.61}$$

The physical meaning of $\bar{\theta}$ is the normalised shift $\bar{\tau} = \bar{\theta}/\omega = \tau - t + \bar{\tau}_0$ between the orbit time τ of the unperturbed trajectory and the actual time in the perturbed system. Intuitively, this shift will develop faster with larger perturbation amplitudes. As we will see, the dynamics of $\bar{\theta}$ close to the resonance condition can be modelled by a "super"-pendulum Hamiltonian with a non-linear (super)bounce frequencies ω_{bN}. To allow for a perturbative treatment in this way, the time-scale of this new kind of motion should be much longer than the bounce time τ. The task of the further derivation is to find quantitative expressions to describe this behaviour.

For the 1D case, a canonical transformation replacing θ by $\bar{\theta}$ together with its resonant action $\bar{J}$ is produced by the type-2 generating function

$$\begin{aligned} F_2(\theta, \bar{J}) &= \bar{J}\,\bar{\theta}(\theta) \\ &= \bar{J}\,(m\theta - \omega t - \bar{\theta}_0). \end{aligned} \tag{1.62}$$

The original action J is related to $\bar{J}$ by

$$J = \frac{\partial F_2}{\partial \theta} = m\bar{J}. \tag{1.63}$$

Specifically for non-zero ω, the explicit time dependence in F_2 enters the unperturbed Kamiltonian (1.18) given by

$$\bar{H}_0(\bar{J}) = H_0 + \frac{\partial F_2}{\partial t} = H_0 - \omega\bar{J}\,. \tag{1.64}$$

The new canonical frequency $\bar{\Omega}$ is

$$\bar{\Omega} = \frac{\partial}{\partial \bar{J}}(H_0(\bar{J}) - \omega\bar{J}) = \frac{\partial J}{\partial \bar{J}}\frac{\partial H_0(J)}{\partial J} - \omega = m\Omega - \omega. \tag{1.65}$$

This expression vanishes at the 1D resonance condition (1.57), which is the intended result of our choice of the canonical transformation.

In the N-dimensional case the situation is similar. In contrast to the 1D case, we now choose a specific action, e.g. J_N (without loss of generality), to be replaced by the resonant action $\bar{J} = \bar{J}_N$. This approach is similar to the one of Bécoulet et al. (1991), where a general description in the direction perpendicular to the resonance is used. A canonical transformation replacing a single angular coordinate by $\bar{\theta}$ is produced by the type-2 generating function

$$\begin{aligned} F_2(\boldsymbol{\theta}, \bar{\boldsymbol{J}}) &= \sum_{k\neq N} \bar{J}_k\theta^k + \bar{J}\,\bar{\theta}(\boldsymbol{\theta}) \\ &= \sum_{k\neq N} \bar{J}_k\theta^k + \bar{J}\,(\boldsymbol{m}\cdot\boldsymbol{\theta} - \omega t - \bar{\theta}_0)\,. \end{aligned} \tag{1.66}$$

In this transformation, the new resonant phase $\bar{\theta} = \bar{\theta}^N$ is defined as in Eq. 1.58, but all other angles stay the same with

$$\bar{\theta}^N = \bar{\theta} = \boldsymbol{m}\cdot\boldsymbol{\theta} - \omega t - \bar{\theta}_0, \tag{1.67}$$

$$\bar{\theta}^{k\neq N} = \frac{\partial F_2}{\partial \bar{J}_k} = \theta^k. \tag{1.68}$$

The action J_N is related to the resonant action $\bar{J}$ as in Eq. (1.63) via

$$J_N = m_N\bar{J}, \tag{1.69}$$

and the remaining original actions are modified via the components of their respective component in the mode-number vector,

$$J_{k\neq N} = \frac{\partial F_2}{\partial \theta^k} = \bar{J}_k + m_k\bar{J}. \tag{1.70}$$

This yields the transformed actions in terms of the original actions as

$$\bar{J}_N = \bar{J} = \frac{1}{m_N} J_N, \tag{1.71}$$

$$\bar{J}_{k\neq N} = J_k - \frac{m_k}{m_N} J_N. \tag{1.72}$$

Since the perturbation

$$\bar{H}_1(\bar{\boldsymbol{\theta}}, \bar{\boldsymbol{J}}) = -|H_{\boldsymbol{m}}(\bar{\boldsymbol{J}})| \cos\bar{\theta} \tag{1.73}$$

depends only on the single angle $\bar{\theta}$ in addition to the actions, all actions with $k \neq N$ are constants of motion which can be treated as parameters and their dependency dropped in the notation of the Hamiltonian. In this step, the problem becomes formally equivalent to the one-dimensional case in Eq. (1.64), where we treat a one-dimensional perturbed Kamiltonian system in $(\bar{\theta}, \bar{J})$ with

$$\begin{aligned} \bar{H}(\bar{\theta}, \bar{J}) &= \bar{H}_0(\bar{J}) - |H_{\boldsymbol{m}}(\bar{J})| \cos\bar{\theta} \\ &= H_0(\bar{J}) - \omega\bar{J} - |H_{\boldsymbol{m}}(\bar{J})| \cos\bar{\theta}. \end{aligned} \tag{1.74}$$

For an originally N-dimensional system, the associated single canonical frequency is

$$\bar{\Omega} = \frac{\partial}{\partial \bar{J}}(H_0(\bar{J}) - \omega\bar{J}) = \frac{\partial J_k}{\partial \bar{J}} \frac{\partial H_0(\boldsymbol{J})}{\partial J_k} - \omega = \boldsymbol{m} \cdot \boldsymbol{\Omega} - \omega, \tag{1.75}$$

which vanishes at the resonance condition in analogy to the one-dimensional case of Eq. (1.65).

Keeping in mind that the main effect of the perturbation should be located around the resonance, we now expand the system around $\bar{\Omega} = 0$, with $\bar{J} = \bar{J}_{\text{res}} + \Delta\bar{J}$ close to the resonant action $\bar{J}_{\text{res}}$ for a specific set of remaining actions $\{\bar{J}_{k\neq n}\}$. In this approximation, the unperturbed part of Eq. (1.74) is expanded up to the second order as

$$\begin{aligned} \bar{H}_0(\bar{J}) - \bar{H}_0(\bar{J}_{\text{res}}) &= \Delta J \frac{\partial \bar{H}_0}{\partial \bar{J}} + \frac{1}{2}\Delta\bar{J}^2 \frac{\partial^2 \bar{H}_0}{\partial \bar{J}^2} \\ &= \bar{\Omega}\Delta\bar{J} + \frac{1}{2}\bar{\Omega}'\Delta\bar{J}^2, \end{aligned} \tag{1.76}$$

where the first-order term vanishes in the resonance condition. The second derivative of the unperturbed Kamiltonian,

$$\bar{\Omega}' = \frac{\partial^2 \bar{H}_0}{\partial \bar{J}^2}, \tag{1.77}$$

is also called the nonlinearity parameter of the system (Lichtenberg and Lieberman, 1983). In 1D,

$$\bar{\Omega}' = m\frac{\mathrm{d}}{\mathrm{d}J}\left(m\Omega - \omega\right) = m^2\frac{\mathrm{d}\Omega}{\mathrm{d}J} = m^2\Omega\frac{\mathrm{d}\Omega}{\mathrm{d}H_0}. \tag{1.78}$$

Subtracting the constant $\bar{H}_0(\bar{J}_{\mathrm{res}}) - |H_{\boldsymbol{m}}(\bar{J}_{\mathrm{res}})|$ and evaluating the perturbation for $J = J_{\mathrm{res}}$ in Eq. (1.74), we obtain a simplified Hamiltonian in $(\bar{\theta}, \Delta\bar{J})$ close to the resonance with

$$H(\bar{\theta}, \Delta\bar{J}) = \frac{1}{2}\bar{\Omega}'\Delta\bar{J}^2 + |H_{\boldsymbol{m}}|(1 - \cos\bar{\theta}), \tag{1.79}$$

with $\bar{\Omega}'$ and $H_{\boldsymbol{m}}$ constant. This is the pendulum Hamiltonian (1.36) with position $\bar{\theta}$, momentum $\Delta\bar{J}$, "mass" $1/\bar{\Omega}'$ and potential normalisation $U_0 = 2|H_{\boldsymbol{m}}|$. Orbits can be trapped in this resonance with turning points[3] from Eq. (1.38) if

$$H < 2|H_{\boldsymbol{m}}|. \tag{1.80}$$

This kind of orbit arising via this weakly non-linear treatment of the perturbation will be called *supertrapped* and their passing counterparts *superpassing*. The non-linear bounce frequency ω_{bN} of such orbits is given by complete elliptic integrals as specified in section 1.3. The highest non-linear bounce frequency of supertrapped orbits is achieved in the harmonic limit (1.49) with

$$\omega_{0N} = \sqrt{\bar{\Omega}'|H_{\boldsymbol{m}}|}, \tag{1.81}$$

which appears also as a common scaling factor in the anharmonic range. As long as the relative perturbation amplitude $|H_{\boldsymbol{m}}|/H_0$ is small enough, $|\omega_{bN}|$ will be much smaller than $|\omega_b|$. Clearly, if they approach the same order, this kind of perturbation theory will break down and more complicated types of motion will set in.

For the applicability of the developed method, we should keep in mind that its underlying principle in 1D is a resonance condition fulfiled only at specific energy levels linked to a certain canonical frequency. Chirikov (1979) refers to the terminology of *isochronicity* and *steepness*. On the one hand, it is impossible to apply the theory to an originally harmonic oscillator, where the oscillation frequency does not depend on energy (isochronicity). In such a system the resonance condition is fulfiled either at all times, if $\omega = \omega_0$, or otherwise never. Thus the unperturbed system has to be *non-isochronous*, i.e. a non-linear oscillator. On the other hand, *steepness* is linked to the convexity of H in action space. Problems can arise if H is not convex, such that $\bar{\Omega}'$ (classifying convexity of H in action space) can change sign at some point. In this case both Hamiltonians (1.79) with positive and negative "super"-mass can influence the motion, which becomes more complicated as a result.

[3] In case of negative $\bar{\Omega}'$ they are shifted in $\bar{\theta}$ by π, what will be recalled in section 2.3.

Finally, we remark that the results described in this section are *general* within the approximations made, and do not rely on the specific original system, as long as it is integrable and can thus be written in terms of action-angle variables[4]. The described method is limited to the collisionless case of perfectly Hamiltonian orbits up to now. However, as soon as collisions enter the picture, decorrelation of orbits within the non-linear bounce time can occur. The kinetic treatment of this problem will be a topic of chapter 2.

1.5 Fourier harmonics in canonical angles

Here, the computation of Fourier harmonics in canonical angles from given functions in real space is briefly pointed out. This process is necessary in particular to obtain the form of Eq. (1.56) for the Hamiltonian perturbation.

In an N-dimensional system, harmonics in canonical angles of a function $a(\boldsymbol{\theta}, \boldsymbol{J})$ are given by the integral

$$a_m(\boldsymbol{J}) = \frac{1}{(2\pi)^N} \int_0^{2\pi} \mathrm{d}^N\theta \, a(\boldsymbol{\theta}, \boldsymbol{J}) \, e^{-\mathrm{i}\boldsymbol{m}\cdot\boldsymbol{\theta}}. \tag{1.82}$$

For a one-dimensional system we consider a function originally dependent on x with additional harmonic time dependence,

$$a(x,t) = a(x)\, e^{-\mathrm{i}\omega t} = \sum_m a_m(J)\, e^{\mathrm{i}(m\theta - \omega t)}. \tag{1.83}$$

Harmonics (1.82) in the single angle θ depending on the action J are

$$a_m(J) = \frac{1}{2\pi} \int_0^{2\pi} \mathrm{d}\theta \, a(x(\theta, J)) \, e^{-\mathrm{i}m\theta}. \tag{1.84}$$

With the angle $\theta = \tau/\tau_b$ taking the role of the normalised orbit time according to Eq. (1.53) we can write this as

$$\begin{aligned} a_m &= \frac{1}{\tau_b} \int_0^{\tau_b} \mathrm{d}\tau \, a(x(\tau)) \, e^{-\mathrm{i}m\tau/\tau_b} \\ &= \left\langle a(x(\tau)) \, e^{-\mathrm{i}\, m\tau/\tau_b} \right\rangle_b , \end{aligned} \tag{1.85}$$

where the bounce average

$$\langle b(\tau) \rangle_b = \frac{1}{\tau_b} \int_0^{\tau_b} \mathrm{d}\tau \, b(\tau) \tag{1.86}$$

[4] or, as a theoretical physicist would put it: "Everything is a pendulum in sufficient approximation."

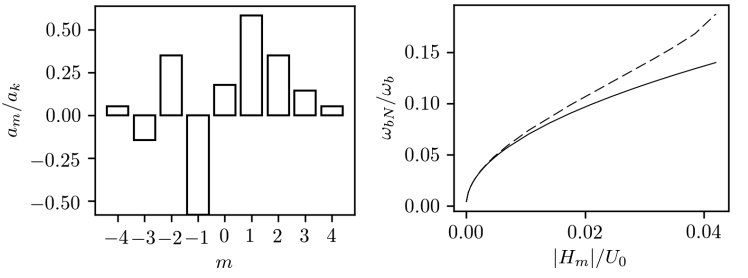

Figure 1.3: Left: spectrum (fully real coefficients) for a perturbation $\propto \cos(kx)$ with $k = 1$ in harmonics m of the canonical angle from Eq. (1.87) for the pendulum Hamiltonian. Right: non-linear super-bounce frequency ω_{bN} for harmonic $m = 2$ for $\omega = 1.5\omega_0$: small-oscillation limit ω_{N0} of Eq. (1.81) (solid line) and numerically computed value close to the resonance (dashed) over perturbation amplitude $|H_m|/U_0$.

has been introduced for an orbit evaluated at a specific J. In the 1D case, harmonics in canonical angle are identical to harmonics in bounce time (bounce harmonics). For $f(x) = f_k e^{\mathrm{i}kx}$ of harmonic form in x, those are

$$\begin{aligned} a_m &= \frac{a_k}{2\pi}\int_0^{2\pi} \mathrm{d}\theta\; e^{\mathrm{i}(kx - m\theta)} \\ &= a_k \left\langle e^{\mathrm{i}(kx(\tau) - 2\pi m\tau/\tau_b)} \right\rangle_b . \end{aligned} \tag{1.87}$$

In conclusion, for one-dimensional systems, the computation of harmonics in θ has been reformulated as a bounce average over the orbit. We will see later that this idea remains valid in integrable systems of higher dimension. In practice, bounce averages can be performed alongside (usually numerical) orbit integration of Hamilton's equations of motion (1.8).

1.6 A numerical experiment for the pendulum

To illustrate the effect of small Hamiltonian perturbations at resonances and assess the validity range of the discussed perturbation theory, we take a look at a numerical solution of Hamilton's equations of motion for an unperturbed and a perturbed pendulum. A time-harmonic perturbation is introduced with

$$H = H_0 + |H_k| \cos(kx - \omega t), \tag{1.88}$$

where the harmonic in the x-direction of real space has been chosen to be $k = 1$ and the perturbation frequency $\omega = 1.5\omega_0$. The phase of the chosen perturbation

at $t = 0$ is opposite to the x-dependency of the unperturbed system's potential $U(x) \propto 1 - \cos(x)$. This makes it easier to initialize a supertrapped orbit at $t = 0$ in practice. The spectrum of such a perturbation in canonical angle θ is plotted in Fig. 1.3. In our case, the first resonance $m\Omega - \omega = 0$ appears at $m = 2$ with energy $H_0 = E \approx 1.4252\, U_0$, with resonances for higher m close to the separatrix $U_0 = 2$. If ω had been chosen smaller than ω_0, also the first harmonic $m = 1$ could form a resonance.

The right side of Fig. 1.3 shows a comparison between the analytically computed value of ω_{N0} from Eq. (1.81) and the value for ω_{bN} computed from the large-scale periodicity of the numerical solution. In this example the match between analytical and numerical values is accurate below a relative perturbation amplitude of 1% and reasonable as long as the qualitative behaviour of the system remains the same. Slightly below a relative amplitude of 5% the method breaks down due to chaos setting in. This behaviour is illustrated in Fig. 1.4, where orbits and development of energy over time are plotted at selected perturbation amplitudes.

While this example is by far not exhaustive, it confirms the usual expectation of a "small" perturbation being of the order of a few percent, leading to a separation of scales between ω_b and ω_{bN}. For the remaining developments, we will assume the method to be generally applicable in such cases. However, problems can arise for very high values of $\bar{\Omega}'$ or where it changes sign, in particular close to the separatrix of the unperturbed system.

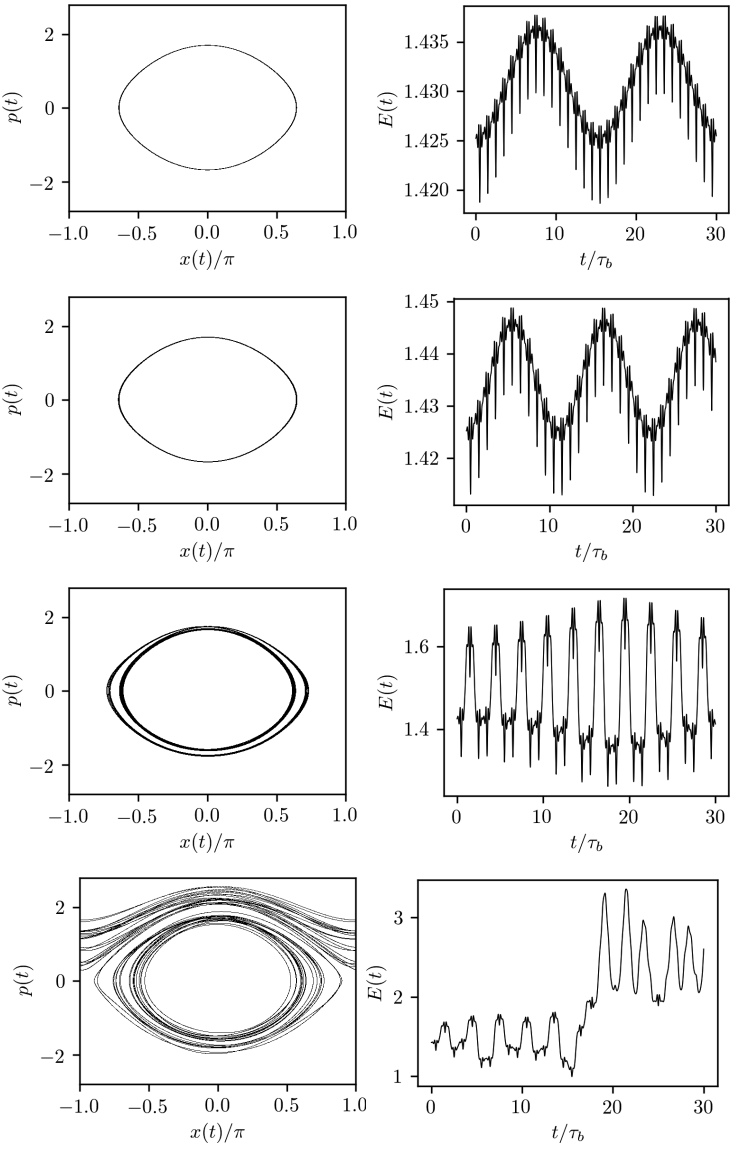

Figure 1.4: Motion close to the resonance for perturbation harmonic $m = 2$ and frequency $\omega = 1.5\omega_0$: orbits (left) and total energy over time (right) at amplitudes $|H_m|/U_0 = 0.0028, 0.0052, 0.042, 0.046$ (top to bottom). The non-linear super-bounce frequency ω_{bN} decreases with $|H_m|$, while the covered energy range increases. Here the transition to chaotic motion occurs between the last two cases.

Chapter 2

Kinetic description and resonant interaction

In this chapter a weakly non-linear kinetic description for resonant interaction with a Hamiltonian perturbation will be derived. The method is related to the treatment of damping of plasma waves, where a quasilinear (Romanov and Filippov, 1961; Vedenov et al., 1961) and a non-linear regime (Zakharov and Karpman, 1963) emerge as the limiting cases. The advantage of the present formulation is its universal applicability to weakly perturbed non-linear Hamiltonian systems with well-separated resonances described in section 1.4 and a consistent description of the transition region. For the latter, a numerical solution is provided, which will later be useful for the transition between quasilinear and non-linear resonant transport regimes in non-axisymmetrically perturbed tokamak plasmas.

2.1 Liouville's theorem

For the treatment of systems with a large number of degrees of freedom it is convenient to introduce a distribution function, which does not describe the exact system but rather an evolving probability density in phase space.

The classical approach is the definition of a distribution function $f(\boldsymbol{q}, \boldsymbol{p}, t)$ in $2N$-dimensional phase space. In the statistical interpretation it describes the distribution of states in an ensemble of identical systems at time t with different initial conditions at $t = 0$. The latter are described by an initial distribution function at $f(\boldsymbol{q}, \boldsymbol{p}, 0) = f_a(\boldsymbol{q}, \boldsymbol{p})$. In a bounded region of phase space such a distribution is well-defined down to an arbitrarily small length scale as long as the number of ensembles is chosen sufficiently high. In the probabilistic point of view, $f(\boldsymbol{q}, \boldsymbol{p}, t)$ describes the probability density of where to find a single system in phase space at a specific time

if initial conditions are only known in terms of a probability density and no further statistical argument is necessary.

In any case, the evolution of a region in phase space subject to the flow generated by the canonical equations is subject to Liouville's theorem (see e.g. Arnold (1989)), which states that its volume is conserved over time. For a heuristic proof involving a time-independent Hamiltonian H with $N = 1$, we define an arbitrarily small rectangle with corners $\{(q_0, p_0), (q_1, p_0), (q_1, p_1), (q_0, p_1)\}$ and volume (area)

$$V = (q_1 - q_0)(p_1 - p_0)\,. \tag{2.1}$$

After an infinitesimal time-step $\mathrm{d}t$, this rectangle has been deformed to a quadrangle with corners $\{(q_0, p_0)', (q_1, p_0)', (q_1, p_1)', (q_0, p_1)'\}$, where

$$\begin{aligned}(q_0, p_0)' &= (q_0, p_0) + \mathrm{d}t\,(\dot{q}, \dot{p})|_{q_0, p_0} \\ &= (q_0, p_0) + \mathrm{d}t\,\left[\frac{\partial H}{\partial p}, -\frac{\partial H}{\partial q}\right]_{q_0, p_0},\end{aligned} \tag{2.2}$$

and so on. If the region is chosen small enough with $q_1 - q_0 = \mathrm{d}q$, $p_1 - p_0 = \mathrm{d}p$ and only leading order terms are retained expanding around $(q_0, p_0)'$, we obtain an infinitesimal parallelogram with

$$(q_1, p_0)' - (q_0, p_0)' = (\mathrm{d}q, 0) + \mathrm{d}t\,\mathrm{d}q \frac{\partial}{\partial q}\left(\frac{\partial H}{\partial p}, -\frac{\partial H}{\partial q}\right), \tag{2.3}$$

$$(q_1, p_1)' - (q_0, p_0)' = (\mathrm{d}q,\ \mathrm{d}p) + \mathrm{d}t\,\mathrm{d}q \frac{\partial}{\partial q}\left(\frac{\partial H}{\partial p}, -\frac{\partial H}{\partial q}\right) + \mathrm{d}t\,\mathrm{d}p \frac{\partial}{\partial p}\left(\frac{\partial H}{\partial p}, -\frac{\partial H}{\partial q}\right), \tag{2.4}$$

$$(q_0, p_1)' - (q_0, p_0)' = (0,\ \mathrm{d}p) + \mathrm{d}t\,\mathrm{d}p \frac{\partial}{\partial p}\left(\frac{\partial H}{\partial p}, -\frac{\partial H}{\partial q}\right). \tag{2.5}$$

The area of this parallelogram is given by the 2×2 determinant

$$\begin{aligned}V' &= \mathrm{d}q\left(1 + \mathrm{d}t\,\frac{\partial^2 H}{\partial q \partial p}\right)\mathrm{d}p\left(1 - \mathrm{d}t\,\frac{\partial^2 H}{\partial q \partial p}\right) - \mathrm{d}t\,\mathrm{d}p \frac{\partial^2 H}{\partial p^2}\left(-\mathrm{d}t\,\mathrm{d}q \frac{\partial^2 H}{\partial q^2}\right) \\ &= \mathrm{d}q\mathrm{d}p\left(1 + \mathrm{d}t^2\left(\frac{\partial^2 H}{\partial q^2}\frac{\partial^2 H}{\partial p^2} - \left(\frac{\partial^2 H}{\partial q \partial p}\right)^2\right)\right) = V + \mathcal{O}(\mathrm{d}t^2),\end{aligned} \tag{2.6}$$

which is equal to S retaining only linear order terms in $\mathrm{d}t$ in the infinitesimal limit. This result can be generalised to finite regions and time differences by integration over phase space and time and to more degrees of freedom and time-dependent Hamiltonians (Arnold, 1989).

Liouville's theorem has an important consequence on the time evolution of the distribution function $f(\boldsymbol{q}, \boldsymbol{p}, t)$. Since the phase space volume occupied by a number of

system realisations in an ensemble does not change along the orbits, their density remains constant with

$$\frac{\mathrm{d}}{\mathrm{d}t} f(\boldsymbol{q}(t), \boldsymbol{p}(t), t) = 0\,. \tag{2.7}$$

The phase space volume V is moving along the orbits in time, so the described picture is of Lagrangian nature. In the Eulerian picture, defining $f(\boldsymbol{q}, \boldsymbol{p}, t)$ in a fixed point of phase space and using Eq. (1.11), we obtain

$$\frac{\partial f(\boldsymbol{q}, \boldsymbol{p}, t)}{\partial t} + \{f, H\} = 0\,, \tag{2.8}$$

or

$$\frac{\partial f(\boldsymbol{q}, \boldsymbol{p}, t)}{\partial t} + \frac{\partial H}{\partial \boldsymbol{p}} \cdot \frac{\partial f(\boldsymbol{q}, \boldsymbol{p}, t)}{\partial \boldsymbol{q}} - \frac{\partial H}{\partial \boldsymbol{q}} \cdot \frac{\partial f(\boldsymbol{q}, \boldsymbol{p}, t)}{\partial \boldsymbol{p}} = 0\,. \tag{2.9}$$

Due to its origin, this equation is often called Liouville's equation for Hamiltonian systems.

2.2 Collisions and the kinetic equation

We now consider a modification to our original one-dimensional system by exposing it to random collisions with a thermal background consisting of particles with small mass as compared to m_α and thermal momentum p_T. This corresponds to a generalised of one-dimensional Brownian motion of a particle (see e.g. Van Kampen (1983)) described by a Langevin equation (the analogy to collisional processes in plasma will be pointed out in section 4.1). For a sufficiently small time-step Δt we add a collisional contribution Δp_c to the dynamical evolution of p from Eq. (1.31),

$$p(t + \Delta t) = p(t) - U'(x)\Delta t + \Delta p_c + \mathcal{O}(\Delta t^2)\,. \tag{2.10}$$

Collisions shall lead to a random distribution of Δp_c that is slowed down towards $p = 0$ with the average rate ν, so

$$\frac{\langle \Delta p_c \rangle}{\Delta t} = -\nu p\,, \tag{2.11}$$

and is randomised with a variance

$$\frac{\langle \Delta p_c^2 \rangle}{\Delta t} = 2\nu p_T^2\,. \tag{2.12}$$

This random process on p is known as the Ornstein-Uhlenbeck process. To implement it in a numerical time-stepping routine for the orbit, we can use rescaled

samples from computer-generated random numbers to produce a distribution Θ with $\langle\Theta\rangle = 0$ and $\langle\Theta^2\rangle = 1$ and compute

$$\Delta p_c = -\nu p \Delta t + \sqrt{2\nu p_T^2}\Theta\sqrt{\Delta t}\,. \tag{2.13}$$

For our 1-dimensional model system, Liouville's equation (2.9) for the distribution function $f(x,p,t)$ is given by

$$\frac{\mathrm{d}f}{\mathrm{d}t} = \frac{\partial f}{\partial t} + \frac{p}{m_\alpha}\frac{\partial f}{\partial x} - U'(x)\frac{\partial f}{\partial p} = 0. \tag{2.14}$$

The described effects of collisions along the particle trajectory are accounted for by replacing the right-hand side of Eq. (2.14) by a linear collision operator acting on f,

$$\hat{L}_C f = \nu\frac{\partial}{\partial p}\left(p_T^2\frac{\partial f}{\partial p} + p\, f\right), \tag{2.15}$$

which results in a kinetic equation known as Kramers' equation (Kramers, 1940),

$$\frac{\partial f}{\partial t} + \frac{p}{m_\alpha}\frac{\partial f}{\partial x} - U'(x)\frac{\partial f}{\partial p} = \hat{L}_C f, \tag{2.16}$$

which is a generalisation of the original results on Brownian motion by Uhlenbeck and Ornstein (1930). The constant ν describes a collision frequency that quantifies the collisional decorrelation in time, and the thermal momentum p_T is a momentum scale corresponding to the width of the stationary distribution, i.e. its temperature

$$T = \frac{p_T^2}{2m_\alpha}. \tag{2.17}$$

This stationary distribution for which $\hat{L}_C f(x,p)$ vanishes is given by the local Maxwellian in energy $E = p^2/2m_\alpha + U(x)$, which is a Gaussian in momentum p,

$$f_M(x,p) = \frac{n_0}{\sqrt{2\pi p_T^2}}\exp\left(-\frac{p^2 + 2m_\alpha U(x)}{2p_T^2}\right), \tag{2.18}$$

where n_0 is the average density $n(x)$. Eq. (2.16) is fulfiled by f_M since also the left-hand-side is evaluated to zero, which is the reason why $U(x)$ has to enter the exponent. In the picture of randomized orbits, Eq. (2.18) describes the statistical distribution generated by the process (2.13) after a sufficiently long time.

A generalisation of Eq. (2.16) in arbitrary dimension is given by the kinetic equation

$$\frac{\partial f}{\partial t} + \{f, H\} = \hat{L}_C f \tag{2.19}$$

for the distribution function $f = f(\boldsymbol{x}, \boldsymbol{p}, t)$ in $2N$-dimensional phase space plus one time dimension. The general Fokker-Planck collision operator

$$\hat{L}_C f = \frac{\partial}{\partial p_i} \left(D_{ik}(\boldsymbol{x}, \boldsymbol{p}) \frac{\partial f}{\partial p_k} - F_i(\boldsymbol{x}, \boldsymbol{p}) f \right), \tag{2.20}$$

contains components D_{ik} of the momentum space diffusivity tensor $\hat{D}(\boldsymbol{p}, t)$ and drag coefficients F_i. As we can see from Eq. 2.15, in our simplified one-dimensional example those quantities are related to ν, p_T and p by[1]

$$D_{11} = \nu p_T^2, \qquad F_1 = -\nu p. \tag{2.21}$$

2.3 Weakly non-linear kinetic theory

For a sufficiently small perturbation H_1 as described in section 1.4 and sufficiently low collisionality (small enough ν in the 1D case), it is possible to construct a perturbation theory based on an unperturbed steady-state solution f_0 of a kinetic equation (2.19) with Hamiltonian H_0. The unperturbed steady-state equation is

$$\{f_0, H_0\} = \hat{L}_C f_0. \tag{2.22}$$

The steady-state equation for the perturbed system with $H = H_0 + H_1$ and $f = f_0 + f_1$ is

$$\{f_1, H_0 + H_1\} - \hat{L}_C f_1 = \{f_0, H_1\} = \boldsymbol{m} \cdot \frac{\partial f_0}{\partial \boldsymbol{J}} |H_{\boldsymbol{m}}| \sin \bar{\theta}, \tag{2.23}$$

where the right-hand side has been evaluated from the harmonic form of the perturbation in Eq. (1.59).

Looking at the 1D example, the result is a simplified collision operator

$$\hat{L}_C f_1 = D_{\text{res}} \frac{\partial^2 f_1}{\partial \Delta \bar{J}^2}, \tag{2.24}$$

that describes scattering across the resonance zone around $\bar{J} = \bar{J}_{\text{res}}$. The assumption of a sufficiently small ν leads to this process happening slowly in comparison to the original canonical frequency Ω allows us to use a canonically averaged resonant diffusivity,

$$D_{\text{res}} = \left\langle D_{11} \left(\frac{\partial p}{\partial \Delta \bar{J}} \right)^2 \right\rangle_\theta = \nu p_T^2 \left\langle \left(\frac{\partial p}{\partial \Delta \bar{J}} \right)^2 \right\rangle_b. \tag{2.25}$$

In the N-dimensional case we approximate the collision operator $\hat{L}_C$ by

$$\hat{L}_C f \approx \left\langle D_{ik}^{(\bar{\boldsymbol{J}})} \right\rangle_{\boldsymbol{\theta}} \frac{\partial^2 f}{\partial \bar{J}_i \partial \bar{J}_k}, \tag{2.26}$$

[1] The notation D_{11} here should not be confused with the one used later for transport coefficients

with canonically averaged diffusion coefficient $\left\langle D_{ik}^{(\bar{\boldsymbol{J}})} \right\rangle_{\boldsymbol{\theta}}$ in action space, where the relation

$$D_{ik}^{(\bar{\boldsymbol{J}})} = \frac{\partial J_i}{\partial p_l} \frac{\partial J_k}{\partial p_m} D_{lm} \tag{2.27}$$

to the momentum space diffusivity D_{lm} holds.

Following the approximation of closeness to the resonance in action space from section 1.4 with the distance from the resonance $\Delta\bar{J} = \bar{J} - \bar{J}_{\text{res}}(\{\bar{J}_{k\neq n}\})$, we consider only scattering across the resonance $\bar{J} = \bar{J}_{\text{res}}$ via $\Delta\bar{J}$, as in the 1D case. Once more, we emphasize that this is a variable change from $\bar{J} = \bar{J}_N$ to $\Delta\bar{J}$ depending on a specific set of non-resonant actions $\bar{J}_{k\neq N}$, which are treated as parametric constants. This leads to the approximation

$$\hat{L}_C f \approx D_{\text{res}} \frac{\partial^2 f}{\partial \Delta\bar{J}^2}, \tag{2.28}$$

with the diffusivity D_{res} across the resonance given by

$$D_{\text{res}} = \left\langle D_{ik}^{(\bar{\boldsymbol{J}})} \right\rangle_{\boldsymbol{\theta}} \frac{\partial \Delta\bar{J}}{\partial \bar{J}_i} \frac{\partial \Delta\bar{J}}{\partial \bar{J}_k}. \tag{2.29}$$

The derivatives of

$$\Delta\bar{J} = \bar{J} - \bar{J}_{\text{res}}(\{\bar{J}_{k\neq N}\}) \tag{2.30}$$

arising from the variable transformation in action space can be evaluated by using the expansion of the frequency $\bar{\Omega}$ close to the resonance condition $\bar{\Omega} = 0$,

$$\bar{\Omega}(\bar{J} \approx \bar{J}_{\text{res}}) = \left.\frac{\partial \bar{\Omega}}{\partial \bar{J}}\right|_{\bar{J}_{\text{res}}} \Delta\bar{J} \tag{2.31}$$

$$\Rightarrow \Delta\bar{J} = \left.\frac{\partial \bar{\Omega}}{\partial \bar{J}}\right|^{-1}_{\bar{J}_{\text{res}}} \bar{\Omega} = \frac{\bar{\Omega}}{\bar{\Omega}'}. \tag{2.32}$$

For the derivatives with respect to $\bar{J}_k$ this means

$$\frac{\partial \Delta\bar{J}}{\partial \bar{J}_k} = \frac{1}{\bar{\Omega}'} \frac{\partial \bar{\Omega}}{\partial \bar{J}_k}. \tag{2.33}$$

In the resulting expression

$$D_{\text{res}} = (\bar{\Omega}')^{-2} \left\langle D_{ik}^{(\bar{\boldsymbol{J}})} \right\rangle_{\boldsymbol{\theta}} \frac{\partial \bar{\Omega}}{\partial \bar{J}_i} \frac{\partial \bar{\Omega}}{\partial \bar{J}_k}, \tag{2.34}$$

we can finally transform back to the original actions $\boldsymbol{J}$. This yields

$$D_{\text{res}} = (\bar{\Omega}')^{-2} \left\langle D_{ik}^{(\boldsymbol{J})} \right\rangle_{\boldsymbol{\theta}} \frac{\partial \bar{\Omega}}{\partial J_i} \frac{\partial \bar{\Omega}}{\partial J_k}, \tag{2.35}$$

with diffusion coefficients $D_{ik}^{(J)}$ in action space given by the transformation from momentum diffusion coefficients D_{lm}.

The kinetic equation around the resonance condition (2.23) becomes

$$\frac{\partial f_1}{\partial \bar{\theta}} \bar{\Omega}' \Delta \bar{J} - \frac{\partial f_1}{\partial \Delta \bar{J}} |H_{\boldsymbol{m}}| \sin \bar{\theta} - D_{\rm res} \frac{\partial^2 f_1}{\partial \Delta \bar{J}^2} = \boldsymbol{m} \cdot \frac{\partial f_0}{\partial \boldsymbol{J}} |H_{\boldsymbol{m}}| \sin \bar{\theta}, \tag{2.36}$$

where the right-hand-side is evaluated at the resonance with $\bar{J} = \bar{J}_{\rm res}$ and is independent of $\Delta \bar{J}$.

To reach a dimensionless form, we introduce the substitution

$$\Delta \bar{J} = \mathrm{sgn}\left(\bar{\Omega}'\right) \left| \frac{H_{\boldsymbol{m}}}{\bar{\Omega}'} \right|^{1/2} y, \tag{2.37}$$

with expressions for derivatives

$$\frac{\partial f_1}{\partial \Delta \bar{J}} = \mathrm{sgn}\left(\bar{\Omega}'\right) \left| \frac{H_{\boldsymbol{m}}}{\bar{\Omega}'} \right|^{-1/2} \frac{\partial f_1}{\partial y}, \tag{2.38}$$

$$\frac{\partial^2 f_1}{\partial \Delta \bar{J}^2} = \left| \frac{H_{\boldsymbol{m}}}{\bar{\Omega}'} \right|^{-1} \frac{\partial^2 f_1}{\partial y^2}. \tag{2.39}$$

The Hamiltonian of Eq. (1.79) in variables $(\bar{\theta}, y)$ is

$$H(\bar{\theta}, y) = |H_{\boldsymbol{m}}| \left(\mathrm{sgn}\left(\bar{\Omega}'\right) \frac{y^2}{2} + (1 - \cos \bar{\theta}) \right), \tag{2.40}$$

with "negative mass" or rather inverted potential if $\bar{\Omega}' < 0$.

Substituting in Eq. (2.36) leads to a kinetic equation in $\bar{\theta}$ and y with

$$\frac{\partial f_1}{\partial \bar{\theta}} y - \mathrm{sgn}\left(\bar{\Omega}'\right) \frac{\partial f_1}{\partial y} \sin \bar{\theta} - D \frac{\partial^2 f_1}{\partial y^2} = \boldsymbol{m} \cdot \frac{\partial f_0}{\partial \boldsymbol{J}} \left| \frac{H_{\boldsymbol{m}}}{\bar{\Omega}'} \right|^{1/2} \sin \bar{\theta}, \tag{2.41}$$

where we have introduced the dimensionless diffusivity

$$D = D_{\rm res} \frac{\left|\bar{\Omega}'\right|^{1/2}}{\left|H_{\boldsymbol{m}}\right|^{3/2}}. \tag{2.42}$$

Shifting the resonant angle $\bar{\theta}$ by π if $\bar{\Omega}' < 0$, the sign of $\sin \bar{\theta}$ is switched in that case, and the sign-dependent part of Eq. (2.41) appears now in the right-hand side,

$$\frac{\partial f_1}{\partial \bar{\theta}} y - \frac{\partial f_1}{\partial y} \sin \bar{\theta} - D \frac{\partial^2 f_1}{\partial y^2} = \mathrm{sgn}\left(\bar{\Omega}'\right) \boldsymbol{m} \cdot \frac{\partial f_0}{\partial \boldsymbol{J}} \left| \frac{H_{\boldsymbol{m}}}{\bar{\Omega}'} \right|^{1/2} \sin \bar{\theta}. \tag{2.43}$$

The source term on the right-hand side can be normalised by rescaling f_1 with

$$f_1 = \mathrm{sgn}\left(\bar{\Omega}'\right) \left| \frac{H_{\boldsymbol{m}}}{\bar{\Omega}'} \right|^{1/2} \boldsymbol{m} \cdot \frac{\partial f_0}{\partial \boldsymbol{J}} \, g, \tag{2.44}$$

which leads to a universal dimensionless equation

$$y\frac{\partial g}{\partial \bar{\theta}} - \sin\bar{\theta}\left(\frac{\partial g}{\partial y} + 1\right) - D\frac{\partial^2 g}{\partial y^2} = 0. \tag{2.45}$$

This corresponds to a 1D kinetic equation (2.16) for a particle of mass normalised to one with position $\bar{\theta}$ and momentum y, subject to a cosine-shaped potential as in Eq. (1.36) with $U_0 = 1$. In addition to a diffusive term with diffusivity D, a source term $\sin\bar{\theta}$ originating from the interaction of the unperturbed steady-state solution f_0 with the Hamiltonian perturbation H_1 in Eq. (2.23) influences the result. At $\bar{\theta} = \pm\pi$, periodic boundary conditions should be used. At infinite momentum $y \to \pm\infty$ the solution should vanish sufficiently fast. Let us first consider the limiting cases of this equation and then continue to the overall solution.

2.4 Quasilinear limit

On one end, there is the case of $D \gg 1$, where scattering across the resonance dominates the process. In this case, the first derivative of g with respect to y can be neglected in Eq. (2.45), leading to the diffusion-dominated equation of the quasilinear limit,

$$y\frac{\partial g}{\partial \bar{\theta}} - D\frac{\partial^2 g}{\partial y^2} = \sin\bar{\theta}. \tag{2.46}$$

An even more simplified version of this equation is obtained, if a Krook model is used, replacing the differential operator $D\frac{\partial^2}{\partial y^2}$ by the constant factor $-\bar{\nu}$, so

$$y\frac{\partial g}{\partial \bar{\theta}} + \bar{\nu} g = \sin\bar{\theta}. \tag{2.47}$$

The solution within this model is

$$g(\bar{\theta}, y) = \mathrm{Re}\left(\frac{-\mathrm{i}e^{\mathrm{i}\bar{\theta}}}{\mathrm{i}y + \bar{\nu}}\right). \tag{2.48}$$

For the actual solution of Eq. (2.46), a separation

$$g(\bar{\theta}, y) = T(\bar{\theta})Y(y) \tag{2.49}$$

yields

$$\frac{T'}{T} = \frac{D}{y}\frac{Y''}{Y} = \mathrm{i}k \tag{2.50}$$

with complex separation parameter $\mathrm{i}k$. The homogeneous ordinary differential equation for T,

$$T' - \mathrm{i}kT = 0, \tag{2.51}$$

has solutions of the type

$$T(\bar{\theta}) = e^{\mathrm{i}k\bar{\theta}}. \tag{2.52}$$

The constant k must be real, since periodic boundary conditions are required. We take this solution as the ansatz for the inhomogeneous equation 2.46, which we solve in its complex form

$$y\frac{\partial g}{\partial \bar{\theta}} - D\frac{\partial^2 g}{\partial y^2} = \mathrm{Re}(-\mathrm{i}e^{\mathrm{i}\bar{\theta}}), \tag{2.53}$$

considering only its real part in the end. Due to linearity and the form of the inhomogeneity, we obtain only a non-zero contribution from $k = 1$. More specifically, we specify

$$g(\bar{\theta}, y) = Z(y)\sin\bar{\theta} = -\mathrm{Re}(\mathrm{i}Z(y)e^{\mathrm{i}\bar{\theta}}). \tag{2.54}$$

The inhomogeneous ordinary differential equation for Z is

$$yZ + \mathrm{i}DZ'' = -\mathrm{i}. \tag{2.55}$$

Choosing $u = -\mathrm{i}D^{-1/3}y$ and $Z(y) = U(u)$ we have

$$Z' = -\mathrm{i}D^{-1/3}U', \tag{2.56}$$

$$Z'' = -D^{-2/3}U'', \tag{2.57}$$

and the result is the inhomogeneous Airy equation

$$U'' - uU = D^{-1/3}. \tag{2.58}$$

Substituting back in Eq. (2.55), we obtain the homogeneous solution

$$Z_{\mathrm{h}}(y) = C_1\mathrm{Ai}(-\mathrm{i}D^{-1/3}y) + C_2\mathrm{Bi}(-\mathrm{i}D^{-1/3}y)$$

involving Airy functions

$$\mathrm{Ai}(x) = \frac{1}{\pi}\int_0^\infty \mathrm{d}w\, \cos\left(\frac{w^3}{3} + xw\right), \tag{2.59}$$

$$\mathrm{Bi}(x) = \frac{1}{\pi}\int_0^\infty \mathrm{d}w\, \left[\exp\left(-\frac{w^3}{3} + xw\right) + \sin\left(\frac{w^3}{3} + xw\right)\right], \tag{2.60}$$

and at least two possible particular solutions represented by the Scorer functions

$$Z_1(y) = \pi D^{-1/3}\mathrm{Gi}(-\mathrm{i}D^{-1/3}y), \tag{2.61}$$

$$Z_2(y) = \pi D^{-1/3}\mathrm{Hi}(-\mathrm{i}D^{-1/3}y), \tag{2.62}$$

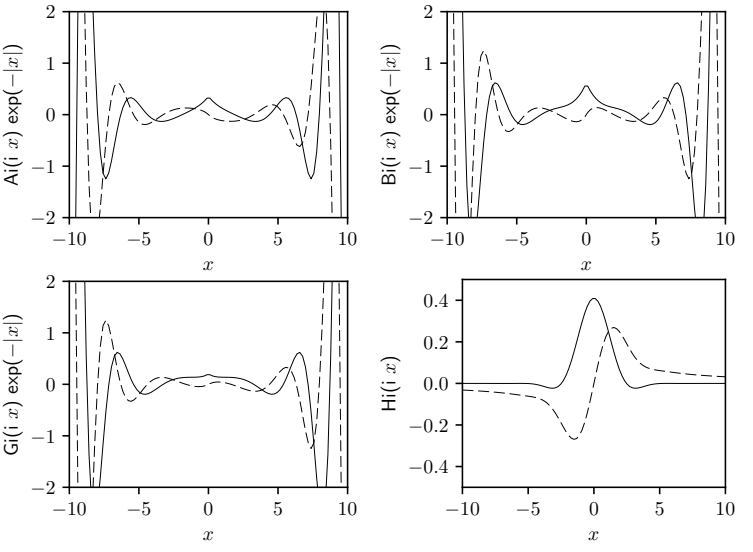

Figure 2.1: Airy functions Ai, Bi and Scorer functions Gi, Hi with imaginary argument $\mathrm{i}x$: real (solid line) and imaginary part (dashed). Despite extra weighting with $e^{-|x|}$, the first three diverge, and only $\mathrm{Hi}(\mathrm{i}x)$ converges for $x \to \pm\infty$.

where

$$\mathrm{Gi}(x) = \frac{1}{\pi}\int_0^\infty \mathrm{d}w\, \sin\left(\frac{w^3}{3} + xw\right), \tag{2.63}$$

$$\mathrm{Hi}(x) = \frac{1}{\pi}\int_0^\infty \mathrm{d}w\, \exp\left(-\frac{w^3}{3} + xw\right). \tag{2.64}$$

Since complex arguments are employed, special care needs to be taken with respect to contour integration in the complex plane. This is described in detail in the book of Gil et al. (2007), where also asymptotic properties of all four functions are given. The only one decaying at $x \to \pm\infty$ for purely imaginary argument is $\mathrm{Hi}(\mathrm{i}x)$, which is illustrated in Fig. 2.1. The conclusion is that there are no contributions to $Z(y)$ from the homogeneous solution, $C_1 = C_2 = 0$, and the solution is directly given as $Z(y) = Z_2(y)$ involving Scorer's Hi from Eq. (2.61). The overall solution for Eq. (2.46) fulfiling the correct boundary conditions at $y \to \pm\infty$ is

$$g(\bar{\theta}, y) = \mathrm{Re}\left[-\mathrm{i}\pi D^{-1/3} e^{\mathrm{i}\bar{\theta}} \mathrm{Hi}(-\mathrm{i}D^{-1/3} y)\right]. \tag{2.65}$$

A comparison between this solution and the simplified Krook model from Eq. (2.47) is plotted in Fig. 2.2 (y-dependent part) and Fig. 2.3 (contours of g) for $D = 100$.

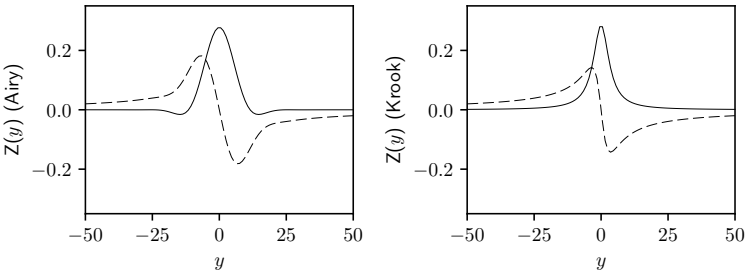

Figure 2.2: Real (solid line) and imaginary part (dashed) of the y-dependent part $Z(y)$ with $D = 100$ for full solution (left) from Eq. (2.65) and Krook model (2.48) with $\bar{\nu} = 3.5$ (right)

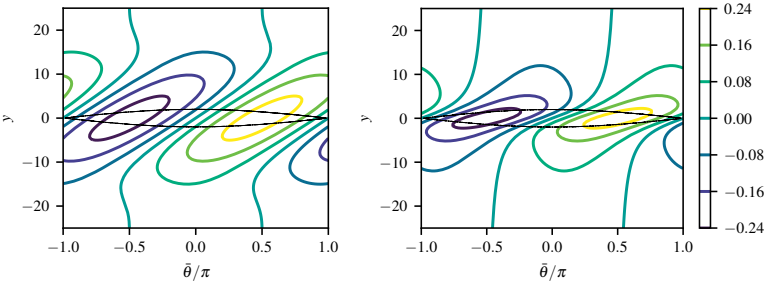

Figure 2.3: Dimensionless distribution function $g(\bar{\theta}, y)$ for $D = 100$ for full quasilinear solution (left, Eq. (2.65)) and Krook model (2.48) with $\bar{\nu} = 3.5$ (right), separatrix of the non-linear oscillation (thin black line).

The results agree qualitatively, and due to the specific choice of $\bar{\nu}$ also quantitatively up to a certain systematic error. This choice has been made manually to roughly match the two models and demonstrate their behaviour. The significance of this similarity will become clear later when applying the method to resonant transport regimes in a tokamak plasma (section 4.9).

2.5 Non-linear limit

At the one end, there is the case of $D \ll 1$. Physically, this means a combination of high-enough perturbation amplitude with low-enough collisionality. This can be seen in Eq. (2.42), where D scales with $|H_{\boldsymbol{m}}|^{-3/2}$ and $\nu^{1/2}$. The resulting equation

in this non-linear limit is obtained by using a perturbative ansatz for g with

$$g = g_0 + Dg_1, \tag{2.66}$$

where Dg_1 is of one order higher in D than g_0. Separation of orders 0 and 1 in D, truncating at D^2 and dividing the first-order equation by D yields

$$y\frac{\partial g_0}{\partial \bar{\theta}} - \sin\bar{\theta}\left(\frac{\partial g_0}{\partial y} + 1\right) = 0, \tag{2.67}$$

$$y\frac{\partial g_1}{\partial \bar{\theta}} - \sin\bar{\theta}\frac{\partial g_1}{\partial y} = \frac{\partial^2 g_0}{\partial y^2}. \tag{2.68}$$

We substitute

$$y = \sigma\sqrt{I + 2\cos\bar{\theta}}, \tag{2.69}$$

where $\sigma = \mathrm{sgn}(y)$, with the inverse transformation

$$I = y^2 - 2\cos\bar{\theta}, \tag{2.70}$$

and derivatives

$$\frac{\partial I(\bar{\theta}, y)}{\partial \bar{\theta}} = 2\sin\bar{\theta}, \tag{2.71}$$

$$\frac{\partial I(\bar{\theta}, y)}{\partial y} = 2\sigma\sqrt{I + 2\cos\bar{\theta}}. \tag{2.72}$$

This transformation is effectively a change from momentum y to two times the normalised shifted total energy I, which is conserved in the particle picture. Thus, contours of constant I are characteristics of the homogeneous variant of Eq. 2.68. The partial differential operator in Eqs. 2.67-2.68 is transformed by

$$\begin{aligned}\left(y\frac{\partial}{\partial\bar{\theta}} - \sin\bar{\theta}\frac{\partial}{\partial y}\right)a(\bar{\theta}, y) &= \sigma\sqrt{I + 2\cos\bar{\theta}}\left(\frac{\partial}{\partial\bar{\theta}} + 2\sin\bar{\theta}\frac{\partial}{\partial I}\right)a(\bar{\theta}, I) \\ &\quad - 2\sigma\sqrt{I + 2\cos\bar{\theta}}\sin\bar{\theta}\frac{\partial}{\partial I}a(\bar{\theta}, I) \\ &= \sigma\sqrt{I + 2\cos\bar{\theta}}\frac{\partial}{\partial\bar{\theta}}a(\bar{\theta}, I).\end{aligned} \tag{2.73}$$

As expected, the transformed differential operator contains only a partial derivative with respect to $\bar{\theta}$ in the new variables $(\bar{\theta}, I)$ on the right-hand-side. Using the shift

$$g_0 = \bar{g}_0 - y, \tag{2.74}$$

the result for $\bar{g}_0$ is an arbitrary function in I, so substituting back, the general solution for Eq. (2.67) is

$$g_0(\bar{\theta}, I) = \bar{g}_0(I) - \sigma\sqrt{I + 2\cos\bar{\theta}}. \tag{2.75}$$

For the second derivative of g_0 with respect to y in Eq. (2.68), only the $\bar{g}_0$ part enters, yielding

$$\frac{\partial g_1}{\partial \bar{\theta}} = 4\sigma \frac{\partial}{\partial I} \left(\sqrt{I + 2\cos\bar{\theta}}\, \bar{g}_0'(I) \right) \tag{2.76}$$

in variables $(\bar{\theta}, I)$. Since $\bar{g}_0$ depends only on I, one partial derivative is denoted as a total derivative $\bar{g}_0'(I) = \mathrm{d}\bar{g}_0(I)/\mathrm{d}I$. The general solution for g_1 is

$$g_1(\bar{\theta}, I) = 4\sigma \frac{\partial}{\partial I} \left(\bar{g}_0'(I) \int \mathrm{d}\bar{\theta} \sqrt{I + 2\cos\bar{\theta}} \right) + \bar{g}_1(I), \tag{2.77}$$

with an indefinite integral over $\bar{\theta}$ and an arbitrary function $\bar{g}_1(I)$.

For the case of superpassing orbits with $I > 2$, the term $\sqrt{I + 2\cos\bar{\theta}}$ is defined over the whole range $-\pi < \bar{\theta} < \pi$. The case $y = 0$ is never reached following a contour. Accordingly, periodic boundary conditions $g_1(\pi) = g_1(-\pi)$ are needed. This requires the solubility condition

$$\frac{\partial}{\partial I} \left(\bar{g}_0'(I) \int_{-\pi}^{\pi} \mathrm{d}\bar{\theta} \sqrt{I + 2\cos\bar{\theta}} \right) = 0\,, \tag{2.78}$$

or rather

$$\begin{aligned} \bar{g}_0'(I) &= C_\mathrm{p}^\sigma \left(\int_{-\pi}^{\pi} \mathrm{d}\bar{\theta} \sqrt{I + 2\cos\bar{\theta}} \right)^{-1} \\ &= \frac{C_\mathrm{p}^\sigma}{4\sqrt{I+2}E\left(\frac{4}{2+I}\right)}\,, \end{aligned} \tag{2.79}$$

with the complete elliptic integral $E(\kappa)$ according the convention given in section 1.3, and

$$\kappa = \frac{I+2}{4}. \tag{2.80}$$

The constant C_p^σ can depend on sign σ. For $I \to \infty$ the asymptotic limit

$$\bar{g}_0'(I)\,|_{I\gg 1} \approx \frac{C_\mathrm{p}^\sigma}{2\pi\sqrt{I}} \tag{2.81}$$

follows from neglecting the dependence on $\bar{\theta}$ in Eq. (2.78). In this limit, we evaluate the derivative of Eq. (2.75) with respect to I as

$$\frac{\partial}{\partial I} g_0(\bar{\theta}, I)\,|_{I\gg 1} \approx \frac{C_\mathrm{p}^\sigma}{2\pi\sqrt{I}} - \frac{\sigma}{2\sqrt{I}}. \tag{2.82}$$

In order to vanish in the limit $I \to \infty$, the constant needs to be fixed by $C_\mathrm{p}^\sigma = \pi\sigma$.

For the supertrapped case $-2 < I < 2$, turning points where the contours of I meet at $y = 0$ are given by

$$\cos\bar{\theta}^{\pm} = -\frac{I}{2}\,. \tag{2.83}$$

The expression $\sqrt{I + 2\cos\bar{\theta}}$ is undefined outside the interval spanned by $\bar{\theta}^{\pm}$. To enforce continuity at $y = 0$ in Eq. (2.75), in contrast to the superpassing case, $\bar{g}_0$ must not depend on the sign σ. Again, we look at the solubility condition from the first-order equation, that is

$$\frac{\partial}{\partial I}\left(\bar{g}_0'(I)\int_{\bar{\theta}-}^{\bar{\theta}+}\mathrm{d}\bar{\theta}\sqrt{I+2\cos\bar{\theta}}\right) = 0\,, \tag{2.84}$$

So

$$\bar{g}_0'(I) = \frac{C_{\mathrm{t}}}{E\left(\frac{2+I}{4}\right) - \left(1 - \frac{\sqrt{2+I}}{2}\right)K\left(\frac{2+I}{4}\right)}. \tag{2.85}$$

Due to the divergence of this expression at the o-point with $I = -2$, we have to set C_t to zero, so $\bar{g}_0$ is constant. Due to symmetry, we set it to zero, and it is in fact possible to absorb it into the equilibrium solution. Thus, in the supertrapped region,

$$g_0(\bar{\theta}, I)|_{I<2} = -\sigma\sqrt{I + 2\cos\bar{\theta}}, \tag{2.86}$$

$$g_1(\bar{\theta}, I)|_{I<2} = \bar{g}_1(I). \tag{2.87}$$

At the separatrix, continuity of g_0 requires the integration constant for $\bar{g}_0$ to be fixed in the superpassing region with $I > 2$ and we obtain the zeroth order expression there as

$$g_0(\bar{\theta}, I)|_{I>2} = \pi\sigma\int_2^I \mathrm{d}I'\left(\int_{-\pi}^{\pi}\mathrm{d}\bar{\theta}\sqrt{I' + 2\cos\bar{\theta}}\right)^{-1} - \sigma\sqrt{I + 2\cos\bar{\theta}}. \tag{2.88}$$

As opposed to the quasilinear limit of the previous section, the distribution function of the non-linear limit is symmetric with respect to angle $\bar{\theta}$, which can be seen in Fig. 2.4, where the evaluated formulas for the non-linear limit that have been obtained in this section are plotted.

2.6 Numerical solution for weakly non-linear kinetics

To solve Eq. (2.45) numerically between the two limiting cases, we combine a harmonic decomposition of g in the angle $\bar{\theta}$ with a finite difference scheme in y for each of the harmonics. The obtained results illustrate the transition and will be useful later to compute non-linear attenuation in resonant transport regimes (section 4.9).

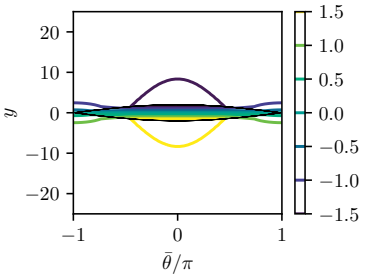

Figure 2.4: Contours of the dimensionless distribution function $g_0(\bar{\theta}, y)$ in the non-linear limit $D \ll 1$, separatrix of the non-linear oscillation (thin black line).

We first develop g as a Fourier series

$$g(y, \bar{\theta}) = \sum_{m=-M}^{M} g_m(y) e^{\mathrm{i}m\bar{\theta}}. \tag{2.89}$$

With this ansatz, Eq. (2.45) becomes

$$\frac{\mathrm{i}}{2}(e^{\mathrm{i}\bar{\theta}} - e^{-\mathrm{i}\bar{\theta}}) + \sum_{m=-M}^{M} \left[\left(\mathrm{i}ymg_m - D\frac{\partial^2 g_m}{\partial y^2} \right) e^{\mathrm{i}m\bar{\theta}} + \frac{\mathrm{i}}{2}\frac{\partial g_m}{\partial y}(e^{\mathrm{i}(m+1)\bar{\theta}} - e^{\mathrm{i}(m-1)\bar{\theta}}) \right] = 0 \tag{2.90}$$

for each harmonic or rather

$$\begin{aligned} &\sum_{m=-M}^{M} \left(\frac{\mathrm{i}}{2}(\delta_{m,1} - \delta_{m,-1}) + \mathrm{i}ymg_m - D\frac{\partial^2 g_m}{\partial y^2} \right) e^{\mathrm{i}m\bar{\theta}} \\ &+\frac{\mathrm{i}}{2} \sum_{m=-M-1}^{M-1} \frac{\partial g_{m-1}}{\partial y} e^{\mathrm{i}m\bar{\theta}} - \frac{\mathrm{i}}{2} \sum_{m=-M+1}^{M+1} \frac{\partial g_{m+1}}{\partial y} e^{\mathrm{i}m\bar{\theta}} = 0, \end{aligned} \tag{2.91}$$

where M is the highest harmonic that we consider. For a harmonic $m \neq \pm M$ this means

$$\mathrm{i}ymg_m + \frac{\mathrm{i}}{2}(g'_{m-1} - g'_{m+1}) - Dg''_m = \frac{\mathrm{i}}{2}(\delta_{m,-1} - \delta_{m,1}), \tag{2.92}$$

where primes are derivatives with respect to the argument y. For the minimum $(-M)$ and the maximum $(+M)$ harmonic ($M > 1$ in any case) follows

$$\mathrm{i}ymg_{-M} - \frac{\mathrm{i}}{2}g'_{-M+1} - Dg''_{-M} = 0, \tag{2.93}$$

$$\mathrm{i}ymg_M + \frac{\mathrm{i}}{2}g'_{M-1} - Dg''_M = 0. \tag{2.94}$$

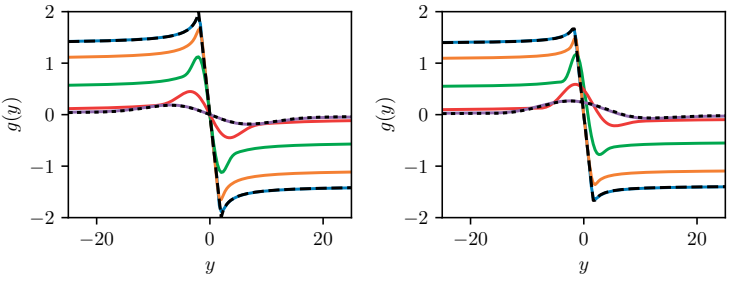

Figure 2.5: Dimensionless distribution function $g(\bar{\theta}, y)$ for $\bar{\theta} = 0$ (left) and $\bar{\theta} = \pi$ plotted over y with $D = 1.2 \cdot 10^{-2}$, 10^{-1}, 1, 10, 10^2 and comparison to quasilinear ($D = 10^2$, dotted) and non-linear limit (dashed).

We discretise g_m on a regular grid with distance Δy using a central difference scheme, so near $y = y_n$ we have

$$g_m(y) \approx g_{mn}, \tag{2.95}$$
$$g'_m(y) \approx (g_{m(n+1)} - g_{m(n-1)})/(2\Delta y), \tag{2.96}$$
$$g''_m(y) \approx (g_{m(n+1)} - 2g_{mn} + g_{m(n-1)})/\Delta y^2. \tag{2.97}$$

The finite difference form of Eq. (2.92) is

$$\begin{aligned} \mathrm{i}ymg_{mn} + \frac{\mathrm{i}}{4\Delta y}(g_{(m-1)(n+1)} - g_{(m-1)(n-1)} - g_{(m+1)(n+1)} + g_{(m+1)(n-1)}) \\ -\frac{D}{\Delta y^2}(g_{m(n+1)} - 2g_{mn} + g_{m(n-1)}) = \frac{\mathrm{i}}{2}(\delta_{m,-1} - \delta_{m,1}), \end{aligned} \tag{2.98}$$

and Eqs. (2.93-2.94) are approximated by

$$\begin{aligned} \mathrm{i}ymg_{-Mn} - \frac{\mathrm{i}}{4\Delta y}(g_{(-M+1)(n+1)} - g_{(-M+1)(n-1)}) \\ -\frac{D}{\Delta y^2}(g_{-M(n+1)} - 2g_{-Mn} + g_{-M(n-1)}) = 0, \end{aligned} \tag{2.99}$$

$$\begin{aligned} \mathrm{i}ymg_{Mn} + \frac{\mathrm{i}}{4\Delta y}(g_{(M-1)(n+1)} - g_{(M-1)(n-1)}) \\ -\frac{D}{\Delta y^2}(g_{M(n+1)} - 2g_{Mn} + g_{M(n-1)}) = 0. \end{aligned} \tag{2.100}$$

As boundary conditions we can either set $g_m(\pm y_0) = 0$ at a distant $y = y_0$ (homogeneous Dirichlet) or rather set the difference between g_m at the boundary to its next neighbour to zero (homogeneous Neumann). To match our non-linear solution we choose the latter condition. For the g_k vector numbering we start from $k = 0$

and use the usual $k = M + (2M+1)n + m$. Our final discrete equations are

$$\mathrm{i}ymg_{mn} + \frac{\mathrm{i}}{2\Delta y}(g_{(m-1)(n+1)} - g_{(m-1)n} - g_{(m+1)n} + g_{(m+1)(n-1)}) \tag{2.101}$$

$$-\frac{D}{\Delta y^2}(g_{m(n+1)} - 2g_{mn} + g_{m(n-1)}) = \frac{\mathrm{i}}{2}(\delta_{m,-1} - \delta_{m,1}), \tag{2.102}$$

and

$$\mathrm{i}ymg_{-Mn} - \frac{\mathrm{i}}{2\Delta y}(g_{(-M+1)n} - g_{(-M+1)(n-1)})$$

$$-\frac{D}{\Delta y^2}(g_{-M(n+1)} - 2g_{-Mn} + g_{-M(n-1)}) = 0, \tag{2.103}$$

$$\mathrm{i}ymg_{Mn} + \frac{\mathrm{i}}{2\Delta y}(g_{(M-1)n} - g_{(M-1)(n-1)})$$

$$-\frac{D}{\Delta y^2}(g_{M(n+1)} - 2g_{Mn} + g_{M(n-1)}) = 0. \tag{2.104}$$

Results of numerical computations using maximum harmonic $M = 10$ and 300 steps in y in the range between -50 and 50 with homogeneous Neumann conditions are shown in Figs. 2.5-2.6 for different values of dimensionless diffusivity D across the resonance. At $D = 1.2 \cdot 10^{-2}$ the solution visually matches the non-linear limit while at $D = 10^2$ a match to the quasilinear case is achieved.

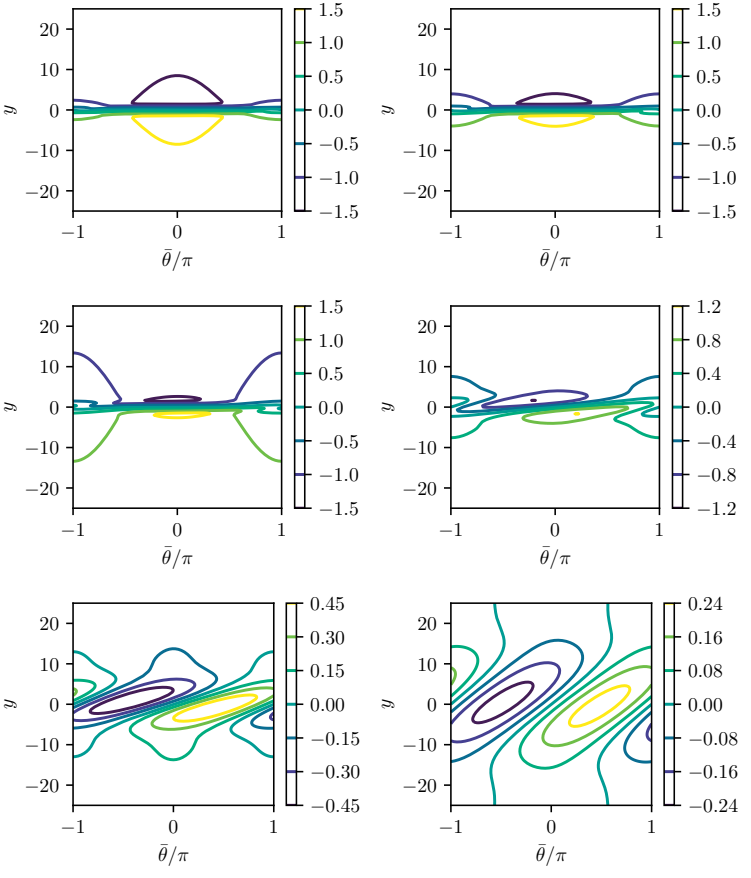

Figure 2.6: Contours of the dimensionless distribution function $g(\bar{\theta}, y)$ with $D = 1.2 \cdot 10^{-2}$, $3 \cdot 10^{-2}$, 10^{-1}, 1, 10, 10^{2} (left to right, top to bottom)

Chapter 3

Hamiltonian theory of guiding-centre motion in a tokamak

The goal in this chapter is to define action-angle variables for charged particle motion in an axisymmetric toroidal system such as an unperturbed electromagnetic field of a tokamak. For this purpose, the guiding-centre Lagrangian in magnetic coordinates is first transformed to a canonical form. Action variables are then found by a canonical transformation as described in section 1.2. The principle of the derivation is identical to the one-dimensional example in section 1.3. However, in contrast to that simple example, the guiding-centre motion in arbitrary axisymmetric geometry cannot be expressed analytically in general. An expansion in orbit width allows for integral expressions for actions, canonical frequencies and angles to the lowest order. Finally, the transformation of quantities given by a Fourier series over angles of magnetic coordinates to a Fourier series in canonical angles is given. The evaluation of the mentioned quantities can be performed via numerical orbit integration. With those ingredients the foundation is laid for the derivations of transport arising from resonances between canonical frequencies, which is performed in the following chapters.

3.1 Guiding-centre Lagrangian

For the purpose of our model, the motion of a charged plasma particle in a magnetic field is described in terms of guiding-centre variables $(\boldsymbol{R}, \phi, J_\perp, H)$ according to Littlejohn (1983). Here, $\boldsymbol{R}$ is the guiding-centre position, ϕ the gyrophase, $J_\perp$ the perpendicular adiabatic invariant and H the Hamiltonian equal to the total energy.

The Lagrangian in these variables is

$$L = (m_\alpha v_\parallel(\boldsymbol{R}, J_\perp, H)\mathbf{h}(\boldsymbol{R}) + \frac{e_\alpha}{c}\boldsymbol{A}(\boldsymbol{R})) \cdot \dot{\boldsymbol{R}} + J_\perp \dot{\phi} - H\,, \tag{3.1}$$

where the parallel velocity $v_\parallel$ is given as a function of $\boldsymbol{R}$, $J_\perp$ and H with

$$v_\parallel(\boldsymbol{R}, J_\perp, H) = \sigma \left(\frac{2}{m_\alpha}(H - e_\alpha \Phi(\boldsymbol{R}) - J_\perp \omega_c(\boldsymbol{R})) \right)^{1/2}. \tag{3.2}$$

The binary variable σ is the sign of the parallel motion along the magnetic field lines and the cyclotron or gyrofrequency is proportional to the magnetic field modulus $B(\boldsymbol{R})$ at the guiding-centre position with

$$\omega_c(\boldsymbol{R}) = \frac{e_\alpha B(\boldsymbol{R})}{m_\alpha c}. \tag{3.3}$$

Since the Lagrangian doesn't depend on ϕ in this approximation, it is clear that $J_\perp$ must be conserved and the two form a pair of action-angle variables already.

If $v_\parallel$ is used to replace H as a variable, the dependency of the latter from the remaining variables is

$$H(\boldsymbol{R}, J_\perp, v_\parallel) = \frac{m_\alpha v^2}{2} + e_\alpha \Phi(\boldsymbol{R}) = \frac{m_\alpha v_\parallel^2}{2} + e_\alpha \Phi(\boldsymbol{R}) + J_\perp \omega_c(\boldsymbol{R}), \tag{3.4}$$

where v is the velocity module containing both, parallel motion and gyration.

For the construction of action-angle variables, we will rely on an originally unperturbed Hamiltonian in the axisymmetric geometry of a tokamak. In such a two-dimensional equilibrium, flux surfaces are closed and straight field-line flux coordinates (r, ϑ, φ) parametrising $\boldsymbol{R} = \boldsymbol{R}(r, \vartheta, \varphi)$ as defined in appendix A can be constructed (D'haeseleer et al., 1991). In those coordinates, the radial component of the vector potential $\boldsymbol{A}$ vanishes and L can be written as

$$L = m_\alpha v_\parallel h_r \dot{r} + (m_\alpha v_\parallel h_\vartheta + \frac{e_\alpha}{c} A_\vartheta)\dot{\vartheta} + (m_\alpha v_\parallel h_\varphi + \frac{e_\alpha}{c} A_\varphi)\dot{\varphi} + J_\perp \dot{\phi} - H. \tag{3.5}$$

If H is used as a variable, the dependencies of $v_\parallel$ on the coordinates is

$$v_\parallel(r, \vartheta, J_\perp, H) = \sigma \left(\frac{2}{m_\alpha}(H - e_\alpha \Phi(r, \vartheta) - J_\perp \omega_c(r, \vartheta)) \right)^{1/2}. \tag{3.6}$$

In the other case, according to Eq. (3.4), the dependency of H is

$$H(r, \vartheta, J_\perp, v_\parallel) = \frac{m_\alpha v_\parallel^2}{2} + e_\alpha \Phi(r, \vartheta) + J_\perp \omega_c(r, \vartheta). \tag{3.7}$$

If cross-field drifts were neglected, r would appear as a parameter in addition to $J_\perp$, and motion would occur purely along magnetic field lines. In this case, there is a

perfect analogy of the system to the 1-dimensional model Hamiltonian discussed in section 1.3. The dynamics are driven mainly by the mirroring force caused by the increase of the magnetic field modulus B on the inboard side of the torus. Generally, in tokamak plasmas, electric forces along the field lines caused by the potential Φ are much smaller than magnetic forces, which is ultimately caused by Debye shielding (Wesson, 2011). The potential is however important for drift motion ($\boldsymbol{E} \times \boldsymbol{B}$ drift), which contributes to toroidal precession.

If we assume variations of $e_\alpha \Phi$ to be small or constant along field lines and consider the limit of large aspect ratio in a tokamak with circular concentric flux surfaces,

$$B(r, \vartheta) \approx B_0(r) \cdot (1 - \varepsilon \cos(\vartheta)), \tag{3.8}$$

with the inverse aspect ratio $\varepsilon = r/R_0$ describing the ratio between minor r and major R_0 radii of the flux surface, the system becomes equivalent to the pendulum Hamiltonian of Eq. (1.36) with

$$H(\vartheta, p_\parallel) = \frac{p_\parallel^2}{2m_\alpha} + \frac{J_\perp e_\alpha}{m_\alpha c} B_0 (1 - \varepsilon \cos(\vartheta)). \tag{3.9}$$

Here we have dropped the constant $e_\alpha \Phi$ from H and defined the parallel kinematic momentum $p_\parallel = m_\alpha v_\parallel$. Those crude simplifications are not required for our task of computing non-ambipolar radial particle fluxes in resonant transport regimes. Still, this zeroth order picture tells us something about the features of guiding-centre orbits that give us hope to be able to apply the concepts of the first two chapters: first of all the description is essentially Hamiltonian. Furthermore, the system is anharmonic, with the oscillation frequency depending on energy, making non-linear resonances possible. Finally, there are trapped and passing orbits and a separatrix in-between, where motion becomes infinitely slow. Keeping these properties in mind, we can now proceed to treat the system in more detail.

3.2 Canonical form of the guiding-centre Lagrangian

For the treatment in the action-angle formalism, we require the system to be of canonical Hamiltonian form. Although the expression for the guiding-centre Lagrangian in Eq. (3.5) seems to be of this form on first sight, it is not. The reason is that four of the six dimensions of phase-space are used up by the coordinates $(r, \vartheta, \varphi, \phi)$. Different approximate and exact approaches to construct a canonical form of the guiding-centre Lagrangian have been undertaken by (White et al., 1982; White, 1990; Meiss and Hazeltine, 1990; Abdullaev and Finken, 2002), and lately by Li et al. (2016), which offers an exact transformation closely related to the one constructed here.

Neglecting finite Larmor radius effects in the guiding-centre approximation, we can immediately identify $J_\perp$ as the canonical momentum for ϕ, being already a canonical action. This leaves only one remaining variable, which is conventionally chosen as the (conserved) total energy H or the parallel velocity $v_\parallel$. Nevertheless we identify (non-canonical) momenta in Eq. (3.5),

$$p_r = m_\alpha v_\parallel h_r, \tag{3.10}$$

$$p_\vartheta = m_\alpha v_\parallel h_\vartheta + \frac{e_\alpha}{c} A_\vartheta, \tag{3.11}$$

$$p_\varphi = m_\alpha v_\parallel h_\varphi + \frac{e_\alpha}{c} A_\varphi, \tag{3.12}$$

where all expressions are functions of phase-space variables. In a toroidally symmetric plasma in the guiding-centre approximation there are no dependencies on ϕ or φ, so the momenta $J_\perp$ and p_φ are conserved. Furthermore, the poloidal momentum p_ϑ (3.11) depends only on ϑ and conserved quantities. If our coordinates $(\{\bar{r} = r\}, \bar{\vartheta}, \bar{\varphi})$ had the additional property that the covariant magnetic field component $B_{\bar{r}}$ vanishes, we could represent L in canonical form,

$$L = (m_\alpha v_\parallel h_{\bar{\vartheta}} + \frac{e_\alpha}{c} A_{\bar{\vartheta}})\dot{\bar{\vartheta}} + (m_\alpha v_\parallel h_{\bar{\varphi}} + \frac{e_\alpha}{c} A_{\bar{\varphi}})\dot{\bar{\varphi}} + J_\perp \dot{\phi} - H, \tag{3.13}$$

and clearly identify canonical momenta for $\bar{\vartheta}$ and $\bar{\varphi}$ being

$$p_{\bar{\vartheta}} = m_\alpha v_\parallel h_{\bar{\vartheta}} + \frac{e_\alpha}{c} A_{\bar{\vartheta}}, \tag{3.14}$$

$$p_{\bar{\varphi}} = m_\alpha v_\parallel h_{\bar{\varphi}} + \frac{e_\alpha}{c} A_{\bar{\varphi}}. \tag{3.15}$$

An exact way to switch to the canonical form is possible by a strategy similar to the one recently pointed out by Li et al. (2016) via the general form of the transformation between straight field-line flux coordinates,

$$\bar{\vartheta}(r, \vartheta, \varphi) = \vartheta - G(r, \vartheta, \varphi), \tag{3.16}$$

$$\bar{\varphi}(r, \vartheta, \varphi) = \varphi - q(r)\, G(r, \vartheta, \varphi). \tag{3.17}$$

In contrast to the reference, we use the inverse form,

$$\vartheta(r, \bar{\vartheta}, \bar{\varphi}) = \bar{\vartheta} + \bar{G}(r, \bar{\vartheta}, \bar{\varphi}), \tag{3.18}$$

$$\varphi(r, \bar{\vartheta}, \bar{\varphi}) = \bar{\varphi} + q(r)\, \bar{G}(r, \bar{\vartheta}, \bar{\varphi}), \tag{3.19}$$

with safety factor $q(r)$ and a function $\bar{G}(r, \bar{\vartheta}, \bar{\varphi})$ that is periodic in the angles. The choice of this function is specified by the condition that the covariant radial magnetic field component $B_{\bar{r}}$ vanishes in new coordinates. This means that

$$\begin{aligned} 0 = B_{\bar{r}} &= \frac{\partial \vartheta}{\partial r} B_\vartheta + \frac{\partial \varphi}{\partial r} B_\varphi + B_r \\ &= \frac{\partial \bar{G}}{\partial r}(B_\vartheta + q B_\varphi) + G \frac{\mathrm{d}q}{\mathrm{d}r} B_\varphi + B_r, \end{aligned} \tag{3.20}$$

or

$$\frac{\partial}{\partial r}\bar{G}(r,\bar{\vartheta},\bar{\varphi}) = -\frac{B_r(r,\vartheta,\varphi) + \bar{G}(r,\bar{\vartheta},\bar{\varphi})\, q'(r)\, B_\varphi(r,\vartheta,\varphi)}{B_\vartheta(r,\vartheta,\varphi) + qB_\varphi(r,\vartheta,\varphi)}. \tag{3.21}$$

Since only a derivative over r occurs, this is an ordinary differential equation in $\bar{G}$. It is non-linear because $\bar{G}$ occurs implicitly in the coordinate dependencies of the magnetic field components in the original coordinates, which are substituted by their functional dependencies (3.18)-(3.19). For sufficiently smooth functions on the right-hand side, standard theory of ordinary differential equations guarantees a unique solution to this equation for each given pair $(\bar{\vartheta},\bar{\varphi})$ that can in principle be found (if no closed analytical form exists, by numerical means).[1] For our purpose, the existence and uniqueness of a solution in this form is sufficient, as we will use $\bar{\vartheta}$ and $\bar{\varphi}$ only as intermediate quantities and finally transform back to ϑ and φ.

In (3.21) for a tokamak field, all quantities are independent of toroidal angle φ so also $\bar{\varphi}$ and $\bar{G} = \bar{G}(r,\bar{\vartheta})$. This leads to an invariance of covariant toroidal vector components, particularly the toroidal momentum (3.12) using the transformation equations (3.18-3.19),

$$p_{\bar{\varphi}} = \frac{\partial\varphi}{\partial\bar{\varphi}}p_\varphi + \frac{\partial\vartheta}{\partial\bar{\varphi}}p_\vartheta + \frac{\partial r}{\partial\bar{\varphi}}p_r = p_\varphi. \tag{3.22}$$

Due to the independence of the Lagrangian on $\bar{\varphi}$, the toroidal momentum is conserved along the orbit and because of the 2π-periodicity of φ and $\bar{\varphi}$ we use it as a canonical action with a yet unknown angle coordinate. With two symmetries in ϕ and φ, separated out from the very beginning, the problem of tokamak orbits is now quasi-one-dimensional in $\bar{\vartheta}$.

A final comment shall be made on the scaling of $\bar{G}$, i.e. G, being roughly of the order $B_r/(B_\vartheta + qB_\varphi) = h_r h^\vartheta$ if r is normalised to 1 at the minor radius. As long as h_r is small, it can be regarded as a small phase shift compared to the range of ϑ and $\bar{\vartheta}$ being 2π. This is confirmed by Li et al. (2016) for symmetry flux coordinates, where the module of G remains below $1.5\cdot10^{-2}$. In this work, we are going to use Boozer magnetic coordinates, which we expect to be even more favourable in terms of the smallness of h_r.

3.3 Transformation of radial dependencies

In phase-space, switching from variables $(r,\vartheta,\varphi,\phi,J_\perp,H)$ to $\boldsymbol{z} = (\phi,\vartheta,\varphi,J_\perp,H,p_\varphi)$ or canonical $(\phi,\bar{\vartheta},\bar{\varphi},J_\perp,p_{\bar{\vartheta}},p_\varphi)$ implies a radially non-local formulation, since r is now a dependent function of coordinates and constants of motion $\boldsymbol{\alpha} = (J_\perp,H,p_\varphi)$

[1] In usual tokamak plasmas the denominator never vanishes (Li et al., 2016).

or momenta $\boldsymbol{p} = (J_\perp, p_{\bar{\vartheta}}, p_\varphi)$, respectively. Instead of flux surfaces of fixed radius, drift surfaces (Kaufman, 1972; Hazeltine et al., 1981) defined by fixed $\boldsymbol{\alpha}$ swept by the actual banana or transit orbit are now relevant for the formulation. On a drift surface the radial guiding-centre position $r = r(\vartheta, \boldsymbol{\alpha})$ is given implicitly from relation (3.12) by

$$p_\varphi = \frac{e_\alpha}{c} A_\varphi(r(\vartheta, \boldsymbol{\alpha})) + m_\alpha v_\parallel(r(\vartheta, \boldsymbol{\alpha}), \vartheta, J_\perp, H) h_\varphi(r(\vartheta, \boldsymbol{\alpha}), \vartheta). \tag{3.23}$$

Here, constants of motion, except for p_φ, enter $v_\parallel$ both directly and via r, namely

$$v_\parallel(r(\vartheta, \boldsymbol{\alpha}), \vartheta, J_\perp, H) = \sigma \left(\frac{2}{m_\alpha} (H - e_\alpha \Phi(r(\vartheta, \boldsymbol{\alpha}), \vartheta) - J_\perp \omega_c(r(\vartheta, \boldsymbol{\alpha}), \vartheta)) \right)^{1/2}. \tag{3.24}$$

The explicit variation of electric potential on a flux surface with ϑ is negligible due to Debye shielding. In addition Φ can contain an implicit dependency on ϑ via the periodic radial drift away from the flux surface during the orbit. The gyrofrequency ω_c also contains this implicit dependency. However, a much bigger variation comes from the explicit ϑ-dependency of B causing the magnetic mirror force, as long as the orbit width is small compared to the radial scale of comparable changes in B.

While the explicit evaluation of $r(\vartheta, \boldsymbol{\alpha})$ usually requires numerical orbit integration, its derivatives are directly known from the magnetic field as

$$\frac{\partial p_\varphi}{\partial z_k} = \frac{e_\alpha}{c} A'_\varphi \frac{\partial r}{\partial z_k} + m_\alpha \frac{\partial (v_\parallel h_\varphi)}{\partial r} \frac{\partial r}{\partial z_k} + m_\alpha \frac{\partial (v_\parallel h_\varphi)}{\partial z_k}, \tag{3.25}$$

where partial derivatives with respect to r are taken for coordinates $(r, \vartheta, J_\perp, H)$. In the case $z_k = p_\varphi$, the left hand side becomes one and partial derivative of $v_\parallel$ vanishes,

$$\frac{\partial r(\vartheta, \boldsymbol{\alpha})}{\partial p_\varphi} = \left[\frac{\partial}{\partial r} \left(\frac{e_\alpha}{c} A_\varphi + m_\alpha v_\parallel h_\varphi \right) \right]^{-1} = \left(\frac{\partial p_\varphi(r, \vartheta, J_\perp, H)}{\partial r} \right)^{-1}. \tag{3.26}$$

For the remaining phase-space variables ϑ, $J_\perp$ and H we obtain

$$\frac{\partial r}{\partial \vartheta} = -m_\alpha \frac{\partial (v_\parallel h_\varphi)}{\partial \vartheta} \left(\frac{\partial p_\varphi}{\partial r} \right)^{-1}, \tag{3.27}$$

$$\frac{\partial r}{\partial J_\perp} = -m_\alpha h_\varphi \frac{\partial v_\parallel}{\partial J_\perp} \left(\frac{\partial p_\varphi}{\partial r} \right)^{-1}, \tag{3.28}$$

$$\frac{\partial r}{\partial H} = -m_\alpha h_\varphi \frac{\partial v_\parallel}{\partial H} \left(\frac{\partial p_\varphi}{\partial r} \right)^{-1}. \tag{3.29}$$

In those expressions, partial derivatives of r on the left-hand side are taken for drift-surface variables $(\vartheta, \boldsymbol{\alpha})$ and translated to radially local ones on the right-hand side

taken with respect to variables $(r, \vartheta, J_\perp, H)$. First we note that we can invert partial derivatives between p_φ and r. The remaining partial derivatives of r taken on drift surfaces follow a chain rule resulting in ratios between radially local derivatives of p_φ with respect to $(\vartheta, J_\perp, H)$ and radial derivatives of p_φ.

For later use, we introduce the approximate radius r_φ defined implicitly by

$$p_\varphi = \frac{e_\alpha}{c} A_\varphi(r_\varphi) = -\frac{e_\alpha}{c} \psi_{\mathrm{pol}}(r_\varphi). \tag{3.30}$$

For trapped orbits, $r = r_\varphi$ is realised in the turning points (banana tip) where the parallel velocity $v_\parallel$ vanishes. In contrast, $v_\parallel$ is always finite for passing orbits, so by using the quantity r_φ defined by Eq. (3.30), a small radial shift is introduced in comparison to the actual orbit.

The derivative of p_φ with respect to r_φ is

$$\frac{\mathrm{d}p_\varphi}{\mathrm{d}r_\varphi} = -\frac{e_\alpha}{c} \psi'_{\mathrm{pol}}(r_\varphi) = -\frac{e_\alpha}{c} \sqrt{g} B^\vartheta = -m_\alpha \sqrt{g} h^\vartheta \omega_c. \tag{3.31}$$

It differs from $\partial p_\varphi / \partial r$ by the term $m_\alpha \frac{\partial}{\partial r}(v_\parallel h_\varphi)$, being of first order in $\rho_\parallel = v_\parallel / \omega_c$. In contrast to r, the quantity r_φ is a direct measure for toroidal momentum p_φ, with their ratio from Eq. (3.31) constant on the flux surface at r_φ.

Finally, we consider the Hamiltonian in canonical coordinates $(\phi, \bar{\vartheta}, \bar{\varphi}, J_\perp, p_{\bar{\vartheta}}, p_{\bar{\varphi}})$, given by

$$H = \frac{\pi_i \bar{g}^{ik} \pi_k}{2 m_\alpha} + J_\perp \omega_c,$$

with summation over kinematic momenta

$$\pi_{\bar{\vartheta}} = p_{\bar{\vartheta}} - \frac{e_\alpha}{c} A_{\bar{\vartheta}} = m_\alpha v_\parallel h_{\bar{\vartheta}}, \tag{3.32}$$

$$\pi_{\bar{\varphi}} = \pi_\varphi = p_\varphi - \frac{e_\alpha}{c} A_\varphi = m_\alpha v_\parallel h_\varphi, \tag{3.33}$$

and components $\bar{g}^{ik}$ of the inverse metric in the space spanned by $\bar{\vartheta}$ and $\bar{\varphi}$. Hamilton's equations of motion are valid in canonical coordinates, but originally radial dependencies of $\boldsymbol{A}$, $\boldsymbol{h}$, and ω_c as well as $\bar{g}^{ik}$ have to be resolved with respect to the new coordinates.

3.4 Action-angle variables in quasi-1D systems

Before we continue with the actual problem in the tokamak, we are now going to consider the general case of a general quasi-one-dimensional (time-independent) systems that allow a treatment similar to a one-dimensional system. We define a quasi-one-dimensional system as a Hamiltonian system with N degrees of freedom,

where spatial dependencies are only on one coordinate x^n. Since we could reduce guiding-centre dynamics in an axisymmetric magnetic field to depend only on one coordinate $\bar{\vartheta}$, all results will be immediately applicable to this case. A system defined in this way is for sure integrable, as the Hamiltonian H and the remaining canonical momenta p_k with $k \neq n$ form a set $\boldsymbol{\alpha}$ of N constants of motion. From the Hamiltonian $H = H(x^n, \boldsymbol{p})$, equations of motion are

$$\dot{x}^n = \frac{\partial H}{\partial p_n}, \qquad \dot{p}_n = -\frac{\partial H}{\partial x^n}, \tag{3.34}$$

$$\dot{x}^k = \frac{\partial H}{\partial p_k}, \qquad \dot{p}_k = 0, \quad \text{for } k \neq n. \tag{3.35}$$

Momenta $p_{k\neq 1}$ in the first set of equations in (x^1, p_1) can be treated as constants, so the first two equations are separated and describe dynamics of a one-dimensional system for each given set of $\{p_{k\neq 1}\}$. We evaluate actions for $k \neq 1$ along the trajectory, where their momenta are constant, so

$$J_k = \frac{1}{2\pi} \oint \mathrm{d}x^k \, p_k = \frac{\Delta x^k}{2\pi} p_k, \quad \text{for } k \neq n. \tag{3.36}$$

Here, Δx^k is the total distance travelled in x^k along the full trajectory. In the special case $\Delta x^k = 2\pi$ we can immediately identify p_k with the action J_k. There all but of one coordinate are already "angle-like" with the correct periodicity but not yet uniform temporal evolution. In any case we redefine constants of motion $\boldsymbol{\alpha}$ at this point by rescaling momenta to actions, $\boldsymbol{\alpha} \equiv (H, \{J_k\})$.

For the n-th coordinate we have to compute the action

$$J_n = \frac{1}{2\pi} \oint \mathrm{d}x^n \, p_n(x^n, \boldsymbol{\alpha}), \tag{3.37}$$

from the actual problem as in the one-dimensional case. For passing orbits, this is an integral over the full range of x^n, which we set to 2π without loss of generality,

$$J_n(\boldsymbol{\alpha}) = \int_0^{2\pi} \mathrm{d}x^n p_n(x^n, \boldsymbol{\alpha}). \tag{3.38}$$

In a trapped region we have

$$J_n(\boldsymbol{\alpha}) = \frac{1}{2\pi} \int_{x^{n-}}^{x^{n+}} \mathrm{d}x^{n\prime} \, p_n(x^{n\prime}, \boldsymbol{\alpha})\big|_{\sigma=1} + \frac{1}{2\pi} \int_{x^{n+}}^{x^{n-}} \mathrm{d}x^{n\prime} \, p_n(x^{n\prime}, \boldsymbol{\alpha})\big|_{\sigma=-1}\,, \tag{3.39}$$

For the representation of J_n as an integral over the actual orbit with orbit time τ,

$$J_n = \frac{\sigma}{2\pi} \int_0^{\tau_b} \mathrm{d}\tau \, \dot{x}^n(\tau) \, p_n(x^n(\tau)), \tag{3.40}$$

the upper integration limit is now the bounce time τ_b, after which a period of motion in x^n has been performed. For trapped orbits this is one turn between turning points $x^{n\pm}$, and for passing orbits x^n covers its full periodic range. The global sign is set to $\sigma = 1$ for trapped and co-passing particles moving from $x^n = 0 \dots 2\pi$ and to $\sigma = -1$ for counter-passing orbits moving from $x^n = 2\pi \dots 0$ during τ_b, which is per definition positive.

Canonical frequencies

The canonical frequencies $\boldsymbol{\Omega}$ describing the time evolution of the angles $\boldsymbol{\theta}$ are given from Eq. (1.21) as partial derivatives of $H(\boldsymbol{J})$ written in terms of the actions. The frequency associated to J_n is either computed as the derivative of the Hamiltonian, or found via integrating the orbit over one full turn in x^n until the bounce time τ_b,

$$\Omega^n(\boldsymbol{J}) = \frac{\partial H(\boldsymbol{J})}{\partial J_n} \equiv \sigma \frac{2\pi}{\tau_b}, \tag{3.41}$$

Due to the definition of canonical frequencies, we already know that this frequency should be defined via the bounce time τ_b being identical to the upper integration limit in Eq. (3.40) for the poloidal action, and sign σ positive for trapped and co-passing and negative for counter-passing orbits. We can check this and obtain an explicit expression of τ_b via an integral over coordinates by noting that

$$\Omega^n = \frac{\partial H(\boldsymbol{J})}{\partial J_n} = \left(\frac{\partial (J_n, \{J_k\})}{\partial (H, \{J_k\})} \right)^{-1} = \left(\frac{\partial J_n(H, \{J_k\})}{\partial H} \right)^{-1}. \tag{3.42}$$

This means that

$$\begin{aligned} \tau_b = 2\pi\sigma \frac{\partial J_n}{\partial H} &= \sigma \frac{\partial}{\partial H} \oint \mathrm{d}x^n \, p_n(x^n, \boldsymbol{\alpha}) \\ &= \sigma \oint \mathrm{d}x^n \, \frac{\partial p_n(x^n, \boldsymbol{\alpha})}{\partial H}. \end{aligned} \tag{3.43}$$

Here we could pull the derivative with respect to H inside the integral for passing orbits, where the integration boundaries are constant, and for trapped orbits, since the integral is split into two integrals between the turning points and the derivatives of the turning points $\partial x^{n\pm}/\partial H$ cancel out. Additionally, we verify the consistency of Eq. (3.43) with Eq. (3.40), which together with Hamilton's equations of motion indeed yields

$$\begin{aligned} \tau_b &= \int_0^{\tau_b} \mathrm{d}\tau \, \dot{x}^n \, \frac{\partial p_n(x^n, \boldsymbol{\alpha})}{\partial H} \\ &= \int_0^{\tau_b} \mathrm{d}\tau \, \frac{\partial H(x^n, \boldsymbol{p})}{\partial p_n} \frac{\partial p_n(x^n, H, \{p_k\})}{\partial H} \\ &= \int_0^{\tau_b} \mathrm{d}\tau = \tau_b. \end{aligned} \tag{3.44}$$

For the remaining canonical frequencies we can exploit the fact that we have transformed from invariants $\boldsymbol{\alpha} = (H, \{J_k\})$ to $\boldsymbol{J} = (J_n, \{J_k\})$ with $k \neq n$ by changing only one variable H to J_n. For a specific frequency Ω^k we can use the rule of Jacobians with another formal index i taking neither the value k nor n,

$$\begin{aligned}\Omega^k = \frac{\partial H(\boldsymbol{J})}{\partial J_k} &= \frac{\partial(H, J_n, \{J_i\})}{\partial(J_k, J_n, \{J_i\})} = \frac{\partial(H, J_n, \{J_i\})}{\partial(J_k, H, \{J_i\})} \left(\frac{\partial(J_k, J_n, \{J_i\})}{\partial(J_k, H, \{J_i\})}\right)^{-1} \\ &= -\frac{\partial J_n(H, J_k, \{J_i\})}{\partial J_k} \frac{\partial H(\boldsymbol{J})}{\partial J_n} = -\frac{\partial J_n(\boldsymbol{\alpha})}{\partial J_k} \Omega^n \quad \text{for } k \neq n. \end{aligned} \tag{3.45}$$

As we can see, the canonical frequencies Ω^k are proportional to Ω^n with a factor equal to the negative partial derivatives of J_n as a function of invariants $\boldsymbol{\alpha}$ with respect to the corresponding action J_k. This expression can be further simplified by transforming the action integral to an integral over orbit time τ and using the equation of motion (3.34) for x^n,

$$\begin{aligned}\frac{\partial J_n(\boldsymbol{\alpha})}{\partial J_k} &= \frac{1}{2\pi} \oint \mathrm{d}x^n \, \frac{\partial p_n(x^n, \boldsymbol{\alpha})}{\partial J_k} \\ &= \frac{\sigma}{2\pi} \int_0^{\tau_b} \mathrm{d}\tau \, \dot{x}^n(\tau) \, \frac{\partial p_n(x^n, \boldsymbol{\alpha})}{\partial J_k} \\ &= \frac{\sigma}{2\pi} \int_0^{\tau_b} \mathrm{d}\tau \, \frac{\partial H(x^n, p_n, J_k, \{J_i\})}{\partial p_n} \, \frac{\partial p_n(x^n, H, J_k, \{J_i\})}{\partial J_k} \\ &= \frac{\sigma}{2\pi} \int_0^{\tau_b} \mathrm{d}\tau \, \frac{\partial(x^n, H, J_k, \{J_i\})}{\partial(x^n, p_n, J_k, \{J_i\})} \, \frac{\partial(x^n, H, p_n, \{J_i\})}{\partial(x^n, H, J_k, \{J_i\})} \\ &= \frac{\sigma}{2\pi} \int_0^{\tau_b} \mathrm{d}\tau \, \frac{\partial(x^n, H, p_n, \{J_i\})}{\partial(x^n, p_n, J_k, \{J_i\})} \\ &= -\frac{\sigma}{2\pi} \int_0^{\tau_b} \mathrm{d}\tau \, \frac{\partial H(x^n, \boldsymbol{p})}{\partial J_k} = -\frac{\sigma}{2\pi} \frac{2\pi}{\Delta x^k} \int_0^{\tau_b} \mathrm{d}\tau \, \dot{x}^k(\tau), \quad \text{for } k \neq n. \end{aligned} \tag{3.46}$$

As in the one-dimensional example of the first chapter, we could pull the derivative inside the integral because boundary terms cancel out due to periodicity. Together with Ω^n from Eq. (3.41) the final result for is

$$\Omega^k = \frac{2\pi}{\Delta x^k} \frac{1}{\tau_b} \int_0^{\tau_b} \mathrm{d}\tau \, \dot{x}^k(\tau) = \frac{2\pi}{\Delta x^k} \left\langle v^k \right\rangle_b, \quad \text{for } k \neq n. \tag{3.47}$$

This expression is a normalised bounce-averaged velocity $v^k \equiv \dot{x}^k$ in the specific coordinate k during one bounce period in x^n, where the bounce-average is defined as in the 1D case. Such a velocity average can immediately be translated to an expression depending only on the end-points,[2]

$$\Omega^k = \frac{2\pi}{\Delta x^k} \frac{1}{\tau_b} \Big(x^k(\tau_b) - x^k(0) \Big), \quad \text{for } k \neq n, \tag{3.48}$$

[2]This is related to a popular example of school-math: if starting and arrival time are fixed, the average velocity is computable from the total distance and doesn't depend on details during the journey.

which is the ratio of the distance travelled in x^k-direction during one bounce in x^n divided by its full range during a period of motion of x^k. From our earlier observation with regard to the actions in Eq. (3.36) this makes sense, as the canonical frequency "smoothes out" the velocity of the coordinates that are not yet canonical angles.

Canonical transformation and generating function

The actions J_k which are rescaled conserved momenta appear only as a sum over linear terms $x^k J_k$ in the generating function (1.26),

$$W(\boldsymbol{q}, \boldsymbol{\alpha}) = W_n(x^n, \boldsymbol{\alpha}) + \sum_k \frac{2\pi}{\Delta x^k} x^k J_k. \tag{3.49}$$

For passing particles, W_n is given by

$$W_n(x^n, \boldsymbol{\alpha}) = \int_0^{x^n} \mathrm{d}x^{n\prime} p_n(x^{n\prime}, \boldsymbol{\alpha}). \tag{3.50}$$

For trapped particles, the sign of $\dot{x}^n$ changes during the motion. Heading towards the first turning point x^{n+}, $\sigma = 1$ and $x^n > x_0^n$, W_n is given by

$$W_n^{t,1}(x^n, \boldsymbol{\alpha}) = \int_{x_0^n}^{x^n} \mathrm{d}x^{n\prime}\, p_n(x^{n\prime}, \boldsymbol{\alpha})\big|_{\sigma=1}\,, \tag{3.51}$$

for negative parallel velocity ($\sigma = -1$) returning from x^{n+} by

$$W_n^{t,2}(x^n, \boldsymbol{\alpha}) = \int_{x^{n+}}^{x^n} \mathrm{d}x^{n\prime}\, p_n(x^{n\prime}, \boldsymbol{\alpha})\big|_{\sigma=-1} + \int_{x_0^n}^{x^{n+}} \mathrm{d}x^{n\prime}\, p_n(x^{n\prime}, \boldsymbol{\alpha})\big|_{\sigma=1}\,, \tag{3.52}$$

and for particles returning again from x^{n-} with $\sigma = 1$ and $x^n < x_0^n$ by

$$W_n^{t,3}(x^n, \boldsymbol{\alpha}) = \int_{x_0^n}^{x^n} \mathrm{d}x^{n\prime}\, p_n(x^{n\prime}, \boldsymbol{\alpha})\big|_{\sigma=1} + 2\pi J_n(\boldsymbol{\alpha})\,, \tag{3.53}$$

with turning points at x^{n+} and x^{n-}.

Canonical angles

For the calculation of the canonical angles, the generating function W must be defined in terms of $(x^n, \boldsymbol{J})$. The canonical angles are then computed by derivatives over the generating function for the canonical transformation defined in Eq. (3.49). We start with

$$\theta^n = \frac{\partial W_n(x^n, \boldsymbol{J})}{\partial J_n} \tag{3.54}$$

The derivative is evaluated similar to canonical frequencies by transforming between actions $\boldsymbol{J} = (J_n, \{J_k\})$ and the original invariants $\boldsymbol{\alpha} = (H, \{J_k\})$ using Jacobians,

$$\begin{aligned}\frac{\partial W_n(x^n, \boldsymbol{J})}{\partial J_n} &= \frac{\partial(x^n, W_n, \{J_k\})}{\partial(x^n, J_n, \{J_k\})} = \frac{\partial(x^n, W_n, \{J_k\})}{\partial(x^n, H, \{J_k\})} \frac{\partial(x^n, H, \{J_k\})}{\partial(x^n, J_n, \{J_k\})} \\ &= \frac{\partial H(\boldsymbol{J})}{\partial J^n} \frac{\partial W_n(x^n, \boldsymbol{\alpha})}{\partial H} = \Omega^n \frac{\partial W_n(x^n, \boldsymbol{\alpha})}{\partial H} \\ &= \Omega^n \int_{x_0^n}^{x^n} \mathrm{d}x^{n\prime} \frac{\partial p_n(x^{n\prime}, \boldsymbol{\alpha})}{\partial H}. \end{aligned} \tag{3.55}$$

The last integral is the orbit parameter τ, i.e. the time spent in the bounce orbit, normalised to reach $\theta^n = 2\pi$ after a full turn. While formally written in the range from x_0^n to x^n, we should carefully set the integration boundaries as in the case of the general function also here. The correct sign convention is based on the pendulum: for trapped orbits, initially $\sigma = 1$, and for passing orbits, the direction of positive θ^n shall be independent of σ, as in Fig. 1.2. This means that since τ given differentially by Eq. 3.110 *increases* during the motion, θ^n should decrease for passing orbits with $\sigma = -1$, as mentioned before. In summary, we have the same case as for the 1D example in Eq. (1.53), with

$$\theta^n = \Omega^n \tau = 2\pi\sigma \frac{\tau}{\tau_b}, \tag{3.56}$$

with a minus sign only for counter-passing orbits with $\sigma = -1$ throughout the orbit. The 2π-periodicity of θ^n is the same as the one of x^n for passing orbits. For trapped orbits, a turn back and forth between the turning points $x^{n\pm}$ leads to an increase of θ^n by 2π.

The remaining canonical angles with index $k \neq n$ include a linear term of the original coordinate x^k normalised to 2π from the generating function,

$$\theta^k = \frac{\partial W(x^n, \boldsymbol{J})}{\partial J_k} = \frac{2\pi}{\Delta x^k} x^k + \frac{\partial W_n(x^k, \boldsymbol{J})}{\partial J_k}. \tag{3.57}$$

The remaining term depends only on x^n and the actions $\boldsymbol{J}$ and is given by

$$\begin{aligned}\frac{\partial W_n(x^n, \boldsymbol{J})}{\partial J_k} &= \frac{\partial(x^n, W_n, J_n, \{J_i\})}{\partial(x^n, J_k, J_n, \{J_i\})} = \frac{\partial(x^n, W_n, J_n, \{J_i\})}{\partial(x^n, J_k, H, \{J_i\})} \frac{\partial(x^n, J_k, H, \{J_i\})}{\partial(x^n, J_k, J_n, \{J_i\})} \\ &= \left(\frac{\partial W_n(x^k, \boldsymbol{\alpha})}{\partial J_k} \frac{\partial J_n(\boldsymbol{\alpha})}{\partial H} - \frac{\partial W_n(x^n, \boldsymbol{\alpha})}{\partial H} \frac{\partial J_n(\boldsymbol{\alpha})}{\partial J_k} \right) \Omega^n \\ &= \frac{\partial W_n(x^k, \boldsymbol{\alpha})}{\partial J_k} + \Omega^k \frac{\partial W_n(x^k, \boldsymbol{\alpha})}{\partial H} \\ &= \Omega^k \tau + \int_{x_0^n}^{x^n} \mathrm{d}x^{n\prime} \frac{\partial p_n(x^{n\prime}, \boldsymbol{\alpha})}{\partial J_k}. \end{aligned} \tag{3.58}$$

Here, the first term is the normalised time spent in the orbit period of x^k. The second term can be evaluated similar to the one for canonical frequencies,

$$\begin{aligned}\int_{x_0^n}^{x^n} \mathrm{d}x^{n\prime} \frac{\partial p_n(x^{n\prime}, \boldsymbol{\alpha})}{\partial J_n} &= \int_0^\tau \mathrm{d}\tau' \dot{x}^n(\tau') \frac{\partial p_n(x^n(\tau'), \boldsymbol{\alpha})}{\partial J_n} \\ &= \frac{2\pi}{\Delta x^k} \int_0^\tau \mathrm{d}\tau' \frac{\partial H(x^n(\tau'), \boldsymbol{p})}{\partial p_n} \frac{\partial p_n(x^n(\tau'), H, p_k, \{p_i\})}{\partial p_k} \\ &= \frac{2\pi}{\Delta x^k} \int_0^\tau \mathrm{d}\tau' \frac{\partial(x^n, H, p_k, \{p_i\})}{\partial(x^n, p_n, p_k, \{p_i\})} \frac{\partial(x^n, H, p_n, \{p_i\})}{\partial(x^n, H, p_k, \{p_i\})} \\ &= \frac{2\pi}{\Delta x^k} \int_0^\tau \mathrm{d}\tau' \frac{\partial(x^n, H, p_n, \{p_i\})}{\partial(x^n, p_n, p_k, \{p_i\})} = -\frac{2\pi}{\Delta x^k} \int_0^\tau \mathrm{d}\tau' \frac{\partial H(x^n, \boldsymbol{p})}{\partial p_k} \\ &= -\frac{2\pi}{\Delta x^k} \int_0^\tau \mathrm{d}\tau' \dot{x}^k(\tau') = -\frac{2\pi}{\Delta x^k} \left(x^k(\tau) - x^k(0) \right). \end{aligned} \tag{3.59}$$

This means on the one hand, that the linear term in Eq. (3.57) can be cancelled out and we can represent $\theta^k(\tau)$ during the orbit as

$$\theta^k(\tau) = \frac{2\pi}{\Delta x^k} x_0^k + \Omega^k \tau. \tag{3.60}$$

As expected this is the phase linear in time for the periodic motion in x^k which can be shifted by $x_0^k \equiv x^k(0)$ – the point in time where the bounce motion in x^n is initiated. To reach a full period, τ can run shorter or longer than τ_b, depending on Ω^k.

On the other hand, we can keep the linear term and express the canonical angle via

$$\theta^k = \frac{2\pi}{\Delta x^k} \left(x^k + \left\langle v^k \right\rangle_b \tau - \int_0^\tau \mathrm{d}\tau' v^k(\tau') \right). \tag{3.61}$$

In addition to the constant shift by x_0^k, the last two terms measure the deviation of the velocity v^k from its bounce-averaged value during the orbit. If this difference is small, the canonical angle is approximately given by the normalised distance in the original coordinate,

$$\theta^k \approx \frac{2\pi}{\Delta x^k} \left(x^k - x_0^k \right). \tag{3.62}$$

As we will see for the construction of Fourier series in canonical angles, either of these expressions for θ^k can be useful.

3.5 Action-angle variables in a tokamak

We are now going to introduce action-angle variables for guiding-centre orbits in an axisymmetric magnetic field, starting from phase-space coordinates $(\phi, \bar{\vartheta}, \bar{\varphi}, \boldsymbol{\alpha})$ with constants of motion $\boldsymbol{\alpha} = (J_\perp, H, p_\varphi)$, where we have used the conserved energy H to

replace $p_{\bar{\vartheta}}$. Since $H = H(\bar{\vartheta}, \boldsymbol{\alpha})$, this is a quasi-1D system with $x^n = \bar{\vartheta}$, as described in section 3.4. Since the range of ϕ and $\bar{\varphi}$ is 2π, their two invariant momenta can be immediately used as actions – perpendicular invariant $J_\perp \equiv J_1$ and toroidal momentum $p_\varphi \equiv J_3$. The last remaining (poloidal) action is $J_2 = J_\vartheta$, where we drop the bar in the notation since a full period in $\bar{\vartheta}$ means also a full period in ϑ. The bounce time τ_b measures the time taken for such a period of motion in the poloidal plane. For passing particles the action is computed by an integral over the full range of motion of $\bar{\vartheta}$, and trapped particles, J_ϑ is composed of two integrals between the turning points at vanishing parallel velocity

$$v_\parallel(\bar{\vartheta}^\pm, \boldsymbol{\alpha}) = 0, \tag{3.63}$$

and is positive per definition. It is also possible to represent J_ϑ in terms of integrals of original guiding-centre coordinates r, ϑ instead. The difference of Eqs. (3.5) and (3.13) identifies

$$p_{\bar{\vartheta}}\dot{\bar{\vartheta}} = p_r\dot{r} + p_\vartheta\dot{\vartheta} + \frac{\mathrm{d}}{\mathrm{d}t}\left(p_\varphi(\varphi - \bar{\varphi})\right) \tag{3.64}$$

up to a total time derivative of $p_\varphi(\varphi - \bar{\varphi}) = p_\varphi q(r)\bar{G}(r, \bar{\vartheta}) = p_\varphi q(r)G(r, \vartheta)$ of a function periodic in $\bar{\vartheta}$ as well as ϑ. During integration in Eq. (3.40) it is cancelled at the boundaries, and we can identify

$$\begin{aligned} J_\vartheta &= \frac{\sigma}{2\pi}\int_0^{\tau_b} \mathrm{d}\tau \left(v_\parallel h_r\dot{r} + (m_\alpha v_\parallel h_\vartheta + \frac{e_\alpha}{c}A_\vartheta)\dot{\vartheta}\right) \\ &= \frac{1}{2\pi}\oint \left(\mathrm{d}r\, m_\alpha v_\parallel h_r + \mathrm{d}\vartheta\,(m_\alpha v_\parallel h_\vartheta + \frac{e_\alpha}{c}A_\vartheta)\right), \end{aligned} \tag{3.65}$$

where the first integral is evaluated along the orbit, and the second one for constant $\boldsymbol{\alpha}$. This is the same expression as given by Kolesnichenko et al. (1998; 2003), who also perform a second order expansion of this expression with respect to radial orbit width. Using Eq. (3.27) with constant $\boldsymbol{\alpha}$, we can switch back to an integration purely over ϑ with

$$\begin{aligned} J_\vartheta &= \frac{1}{2\pi}\oint \mathrm{d}\vartheta \left(p_\vartheta(r(\vartheta, \boldsymbol{\alpha}), \vartheta, \boldsymbol{\alpha}) + \frac{\partial r(\vartheta, \boldsymbol{\alpha})}{\partial\vartheta} p_r(r(\vartheta, \boldsymbol{\alpha}), \vartheta, \boldsymbol{\alpha})\right) \\ &= \frac{1}{2\pi}\oint \mathrm{d}\vartheta \left(m_\alpha v_\parallel \left(h_\vartheta - h_r m_\alpha \frac{\partial(v_\parallel h_\varphi)}{\partial\vartheta}\left(\frac{\partial p_\varphi}{\partial r}\right)^{-1}\right) + \frac{e_\alpha}{c}A_\vartheta\right). \end{aligned} \tag{3.66}$$

The second term in the last line describes a correction that we estimate using Eq. 3.31,

$$-h_r m_\alpha \frac{\partial(v_\parallel h_\varphi)}{\partial\vartheta}\left(\frac{\partial p_\varphi}{\partial r}\right)^{-1} \approx \frac{h_r}{\sqrt{g}h^\vartheta\omega_c}\frac{\partial(v_\parallel h_\varphi)}{\partial\vartheta}, \tag{3.67}$$

being of order $\rho_\parallel h_r$. Another influence from the deviation of the orbit's drift surface from the flux surface at r_φ appears via the non-local evaluation of terms $m_\alpha v_\parallel h_\vartheta$ and $\frac{e_\alpha}{c} A_\vartheta$ at $r(\vartheta, \boldsymbol{\alpha})$. For trapped orbits moving inside and outside of r_φ, we expect those effects to average out during a full bounce in good approximation. However, passing orbits, never reaching $r = r_\varphi$, will maintain a shift in respective opposite radial direction for co- and counter-passing particles if treated exactly.

Canonical frequencies

By the general results for quasi-1D systems, we have already confirmed that the poloidal canonical frequency is per definition equal to the bounce frequency,

$$\Omega^\vartheta = \sigma \frac{2\pi}{\tau_b} \equiv \omega_b \,, \tag{3.68}$$

which can take positive or negative values.

According to the general result in Eq. (3.45), the remaining two canonical frequencies are equal to bounce-averaged velocities

$$\Omega^\phi = \frac{\partial H(\boldsymbol{J})}{\partial J_\perp} = \left\langle v^\phi \right\rangle_b = \frac{\phi(\tau_b)}{\tau_b} \,, \tag{3.69}$$

$$\Omega^\varphi = \frac{\partial H(\boldsymbol{J})}{\partial p_\varphi} = \langle v^\varphi \rangle_b = \frac{\bar{\varphi}(\tau_b)}{\tau_b} = \frac{\varphi(\tau_b)}{\tau_b} \,. \tag{3.70}$$

Here we have, without loss of generality, started the bounce integral at phase $\varphi(0) = \phi(0) = 0$ and used the periodicity in $\bar{\vartheta}$ of the transformation function $\bar{G}$ in Eq. (3.19). Consequently, there is no difference whether we use φ of $\bar{\varphi}$ for the toroidal canonical frequency.

The generalised velocity v^ϕ associated with the gyrophase is not exactly the gyrofrequency ω_c, which can be seen from the equation of motion,

$$\begin{aligned} v^\phi = \frac{\partial H(\bar{\vartheta}, p_{\bar{\vartheta}}, J_\perp, p_\varphi)}{\partial J_\perp} &= \frac{\partial H(r, \bar{\vartheta}, J_\perp, p_\varphi)}{\partial J_\perp} + \frac{\partial H(r, \bar{\vartheta}, J_\perp, p_\varphi)}{\partial r} \frac{\partial r(\bar{\vartheta}, H, J_\perp, p_\varphi)}{\partial J_\perp} \\ &= \omega_c + \frac{\partial H(r, \bar{\vartheta}, J_\perp, p_\varphi)}{\partial r} \frac{\partial r(\bar{\vartheta}, H, J_\perp, p_\varphi)}{\partial J_\perp} . \end{aligned} \tag{3.71}$$

Due to the ordering with large gyrofrequency ω_c and furthermore the insignificance of the gyrophase ϕ for later computations, this correction can safely be neglected. For v^φ we similarily obtain

$$v^\varphi = \frac{\partial H(\bar{\vartheta}, p_{\bar{\vartheta}}, J_\perp, p_\varphi)}{\partial p_\varphi} = \frac{\partial H(r, \bar{\vartheta}, J_\perp, p_\varphi)}{\partial p_\varphi} + \frac{\partial H(r, \bar{\vartheta}, J_\perp, p_\varphi)}{\partial r} \frac{\partial r(\bar{\vartheta}, H, J_\perp, p_\varphi)}{\partial p_\varphi} . \tag{3.72}$$

In the previous two equations, we could also have chosen ϑ instead of $\bar{\vartheta}$ for poloidal dependencies, as they influence neither derivatives over radius nor actions.

Canonical transformation and angles

As above, the two conserved momenta $J_\perp$ and p_φ appear as linear terms $\phi J_\perp$ and $\bar{\varphi} p_\varphi$ in the generating function (1.26),

$$W(\boldsymbol{q}, \boldsymbol{\alpha}) = \phi J_\perp + W_{\bar{\vartheta}}(\bar{\vartheta}, \boldsymbol{\alpha}) + \bar{\varphi} p_\varphi. \tag{3.73}$$

Generally, W_ϑ is given by an incomplete integral, where the dependency via the transformation back to original coordinates r, ϑ, φ does not cancel out in the integral,

$$\begin{aligned} W_\vartheta(\bar{\vartheta}, \boldsymbol{\alpha}) &= \int_{\bar{\vartheta}_0}^{\bar{\vartheta}} \mathrm{d}\bar{\vartheta}' p_{\bar{\vartheta}}(\bar{\vartheta}', \boldsymbol{\alpha}) \\ &= \int_{(r_0,\vartheta_0)}^{(r,\vartheta)} \left(\mathrm{d}\vartheta' (p_\vartheta + p_\varphi q \frac{\partial G}{\partial \vartheta}) + \mathrm{d}r' (p_r + p_\varphi \frac{\partial (qG)}{\partial r}) \right). \end{aligned} \tag{3.74}$$

As in the computation for the action, there is an influence of the orbit moving away from $r = r_\varphi$ via the radial dependencies inside p_ϑ and also the remaining terms. With the convention $h^\vartheta > 0$, the sign of $\dot{\bar{\vartheta}}$ is also given by σ. We follow the trajectory of a trapped particle starting from $\bar{\vartheta} = \bar{\vartheta}_0$ at a global maximum of $v_\parallel$ with respect to $\bar{\vartheta}$. Due to symmetry, we consider only trapped orbits with positive $v_\parallel$ on the outboard side of the banana $-\pi/2 < \bar{\vartheta} < \pi/2$, where we also choose $\bar{\vartheta}_0$.

For canonical angles, we can again use the general expressions from the quasi-1D case. The first canonical angle is essentially the gyrophase with

$$\theta^1 = \phi_c = \frac{\partial W(\bar{\vartheta}, \boldsymbol{J})}{\partial J_\perp} = \phi + \frac{\partial W_\vartheta(\bar{\vartheta}, \boldsymbol{J})}{\partial J_\perp}, \tag{3.75}$$

where the difference depends only on $\bar{\vartheta}$ and actions. The second canonical angle associated to poloidal motion is the bounce phase

$$\theta^2 = \Omega^\vartheta \tau = 2\pi\sigma \frac{\tau}{\tau_b}. \tag{3.76}$$

For the remaining toroidal canonical angle, we have

$$\theta^3 = \varphi_c + \frac{\partial W_\vartheta(\bar{\vartheta}, \boldsymbol{J})}{\partial p_\varphi} = \varphi - q(r)\, G(r, \vartheta) + \frac{\partial W_\vartheta(\bar{\vartheta}, \boldsymbol{J})}{\partial p_\varphi}, \tag{3.77}$$

with the last term again independent from φ or $\bar{\varphi}$.

As described in section (1.5) we now proceed to compute Fourier harmonics in canonical angles of a quantity given on a flux surface at radius r by a Fourier series in ϕ and φ,

$$a(\phi, \vartheta, \varphi) = \sum_{l,n} a_{ln}(\vartheta) e^{i(l\phi + n\varphi)}, \tag{3.78}$$

where the poloidal dependency on ϑ remains in the Fourier coefficients. In principle, finite Larmor radius effects can be considered by the harmonic of index l, but for our application involving quasi-static perturbation fields, only $l = 0$ will allow to fulfil a resonance condition (1.57), since ω_c is much larger than ω_b and Ω^φ by modulus. Non-zero harmonics l would be required to consider, in particular, radiofrequency heating by resonant wave-particle interaction (Bécoulet et al., 1991; Kasilov et al., 1997). Our goal is to obtain a Fourier series in canonical angles,

$$a(\boldsymbol{\theta}) = \sum_{m_1,m_2,m_3} a_{\boldsymbol{m}} e^{i(m_k\theta^k)}. \tag{3.79}$$

We notice that due to the guiding-centre approximation and toroidal symmetry, neither ϕ nor φ appear in the transformation equations to canonical angles. Since $\bar{\vartheta}$ can be expressed by $\theta^2 = \vartheta_c$ via the inverse relation of Eq. (3.54), we can formally write $\theta^1 = \phi - \Delta\phi(\theta^2, \boldsymbol{J})$, $\theta^3 = \varphi - \Delta\varphi(\theta^2, \boldsymbol{J})$. Fourier coefficients in canonical $\boldsymbol{\theta}$ are

$$\begin{aligned} a_{\boldsymbol{m}} &= \sum_{l,n} \frac{1}{(2\pi)^3} \int \mathrm{d}^3\theta \, a_{ln}(\vartheta) e^{i(l\phi + n\varphi - m_k\theta^k)} \\ &= \sum_{l,n} \frac{1}{(2\pi)^3} \int \mathrm{d}^3\theta \, a_{ln}(\vartheta) e^{i((l-m)\theta^1 + (n-m_3)\theta^3 + l\Delta\phi(\theta^2,\boldsymbol{J}) + n\Delta\varphi(\theta^2,\boldsymbol{J}) - m_2\theta^2)}. \end{aligned} \tag{3.80}$$

The differences $\Delta\phi$ and $\Delta\varphi$ introduce only a phase-shift in ϕ and φ that keeps integrals over the full range of the angle invariant. As a consequence, only harmonics $m_1 = l$ and $m_3 = n$ contribute to the result with a factor of $4\pi^2$ at evaluation. Still, a single poloidal mode m in ϑ contributes to several canonical modes m_2 in θ^2, similar to the 1D case illustrated in Fig. 1.3. This dependency with $l = 0$ is

$$a_{\boldsymbol{m}} = \frac{1}{2\pi} \int \mathrm{d}\theta^2 \, a_{ln}(\vartheta) e^{i(n\Delta\varphi(\theta^2,\boldsymbol{J}) - m_2\theta^2)}.$$

3.6 Thin orbit approximation

To be able to perform more steps in an analytical way, we rely on a *thin orbit approximation*: We assume variations of unperturbed fields across the whole range of r during an orbit to be small enough so that second order contributions have negligible influence on canonical actions, angles and frequencies. This approximation is not necessary for the formalism, which could in principle be performed even for the full particle orbit taking into account the scale of the Larmor radius. However, the resulting expressions would be much more complicated and less efficiently computable. Since zero orbit width means $\mathrm{d}r = 0$ in integrals such as Eq. (3.65), we can formally replace $\bar{\vartheta}$ by ϑ in the following computations.

It is also important to note that this approximation made for canonical variables is independent from the later choice of integration along the full or rather the lowest order orbit for bounce averages. The latter can be used to take into account small-scale effects of perturbation fields if unperturbed fields vary slowly in space.

Using the approximate (banana-tip) radius r_φ implicitly defined in Eq. 3.30, we perform a first-order expansion of Eq. (3.12) around $r = r_\varphi$ with

$$\begin{aligned} p_\varphi - m_\alpha v_\parallel h_\varphi(r) &= -\frac{e_\alpha}{c}\psi_{\mathrm{pol}}(r) \\ &= -\frac{e_\alpha}{c}\left(\psi_{\mathrm{pol}}(r_\varphi) + (r-r_\varphi)\psi'_{\mathrm{pol}}(r_\varphi)\right) + \mathcal{O}((r-r_\varphi)^2\psi''_{\mathrm{pol}}(r_\varphi)). \end{aligned} \tag{3.81}$$

Replacing p_φ by Eq. (3.30) and with $m_\alpha v_\parallel h_\varphi$ of first order in $\rho_\parallel$ compared to $\frac{e_\alpha}{c}\psi_{\mathrm{pol}}$ allows us to express r to the first order in $\rho_\parallel$ by

$$r = r_\varphi + \frac{c m_\alpha v_\parallel h_\varphi}{e_\alpha \psi'_{\mathrm{pol}}} + \mathcal{O}(\varepsilon^2)\,, \tag{3.82}$$

where we assumed both $(r-r_\varphi)^2\psi''_{\mathrm{pol}}(r_\varphi)$ and $\rho_\parallel^2$ to be of the order ε^2. Here and in the remaining expansions in this section, all quantities on the right-hand side are evaluated at $r = r_\varphi$. Noting that in magnetic coordinates

$$\psi'_{\mathrm{pol}} = \sqrt{g}Bh^\vartheta = h^\vartheta \omega_c \sqrt{g} c m_\alpha / e_\alpha, \tag{3.83}$$

we can also write Eq. (3.82) as

$$r = r_\varphi + \frac{v_\parallel h_\varphi}{\omega_c \sqrt{g} h^\vartheta} + \mathcal{O}(\varepsilon^2). \tag{3.84}$$

To this order, the poloidal momentum is approximated by

$$\begin{aligned} p_\vartheta + \mathcal{O}(\varepsilon^2) &= \frac{e_\alpha}{c}A_\vartheta + m_\alpha v_\parallel h_\vartheta - \frac{m_\alpha v_\parallel h_\varphi}{A'_\varphi}A'_\vartheta \\ &= \frac{e_\alpha}{c}A_\vartheta + m_\alpha v_\parallel (h_\vartheta + q h_\varphi) \\ &= \frac{e_\alpha}{c}A_\vartheta + \frac{m_\alpha v_\parallel}{h^\vartheta}. \end{aligned} \tag{3.85}$$

This results in an approximate expression for the poloidal action from Eq. (3.65), now taken locally in radius with $\mathrm{d}r = 0$,

$$J_\vartheta = \frac{1}{2\pi}\oint \mathrm{d}\vartheta\, p_\vartheta = \frac{e_\alpha}{c}A_\vartheta \delta_{\mathrm{tp}} + J_\parallel + \mathcal{O}(\varepsilon^2), \tag{3.86}$$

where the first term exists only for passing orbits and vanishes for trapped orbits while integrating back and forth between the turning points. This is formally written

by the expression

$$\delta_{\mathrm{tp}} = \begin{cases} 0 & \text{for trapped orbits} \\ 1 & \text{for passing orbits} \end{cases}. \tag{3.87}$$

The second term is the parallel adiabatic invariant given by

$$J_\parallel = \frac{1}{2\pi} \oint \mathrm{d}\vartheta \, \frac{m_\alpha v_\parallel}{h^\vartheta} = \frac{m_\alpha \tau_b}{2\pi} \sigma \left\langle v_\parallel^2 \right\rangle_b , \tag{3.88}$$

with bounce time τ_b and bounce average $\langle a \rangle_b$ of a function $a(r, \vartheta)$ respectively given by

$$\tau_b = \sigma \oint \mathrm{d}\tau = \sigma \oint \frac{\mathrm{d}\vartheta}{\dot{\vartheta}_{\mathrm{orb}}(\tau)} = \sigma \oint \frac{\mathrm{d}\vartheta}{v_\parallel h^\vartheta}, \tag{3.89}$$

$$\langle a \rangle_b = \frac{\sigma}{\tau_b} \oint \mathrm{d}\tau a = \frac{\sigma}{\tau_b} \oint \mathrm{d}\vartheta \, \frac{a}{v_\parallel h^\vartheta}. \tag{3.90}$$

In those definitions, the sign σ of the parallel velocity has been included for passing particles to yield $\tau_b > 0$ and σ is set to 1 per convention for the trapped case. Note that in contrast to the simpler case of the pendulum in Eq. (1.41), the velocity sign σ appears only in a the second part of J_ϑ. Close to the trapped-passing boundary with $v_\parallel \ll \frac{e_\alpha A_\vartheta}{m_\alpha c}$ the sign of $v_\parallel$ and J_ϑ can for example be equal for co-passing ($\sigma = 1$) and different for counter-passing particles ($\sigma = -1$).

Canonical frequencies

In the thin orbit approximation we note that in Eq. (3.86) the only dependence of $J_\vartheta(J_\perp, H, p_\varphi)$ on H is inside $J_\parallel$, the second (poloidal) canonical frequency can be expressed as

$$\begin{aligned} \Omega^\vartheta = \frac{\partial H}{\partial J_\vartheta} &= \left(\frac{\partial (J_\perp, J_\vartheta, p_\varphi)}{\partial (J_\perp, H, p_\varphi)} \right)^{-1} = \left(\frac{\partial J_\vartheta (J_\perp, H, p_\varphi)}{\partial H} \right)^{-1} \\ &= \left(\frac{\partial J_\parallel (J_\perp, H, p_\varphi)}{\partial H} \right)^{-1}. \end{aligned} \tag{3.91}$$

Accordingly, the sign of Ω^ϑ is σ for passing particles and 1 for trapped particles, independent from A_ϑ. Using the parallel velocity defined in Eq. 3.2 written in terms of invariants,

$$v_\parallel(\boldsymbol{q}, \boldsymbol{\alpha}) = \sigma \sqrt{2/m_\alpha (H - e_\alpha \Phi(p_\varphi) - J_\perp \omega_c(\vartheta, p_\varphi))}, \tag{3.92}$$

we take the derivative

$$\begin{aligned} \frac{\partial J_\parallel}{\partial H} &= \frac{1}{2\pi} \oint \mathrm{d}\vartheta \, \frac{m_\alpha}{h^\vartheta(\vartheta, p_\varphi)} \frac{\partial v_\parallel(\vartheta, J_\perp, H, p_\varphi)}{\partial H} \\ &= \frac{1}{2\pi} \oint \mathrm{d}\vartheta \, \frac{m_\alpha}{h^\vartheta} \frac{1}{m_\alpha v_\parallel} = \sigma \frac{\tau_b}{2\pi}. \end{aligned} \tag{3.93}$$

The relative magnitudes of the remaining canonical frequencies,

$$\Omega^\phi = \frac{\partial H}{\partial J_\perp} = -\frac{\partial J_\parallel(J_\perp, H, p_\varphi)}{\partial J_\perp}\Omega^\vartheta \,,$$
$$\Omega^\varphi = \frac{\partial H}{\partial p_\varphi} = -\frac{\partial J_\vartheta(J_\perp, H, p_\varphi)}{\partial p_\varphi}\Omega^\vartheta \,, \tag{3.94}$$

can now be computed explicitly. Here we have used again a vanishing derivative of A_ϑ with respect to $J_\perp$, but its dependency on p_φ remains via the radial dependency evaluated at r_φ. The factor for Ω^ϕ is

$$\begin{aligned}\frac{\partial J_\parallel}{\partial J_\perp} &= \frac{1}{2\pi}\oint \mathrm{d}\vartheta\, \frac{m_\alpha}{h^\vartheta(\vartheta, p_\varphi)}\frac{\partial v_\parallel(\vartheta, J_\perp, H, p_\varphi)}{\partial J_\perp} \\ &= -\frac{1}{2\pi}\oint \mathrm{d}\vartheta\, \frac{\omega_c}{v_\parallel h^\vartheta} = -\sigma\frac{\tau_b}{2\pi}\left\langle\omega_c\right\rangle_b \,,\end{aligned} \tag{3.95}$$

so the first canonical frequency is exactly the bounce-averaged gyrofrequency here,

$$\Omega^\phi = \left\langle\omega_c\right\rangle_b . \tag{3.96}$$

The third (toroidal) canonical frequency Ω^φ differs between passing and trapped orbits due to the dependence on p_φ of the vector potential component A_ϑ in Eq. (3.86). In our approximation, following (3.31), this is equivalent to a radial dependency evaluated at $r = r_\varphi$,

$$\frac{\partial A_\vartheta(p_\varphi)}{\partial p_\varphi} = A'_\vartheta(r_\varphi)\frac{\mathrm{d}r_\varphi}{\mathrm{d}p_\varphi} = -\frac{c}{e_\alpha}\frac{\psi'_\mathrm{tor}(r_\varphi)}{\psi'_\mathrm{pol}(r_\varphi)} = -\frac{c}{e_\alpha}q(r_\varphi) \,. \tag{3.97}$$

Thus, the extra term in Ω^φ entering for passing particles is the safety factor q defined for straight field-line magnetic flux coordinates in Eq. (A.14), and Eq. (3.94) becomes

$$\begin{aligned}\Omega^\varphi =& q\Omega^\vartheta\delta_\mathrm{tp} - \frac{\partial J_\parallel(J_\perp, H, p_\varphi)}{\partial p_\varphi}\Omega^\vartheta \\ =& q\omega_b\delta_\mathrm{tp} + \Omega_t \,.\end{aligned} \tag{3.98}$$

The parallel velocity sign σ relevant for passing particles remains in the first, but is cancelled out in the second term. We write the remaining term as a bounce average by

$$\begin{aligned}\Omega_t = -\frac{\partial J_\parallel}{\partial p_\varphi}\Omega^\vartheta &= -\sigma\frac{m_\alpha}{\tau_b}\oint \mathrm{d}\vartheta\, \frac{\mathrm{d}r_\varphi}{\mathrm{d}p_\varphi}\frac{\partial}{\partial r}\left(\frac{v_\parallel(\vartheta, J_\perp, H, r)}{h^\vartheta(\vartheta, r)}\right) \\ &= \frac{\sigma}{\tau_b}\oint \mathrm{d}\vartheta\, \frac{1}{\sqrt{g}\omega_c h^\vartheta}\frac{\partial}{\partial r}\left(\frac{v_\parallel}{h^\vartheta}\right) \\ &= \left\langle \frac{v_\parallel}{\sqrt{g}\omega_c}\frac{\partial}{\partial r}\left(\frac{v_\parallel}{h^\vartheta}\right)\right\rangle_b = \left\langle v_g^\varphi\right\rangle_b .\end{aligned} \tag{3.99}$$

This is the bounce average of the toroidal precession frequency v_g^φ generated by $\boldsymbol{E}\times\boldsymbol{B}$ and magnetic drift on the flux surface. Evaluation of the radial derivative inside the brackets with $r = r_\varphi$ results in

$$\frac{\partial}{\partial r}\left(\frac{v_\parallel}{h^\vartheta}\right) = \frac{1}{m_\alpha h^\vartheta v_\parallel}\left(-e_\alpha\frac{\partial\Phi}{\partial r} - \frac{e_\alpha J_\perp}{m_\alpha c}\frac{\partial B}{\partial r}\right) + v_\parallel\frac{\partial}{\partial r}\left(\frac{1}{h^\vartheta}\right) . \tag{3.100}$$

Together with the relation in straight field-line flux coordinates

$$\frac{1}{m_\alpha\sqrt{g}\omega_c h^\vartheta} = \frac{c}{e_\alpha\psi'_{\mathrm{pol}}} , \tag{3.101}$$

this yields

$$\Omega_t = \frac{1}{\psi'_{\mathrm{pol}}}\left\langle -c\frac{\partial\Phi}{\partial r} - \frac{J_\perp}{m_\alpha}\frac{\partial B}{\partial r} + \frac{v_\parallel^2 B}{\omega_c}h^\vartheta\frac{\partial}{\partial r}\left(\frac{1}{h^\vartheta}\right)\right\rangle_b$$

We can now decompose Ω_t in its electric and magnetic part,

$$\Omega_t = \langle\Omega_{tE}\rangle_b + \langle\Omega_{tB}\rangle_b , \tag{3.102}$$

with $\boldsymbol{E}\times\boldsymbol{B}$ drift frequency Ω_{tE} and its bounce average

$$\langle\Omega_{tE}\rangle_b = -\frac{c}{\psi'_{\mathrm{pol}}}\left\langle\frac{\partial\Phi}{\partial r}\right\rangle_b , \tag{3.103}$$

and magnetic drift frequency Ω_{tB} containing the remaining terms related to ∇B and curvature drift. A transformation to covariant components is advantageous, especially for the case of Boozer magnetic coordinates, where the former are flux functions. With $B^2 = B^\vartheta(B_\vartheta + qB_\varphi)$ it follows that $h^\vartheta = (h_\vartheta - qh_\varphi)^{-1}$ and

$$\begin{aligned}\frac{\partial}{\partial r}\left(\frac{1}{h^\vartheta}\right) &= \frac{\partial}{\partial r}\left(\frac{B_\vartheta - qB_\varphi}{B}\right)\\ &= -\frac{1}{B^\vartheta}\frac{\partial B}{\partial r} + \frac{1}{B}\frac{\partial}{\partial r}\left(B_\vartheta - qB_\varphi\right) .\end{aligned} \tag{3.104}$$

The bounce averaged magnetic drift frequency is given by

$$\langle\Omega_{tB}\rangle_b = \frac{1}{\psi'_{\mathrm{pol}}}\left\langle -\frac{J_\perp\omega_c + m_\alpha v_\parallel^2}{m_\alpha\omega_c}\frac{\partial B}{\partial r} + \frac{v_\parallel^2}{\omega_c}h^\vartheta\left(\frac{\partial B_\vartheta}{\partial r} - q\frac{\partial B_\varphi}{\partial r} - \frac{\mathrm{d}q}{\mathrm{d}r}B_\varphi\right)\right\rangle_b . \tag{3.105}$$

The last term containing the radial derivative of the safety factor in this form is absent in standard local neoclassical theory and has only recently been considered for the case of the superbanana resonance by Shaing (2015), where it appears as a secular term resolved by bounce averaging.

For actual computations, we will use a parametrization of velocity space by velocity modulus v and and normalized perpendicular invariant η related to $J_\perp$ and $v_\parallel$ by

$$J_\perp = \frac{m_\alpha v^2}{2}\frac{m_\alpha c}{e_\alpha}\eta, \tag{3.106}$$

$$v_\parallel = \sigma v\sqrt{1-\eta B}\,. \tag{3.107}$$

From the conserved Hamiltonian (3.4) it follows that also v and subsequently η are exactly conserved if the electric potential is assumed to be constant on a flux surface and the orbit integration is performed in the lowest order in orbit width. As long as the thermal energy $\frac{m_\alpha v^2}{2}$ is much higher than the change in the electric energy $e_\alpha\Phi$ during the orbit, this still holds in very good approximation. The absolute value of the bounce frequency in those variables is

$$|\omega_b| = 2\pi v\left(\oint \mathrm{d}\vartheta\,\frac{1}{h^\vartheta\sqrt{1-\eta B}}\right)^{-1}, \tag{3.108}$$

and the bounce-averaged magnetic drift frequency becomes

$$\langle\Omega_{tB}\rangle_b = \frac{v^2}{\psi'_{\mathrm{pol}}}\left\langle -\frac{2-\eta B}{2\omega_c}\frac{\partial B}{\partial r} + \frac{1-\eta B}{\omega_c}h^\vartheta\left(\frac{\partial B_\vartheta}{\partial r} - q\frac{\partial B_\varphi}{\partial r} - \frac{\mathrm{d}q}{\mathrm{d}r}B_\varphi\right)\right\rangle_b . \tag{3.109}$$

We notice that the involved bounce integrals do not depend on velocity v. This means that we can efficiently pre-compute the dependency of those integrals on η and just use v and v^2 as the respective scaling when needed. In practice, a numerical integration based on ordinary differential equations of orbits can be used to perform bounce averages. The differential of the orbit parameter τ equal to time for the unperturbed orbits is related to the differential $\mathrm{d}\vartheta$ by

$$\mathrm{d}\tau = \left|\frac{\mathrm{d}\vartheta}{h^\vartheta v_\parallel}\right|, \tag{3.110}$$

where $\mathrm{d}\vartheta$ is evaluated as it increases or decreases during the motion in the orbit.

Canonical angles and Fourier harmonics

Explicit expressions for canonical angles from section 3.5 can be computed close to $r = r_\varphi$, where setting $\mathrm{d}r = 0$ in integrals allows us to replace $\bar\vartheta$ by the original ϑ. The canonical gyrophase becomes

$$\begin{aligned}\theta^1 = \phi_c &= \phi + \Omega^\phi\tau - \int_{\vartheta_0}^{\vartheta}\mathrm{d}\vartheta'\,\frac{\omega_c}{v_\parallel h^\vartheta}\\ &= \phi + \langle\omega_c\rangle_b\,\tau - \int_0^\tau \mathrm{d}\tau'\,\omega_c\end{aligned} \tag{3.111}$$

The last two terms measure the deviation of the current gyrofrequency from its average value during the orbit.

The canonical poloidal angle, i.e. the bounce phase, is given by

$$\theta^2 = \vartheta_c = \omega_b \int_{\vartheta_0}^{\vartheta} \mathrm{d}\vartheta' \frac{\mathrm{d}\vartheta'}{v_\parallel h^\vartheta}. \tag{3.112}$$

For the toroidal canonical angle we evaluate

$$\begin{aligned}\frac{\partial W_\vartheta(\vartheta, \boldsymbol{J})}{\partial p_\varphi} &= \Omega^\varphi \tau + \frac{\partial}{\partial p_\varphi} \int_{\vartheta_0}^{\vartheta} \mathrm{d}\vartheta' \left[\frac{e_\alpha}{c} A_\vartheta + \frac{m_\alpha v_\parallel}{h^\vartheta} + p_\varphi q \frac{\partial G}{\partial \vartheta}\right] \\ &= (\Omega_t + q\omega_b \delta_{\mathrm{tp}})\,\tau - q\,(\vartheta - G(r,\vartheta) - \vartheta_0 + G(r,\vartheta_0)) - \int_0^\tau \mathrm{d}\tau' \frac{v_\parallel}{\sqrt{g}\omega_c} \frac{\partial}{\partial r} \frac{v_\parallel}{h^\vartheta} \\ &= 2\pi\sigma \frac{\tau}{\tau_b} \delta_{\mathrm{tp}} - q(\vartheta - G(r,\vartheta) - \vartheta_0 + G(r,\vartheta_0)) + \tau \left\langle v_g^\varphi \right\rangle_b - \int_0^\tau \mathrm{d}\tau' v_g^\varphi.\end{aligned} \tag{3.113}$$

The first term in this expression is only present for passing particles and the last two terms measure the deviation of the toroidal drift velocity v_g^φ from its bounce averaged value $\langle v_g^\varphi \rangle_b = \Omega_t$. Compared to the other terms of order one, this difference is of the order of the Larmor radius and can be neglected.

Finally, terms involving the transformation function G at the upper boundary cancel out and we obtain

$$\begin{aligned}\theta^3 = \varphi_c &= \varphi - q(\vartheta - \vartheta_0 + G(r,\vartheta_0)) + q\theta^2 \delta_{\mathrm{tp}} \\ &= \varphi - q(\vartheta_{\mathrm{orb}}(\vartheta_0,\, \tau) + G(r,\vartheta_0) - 2\pi\sigma \frac{\tau}{\tau_b} \delta_{\mathrm{tp}}),\end{aligned} \tag{3.114}$$

where

$$\vartheta_{\mathrm{orb}}(\vartheta_0,\, \tau) = \vartheta(\tau) - \vartheta_0 \tag{3.115}$$

is the angle as evaluated in the integration of unperturbed orbits with initial position ϑ_0 and time parameter τ.

Up to the additional last term for passing orbits, Eq. (3.114) and the constant shift involving G, the toroidal canonical angle θ^3 is identical to the definition of the toroidal angle $\varphi_0 = \varphi - q\vartheta$ used in the works of Shaing et al. (2009b; 2009a; 2010; 2015) and Park et al. (2009), where the orientation of φ is switched in addition, as well as Kasilov et al. (2014). This choice is usually made for geometrical reasons, namely because φ_0 is constant on magnetic field lines on a flux surface. As we have demonstrated here, its generalisation for passing orbits via the canonical angle contains an additional contribution from the canonical poloidal angle $\theta^2 = \vartheta_c = 2\pi\tau/\tau_b$, i.e. the time spent in the transit orbit.

Fourier harmonics in canonical angles become

$$\begin{aligned} a_{\boldsymbol{m}} &= \frac{1}{2\pi}\int \mathrm{d}\theta^2\, a_{ln}(\vartheta) e^{i(n\Delta\varphi(\theta^2,\boldsymbol{J})-m_2\theta^2)} \\ &= \left\langle a_{0n}(\vartheta) e^{inq\vartheta_{\mathrm{orb}}-i(m_2+nq\delta_{\mathrm{tp}})\omega_b\tau}\right\rangle_b . \end{aligned} \tag{3.116}$$

The evaluation of this expression, $\vartheta_{\mathrm{orb}}(\vartheta_0,\tau)$ is integrated along the orbit from initial ϑ_0 ignoring the constant phase shift via G. The sign of the bounce frequency ω_b is $\sigma=-1$ for the case of counter-passing particles, and $\sigma=1$ for trapped and co-passing particles, while the integration over τ always runs in the positive direction. This means that ϑ decreases during the integration for counter-passing particles and increases for the other cases.

3.7 Approximate transformation to canonical coordinates

An alternative approach to reach a canonical form for the guiding-centre Lagrangian lies in a transformation of only the toroidal angle coordinate $\bar{\varphi}$. A similar step is taken by White (1984; 1990) where the poloidal angle ϑ is transformed instead. Noticing that

$$m_\alpha v_\parallel h_r \dot{r} = \frac{\mathrm{d}}{\mathrm{d}t}\left(v_\parallel h_r r\right) - r\frac{\mathrm{d}}{\mathrm{d}t}(v_\parallel h_r), \tag{3.117}$$

we define the new toroidal angle by

$$\bar{\varphi} = \varphi - \frac{c m_\alpha v_\parallel h_r}{e_\alpha A'_\varphi}. \tag{3.118}$$

Subtracting the total time derivative

$$\begin{aligned} \frac{\mathrm{d}}{\mathrm{d}t}\left(A_\varphi \frac{m_\alpha v_\parallel h_r}{A'_\varphi}\right) &= m_\alpha A_\varphi \frac{\mathrm{d}}{\mathrm{d}t}\left(\frac{v_\parallel h_r}{A'_\varphi}\right) + m_\alpha \frac{\mathrm{d}A_\varphi}{\mathrm{d}t}\left(\frac{v_\parallel h_r}{A'_\varphi}\right) \\ &= \frac{e_\alpha}{c} A_\varphi(\dot{\varphi}-\dot{\bar{\varphi}}) + m_\alpha v_\parallel h_r \dot{r} \end{aligned} \tag{3.119}$$

from the Lagrangian (3.5) results in

$$\begin{aligned} L &= p_\vartheta \dot{\vartheta} + p_\varphi \dot{\bar{\varphi}} + J_\perp \dot{\phi} - H + m_\alpha v_\parallel h_\varphi(\dot{\varphi}-\dot{\bar{\varphi}}) \\ &= p_\vartheta \dot{\vartheta} + p_\varphi \dot{\bar{\varphi}} + J_\perp \dot{\phi} - H + \frac{c m_\alpha^2 v_\parallel h_\varphi}{e_\alpha}\frac{\mathrm{d}}{\mathrm{d}t}\left(\frac{v_\parallel h_r}{A'_\varphi}\right), \end{aligned} \tag{3.120}$$

with the canonical momenta

$$p_\vartheta = m_\alpha v_\parallel h_\vartheta + \frac{e_\alpha}{c} A_\vartheta, \tag{3.121}$$

$$p_\varphi = m_\alpha v_\parallel h_\varphi + \frac{e_\alpha}{c} A_\varphi. \tag{3.122}$$

The last term in Eq. (3.120) is of second order in $\rho_\parallel = v_\parallel/\omega_c$ compared to the other terms and can be neglected. Since the correction term in Eq. (3.118) does not depend on φ, we can retain the exact expression for the original canonical momentum p_φ here. The important point of this approximate transformation is that the correction $\varphi - \bar{\varphi}$ is of first order in $\rho_\parallel h_r$. This means that in the thin orbit approximation, where we have neglected other terms of this order, this alternatively justifies just setting $\bar{\varphi} = \varphi$ and $\bar{\vartheta} = \vartheta$ in the derivation of action-angle coordinates and canonical frequencies, which confirms the more general procedure performed above.

Chapter 4

Resonant transport regimes

4.1 Basic kinetic theory

Particularly in the context of fusion plasmas, a large number of particles ($10^{19} - 10^{21}$ per m^3) interacting via long-range Coulomb forces and exposed to an externally imposed electromagnetic field has to be described. This means that Eq. (2.9) is of little practical use, as long as it is defined for such a high-dimensional system. The reduction to an effective low-dimensional equation is possible via the BBGKY hierarchy (named after Bogolyubov, Bom, Green, Kirkwood and Yvon), which is e.g. described in the books of and Nicholson (1983)[1].

For this purpose, velocity coordinates are usually employed instead of momenta. Neglecting three-particle interactions, a one-particle distribution function $\bar{f}(\boldsymbol{r}, \boldsymbol{v})$ defined for a particle subject to two-particle collisions with the remaining particles follows the plasma kinetic equation

$$\frac{\partial \bar{f}(\boldsymbol{r}, \boldsymbol{v}, t)}{\partial t} + \boldsymbol{v} \cdot \frac{\partial \bar{f}}{\partial \boldsymbol{r}} + \frac{e_\alpha}{m_\alpha} \left(\bar{\boldsymbol{E}} + \frac{1}{c} \boldsymbol{v} \times \bar{\boldsymbol{B}} \right) \cdot \frac{\partial \bar{f}}{\partial \boldsymbol{v}} = -n_0 \int \mathrm{d}^3 r_2 \mathrm{d}^3 v_2 \boldsymbol{a}_{12} \cdot \nabla_{\boldsymbol{v}} g_{12}(\boldsymbol{r}, \boldsymbol{r}_2, \boldsymbol{v}, \boldsymbol{v}_2, t) \,. \tag{4.1}$$

Here n_0 is the average mass density, $\boldsymbol{a}_{12}$ describes the accelerations due to interaction forces, and g_{12} is the two-particle correlation function. Except for the right hand side, this equation is formally similar to the Liouville equation (2.9) with an electromagnetic Hamiltonian. However, Eq. (4.1) is defined for positions $\boldsymbol{r}$ and velocities $\boldsymbol{v}$ of a single particle in 6-dimensional phase space, with the fields $\bar{\boldsymbol{E}}$ and $\bar{\boldsymbol{B}}$ containing only ensemble-averaged terms from a smoothed density function and external forces. Making use of the long-range Coulomb forces leading to small-angle

[1] The mentioned book also contains an instructive derivation of the Liouville equation based on individual particles represented by δ distribution terms inside f.

collisions and assuming g_{12} to decay on a much faster timescale than the one-particle distribution function $\bar{f}$ (Bogoliubov's hypothesis), the right-hand side of 4.1 can be modelled by a Fokker-Planck operator $\hat{C}$ acting on $\bar{f}$. Taking into account possibly different particle species a and b and omitting the bar in the notation of Eq. (4.1), we can write the plasma kinetic equation for the one-particle distribution function f_a for a species a as

$$\frac{\partial f_a}{\partial t} + \boldsymbol{v} \cdot \frac{\partial f_a}{\partial \boldsymbol{r}} + \frac{e_\alpha}{m_\alpha} \left(\boldsymbol{E} + \frac{1}{c} \boldsymbol{v} \times \boldsymbol{B} \right) \cdot \frac{\partial f_a}{\partial \boldsymbol{v}} = \hat{C}_a f_a, \tag{4.2}$$

where collision operator

$$\hat{C}_a f_a = \sum_b \hat{C}_{ab} f_a \tag{4.3}$$

includes collisions with all species b given by

$$\hat{C}_{ab} f_a = \frac{\partial}{\partial v^k} \left(\frac{\partial}{\partial v^l} \left(D^{ab}_{kl}(\boldsymbol{v}, f_b)\, f_a \right) - F^{ab}_k(\boldsymbol{v}, f_b)\, f_a \right) \equiv \hat{C}_{ab}[f_a, f_b]. \tag{4.4}$$

Despite various approximative assumptions, the collision operator (4.3) retains important physical features such as convergence towards a Maxwellian distribution as time approaches infinity as well as momentum and energy conservation. As an alternative to the derivation of this result without employing the BBGKY hierarchy, the book of Helander and Sigmar (2005) provides an instructive derivation based on more heuristic arguments of two-particle Coulomb collisions.

While formally of Fokker-Planck type, the complexity of the problem in Eq. (4.2) is now hidden inside the velocity-dependent drag coefficients F^{ab}_k and diffusion coefficients D^{ab}_{kl}, that are defined via integral operators acting on f_b written in terms of Rosenbluth or Trubnikov potentials (see e.g. the book of Helander and Sigmar (2005)). In the coefficients with $b = a$, f_a itself appears inside the integrals, which is even the case for a single-species model, so further measures are necessary for the analytical or numerical treatment of Eq. (4.2). For plasmas close to thermodynamic equilibrium $f_a \approx f_{a0} + f_{a1}$, with f_{a0} given by a Maxwellian for all species, in particular for neoclassical theory of toroidal plasma confinement (Hinton and Hazeltine (1976), Hirshman and Sigmar (1981)), the collision operator is often used in its linearised form

$$\hat{C}_{ab}[f_a, f_b] \approx \hat{C}_{ab}[f_{a0}, f_{b0}] + \hat{C}_{ab}[f_{a1}, f_{b0}] + \hat{C}_{ab}[f_{a0}, f_{b1}]\,. \tag{4.5}$$

The first term describes temperature equilibration which is usually neglected either by the assumption of already equal temperatures of different species or by the process happening on the slower transport timescale due to the smallness of the electron-ion mass ratio. The second term is a differential operator acting on f_{a1} describing the linear order approximation of f_a subject to a Maxwellian background

f_{b0}. The third term is an integral operator acting on f_{b1}, which is required, in particular, to retain the property of momentum and energy conservation.

For our purpose at the low collisionality limit, we are going to use a *linearised collision operator* on a single species plasma, given by

$$\hat{L}_C f_1 = \hat{C}_{ab}[f_1, f_0]\,. \tag{4.6}$$

Since it is of the form of a differential Fokker-Planck operator defined in Eq. (2.20), we can immediately use all the universal results obtained in chapter 2. To justify all approximations for the intended application on resonant transport regimes in the low-collisionality limit, some further investigations will be necessary, described in the subsequent sections.

4.2 Kinetic equation and conservation laws

In canonically conjugate variables, in particular for Cartesian coordinates and their respective momenta $(\boldsymbol{r}, \boldsymbol{p})$ or action-angle variables $(\boldsymbol{\theta}, \boldsymbol{J})$ of the unperturbed system, the plasma kinetic equation for the distribution function $f = f(t, \boldsymbol{r}, \boldsymbol{p}) = f(t, \boldsymbol{r}(\boldsymbol{\theta}, \boldsymbol{J}), \boldsymbol{p}(\boldsymbol{\theta}, \boldsymbol{J}))$ can be written employing the Poisson brackets (1.10),

$$\frac{\mathrm{d}f}{\mathrm{d}t} = \frac{\partial f}{\partial t} + \{f, H\} = \hat{L}_c f, \tag{4.7}$$

where $\hat{L}_c$ is the collision operator. With help of Eq. (4.7) we are going to formulate a flux-surface averaged conservation law for a quantity $a(\boldsymbol{r}, \boldsymbol{p})$ defined in phase space. We first define the reduced (Eulerian) quantity $A(t, \boldsymbol{r})$ by integration over momentum space,

$$A(t, \boldsymbol{r}) \equiv \int \mathrm{d}^3 p a\, f\,. \tag{4.8}$$

The time derivative of A is

$$\begin{aligned} \frac{\partial A}{\partial t} &= \int \mathrm{d}^3 p a\, \frac{\partial f}{\partial t} \\ &= \int \mathrm{d}^3 p a\, (\hat{L}_c f - \{f, H\})\,. \end{aligned} \tag{4.9}$$

The first term is a source term arising from collisions, which we denote by

$$s_A^{(c)} \equiv \int \mathrm{d}^3 p a \hat{L}_c f\,, \tag{4.10}$$

whereas the second term involving the Poisson brackets can be written as

$$\begin{aligned}\int \mathrm{d}^3p\, a\{f,H\} &= \int \mathrm{d}^3p a \left(\frac{\partial}{\partial r^i}\left(f\frac{\partial H}{\partial p_i}\right) - \frac{\partial}{\partial p_i}\left(f\frac{\partial H}{\partial r^i}\right)\right)\\ &= \int \mathrm{d}^3p \left(\frac{\partial}{\partial r^i}\left(af\frac{\partial H}{\partial p_i}\right) - \frac{\partial}{\partial p_i}\left(af\frac{\partial H}{\partial r^i}\right)\right)\\ &- \int \mathrm{d}^3p \left(f\frac{\partial a}{\partial r^i}\frac{\partial H}{\partial p_i} - f\frac{\partial a}{\partial p_i}\frac{\partial H}{\partial r^i}\right)\\ &= \frac{\partial}{\partial r^i}\int \mathrm{d}^3p\, af\frac{\partial H}{\partial p_i} - \int \mathrm{d}^3p\,\{a,H\}f, \end{aligned} \tag{4.11}$$

where we have used the condition of f vanishing sufficiently fast at $|\boldsymbol{p}| \to \infty$ and swapped integration over $\boldsymbol{p}$ and the derivative over $\boldsymbol{r}$.

Since $\partial H/\partial p_i = \{r^i, H\}$ (1.14), the first term in (4.11) can be interpreted as the divergence of a flux density defined by

$$\begin{aligned}\boldsymbol{\Gamma}_A(t,\boldsymbol{r}) &\equiv \int \mathrm{d}^3p \boldsymbol{v}\, a\, f\\ &= \int \mathrm{d}^3p \{\boldsymbol{r}, H\} a\, f\,. \end{aligned} \tag{4.12}$$

The remaining term is identified with a collision-independent source

$$s_A \equiv \int \mathrm{d}^3p\,\{a,H\}f\,. \tag{4.13}$$

Finally, we can write down the local conservation law

$$\frac{\partial A}{\partial t} + \nabla\cdot\boldsymbol{\Gamma}_A = s_A + s_A^{(c)}. \tag{4.14}$$

If a is not affected by collisions, which is particularly the case for the toroidal momentum p_φ in a single-species model, the collisional source term $s_A^{(c)}$ vanishes.

For the formulation of flux surfaced averaged conservation laws we use curvilinear magnetic flux coordinates (see D'haeseleer et al. (1991)) $\boldsymbol{x} = (r,\vartheta,\varphi)$ with Jacobian $\sqrt{g}$ and define the flux average $\langle a(\boldsymbol{r})\rangle$ of a quantity $a(\boldsymbol{r})$ as the limit of a volume integral with vanishing radial width around a flux surface,

$$\langle a(\boldsymbol{r})\rangle = \frac{1}{S}\int_{-\pi}^{\pi}\mathrm{d}\vartheta\int_{-\pi}^{\pi}\mathrm{d}\varphi\sqrt{g}a(\boldsymbol{r}). \tag{4.15}$$

The radial variable r is chosen as the effective radius r_{eff} (see Nemov et al., 1999) fixed by the condition

$$\langle|\nabla r_{\mathrm{eff}}|\rangle = 1, \tag{4.16}$$

so the normalisation constant S is equal to the geometrical area of a flux surface given by

$$\begin{aligned}\int_{-\pi}^{\pi}\mathrm{d}\vartheta\int_{-\pi}^{\pi}\mathrm{d}\varphi\sqrt{g}\frac{\partial\boldsymbol{r}}{\partial\vartheta}\times\frac{\partial\boldsymbol{r}}{\partial\varphi}\cdot\frac{\nabla r}{|\nabla r|} &= \int_{-\pi}^{\pi}\mathrm{d}\vartheta\int_{-\pi}^{\pi}\mathrm{d}\varphi\sqrt{g}\overbrace{\boldsymbol{E}_\vartheta\times\boldsymbol{E}_\varphi}^{\boldsymbol{E}^r}\cdot\frac{\boldsymbol{E}^r}{\sqrt{g^{rr}}}\\ &= \int_{-\pi}^{\pi}\mathrm{d}\vartheta\int_{-\pi}^{\pi}\mathrm{d}\varphi\sqrt{g}|\nabla r|\\ &= \langle|\nabla r|\rangle\int_{-\pi}^{\pi}\mathrm{d}\vartheta\int_{-\pi}^{\pi}\mathrm{d}\varphi\sqrt{g}=S. \end{aligned}\tag{4.17}$$

This definition of r will be assumed in the following derivation.

From the definition of the Poisson brackets (1.14), we notice that

$$\{\boldsymbol{r},H\}\cdot\nabla x^k=\frac{\partial x^k}{\partial r^k}\cdot\frac{\partial H}{\partial p_k}=\{x^k,H\}.\tag{4.18}$$

This can be used to write the flux-averaged radial component of $\boldsymbol{\Gamma}_A$ as

$$\begin{aligned}\langle\Gamma_A^r\rangle &= \langle\boldsymbol{\Gamma}_A\cdot\nabla r\rangle\\ &= \left\langle\int\mathrm{d}^3p\,a\,f\,\{\boldsymbol{r},H\}\cdot\nabla r\right\rangle\\ &= \left\langle\int\mathrm{d}^3p\{r,H\}\,a\,f\right\rangle. \end{aligned}\tag{4.19}$$

The flux surface average of the divergence of $\boldsymbol{\Gamma}_A$ can be expressed by

$$\begin{aligned}\langle\nabla\cdot\boldsymbol{\Gamma}_A\rangle &= \left\langle\frac{1}{\sqrt{g}}\frac{\partial}{\partial x^k}(\sqrt{g}\,\Gamma_A^k)\right\rangle\\ &= \frac{1}{S}\int_{-\pi}^{\pi}\mathrm{d}\vartheta\int_{-\pi}^{\pi}\mathrm{d}\varphi\frac{\partial}{\partial x^k}(\sqrt{g}\,\Gamma_A^k)\\ &= \frac{1}{S}\frac{\partial}{\partial r}\int_{-\pi}^{\pi}\mathrm{d}\vartheta\int_{-\pi}^{\pi}\mathrm{d}\varphi(\sqrt{g}\,\Gamma_A^r)\\ &= \frac{1}{S}\frac{\partial}{\partial r}S\,\langle\Gamma_A^r\rangle. \end{aligned}\tag{4.20}$$

Due to the periodicity of the integral, only a radial derivative remained in this expression. Finally, we obtain the flux-surface averaged conservation law

$$\frac{\partial}{\partial t}\langle A\rangle+\frac{1}{S}\frac{\partial}{\partial r}S\,\langle\Gamma_A^r\rangle=\langle s_A\rangle+\left\langle s_A^{(c)}\right\rangle.\tag{4.21}$$

In this one-dimensional law, the radial derivative describes the divergence where the flux surface area S has taken the role of the Jacobian, which could be anticipated from its definition as the flux-averaged Jacobian in Eq. (4.17).

We can also write integrals over momentum of a local quantities as defined in Eq. (4.8) by an integral over action-angle variables parametrising phase space. The

correct integration submanifold at constant spatial location $\boldsymbol{r}$ is chosen by a Dirac delta fixing it to the orbital position $\boldsymbol{r}_c(\boldsymbol{\theta}, \boldsymbol{J})$ depending on actions $\boldsymbol{J}$ and angles $\boldsymbol{\theta}$,

$$A(t, \boldsymbol{r}) = \int \mathrm{d}^3 p \, a \, f \tag{4.22}$$

$$= \int \mathrm{d}^3\theta \int \mathrm{d}^3 J \, \delta(\boldsymbol{r}_c(\boldsymbol{\theta}, \boldsymbol{J}) - \boldsymbol{r}) a \, f \, . \tag{4.23}$$

The flux surface average of A is then given by

$$\begin{aligned} \langle A \rangle &= \left\langle \int \mathrm{d}^3\theta \int \mathrm{d}^3 J \delta(\boldsymbol{r}_c(\boldsymbol{\theta}, \boldsymbol{J}) - \boldsymbol{r}) a \, f \right\rangle \\ &= \left\langle \frac{1}{\sqrt{g}} \int \mathrm{d}^3\theta \int \mathrm{d}^3 J \delta(\boldsymbol{r}_c(\boldsymbol{\theta}, \boldsymbol{J}) - \boldsymbol{r}) a \, f \right\rangle \\ &= \frac{1}{S} \int \mathrm{d}^3\theta \int \mathrm{d}^3 J \, \delta(r_c(\boldsymbol{\theta}, \boldsymbol{J}) - r) a \, f \, , \end{aligned} \tag{4.24}$$

where the δ has been transformed to coordinates $\boldsymbol{x}$ and resolved for the two angular variables ϑ and φ by the flux surface integral in (4.15). The particle radial position has been denoted by $r_c = r(\boldsymbol{r}_c(\boldsymbol{\theta}, \boldsymbol{J})) = r_c(\boldsymbol{\theta}, \boldsymbol{J})$. Similarly, by taking averages of expressions (4.10) and (4.13) for the source terms, we obtain

$$\left\langle s_A^{(c)} \right\rangle = \frac{1}{S} \int \mathrm{d}^3\theta \int \mathrm{d}^3 J \, \delta(r_c(\boldsymbol{\theta}, \boldsymbol{J}) - r) a \hat{L}_c f \, , \tag{4.25}$$

$$\langle s_A \rangle = \frac{1}{S} \int \mathrm{d}^3\theta \int \mathrm{d}^3 J \, \delta(r_c(\boldsymbol{\theta}, \boldsymbol{J}) - r) \{a, H\} f \, . \tag{4.26}$$

4.3 Toroidal torque density and flux-force relation

In particular by setting $a = 1$ in (4.21), we obtain a vanishing source term $\langle s_A \rangle = 0$ and the radial particle flux

$$\Gamma_n = \frac{1}{S} \int \mathrm{d}^3\theta \int \mathrm{d}^3 J \, \delta(r_c(\boldsymbol{\theta}, \boldsymbol{J}) - r) \, \{r, H\} \, f \, , \tag{4.27}$$

where we have dropped the index r by using the notation $\Gamma_n \equiv \langle \Gamma_n^r \rangle$.

For the toroidal momentum conservation law we choose $a = p_\varphi$ as defined in Eq. (3.12). In this case, the source term $\langle s_A \rangle$ in Eq. (4.15) is the torque density

$$\begin{aligned} T_\varphi &= \left\langle \int \mathrm{d}^3 p \, \{p_\varphi, H\} f \right\rangle \\ &= -\left\langle \int \mathrm{d}^3 p \, \frac{\partial H}{\partial \varphi} f \right\rangle \\ &= -\frac{1}{S} \int \mathrm{d}^3\theta \int \mathrm{d}^3 J \, \delta(r_c(\boldsymbol{\theta}, \boldsymbol{J}) - r) \frac{\partial H}{\partial \varphi_c} f. \end{aligned} \tag{4.28}$$

From this equation, it is immediately clear that radial torque appears only if there are non-axisymmetric contributions to the Hamiltonian H. In contrast to this, the radial particle flux in Eq. (4.27) does not necessarily vanish in the axisymmetric case, where it is given by

$$\Gamma_n^0 = \frac{1}{S}\int \mathrm{d}^3\theta \int \mathrm{d}^3 J\, \delta(r_c(\boldsymbol{\theta},\boldsymbol{J}) - r)\, \frac{\partial r_c(\boldsymbol{\theta},\boldsymbol{J})}{\partial \boldsymbol{\theta}} \cdot \boldsymbol{\Omega}\, f_0. \tag{4.29}$$

To the lowest order in orbit width with $r_c(\boldsymbol{\theta},\boldsymbol{J}) = r_\varphi(p_\varphi)$ defined in Eq. (3.30), it is possible to immediately resolve the δ via an integration over p_φ as

$$\begin{aligned}\int \mathrm{d}p_\varphi\, \delta(r_\varphi(p_\varphi) - r)\, g(p_\varphi, \dots) &= \int \mathrm{d}r_\varphi \left|\frac{\mathrm{d}p_\varphi(r_\varphi)}{\mathrm{d}r_\varphi}\right| \delta(r_\varphi - r)\, g(p_\varphi(r_\varphi), \dots) \\ &= \left|\frac{\mathrm{d}p_\varphi(r_\varphi)}{\mathrm{d}r_\varphi}\right| g(p_\varphi(r_\varphi), \dots)\,|_{r_\varphi = r}. \end{aligned} \tag{4.30}$$

In this approximation, the axisymmetric flux in Eq. 4.29 vanishes and the total radial flux is determined by the perturbation with

$$\begin{aligned}\Gamma_n &= -\frac{1}{S}\left|\frac{\mathrm{d}p_\varphi}{\mathrm{d}r_\varphi}\right| \int \mathrm{d}^3\theta \int \mathrm{d}J_\perp \int \mathrm{d}J_\vartheta\, \frac{\partial r_\varphi}{\partial(J_\perp, J_\vartheta, p_\varphi)} \cdot \frac{\partial H}{\partial \boldsymbol{\theta}}\, f \\ &= -\frac{1}{S}\,\mathrm{sign}\left(\frac{\mathrm{d}p_\varphi}{\mathrm{d}r_\varphi}\right) \int \mathrm{d}^3\theta \int \mathrm{d}J_\perp \int \mathrm{d}J_\vartheta\, \frac{\partial H}{\partial \varphi_c}\, f. \end{aligned} \tag{4.31}$$

The torque density is proportional to the radial particle flux with

$$\begin{aligned} T_\varphi &= -\frac{1}{S}\left|\frac{\mathrm{d}p_\varphi}{\mathrm{d}r_\varphi}\right| \int \mathrm{d}^3\theta \int \mathrm{d}J_\perp \int \mathrm{d}J_\vartheta\, \frac{\partial H}{\partial \varphi_c} f \\ &= \frac{\mathrm{d}p_\varphi}{\mathrm{d}r_\varphi}\Gamma_n. \end{aligned} \tag{4.32}$$

This is the flux-force relation introduced by Hirshman (1978) in the context of axisymmetric plasmas and described in Shaing and Callen (1983) for non-axisymmetric perturbations. The sign of $\mathrm{d}p_\varphi/\mathrm{d}r_\varphi$ is dependent on the sign of the charge in Eq. (4.31), which means that the transport produced by the non-axisymmetric perturbation separates charges, it is non-ambipolar.

4.4 Hamiltonian perturbation

Let us consider a perturbed Hamiltonian of the form $H = H_0 + \tilde{H}$. Actions $\boldsymbol{J}$ and angles $\boldsymbol{\theta}$ shall be defined for the unperturbed axisymmetric case with H_0 which then depends only on actions $\boldsymbol{J}$. The Hamiltonian perturbation $\tilde{H}$ and the perturbation of the distribution function, shall be time-harmonic with frequency ω (which can also be zero) and written as a Fourier series in the canonical angles $\boldsymbol{\theta}$ without

constant part (it can be absorbed in H_0 to define a new unperturbed axisymmetric equilibrium),

$$H(t, \boldsymbol{J}, \boldsymbol{\theta}) = H_0(t, \boldsymbol{J}) + \mathrm{Re} \sum_{\boldsymbol{m} \neq \boldsymbol{0}} \tilde{H}_{\boldsymbol{m}}(t, \boldsymbol{\theta}, \boldsymbol{J}) \,, \tag{4.33}$$

where

$$\tilde{H}_{\boldsymbol{m}} = H_{\boldsymbol{m}}(\boldsymbol{J})\, e^{\mathrm{i}(\mathbf{m}\cdot\boldsymbol{\theta} - \omega t)} \,. \tag{4.34}$$

In the kinetic equation for $f = f(t, \boldsymbol{\theta}, \boldsymbol{J})$ in the perturbed system,

$$\frac{\mathrm{d}f}{\mathrm{d}t} = \frac{\partial f}{\partial t} + \{f, H\} = \hat{L}_c f \,, \tag{4.35}$$

we split f into an averaged part $\bar{f}$ and an oscillating part $\tilde{f}$,

$$f = \bar{f} + \tilde{f} \,, \tag{4.36}$$

$$\bar{f} \equiv \langle f \rangle_{t,\boldsymbol{\theta}} = \frac{1}{(2\pi)^3 t_0} \int_0^{t_0} \mathrm{d}t \int_0^{2\pi} \mathrm{d}^3\theta \, f(t, \boldsymbol{J}, \boldsymbol{\theta}) \,, \tag{4.37}$$

$$\left\langle \tilde{f} \right\rangle_{t,\boldsymbol{\theta}} = 0 \,, \tag{4.38}$$

where $\langle\rangle_{t,\boldsymbol{\theta}}$ denotes the average over canonical angles and over a sufficiently long timescale t_0 if $\tilde{H}$ depends on time explicitly. The latter average is not required for a time-independent perturbation. At this point we make the assumption that $\hat{L}_c = \hat{L}_c(\boldsymbol{J})$ depends only on actions and not on angles. The operator $\hat{L}_c$ acts in velocity space $\boldsymbol{v}$ independently from position $\boldsymbol{x}$. However, this distinction breaks down in action-angle coordinates, where velocities are functions of both, actions and angles. Thus we expect the assumption to be justified if the collision frequency ν_c is of lower order than all canonical frequencies. A quantitative description for the collisionality dependency will be offered in section (4.9) based on the universal kinetic equation of resonant regimes.

In our specific case this means the following: since we are working on scales where the gyrophase $\theta^1 = \phi$ has been averaged out from the very beginning, there are no dependencies on it. Furthermore our problem is nearly axisymmetric, so the dependency on $\theta^3 = \varphi_c$ will enter only at higher order. However, $\theta^2 = \vartheta_c = \sigma\tau/\tau_b$ which describes the phase of the bounce motion affects collisions. Especially orbits near the trapped-passing boundary will spend significantly more time near the turning points of marginally trapped orbits with $v_\parallel(\vartheta_c, \boldsymbol{J}) = 0$, where collisions are most likely to occur in the particle picture. This means that the limiting timescale is the bounce frequency ω_b, which should be much larger by module than the effective collision frequency ν_c. In tokamaks, this limits the range of applicability of this approach to the low-collisional banana regime. As will become clear later, there is

also a lower limit on ν_c for the applicability of quasilinear theory – a transition to a non-linear regime analogous to the one from banana plateau to banana regime will occur below this collisionality. At this point, collisionality will enter the results again and special care needs to be taken regarding $\hat{L}_c$ and its averaging.

To continue the construction of the perturbation theory, we split Eq. 4.35 written as

$$\frac{\mathrm{d}f}{\mathrm{d}t} = \frac{\partial \bar{f}}{\partial t} + \frac{\partial \tilde{f}}{\partial t} + \{\bar{f}, H_0\} + \{\tilde{f}, H_0\} + \{\bar{f}, \tilde{H}\} + \{\tilde{f}, \tilde{H}\} = \hat{L}_c \bar{f} + \hat{L}_c \tilde{f}\,, \tag{4.39}$$

into an averaged part

$$\frac{\partial \bar{f}}{\partial t} + \left\langle \{\tilde{f}, \tilde{H}\} \right\rangle_{t,\boldsymbol{\theta}} = \hat{L}_c \bar{f}\,, \tag{4.40}$$

and an oscillating part with zero $(t, \boldsymbol{\theta})$ average,

$$\frac{\partial \tilde{f}}{\partial t} + \{\bar{f}, \tilde{H}\} + \{\tilde{f}, H_0\} + \left(\{\tilde{f}, \tilde{H}\} - \left\langle \{\tilde{f}, \tilde{H}\} \right\rangle_{t,\boldsymbol{\theta}} \right) = \hat{L}_c \tilde{f}\,. \tag{4.41}$$

Here, the Poisson bracket $\{\bar{f}(\boldsymbol{J}), H_0(\boldsymbol{J})\}$ of two angle-independent quantities is identically zero and oscillating terms average out to zero.

4.5 Quasilinear approximation

Let us now construct a perturbation expansion from Eqs. (4.40) and (4.41), which are still exact up to the assumption of a canonically averaged $\hat{L}_c$. The order of the perturbation is set to be the amplitude of the Hamiltonian perturbation $\tilde{H}/H_0$ from (4.33). We start with the first-order equation constructed from Eq. (4.41),

$$\frac{\partial f_1}{\partial t} + \{f_0, \tilde{H}\} + \{f_1, H_0\} = \hat{L}_c f_1\,, \tag{4.42}$$

and collect the remaining terms in

$$\frac{\partial}{\partial t}(\tilde{f} - f_1) + \{\bar{f} - f_0, \tilde{H}\} + \{\tilde{f} - f_1, H_0\} + \left(\{\tilde{f}, \tilde{H}\} - \left\langle \{\tilde{f}, \tilde{H}\} \right\rangle_{t,\boldsymbol{\theta}} \right) = \hat{L}_c(\tilde{f} - f_1)\,. \tag{4.43}$$

The zeroth order term f_0 shall be sufficiently close to $\bar{f}$ without dependency on angles $\boldsymbol{\theta}$ and will be specified later. In terms of action-angle variables with canonical frequencies $\boldsymbol{\Omega}$, Eq. (4.42) becomes

$$\frac{\partial f_1}{\partial t} - \frac{\partial f_0}{\partial \boldsymbol{J}} \frac{\partial H_1}{\partial \boldsymbol{\theta}} + \frac{\partial f_1}{\partial \boldsymbol{\theta}} \cdot \boldsymbol{\Omega} = \hat{L}_c f_1\,. \tag{4.44}$$

Expanding f_1 in Fourier harmonics in $\boldsymbol{\theta}$ as in Eqs. (4.33-4.34), we obtain an equation for each individual set of harmonic indices $\boldsymbol{m}$,

$$-\mathrm{i}\omega f_{\boldsymbol{m}} - \mathrm{i}\boldsymbol{m}\cdot\frac{\partial f_0}{\partial \boldsymbol{J}} H_{\boldsymbol{m}} + \mathrm{i}\boldsymbol{m}\cdot\boldsymbol{\Omega} f_{\boldsymbol{m}} = \hat{L}_c f_{\boldsymbol{m}}\,. \tag{4.45}$$

At the low collisionality limit $\hat{L}_c f_{\boldsymbol{m}} \to 0$, we use a Krook term $\hat{L}_c f_{\boldsymbol{m}} = -\nu f_{\boldsymbol{m}}$ with infinitesimal scalar $\nu > 0$. This approximation is justified from the results of section 2.3, where this approximation resulted in similar perturbed distribution functions, as long as collisionality is not too low. A more detailed derivation based on the exact solution will be performed later. The solution for $f_{\boldsymbol{m}}$ with a Krook term follows as

$$f_{\boldsymbol{m}} = \lim_{\nu\to 0^+} \frac{H_{\boldsymbol{m}}}{\boldsymbol{m}\cdot\boldsymbol{\Omega} - \omega - \mathrm{i}\nu}\boldsymbol{m}\cdot\frac{\partial f_0}{\partial \boldsymbol{J}}\,. \tag{4.46}$$

At the resonance condition

$$\boldsymbol{m}\cdot\boldsymbol{\Omega} - \omega = 0\,, \tag{4.47}$$

the expression for $f_{\boldsymbol{m}}$ will diverge if ν is set exactly to zero. The term $\mathrm{i}\nu$ retains causality, i.e. the direction of time, and approaches the resonance from the correct direction in the complex plane, as in the derivation of Landau damping. Still, we have to keep this localized divergence in action space in mind when constructing the zeroth order f_0.

In Eq. (4.40), we assume $f_0 - \bar{f}$ and the collision term of second or higher order. Retaining the locally divergent linear order term in the averaged Poisson bracket term inside the zeroth order time evolution leads to the quasilinear time evolution equation

$$\frac{\partial f_0}{\partial t} = -\left\langle \{f_1, \tilde{H}\}\right\rangle_{t,\boldsymbol{\theta}}\,, \tag{4.48}$$

and a second-order equation for the averaged part

$$\frac{\partial}{\partial t}(\bar{f} - f_0) + \left\langle \{\tilde{f} - f_1, \tilde{H}\}\right\rangle_{t,\boldsymbol{\theta}} = \hat{L}_c \bar{f}\,. \tag{4.49}$$

The source term $\left\langle \{f_1, \tilde{H}\}\right\rangle_{t,\boldsymbol{\theta}}$ obtained from the linear order solution causes f_0 to change in time even if collisions have no direct influence on it. Namely, Eq. (4.48)

is evaluated to

$$\begin{aligned}\frac{\partial f_0}{\partial t} &= -\left\langle \{f_1, \tilde{H}\}\right\rangle_{t,\boldsymbol{\theta}} = \left\langle \frac{\partial \tilde{H}}{\partial \boldsymbol{\theta}} \cdot \frac{\partial f_1}{\partial \boldsymbol{J}} - \frac{\partial \tilde{H}}{\partial \boldsymbol{J}} \cdot \frac{\partial f_1}{\partial \boldsymbol{\theta}} \right\rangle_{t,\boldsymbol{\theta}} \\ &= \sum_{\boldsymbol{m}} \left\langle \mathrm{Re}(\mathrm{i}\tilde{H})\boldsymbol{m} \cdot \frac{\partial f_1}{\partial \boldsymbol{J}} - \boldsymbol{m} \cdot \frac{\partial \tilde{H}}{\partial \boldsymbol{J}} \mathrm{Re}(\mathrm{i}f_1) \right\rangle_{t,\boldsymbol{\theta}} \\ &= \sum_{\boldsymbol{m}} \left\langle \frac{1}{2}\mathrm{Re}\left(-\mathrm{i}\tilde{H}^\star_{\boldsymbol{m}} \boldsymbol{m} \cdot \frac{\partial \tilde{f}_{\boldsymbol{m}}}{\partial \boldsymbol{J}} + \mathrm{i}\tilde{f}_{\boldsymbol{m}} \boldsymbol{m} \cdot \frac{\partial \tilde{H}^\star_{\boldsymbol{m}}}{\partial \boldsymbol{J}} \right) \right\rangle_{t,\boldsymbol{\theta}} \\ &= \frac{1}{2}\mathrm{Re}\sum_{\boldsymbol{m}} \{\tilde{H}^\star_{\boldsymbol{m}}, \tilde{f}_{\boldsymbol{m}}\} = -\frac{1}{2}\mathrm{Re}\sum_{\boldsymbol{m}} \mathrm{i}\boldsymbol{m} \cdot \frac{\partial}{\partial \boldsymbol{J}} (H^\star_{\boldsymbol{m}} f_{\boldsymbol{m}}) \,. \end{aligned} \tag{4.50}$$

Inserting the result from Eq. (4.48) yields

$$\begin{aligned}\frac{\partial f_0}{\partial t} &= -\frac{1}{2}\mathrm{Re}\sum_{\boldsymbol{m}} \mathrm{i}\boldsymbol{m} \cdot \frac{\partial}{\partial \boldsymbol{J}} \left(H^\star_{\boldsymbol{m}} \lim_{\nu\to 0^+} \frac{H_{\boldsymbol{m}}}{\boldsymbol{m}\cdot\boldsymbol{\Omega} - \omega - \mathrm{i}\nu} \boldsymbol{m} \cdot \frac{\partial f_0}{\partial \boldsymbol{J}} \right) \\ &= \frac{1}{2}\sum_{\boldsymbol{m}} \boldsymbol{m} \cdot \frac{\partial}{\partial \boldsymbol{J}} \mathrm{Im} \lim_{\nu\to 0^+} \frac{|H_{\boldsymbol{m}}|^2}{\boldsymbol{m}\cdot\boldsymbol{\Omega} - \omega - \mathrm{i}\nu} \boldsymbol{m} \cdot \frac{\partial f_0}{\partial \boldsymbol{J}} \,. \end{aligned} \tag{4.51}$$

Using the relation

$$\mathrm{Im}\frac{1}{x \pm \mathrm{oi}} = \mp \pi \delta(x) \,, \tag{4.52}$$

for the δ distribution, the solution for the time evolution of f_0 follows as

$$\frac{\partial f_0}{\partial t} = \sum_{\boldsymbol{m}} \boldsymbol{m} \cdot \frac{\partial}{\partial \boldsymbol{J}} \cdot Q_{\boldsymbol{m}} \,, \tag{4.53}$$

with the quasilinear resonant term

$$Q_{\boldsymbol{m}} = \frac{\pi}{2} |H_{\boldsymbol{m}}|^2 \delta(\boldsymbol{m}\cdot\boldsymbol{\Omega} - \omega) \boldsymbol{m} \cdot \frac{\partial f_0}{\partial \boldsymbol{J}} \,. \tag{4.54}$$

We have thus reached the main result of this section in Eq. (4.53) and (4.54), where resonant diffusion occurs in action space around $\boldsymbol{m}\cdot\boldsymbol{\Omega} - \omega$ for f_0, which should remain close to the averaged $\bar{f}$.

In order to construct a higher orders perturbation theory, one would consider the sum of the second and higher order Eqs. (4.43) and (4.49) given by

$$\frac{\partial}{\partial t}(f - f_0 - f_1) + \{f - f_0 - f_1, H\} + \left(\{f_1, \tilde{H}\} - \left\langle \{f_1, \tilde{H}\} \right\rangle_{t,\boldsymbol{\theta}} \right) = \hat{L}_c (f - f_1) \,, \tag{4.55}$$

where the extraction of Eq. (4.49) is possible by averaging.

4.6 Non-axisymmetric magnetic perturbation

For the intended application of NTV torque, we will introduce a non-axisymmetric quasistatic magnetic perturbation with $\omega = 0$ to the originally axisymmetric field. We take into account only the magnetically non-resonant part of the perturbation field, that does not change topology. In Boozer magnetic coordinates (see e.g. the book of D'haeseleer et al. (1991)) such a perturbation can be fully described by a change of the magnetic module $B = |\boldsymbol{B}|$ (see e.g. (Kasilov et al., 2014)). In addition, Boozer coordinates have the specific property that covariant components B_ϑ and B_φ are constant on each flux surface.

For the computation of the perturbation amplitude it is necessary to evaluate this magnetic field modulus on the slightly distorted flux surfaces of the perturbed equilibrium, which has been pointed out by Boozer (2006). We construct our perturbation theory with orbits and canonical frequencies left unchanged from the axisymmetric equilibrium but formally on those distorted flux surfaces. The magnetic perturbation enters the guiding-centre Hamiltonian (3.7) via the parallel velocity $v_\parallel$ and the gyrofrequency ω_c. The former is defined implicitly via Eqs. (3.11-3.12) together with radius r,

$$p_\vartheta = m_\alpha v_\parallel \frac{B_\vartheta(r)}{B(r,\vartheta,\varphi)} + \frac{e_\alpha}{c} A_\vartheta(r), \tag{4.56}$$

$$p_\varphi = m_\alpha v_\parallel \frac{B_\vartheta(r)}{B(r,\vartheta,\varphi)} + \frac{e_\alpha}{c} A_\varphi(r). \tag{4.57}$$

Expanding up to first order via $B = B_0 + B_1$ and $v_\parallel = v_{\parallel 0} + v_{\parallel 1}$ yields

$$p_\vartheta - \frac{e_\alpha}{c} A_\vartheta - m_\alpha v_{\parallel 0} \frac{B_\vartheta}{B_0} = -m_\alpha v_{\parallel 0} \frac{B_1}{B_0} \frac{B_\vartheta}{B_0} + m_\alpha v_{\parallel 1} \frac{B_\vartheta}{B_0} + \mathcal{O}((B_1/B_0)^2), \tag{4.58}$$

with a similar equation for p_φ. To balance the left-hand side, we require

$$v_{\parallel 1} = v_{\parallel 0} \frac{B_1(r,\varphi,\vartheta)}{B_0(r,\vartheta)}. \tag{4.59}$$

Up to linear order in the perturbation field, our Hamiltonian is thus given by $H = H_0 + H_1 + \mathcal{O}((B_1/B_0)^2)$, with

$$\begin{aligned} H_0 &= \frac{m_\alpha v_{\parallel 0}^2}{2} + J_\perp \omega_{c0}, \\ H_1 &= \left(J_\perp \omega_{c0} + m_\alpha v_{\parallel 0}^2 \right) \frac{B_1}{B_0}. \end{aligned} \tag{4.60}$$

It can be shown that in Hamada coordinates a similar choice is possible setting $v_{\parallel 1} = v_{\parallel 0} B_0/B_1$ to the inverse value.

With the non-axisymmetric magnetic perturbation given as a series in the toroidal angle

$$B_1(\vartheta,\varphi) = \sum_n B_n(\vartheta) e^{in\varphi}, \tag{4.61}$$

Fourier modes of H_1 in canonical $\boldsymbol{\theta}$ follow via bounce averages along unperturbed orbits from Eq. (3.116),

$$H_{\boldsymbol{m}} = \left\langle \left(\frac{e_\alpha}{m_\alpha c} J_\perp B_0(\vartheta) + m_\alpha v_{\parallel 0}^2 \right) \frac{B_n(\vartheta)}{B_0(\vartheta)} e^{inq\vartheta - i(m_2 + nq\delta_{\mathrm{tp}})\omega_b \tau} \right\rangle_b , \tag{4.62}$$

where $\boldsymbol{m} = (0, m_2, n)$ and $\delta_{\mathrm{tp}} = 0$ for trapped orbits and $\delta_{\mathrm{tp}} = 1$ for passing orbits. Resonances $\boldsymbol{m} \cdot \boldsymbol{\Omega} = m_2\omega_b + n\Omega^\varphi = 0$ according to Eq. (4.47) will occur for

$$(m_2 + nq\delta_{\mathrm{tp}})\omega_b + n\left(\Omega_{tE} + \langle \Omega_{tB} \rangle_b\right) = 0, \tag{4.63}$$

where $\Omega_{tE} = \langle \Omega_{tE} \rangle_b$ due to the approximation of a constant electric potential on a flux surface and with negative value of ω_b for counter-passing particles. The resonance with $m_2 = 0$ for trapped particles is the superbanana resonance

$$\Omega_{tE} + \langle \Omega_{tB} \rangle_b = 0, \tag{4.64}$$

whereas for passing particles, $m_2 = 0$ corresponds to the transit resonance

$$q\omega_b + \Omega_{tE} + \langle \Omega_{tB} \rangle_b = 0, \tag{4.65}$$

which is the only remaining resonance in the inifinite aspect ratio limit, where it is reduced to a Cherenkov (TTMP) resonance. We need not consider the case $n = 0$, since the axisymmetric part of the perturbation can be absorbed in the unperturbed field. Mixed resonances with $m_2, n \neq 0$ require a combination of poloidal bounce/transit motion and toroidal precession drift. Shaing et al. (2009a) has labelled this case as the *bounce-transit and drift resonance* and we will also refer to it as drift-orbit resonance.

4.7 Quasilinear resonant transport regimes and NTV torque

With the Hamiltonian perturbation as a Fourier series in $\boldsymbol{\theta}$, we can evaluate

$$\frac{\partial H}{\partial \varphi_c} = \mathrm{Re}(in\tilde{H}_{\boldsymbol{m}}) = -n\mathrm{Im}(\tilde{H}_{\boldsymbol{m}}), \tag{4.66}$$

where we recall that partial derivatives of H and harmonic number n with respect to φ and φ_c are the same, since those angles differ only by a term independent from φ_c.

The toroidal torque density in Eq. 4.28, with r_c only dependent on canonical $\theta^2 = \vartheta_c$ for guiding-centre orbits in the axisymmetric equilibrium, becomes

$$T_\varphi = \frac{1}{S}\sum_{\boldsymbol{m}} n \int \mathrm{d}^3\theta \int \mathrm{d}^3 J\, \delta(r_c(\vartheta_c, \boldsymbol{J}) - r) \mathrm{Im}(\tilde{H}_{\boldsymbol{m}})\, \mathrm{Re}\,(\tilde{f}_{\boldsymbol{m}}). \tag{4.67}$$

We evaluate the term

$$\begin{aligned}
\int \mathrm{d}\varphi_c \mathrm{Im}(\tilde{H}_{\boldsymbol{m}})\, \mathrm{Re}\,(\tilde{f}_{\boldsymbol{m}}) &= \int \mathrm{d}\varphi_c \mathrm{Im}(\tilde{H}_{\boldsymbol{m}})\, \mathrm{Re}\,(\tilde{f}_{\boldsymbol{m}}) \\
&= \int \mathrm{d}\varphi_c \mathrm{Im}(H_{\boldsymbol{m}} e^{i\boldsymbol{m}\cdot\boldsymbol{\theta}})\, \mathrm{Re}\left(\lim_{\nu\to 0^+} \frac{H_{\boldsymbol{m}}}{\boldsymbol{m}\cdot\boldsymbol{\Omega} - \mathrm{i}\nu} e^{i\boldsymbol{m}\cdot\boldsymbol{\theta}}\right) \boldsymbol{m}\cdot\frac{\partial f_0}{\partial \boldsymbol{J}} \\
&= -\frac{1}{2}\int \mathrm{d}\varphi_c \lim_{\nu\to 0^+} \frac{|H_{\boldsymbol{m}}|^2\, \nu}{\boldsymbol{m}\cdot\boldsymbol{\Omega} + \nu^2} \boldsymbol{m}\cdot\frac{\partial f_0}{\partial \boldsymbol{J}} \\
&= -\frac{\pi}{2}\int \mathrm{d}\varphi_c\, |H_{\boldsymbol{m}}|^2\, \delta(\boldsymbol{m}\cdot\boldsymbol{\Omega})\, \boldsymbol{m}\cdot\frac{\partial f_0}{\partial \boldsymbol{J}}.
\end{aligned} \tag{4.68}$$

This expression is the integral over the quasilinear resonant term $Q_{\boldsymbol{m}}$ from Eq. 4.54 for $\omega = 0$, which we use in the notation for the torque density written in its final form for the quasilinear limit,

$$T_\varphi = -\frac{1}{S}\sum_{\boldsymbol{m}} n \int \mathrm{d}^3\theta \int \mathrm{d}^3 J\, \delta(r_c(\vartheta_c, \boldsymbol{J}) - r)\, Q_{\boldsymbol{m}}. \tag{4.69}$$

In the thin orbit approximation from Eq. (3.30), that allows trivial integration over all three angles, the torque becomes

$$T_\varphi = -\frac{(2\pi)^3}{S}\left|\frac{\mathrm{d}p_\varphi}{\mathrm{d}r_\varphi}\right| \sum_{\boldsymbol{m}} n \int \mathrm{d}J_\perp \int \mathrm{d}J_\vartheta\, Q_{\boldsymbol{m}} \tag{4.70}$$

$$= -\frac{|e_\alpha \psi'_{\mathrm{pol}}|}{c}\,\Gamma_n, \tag{4.71}$$

with the linked radial particle flux from the flux-force relation (4.32) given by

$$\Gamma_n = -\frac{(2\pi)^3}{S}\mathrm{sgn}\left(\frac{\mathrm{d}p_\varphi}{\mathrm{d}r_\varphi}\right) \sum_{\boldsymbol{m}} n \int \mathrm{d}J_\perp \int \mathrm{d}J_\vartheta\, Q_{\boldsymbol{m}}. \tag{4.72}$$

Switching to velocity space variables (v, η) defined in Eqs. (3.106-3.107), we compute the Jacobian

$$\begin{aligned}
\left|\frac{\partial(J_\perp, J_\vartheta)}{\partial(v,\eta)}\right| &= \left|\frac{\partial(J_\perp, H_0)}{\partial(v,\eta)}\right| \left|\frac{\partial(J_\perp, H_0)}{\partial(J_\perp, J_\vartheta)}\right|^{-1} \\
&= \frac{1}{\omega_b}\left|\frac{\partial(J_\perp, H_0)}{\partial(v,\eta)}\right| = \frac{1}{\omega_b}\begin{vmatrix} \frac{\eta m_\alpha^2 v c}{e} & \frac{m_\alpha^2 v^2 c}{2e_\alpha} \\ mv & 0 \end{vmatrix} \\
&= \frac{m_\alpha^3 v^3 c}{2e_\alpha \omega_b}.
\end{aligned} \tag{4.73}$$

After trivial integration over angles, the integral for the particle flux is given by

$$\Gamma = \frac{2\pi^2 m_\alpha^3 c}{e_\alpha S}\mathrm{sgn}\left(\frac{\mathrm{d}p_\varphi}{\mathrm{d}r_\varphi}\right)\sum_{\boldsymbol{m}} n\int_0^\infty \mathrm{d}v\, v^3 \int_0^{1/B_{\min}} \mathrm{d}\eta\, \tau_b Q_{\boldsymbol{m}} \tag{4.74}$$

in those variables.

4.8 Transport coefficients

One of the main differences of the action-angle approach to the standard local neoclassical ansatz is the inherent non-locality of quantities, which we limited by assuming a small orbit width with respect to unperturbed profiles. This means evaluating the unperturbed distribution function with profiles given in r_φ with

$$f_0(\boldsymbol{J}) = \frac{n_\alpha(r_\varphi(p_\varphi))}{(2\pi m_\alpha T(r_\varphi(p_\varphi)))^{3/2}}\exp\left(-\frac{H_0(J_\perp, p_\varphi, J_\vartheta) - e\Phi(r_\varphi(p_\varphi))}{T(r_\varphi(p_\varphi))}\right). \tag{4.75}$$

Consequently, the perpendicular and poloidal actions appear only in the Hamiltonian H_0, so separating the dependency of f_0 on H_0 we obtain

$$\frac{\partial f_0(\boldsymbol{J})}{\partial J_\perp} = \frac{\partial f_0(H_0, p_\varphi)}{\partial H_0}\frac{\partial H_0(\boldsymbol{J})}{\partial J_\perp} = -\frac{\Omega^\phi}{T} f_0, \tag{4.76}$$

$$\frac{\partial f_0(\boldsymbol{J})}{\partial J_\vartheta} = \frac{\partial f_0(H_0, p_\varphi)}{\partial H_0}\frac{\partial H_0(\boldsymbol{J})}{\partial J_\vartheta} = -\frac{\Omega^\vartheta}{T} f_0. \tag{4.77}$$

For the remaining terms, derivatives over p_φ can be replaced by radial derivatives,

$$\begin{aligned}\frac{\partial f_0(\boldsymbol{J})}{\partial p_\varphi} &= \frac{\partial f_0(H_0, p_\varphi)}{\partial p_\varphi} + \frac{\partial f_0(H_0, p_\varphi)}{\partial H_0}\frac{\partial H_0(J_\perp, J_\vartheta, p_\varphi)}{\partial p_\varphi} \\ &= \frac{\mathrm{d}r_\varphi}{\mathrm{d}p_\varphi}\frac{f_0(H_0, r)}{\partial r} - \frac{\Omega^\varphi}{T} f_0.\end{aligned} \tag{4.78}$$

The radial derivative of the local Maxwellian f_0,

$$\frac{f_0(H_0, r)}{\partial r} = (A_1 + A_2 u^2) f_0, \tag{4.79}$$

with normalised thermal velocity $u = v/v_{T\alpha}$ and $v_{T\alpha} = \sqrt{2T_\alpha/m_\alpha}$, is written in terms of thermodynamic forces

$$A_1 = \frac{1}{n_\alpha}\frac{\partial n_\alpha}{\partial r} + \frac{e_\alpha}{T_\alpha}\frac{\partial \Phi}{\partial r} - \frac{3}{2T_\alpha}\frac{\partial T_\alpha}{\partial r}, \tag{4.80}$$

$$A_2 = \frac{1}{T_\alpha}\frac{\partial T_\alpha}{\partial r}. \tag{4.81}$$

The expression containing the gradient of f_0 in action space appearing in the quasi-linear term $Q_{\boldsymbol{m}}$ becomes

$$\boldsymbol{m} \cdot \frac{\partial f_0}{\partial \boldsymbol{J}} = \frac{\mathrm{d}r_\varphi}{\mathrm{d}p_\varphi} \frac{f_0(H_0, r)}{\partial r} - \frac{\boldsymbol{m} \cdot \boldsymbol{\Omega}}{T} f_0. \tag{4.82}$$

For our quasi-static perturbation, the last term vanishes due to the resonance condition, and we can directly identify the expressions for radial transport coefficients D_{11} and D_{12} for the flux defined via

$$\Gamma = -n_\alpha (D_{11} A_1 + D_{12} A_2), \tag{4.83}$$

from Eq. (4.74). Eliminating integration over η in (4.74) by the Dirac δ of the resonance condition inside $Q_{\boldsymbol{m}}$ we obtain

$$\begin{aligned} D_{1k} = \mathrm{sgn}(\psi'_{\mathrm{pol}} e_\alpha) \frac{\pi^{3/2} n^2 c^2 v_{T\alpha}}{e_\alpha^2 S} \int_0^\infty u^3 e^{-u^2} \\ \times \sum_{m_2} \sum_{\mathrm{Res}} \tau_b |H_{\boldsymbol{m}}|^2 \left| m_2 \frac{\partial \omega_b}{\partial \eta} + n \frac{\partial \Omega^\varphi}{\partial \eta} \right|^{-1}_{\eta = \eta_{\mathrm{res}}} w_k, \end{aligned} \tag{4.84}$$

where $w_1 = 1$ and $w_2 = u^2$.

Since we have directly derived the flux-force relation Eq. (4.32) in terms of radial particle flux in Eq. (4.27), this result for thin orbits does not depend on details of the collision operator, which we have chosen as a Krook operator here. In particular, momentum conservation should plays no role in resonant transport. For the super-banana plateau and bounce resonance regimes, only trapped particles contribute, so the reason is the cancellation of parallel momentum generated by the perturbation during a single bounce period. For transit-drift resonances of passing particles a different explanation is required: since the total energy H_0 is not changed by a quasi-static perturbation and resonances with the gyrophase play no role for bulk particles, the perpendicular invariant $J_\perp$ is conserved in addition. This makes a change in parallel velocity $v_\parallel(\boldsymbol{x}, H_0, J_\perp)$ and of bounce frequency $\omega_b(r_\varphi, H_0, J_\perp)$ proportional to the bounce-averaged parallel momentum of passing particles only possible through the spatial coordinates $\boldsymbol{x}$ of the guiding-centre, where r_φ represents the radius. For not too large radial electric fields the variation of the potential energy along the guiding centre orbit with finite radial width is small (of the order of Larmor radius) compared to the thermal energy. In this case of sub-sonic rotations (small toroidal Mach number $M_t \equiv R\Omega_{\mathrm{t}E}/v_T$ with major radius R and thermal velocity v_T), the contribution of the change in kinematic momentum to the overall change of the canonical momentum is small of the same order. Therefore, the momentum restoring term in the collision operator provides a correction proportional to the toroidal Mach number assumed to be small here.

4.9 Transition to non-linear transport regimes

Despite the frequently used terminology of the *low-collisionality limit*, the picture becomes more complicated due to the combination of the smallness of the perturbation and collisionality. As we have seen in section 2.3 a Krook collision model is only justified if collisionality is not too low. The quasilinear limit described in section 2.4 relies on sufficient decorrelation of the orbit during the non-linear super-bounce time in Eq. (1.81). In this case, which is valid for an infinitesimal perturbation amplitude, collisionality does not appear in the final expressions, as we have seen in the previous section. In contrast to that, if the perturbation amplitude is kept small but finite and the limit of collisionality is taken to zero, the non-linear limit of section 2.5 is relevant instead. In a more realistic model, both, perturbation amplitude and collisionality are kept small but finite. For this purpose we will rely on a numerical solution of the perturbed distribution function, as described in (2.6).

An important limitation of the approach is the separate treatment of each harmonic of the perturbed Hamiltonian in Eq. (4.34). In the quasilinear limit, this is simply possible because canonical harmonics are naturally decoupled. Moving towards the non-linear case, we need to assume the resonances with the dominant contributions to be well-separated in phase-space. This is a reasonable assumption as long as the resonances are not too close to the trapped passing boundary, but the latter case should be checked more carefully, possibly depending on the specific problem.

We first introduce our collision model, which we choose as a linearised Fokker-Planck operator in velocity space describing collisions with a Maxwellian background plasma. Coefficients of the collision operator are evaluated in the unperturbed system, where violation of axial symmetry in the background field particle distribution f_{00} is neglected. This approximation may not be valid in the narrow phase space region around the resonance. However, diffusion coefficients are the velocity space integrals, the integral effect of this local violation is negligible small.

The differential operator specified in Eq. (4.4) is then applied with coefficients evaluated for f_{00}, with

$$\hat{L}_C f = \frac{\partial}{\partial v^k}\left(\frac{\partial}{\partial v^l}\left(D^{kl}(\boldsymbol{v})\, f\right) - F^k(\boldsymbol{v})\, f\right). \tag{4.85}$$

This expression has the form of a divergence, so in arbitrary coordinates parametrising velocity space by $\boldsymbol{v} = \boldsymbol{v}(\boldsymbol{z})$, it becomes

$$\hat{L}_C f = \frac{1}{J_z}\frac{\partial}{\partial z^i}\left[J_z\left(\frac{\partial}{\partial z^j}\left(D^{ij}_{(\boldsymbol{z})}\, f\right) - F^i_{(\boldsymbol{z})}\right)\right], \tag{4.86}$$

with Jacobian J_y of the transformation and implicit dependence of the coefficients by $\boldsymbol{y}$. If canonically conjugated variables $(\boldsymbol{x}, \boldsymbol{p})$, $(\boldsymbol{\theta}, \boldsymbol{J})$, or $\bar{\boldsymbol{z}} = (\bar{\boldsymbol{\theta}}, \bar{\boldsymbol{J}})$ are used,

the Jacobian becomes one. Since action-angle-variables mix velocity and spatial components in phase-space, the sum for i and j runs over 6 dimensions instead of just 3 for variables purely in velocity space.

To justify the canonical averaging of diffusion coefficients, we first transform to action-angle variables $(\boldsymbol{\theta}, \boldsymbol{J})$. Since all quantities are evaluated in the unperturbed axisymmetric field, there are no dependencies on the canonical toroidal angle $\theta^3 = \varphi_c$. A transformation to variables $(\bar{\boldsymbol{\theta}}, \bar{\boldsymbol{J}})$ adapted to the resonance condition replaces this angle by

$$\bar{\theta} = \bar{\theta}^3 = \boldsymbol{m} \cdot \boldsymbol{\theta} + \bar{\theta}_0, \tag{4.87}$$

and leaves the two remaining angles $\bar{\theta}^1 = \theta^1 = \phi_c$ and $\bar{\theta}^2 = \theta^2 = \vartheta_c$ unchanged. Canonical averaging of Eq. (4.86) over the non-resonant angles $\bar{\theta}^{1,2}$ can be immediately performed, since it will not influence transport across the resonance. The originally axisymmetric diffusion coefficients will not depend on $\bar{\theta}$ after the transformation, so this means that the diffusion coefficients are already in full canonically averaged form. However, derivatives over $\bar{\theta}$ will stay in the collision operator for now, which can be expanded to

$$\begin{aligned}\hat{L}_C f = &\frac{\partial}{\partial \bar{z}^i}\left[\left(\frac{\partial}{\partial \bar{z}^j}\left(\left\langle D^{ij}_{(\tilde{\boldsymbol{z}})}\right\rangle_{\boldsymbol{\theta}} f\right) - \left\langle F^{i}_{(\tilde{\boldsymbol{z}})}\right\rangle_{\boldsymbol{\theta}} f\right)\right] \\ &+ \frac{\partial}{\partial \bar{\theta}}\left[\left(\frac{\partial}{\partial \bar{z}^j}\left(\left\langle D^{3j}_{(\tilde{\boldsymbol{z}})}\right\rangle_{\boldsymbol{\theta}} f\right) - \left\langle F^{3}_{(\tilde{\boldsymbol{z}})}\right\rangle_{\boldsymbol{\theta}} f\right)\right],\end{aligned}$$

with i and j only running over action indexes $4-6$. To justify that we can neglect derivatives of f with respect to the resonant phase $\bar{\theta}$, we make use of the fast phase decorrelation as compared to the collision time (Kasilov et al., 1997), which allows for an estimate of second derivatives over actions being of higher order than the remaining terms. Finally, we obtain a collision operator with canonically averaged diffusion coefficients acting purely in action space,

$$\hat{L}_C f = \frac{\partial}{\partial \bar{J}^\alpha}\left[\left(\frac{\partial}{\partial \bar{J}^\beta}\left(\left\langle D^{\alpha\beta}_{(\tilde{\boldsymbol{J}})}\right\rangle_{\boldsymbol{\theta}} f\right) - \left\langle F^{\alpha}_{(\tilde{\boldsymbol{J}})}\right\rangle_{\boldsymbol{\theta}} f\right)\right]. \tag{4.88}$$

Neglecting the drag term and retaining only the diffusive part responsible for scattering across the resonance, we finally obtain the form of Eq. (2.26) required for the application of the weakly non-linear kinetic theory with

$$\hat{L}_C f \approx \frac{\partial^2}{\partial \bar{J}^\alpha \partial \bar{J}^\beta}\left(\left\langle D^{\alpha\beta}_{(\tilde{J})}\right\rangle_{\boldsymbol{\theta}} f\right). \tag{4.89}$$

Substituting back the original actions according to Eq. (2.35), we use common velocity space variables (v, η, p_φ) and their transformation to $\boldsymbol{J} = (J_\perp, J_\vartheta, p_\varphi)$ given

via Eqs. (3.106-3.107). Furthermore, we notice that we can neglect derivatives with respect to p_φ, which enter only in the next order in Larmor radius as compared to the remaining variables due to

$$\frac{\partial p_\varphi}{\partial \boldsymbol{v}}\frac{\partial}{\partial p_\varphi} = -\frac{m_\alpha c}{e_\alpha \sqrt{g} B^\vartheta}\frac{\partial \boldsymbol{r}}{\partial \varphi}\frac{\partial}{\partial r_\varphi} \approx \frac{qR\rho_L}{r^2}\frac{1}{v} \ll \frac{1}{v}. \tag{4.90}$$

The resulting resonant diffusion coefficient from Eq. (2.35) is thus given by

$$D_{\text{res}} = \left(\frac{1}{\bar{\Omega}'}\frac{\partial \bar{\Omega}}{\partial v}\right)^2 \langle D^{vv}\rangle_{\boldsymbol{\theta}} + \left(\frac{1}{\bar{\Omega}'}\frac{\partial \bar{\Omega}}{\partial \eta}\right)^2 \langle D^{\eta\eta}\rangle_{\boldsymbol{\theta}}\,, \tag{4.91}$$

since off-diagonal components are zero and $\langle D^{vv}\rangle_{\boldsymbol{\theta}} = D^{vv}$ for constant electric potential on a flux surface. Transforming η to the pitch-angle χ by

$$\eta = \frac{\sin^2\chi}{B}, \tag{4.92}$$

we can use the standard expressions D^{vv} and $D^{\chi\chi}$ (see e.g. the books of Dnestrovskii and Kostomarov (2012) or Helander and Sigmar (2005)) in the collision operator for a Maxwellian background,

$$\hat{L}_C f = \frac{1}{v^2}\frac{\partial}{\partial v} v^2 D^{vv}(v)\left(\frac{\partial f}{\partial v} + \frac{m_\alpha v}{T_\alpha} f\right) + \frac{1}{\sin\chi}\frac{\partial}{\partial \chi}\sin\chi D^{\chi\chi}\frac{\partial f}{\partial \chi}. \tag{4.93}$$

The canonically averaged $D^{\eta\eta}$ follows from the bounce average

$$\langle D^{\eta\eta}\rangle_{\boldsymbol{\theta}} = D^{\chi\chi}\left\langle\left(\frac{\partial \eta}{\partial \chi}\right)^2\right\rangle_b = D^{\chi\chi}\eta\left(\left\langle\frac{1}{B}\right\rangle_b - \eta\right). \tag{4.94}$$

Thus, the final form of the diffusion coefficient describing scattering across the resonance is

$$D_{\text{res}} = D^{vv}\left(\frac{1}{\bar{\Omega}'}\frac{\partial \bar{\Omega}}{\partial v}\right)^2 + D^{\eta\eta}\eta\left(\left\langle\frac{1}{B}\right\rangle_b - \eta\right)\left(\frac{1}{\bar{\Omega}'}\frac{\partial \bar{\Omega}}{\partial \eta}\right)^2. \tag{4.95}$$

To obtain the solution for the perturbed distribution function, coefficient is transformed to the dimensionless D via Eq. 2.42 appearing in the dimensionless kinetic equation (2.45).

As it turns out, for our purpose, this equation only needs to be solved once for various values of D, and the tabulated results can be re-used. This is possible because quantity of interest is the toroidal torque density, where the distribution function appears inside an integral in Eq. 4.28. Using the form of the single-harmonic Hamiltonian perturbation defined in angle $\bar{\theta}$ from Eq. (1.59) we obtain the torque

density

$$\begin{aligned} T_\varphi &= -\frac{m_\varphi}{S}\int \mathrm{d}^3\theta \int \mathrm{d}^3 J\, \delta(r_c(\theta_{1,2}, \boldsymbol{J}) - r)|H_{\boldsymbol{m}}| \sin\bar{\theta}\, f_1 \\ &= -\frac{m_\varphi}{S}\int \mathrm{d}^3\bar{\theta} \int \mathrm{d}^3 \bar{J}\, \delta(r_c(\bar{\theta}_{1,2}, \bar{\boldsymbol{J}}) - r)|H_{\boldsymbol{m}}| \sin\bar{\theta}\, f_1 \\ &= -\frac{m_\varphi}{S}\int \mathrm{d}^2\bar{\theta}^{1,2} \int \mathrm{d}^3 \bar{J}\, \delta(r_c - r)|H_{\boldsymbol{m}}| \int_{-\pi}^{\pi} \mathrm{d}\bar{\theta}\, \sin\bar{\theta}\, f_1. \end{aligned} \tag{4.96}$$

Since contributions come only from the resonant zone, we can insert a Dirac δ term for the resonant action $\bar{J}$,

$$\int \mathrm{d}^3\bar{J} \approx \int \mathrm{d}^3\bar{J}\, \delta(\bar{J} - \bar{J}_{\mathrm{res}}(\bar{J}_{1,2})) \int_{-\infty}^{\infty} \mathrm{d}\Delta\bar{J} \tag{4.97}$$

$$= \int \mathrm{d}^3\bar{J}\, |\bar{\Omega}'|\delta(\bar{\Omega}) \int_{-\infty}^{\infty} \mathrm{d}\Delta\bar{J}. \tag{4.98}$$

The term has been scaled with the total contribution of the integral over $\Delta\bar{J}$ close to the resonance. In this term we substitute via the dimensionless variable y from Eq. (2.37) and distribution function g from Eq. (2.44) to obtain

$$\begin{aligned} \int_{-\infty}^{\infty} \mathrm{d}\Delta\bar{J}\, f_1 &= \left|\frac{H_{\boldsymbol{m}}}{\bar{\Omega}'}\right|^{1/2} \int_{-\infty}^{\infty} \mathrm{d}y\, f_1 \\ &= \left|\frac{H_{\boldsymbol{m}}}{\bar{\Omega}'}\right| \boldsymbol{m}\cdot\frac{\partial f_0}{\partial \boldsymbol{J}} \int_{-\infty}^{\infty} \mathrm{d}y\, g. \end{aligned} \tag{4.99}$$

It is clear that contributions to this integral can come only from the symmetric part of g in y. According to Figs. 2.5 and 2.6, we suspect that this part will reach its maximum in the quasiliniear limit. The nonlinearity parameter $\bar{\Omega}'$ cancels out in the integral but remains in the diffusion coefficient D determining the solution for g. Adding an integral over $\bar{\theta}$ normalised by $1/2\pi$ to restore the complete form in phase-space of the initial part of the integral, we can transform back to original actions and angles with

$$T_\varphi = -\frac{m_\varphi}{2\pi S}\int \mathrm{d}^3\theta \int \mathrm{d}^3 J\, \delta(\boldsymbol{m}\cdot\boldsymbol{\Omega})\delta(r_c - r)|H_{\boldsymbol{m}}|^2 \boldsymbol{m}\cdot\frac{\partial f_0}{\partial \boldsymbol{J}} \int_{-\infty}^{\infty} \mathrm{d}y \int_{-\pi}^{\pi} \mathrm{d}\bar{\theta}\, \sin\bar{\theta}\, g. \tag{4.100}$$

This expression differs to the quasiliniear limit obtained in Eq. (4.69) only via a factor defined via the integral over g on the right end of the expression,

$$T_\varphi = -\frac{m_\varphi}{S}\int \mathrm{d}^3\theta \int \mathrm{d}^3 J\, \delta(r_c - r)\, Q_{\boldsymbol{m}}\, \Theta. \tag{4.101}$$

Since resonant action and angle are integrated, the only parameter that enters in Θ is the dimensionless D from Eq. (2.42) with D_{res} given from Eq. (4.95) in the

plasma. This non-linear attenuation factor (the reason for the name will become clear immediately) is defined as

$$\Theta = \Theta(D) = \frac{1}{\pi^2}\int_{-\infty}^{\infty} \mathrm{d}y \int_{-\pi}^{\pi} \mathrm{d}\bar{\theta}\, \sin\bar{\theta}\, g, \tag{4.102}$$

using the appropriate normalisation.

Quasilinear limit

In the quasilinear limit $D \gg 1$, we obtain the value $\Theta = 1$, which can be checked by inserting the limiting solution for g from Eq. (2.65) into the integral. Namely in this case,

$$\begin{aligned}
\Theta(D \gg 1) &= -\frac{D^{-1/3}}{\pi}\int_{-\infty}^{\infty} \mathrm{d}y \mathrm{Re}\left[\int_{-\pi}^{\pi} \mathrm{d}\bar{\theta}\, \sin\bar{\theta} \mathrm{i} e^{\mathrm{i}\bar{\theta}} \mathrm{Hi}(-\mathrm{i}D^{-1/3}y)\right] \\
&= D^{-1/3}\int_{-\infty}^{\infty} \mathrm{d}y \mathrm{Re}\left[\mathrm{Hi}(-\mathrm{i}D^{-1/3}y)\right] \\
&= \frac{D^{-1/3}}{\pi}\int_{-\infty}^{\infty} \mathrm{d}y \mathrm{Re}\left[\int_0^{\infty} \mathrm{d}w\, \exp\left(\frac{w^3}{3} - \mathrm{i}D^{-1/3}yw\right)\right] \\
&= 2\int_0^{\infty} \mathrm{d}w\, \delta(w)\frac{w^3}{3} = 1,
\end{aligned}$$

in the limit of $D \to \infty$. Alternatively, inserting the approximate solution for g from Eq. 2.48, where the resonant diffusivity parameter D has been replaced by a Krook term $-\bar{\nu}$ leads to the same result as above,

$$\begin{aligned}
\Theta_{\bar{\nu}} &= \frac{1}{\pi^2}\int_{-\infty}^{\infty} \mathrm{d}y \int_{-\pi}^{\pi} \mathrm{d}\bar{\theta}\, \sin\bar{\theta}\, \mathrm{Re}\left(\frac{-\mathrm{i}e^{\mathrm{i}\bar{\theta}}}{\mathrm{i}y + \bar{\nu}}\right) \\
&= \frac{1}{\pi}\int_{-\infty}^{\infty} \mathrm{d}y\, \frac{\mathrm{i}}{y - \mathrm{i}\bar{\nu}} = \frac{1}{\pi}\int_{-\infty}^{\infty} \mathrm{d}y\, \frac{\bar{\nu}}{y^2 + \bar{\nu}^2} = 1.
\end{aligned} \tag{4.103}$$

Those collisionality-independent results confirm the ones of section 4.7 with torque density in Eq. (4.69) obtained via the classical quasilinear method of Kaufman (1972) and Hazeltine et al. (1981) employing an infinitesimal Krook collision term for the actual collision operator.

Non-linear limit

In the non-linear limit $D \ll 1$, direct evaluation of Eq. (4.102) via the first-order term g_1 leads to difficulties with singularities near the separatrix $I = 2$. In this case, we make use of the original dimensionless kinetic equation (2.45). First, we switch to integration variables $(I, \bar{\theta})$ with

$$\int_{-\infty}^{\infty} \mathrm{d}y = \sum_{\sigma=\pm}\int_2^{\infty} \frac{\mathrm{d}I}{2\sqrt{I + 2\cos\bar{\theta}}}, \tag{4.104}$$

leading to distinct terms for superpassing and supertrapped region,

$$\begin{aligned}\Theta &= \frac{1}{2\pi^2}\sum_{\sigma=\pm}\left(\int_2^\infty \mathrm{d}I\int_{-\pi}^{\pi}\mathrm{d}\bar{\theta}\,\frac{\sin\bar{\theta}}{\sqrt{I+2\cos\bar{\theta}}}\,g+\int_{-2}^{2}\mathrm{d}I\int_{\bar{\theta}-}^{\bar{\theta}+}\mathrm{d}\bar{\theta}\,\frac{\sin\bar{\theta}}{\sqrt{I+2\cos\bar{\theta}}}\,g\right)\\ &= \frac{1}{2\pi^2}\sum_{\sigma=\pm}\left(\int_2^\infty \mathrm{d}I\int_{-\pi}^{\pi}\mathrm{d}\bar{\theta}\,\sqrt{I+2\cos\bar{\theta}}\,\frac{\partial g}{\partial\bar{\theta}}+\int_{-2}^{2}\mathrm{d}I\int_{\bar{\theta}-}^{\bar{\theta}+}\mathrm{d}\bar{\theta}\,\sqrt{I+2\cos\bar{\theta}}\,\frac{\partial g}{\partial\bar{\theta}}\right).\end{aligned} \tag{4.105}$$

where we have used partial integration together with periodicity/continuity conditions. The partial derivative of g is taken with I held fixed and from Eq. (2.73) we identify

$$\begin{aligned}\sigma\sqrt{I+2\cos\bar{\theta}}\frac{\partial g(\bar{\theta},I)}{\partial\bar{\theta}} &= \left(y\frac{\partial}{\partial\bar{\theta}}-\sin\bar{\theta}\frac{\partial}{\partial y}\right)g(\bar{\theta},y)\\ &= D\frac{\partial^2 g(\bar{\theta},y)}{\partial y^2}\\ &= 4D\sqrt{I+2\cos\bar{\theta}}\frac{\partial}{\partial I}\left(\sqrt{I+2\cos\bar{\theta}}g(\bar{\theta},I)\right),\end{aligned} \tag{4.106}$$

where we have used the original equation (2.45). Inserting this in the integrals (4.105) and performing one more partial integration yields

$$\Theta = -\frac{D}{\pi^2}\sum_{\sigma=\pm}\sigma\left(\int_2^\infty \mathrm{d}I\int_{-\pi}^{\pi}\mathrm{d}\bar{\theta}\,\frac{\partial g}{\partial I}+\int_{-2}^{2}\mathrm{d}I\int_{\bar{\theta}-}^{\bar{\theta}+}\mathrm{d}\bar{\theta}\,\frac{\partial g}{\partial I}\right). \tag{4.107}$$

This expression allows us to insert the zeroth order solution from Eqs. (2.75) and (2.86). Note that this works despite g_0 cancelling out in the original integral (4.102) because by the replacement via the kinetic equation we are actually also integrating over g_1, containing derivatives $\frac{\partial g_0}{\partial I}$, while avoiding singularities. Those are

$$\frac{\partial g_0}{\partial I} = \bar{g}_0'(I) - \frac{\sigma}{2\sqrt{I+2\cos\bar{\theta}}}, \tag{4.108}$$

with $\bar{g}_0'(I)=0$ for supertrapped and

$$\begin{aligned}\bar{g}_0'(I) &= \sigma\pi\left(\int_{-\pi}^{\pi}\mathrm{d}\bar{\theta}\sqrt{I+2\cos\bar{\theta}}\right)^{-1}\\ &= \sigma\frac{\pi}{4\sqrt{I+2}E\left(\frac{4}{2+I}\right)}\end{aligned} \tag{4.109}$$

for the superpassing region.

The term for the supertrapped region can be immediately computed by adding up $\sigma\pm$ and a change of the integration order,

$$-\sum_{\sigma=\pm}\sigma\int_{-2}^{2}\mathrm{d}I\int_{\bar{\theta}^-}^{\bar{\theta}^+}\mathrm{d}\bar{\theta}\,\frac{\partial g}{\partial I}=\int_{-\pi}^{\pi}\mathrm{d}\bar{\theta}\int_{-2\cos\bar{\theta}}^{2}\mathrm{d}I\,\frac{1}{\sqrt{I+2\cos\bar{\theta}}}$$
$$=\int_{-\pi}^{\pi}\mathrm{d}\bar{\theta}\sqrt{2+2\cos\bar{\theta}}=16. \tag{4.110}$$

In the superpassing region, we need to evaluate

$$2\sigma\int_{2}^{\infty}\mathrm{d}I\int_{-\pi}^{\pi}\mathrm{d}\bar{\theta}\,\frac{\partial g}{\partial I}=\int_{2}^{\infty}\mathrm{d}I\int_{-\pi}^{\pi}\mathrm{d}\bar{\theta}\left[\frac{1}{\sqrt{I+2\cos\bar{\theta}}}-\pi\left(\int_{-\pi}^{\pi}\mathrm{d}\bar{\theta}\sqrt{I+2\cos\bar{\theta}}\right)^{-1}\right]$$
$$=\int_{2}^{\infty}\mathrm{d}I\int_{-\pi}^{\pi}\mathrm{d}\bar{\theta}\left[\frac{1}{\sqrt{I+2\cos\bar{\theta}}}-\frac{\pi}{2\sqrt{I+2}E\left(\frac{4}{2+I}\right)}\right] \tag{4.111}$$

where both terms formally diverge at $I\to\infty$. Swapping again the integration order in the first term, we obtain

$$\int_{2}^{\infty}\mathrm{d}I\int_{-\pi}^{\pi}\mathrm{d}\bar{\theta}\frac{1}{\sqrt{I+2\cos\bar{\theta}}}=\lim_{I\to\infty}\int_{-\pi}^{\pi}\mathrm{d}\bar{\theta}\int_{2}^{I}\mathrm{d}I'\frac{1}{\sqrt{I'+2\cos\bar{\theta}}}$$
$$=\lim_{I\to\infty}2\int_{-\pi}^{\pi}\mathrm{d}\bar{\theta}\left(\sqrt{I+2\cos\bar{\theta}}-\sqrt{2+2\cos\bar{\theta}}\right)$$
$$=4\pi\lim_{I\to\infty}\sqrt{I}-16.$$
$$=4\pi\left(\int_{2}^{\infty}\frac{\mathrm{d}I}{2\sqrt{I}}+\sqrt{2}\right)-16. \tag{4.112}$$

The finite part of this integral cancels out with the supertrapped contribution and we move the divergent term to the last remaining integral arising from $\bar{g}_0'(I)$ in the superpassing region to obtain

$$\Theta(D\ll 1)=D\,\frac{4\sqrt{2}}{\pi}\left(1-\frac{1}{2\sqrt{2}}\int_{2}^{\infty}\mathrm{d}I\,\left(\frac{\pi}{2\sqrt{I+2}E\left(\frac{4}{2+I}\right)}-\frac{1}{\sqrt{I}}\right)\right). \tag{4.113}$$

The last term in the bracket that is subtracted from 1 can be evaluated numerically as ≈ 0.0250500 to yield

$$\Theta(D\ll 1)\approx 1.7555267\cdot D. \tag{4.114}$$

Transition region

For the remaining transition region with D of order one, we can store sampled values of the smooth function $\Theta(D)$ based on the numerical solution described in section

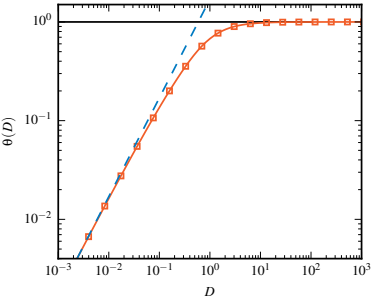

Figure 4.1: Attenuation factor Θ ($\square$) depending on diffusion parameter D. Quasi-linear (solid line) and non-linear limit (dashed) $\Theta \approx 1.7555267 \cdot D$.

(2.6), and interpolate them according to the actual value for D during bounce integrals. The dependency is shown in Fig. 4.1. For a given perturbation amplitude $|H_{\boldsymbol{m}}|$, in the non-linear low-collisionality limit $D \ll 1$, the asymptotic dependency $\Theta(D)$ is linear. For $D \gg 1$, the quasilinear case $\Theta = 1$ without attenuation is reached.

Chapter 5

Results and discussion

5.1 Quasilinear resonant transport regimes

This section can also be found in Albert et al. (2016a), *V. Numerical implementation and results*, and *Conclusion* formulated by the author and including some minor modifications.

In the scope of the quasilinear ansatz of section 4.5, analytical expressions for transport coefficients obtained within the Hamiltonian formalism agree with the corresponding expressions obtained earlier for particular resonant regimes within the validity domains of those results (see appendix B for details). In particular, the agreement with formulas for the superbanana plateau regime, which have been updated recently for a general tokamak geometry by Shaing (2015), is exact. One inconsistency in the treatment of passing particles has been found (see appendix B.5) in comparison to the analytical formulas for bounce-transit resonances of Shaing et al. (2009a). In addition, it has been demonstrated that momentum conservation of the collision operator plays a minor role in resonant regimes in general as long as the toroidal rotation is sub-sonic, which can be seen from the comparison with runs from the code NEO-2, where a full momentum-conserving collision operator is employed.

In addition to the analytical assessment, transport coefficients from Eq. (4.84) have been computed numerically in the code NEO-RT (Albert and Kasilov, 2017) for the general case of a perturbed tokamak magnetic field specified in Boozer coordinates. Bounce averages are performed via numerical time integration of zero order guiding-centre orbits along the field lines as specified in Eq. (3.116). An efficient numerical procedure for finding the roots in Eq. (4.63) is realized using the scalings

$$\omega_b = u\bar{\omega}_b(\eta), \tag{5.1}$$

$$\langle \Omega_{tB} \rangle_b = u^2 \left\langle \bar{\Omega}_{tB} \right\rangle_b . \tag{5.2}$$

Normalized frequencies $\bar{\omega}_b$ and $\bar{\Omega}_{tB}$ (relatively smooth functions) are precomputed on an adaptive η-grid and interpolated via cubic splines in later calculations.

For testing and benchmarking, a tokamak configuration with circular concentric flux surfaces and safety factor shown in Fig. 5.1 is used (the same as in Kasilov et al. (2014)) and results are compared to calculations from the NEO-2 code. The perturbation field amplitude in Eq. (4.60) is taken in the form of Boozer harmonics

$$B_n = \varepsilon_{\mathrm{M}} B_0(\vartheta) e^{\mathrm{i}m\vartheta}.$$

Two kinds of perturbations are considered here: a large scale perturbation with $(m, n) = (0, 3)$ referred below as "RMP-like case" because of the toroidal wavenumber typical for perturbations produced by ELM mitigation coils, and a short scale perturbation with $(m, n) = (0, 18)$ typical for the toroidal field (TF) ripple. The remaining parameters are chosen to be representative for a realistic medium-sized tokamak configuration. In the plots, transport coefficients D_{1k} are normalized by (formally infinitesimal) $\varepsilon_{\mathrm{M}}^2$ times the mono-energetic plateau value

$$D_p = \frac{\pi q v_T^3}{16\, R\, \bar{\omega}_c^2}, \tag{5.3}$$

where R is the major radius, and the reference gyrofrequency $\bar{\omega}_c$ is given by the $(0, 0)$ harmonic of ω_c. Radial dependencies are represented by the flux surface aspect ratio $A = (\psi^a_{\mathrm{tor}}/\psi_{\mathrm{tor}})^{1/2}\, R/a$ of the current flux surface where a is the minor radius of the outermost flux surface and ψ^a_{tor} the toroidal magnetic flux at this surface. The radial electric field magnitude is given in terms of the toroidal Mach number $M_t \equiv R\Omega_{\mathrm{t}E}/v_T$. In all plots there are at least 4 data points between subsequent markers.

Fig. 5.1 shows the radial dependence of the transport coefficient D_{11} in the super-banana plateau regime for the RMP-like perturbation for both positive and negative radial electric field. For this benchmarking case the relation between toroidal precession frequencies due to the $\boldsymbol{E} \times \boldsymbol{B}$ drift, Ω_{tE}, and due to the magnetic drift Ω_{tB}, has been fixed by setting the reference toroidal magnetic drift frequency $\Omega^{\mathrm{ref}}_{tB} \equiv cT_\alpha/(e_\alpha \psi^a_{\mathrm{tor}})$ (not the actual Ω_{tB}) equal to Ω_{tE}. Additional curves are shown for calculations where the magnetic shear term $(\mathrm{d}q/\mathrm{d}r)$ in Eq. (3.109) has been neglected. The results are compared to the analytical formula for the large aspect ratio limit by Shaing et al. (2009b). Resonance lines in velocity space are plotted below the radial profiles for a flux surface relatively close to the axis ($A = 10$) and one further outwards ($A = 5$). Here $\Delta\bar{\eta} = (\eta - \eta_{\mathrm{tp}})/(\eta_{\mathrm{dt}} - \eta_{\mathrm{tp}})$ is the distance to the trapped passing boundary η_{tp} normalized to the trapped region between trapped-passing boundary η_{tp} and deeply trapped η_{dt}. For flux surfaces with $A > 10$ magnetic shear plays a small role due to the flat safety factor profile in the present field configuration: The diffusion coefficient D_{11} is nearly identical to the result without shear

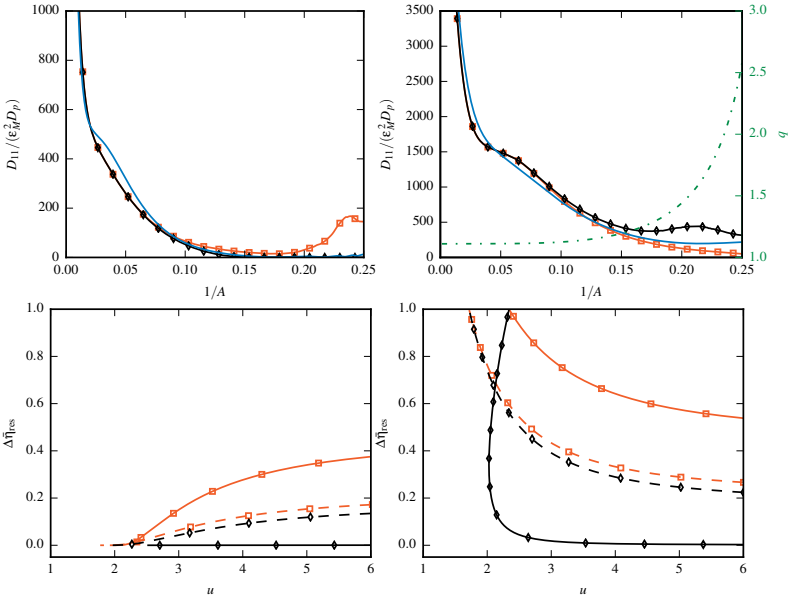

Figure 5.1: Radial dependence of superbanana plateau D_{11} (upper plots) in the RMP case for Mach number $M_t = 0.036$ (left) and -0.036 (right). Comparison of Hamiltonian approach (NEO-RT) to analytical formula by Shaing et al. (2009b) (solid line). Results with ($\diamond$) and without magnetic shear ($\square$) in the magnetic drift frequency (3.109). A safety factor profile (dash-dotted) is shown on the second axis of the upper right plot. The lower plots show resonance lines ranging from deeply trapped ($\Delta\bar{\eta} = 0$) to trapped passing boundary ($\Delta\bar{\eta} = 1$) at flux surfaces of aspect ratio $A = 5$ (solid) and $A = 10$ (dashed).

and stays close to the analytical result for the large aspect ratio limit. For aspect ratio $A = 10$, the agreement between NEO-2 calculations and large aspect ratio limit of Shaing et al. (2009b) has been demonstrated earlier by Kasilov et al. (2014). At larger radii, where the q profile becomes steep, a significant deviation between the cases with and without magnetic shear term is visible. This can be explained by the strong shift of the resonance lines due to the shear term in the rotation frequency Ω_{tB} that is visible in lower plots. For both signs of the electric field, the resonant $\eta_{\rm res}$ is closer to the trapped passing boundary when shear is included.

In Figs. 5.2-5.3 the radial electric field dependence of non-ambipolar transport induced by drift-orbit resonances with magnetic drift neglected (Ω_{tB} set to zero) is pictured. Here, several canonical modes m_2 contribute for both, trapped and passing

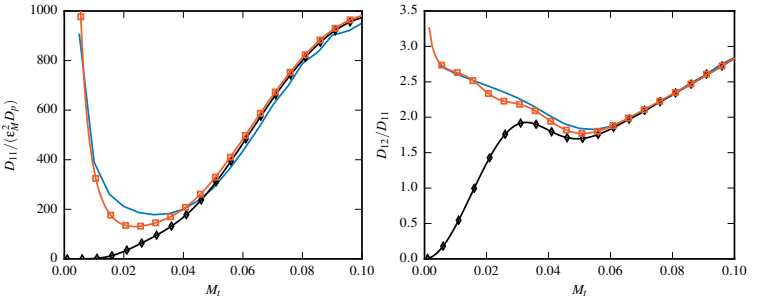

Figure 5.2: Drift-orbit resonances with neglected magnetic drift: Mach number dependence of D_{11} (left) and the ratio D_{12}/D_{11} (right) for an RMP-like perturbation at $A = 10$. Comparison of Hamiltonian approach ($\diamond$), sum of Hamiltonian results and $\nu - \sqrt{\nu}$ regime by Shaing et al. (2010) ($\square$), and results from NEO-2 at collisionality $\nu^\star = 3 \cdot 10^{-4}$ (solid line).

particles.

In Fig. 5.2 the Mach number dependence of transport coefficient D_{11} and the ratio D_{12}/D_{11} is plotted for this regime for an RMP-like perturbation ($n = 3$). NEO-2 calculations shown for the comparison have been performed at rather low collisionality (see the caption) characterized by the parameter $\nu^* = 2\nu q R/v_T$ where ν is the collision frequency. In addition, also the curves with the sum of diffusion coefficients in the collisional $\nu - \sqrt{\nu}$ regime from the joint formula of Shaing et al. (2010) and resonant contributions from the Hamiltonian approach are shown.

For $M_t < 0.02$, in contrast to the superbanana plateau regime, collisionless transport is small compared to collisional effects. Between $M_t = 0.02$ and 0.04 the sum of Hamiltonian and $\nu - \sqrt{\nu}$ results for D_{11} is clearly below NEO-2 values. The reason for this are contributions near the trapped passing boundary, which are illustrated in Fig. 5.3 at $M_t = 0.028$. There the integrand in Eq. (4.84) for the mode m_2 with the strongest contribution is shown together with the resonance line in velocity space. For $M_t > 0.04$ there is a close match between the results with slightly lower D_{11} values from NEO-2 due to remaining collisionality effects.

It should be noted that validity of the "collisionless" Hamiltonian model cannot be accessed with the help of a simple Krook model although this model is fully adequate for the present derivations. The details of the collision model are not important as long as the collisional width of the resonant line in velocity space is smaller than the distance from that line to the trapped-passing boundary where the topology of the orbits changes abruptly. This criterion is much more restrictive than the smallness of the collision frequency compared to the bounce frequency suggested by the Krook

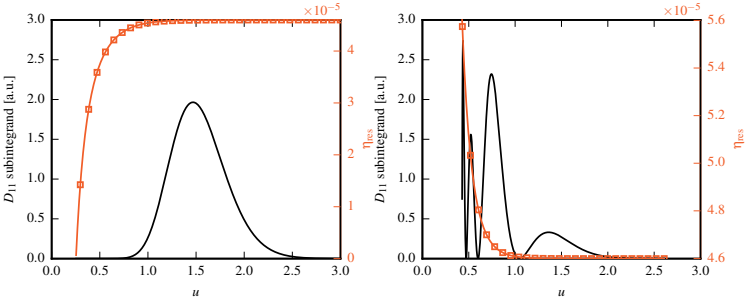

Figure 5.3: Drift-orbit resonances, RMP at $A = 10$ with $M_t = 0.028$. Dependency of the subintegrands in Eq. (4.84) on the normalized velocity u for the dominant mode (solid black line) of passing (left, $m_2 = -3$) and trapped particles (right, $m_2 = -1$) and resonance lines for these modes (□, right axis). Significant contributions are visible where the resonance is close to the trapped passing boundary $\eta_{\rm tp} = 4.6 \cdot 10^{-5}$.

model. At small Mach numbers where the resonant line approaches the trapped-passing boundary rather closely (see Fig. 5.3), the applicability of the "collisionless" approach is violated at much lower collisionality than one could expect from the Krook model, and in that case a collisional boundary layer analysis including the resonant interaction is needed. As one can see from Fig. 5.2, for such transitional Mach numbers where both, $\nu - \sqrt{\nu}$ regime and resonant regime are important, a simple summation of the separate contributions from these regimes obtained in asymptotical limits cannot reproduce the numerical result, similarly to the observation of Sun et al. (2010). With increasing Mach numbers, the resonant curve gets more separated from the trapped-passing boundary, and the collisionless analysis becomes sufficient, as visible for higher Mach numbers in Fig. 5.2.

Fig. 5.4 shows the Mach number dependence of D_{11} as well as D_{12}/D_{11} for a toroidal field ripple ($n = 18$) together with the analytical ripple plateau value Boozer (1980) and results for finite collisionality from NEO-2. At low Mach numbers $M_t < 0.01$ collisional effects are again dominant. A resonance peak of passing particles is visible for D_{12}/D_{11} at $M_t = 2.8 \cdot 10^{-3}$. In the intermediate region between $M_t = 0.01$ and 0.05 oscillations due to trapped particle resonances are shifted and reduced in the collisional case. For $M_t > 0.05$ Hamiltonian results converge towards the ripple plateau. A small deviation of NEO-2 values for D_{11}, which is of the order of Mach number is most likely caused by the low Mach number approximation used in NEO-2.

Finally, in Fig. 5.5 the Mach number dependence of D_{11} for the RMP case is plot-

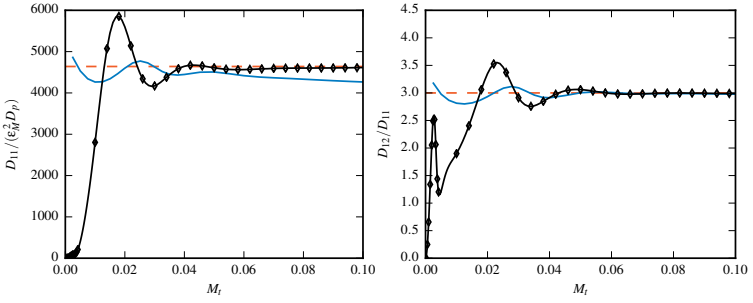

Figure 5.4: Mach number dependence of transport coefficients of drift-orbit resonances for a toroidal field ripple at $A = 10$. Comparison between Hamiltonian approach ($\diamond$), ripple plateau (red) and NEO-2 at collisionality $\nu^\star = 10^{-3}$ (solid line).

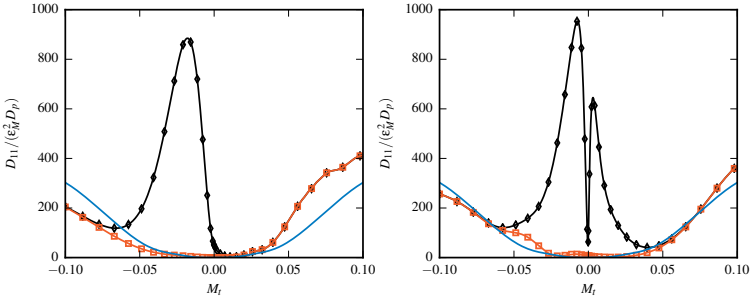

Figure 5.5: Mach number dependence of D_{11} for RMP at $A = 5$ with shear term included (left) and neglected (right) in Eq. (3.109). Total resonant transport ($\diamond$) and contributions by drift-orbit resonances with finite magnetic drift and excluding superbanana plateau ($\square$). Comparison to drift-orbit resonances with Ω_{tB} set to zero (solid line).

ted for both, positive and negative Mach numbers for finite toroidal precession frequency due to the magnetic drift Ω_{tB}. To set the scaling with respect to Ω_{tE}, the reference magnetic drift frequency defined above is fixed by $R\Omega_{tB}^{\mathrm{ref}}/v_T = 3.6 \cdot 10^{-2}$. In this case all resonance types contribute to transport coefficients. Due to the finite magnetic drift, the Mach number dependence is not symmetric anymore. If shear is neglected in Eq. (3.109) the superbanana plateau is centred around slightly negative values of the electric field, and magnetic drift induces some deviation from the idealized case without magnetic drift. In the case with included shear superbanana plateau, contributions for positive Mach numbers vanish and a large deviation from the case without magnetic drift is visible also for drift-orbit resonances.

To sum up, numerical results from NEO-RT based on the Hamiltonian approach agree well with results from the NEO-2 code at relatively high Mach numbers where finite collisionality effects are small ($M_t > 0.04$ in the examples here). At these Mach numbers, both approaches also reproduce the analytical result for the ripple plateau regime (Boozer, 1980). At intermediate Mach numbers $0.02 < M_t < 0.04$ which correspond to the transition between the $\nu-\sqrt{\nu}$ regime and resonant diffusion regime, the combined torque of $\nu - \sqrt{\nu}$ regime and resonant diffusion regime does not reach the numerical values calculated by NEO-2 even at very low collisionality. The reason for this are contributions of the resonant phase space region very close to the trapped-passing boundary. To obtain more accurate results in these regions, an analysis of the collisional boundary layer would be required in the Hamiltonian formalism.

The Hamiltonian approach is of non-local nature, i.e. it does not use truncated "local" orbits bound to a specific magnetic flux surface. Already in the present leading order approximation, an additional term describing the influence of magnetic shear that is absent in the standard local neoclassical ansatz naturally arises in the resonance condition. This term significantly increases the asymmetry of the superbanana plateau resonance with respect to the toroidal Mach numbers of $\boldsymbol{E} \times \boldsymbol{B}$ rotation and may even eliminate this resonance for a given Mach number sign (at positive Mach numbers in the examples here). This shear term has been included into analytical treatment recently Shaing (2015) but was absent in earlier approximate formulas (Shaing et al., 2009b, 2010). This could be one possible reason for the discrepancy with the non-local δf Monte Carlo approach observed by Satake et al. (2011).

It should be noted that term "non-local transport ansatz" is used here with respect to the orbits employed in the computation of the perturbation of the distribution function, and it should not be confused with the non-local transport in the case where the orbit width is comparable to the radial scale of the parameter profiles and where the transport equations cannot be reduced to partial differential equations. In the

sense used here, the shear term appears due to a radial displacement of the guiding-centre, which is a non-local effect. Namely, due to variation of the safety factor with radius, the toroidal connection length between the banana tips of the trapped particle is different at the outer and the inner sides of the flux surface containing these tips. Since particles with positive and negative parallel (and, respectively, toroidal) velocity signs are displaced from this surface in different directions, the sum of the toroidal displacements over the full banana orbit is not balanced to zero. The result is an overall toroidal drift proportional to the shear parameter. This effect cannot be described by the local ansatz in an arbitrary coordinate system but still can be retained within the local ansatz in the field aligned coordinates as the ones used by Shaing (2015). This ambiguity in the description of the magnetic drift within the local ansatz (Smith) results from the fact that setting to zero one of the velocity vector components which are not invariant under a coordinate transformation destroys the covariance of equations of motion during such transformations.

According to the presented results, magnetic shear can also have a strong influence on drift-orbit (bounce-transit and drift) resonances. A comparison between the results in the related resonant diffusion regime with neglected magnetic drift and results including magnetic drift shows a strong discrepancy, especially if magnetic shear is considered. Therefore, for an accurate evaluation of NTV torque in low-collisional resonant transport regimes it is necessary to consider magnetic drift including magnetic shear in the resonance condition. This is especially important for modern tokamaks with poloidal divertors causing high magnetic shear at the plasma edge where the main part of the NTV torque is produced.

An application to the tokamak ASDEX Upgrade with resonant magnetic perturbations published in Martitsch et al. (2016) compares results for NTV torque from different approaches. For deuterium ions, typical values of bounce and toroidal drift frequencies are within a similar order of magnitude in that case. Thich makes it possible for superbanana resonance and drift-orbit resonances to make substantial contributions to non-ambipolar transport and NTV torque.

Results from the computation of ion NTV torque caused by the RMP field in several models are compared in Figs. 5.6 and 5.7. First of all, this includes the quasilinear version of NEO-2 (Kasilov et al., 2014) that is able to numerically compute neoclassical transport over a wide range of collisionalities (Kernbichler et al., 2016). Neglecting magnetic drift, a comparison to the code SFINCS by Landreman et al. (2014) is possible, that additionally includes yet another class of non-linear effects from local particle trapping, which are shown to be insignificant in the RMP case shown here. Analytical results come from the universal formula of Shaing et al. (2010) connecting $1/\nu$, $\nu - \sqrt{\nu}$ and superbanana-plateau transport regimes, which is formulated for the large-aspect-ratio limit and does not include drift-orbit reson-

ances. Finally, results from NEO-RT that implements the semi-analytical Hamiltonian approach from the present text are plotted for the quasilinear case without non-linear attenuation.

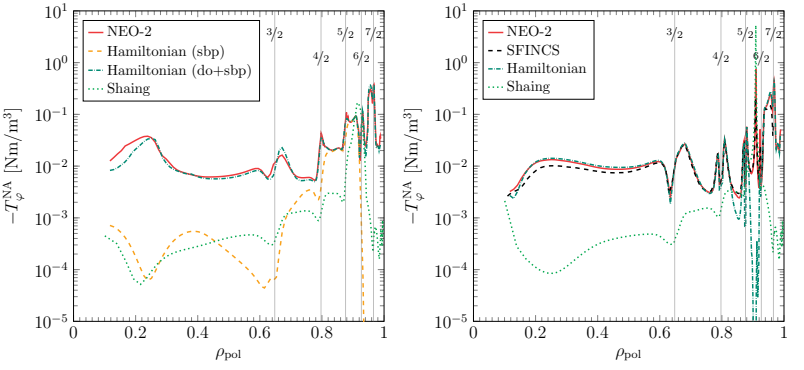

Figure 5.6: Ion contribution to the NTV torque density produced by the RMP coils as a function of the normalized poloidal radius. Left: The NEO-2 (solid) result including both, $\boldsymbol{E} \times \boldsymbol{B}$ drift and magnetic drift (*without magnetic shear*), is compared to the Hamiltonian model (NEO-RT, dashed), as well as to the universal formula by Shaing et al. (2010) (dotted line). Right: Neglecting magnetic drift, the NEO-2 result is compared to SFINCS (dashed), to the Hamiltonian model (dash–dotted) and to the bounce-averaged model by Shaing. Vertical lines mark resonant surfaces with $q(\rho_{\mathrm{pol}}) = m/n$, where m and n are poloidal and toroidal mode number, respectively.

While Fig. 5.6 shows results from the standard local neoclassical ansatz, where magnetic shear is not present, and intentionally switched off also in NEO-RT, Fig. 5.7 displays data from a modified version of NEO-2 taking into account non-local effects that lead to the shear term in the magnetic drift frequency compared to the full Hamiltonian solution. Results from NEO-2, NEO-RT and SFINCS are matching over the whole radial range despite three fundamentally different approach to the problem. Differences between NEO-2 and NEO-RT are mainly due to collisional effects not considered in NEO-RT. Differences to SFINCS can arise due to the mentioned non-linearity, which is different to the one considered here. Analytical results show a match of the same order of magnitude near the electric zero, where the superbanana plateau resonance is relevant, however, due to the large-aspect-ratio limit there is no quantitative match. Apart from that radial range, analytical collisional regimes are masked by resonant transport from drift-orbit resonances.

It should be noted, that formulas for the superbanana plateau regime without re-

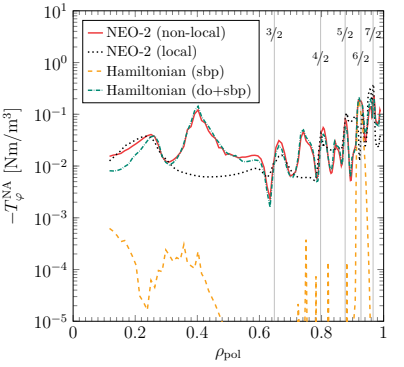

Figure 5.7: Ion contribution to the NTV torque density produced by the ELM mitigation coils with a phase of 90 degrees as a function of the normalized poloidal radius. The non-local NEO-2 result including both, $\boldsymbol{E}\times\boldsymbol{B}$ drift and magnetic drift (*with magnetic shear*), is compared to the NEO-2 result using a local approximation and to the semi- analytical Hamiltonian model taking into account drift-orbit (do) and superbanana-plateau (sbp) resonances. Vertical lines indicate the positions of resonant surfaces.

quiring the large-aspect-ratio limit have recently been published by Shaing (2015), which can be shown to match the present results for bounce harmonic $m_2 = 0$ analytically (see appendix B).

5.2 Non-linear resonant transport regimes

This section can also be found in (Albert et al., 2016b), *Numerical implementation, results and discussion*, and *Conclusion and Outlook* formulated by the author and including some minor modifications. Quasilinear calculations of NTV torque provide an upper limit for contributions from resonant transport regimes. The weak non-linear Hamiltonian treatment that goes beyond the quasilinear limit has been implemented in the code NEO-RT, enabling the prediction of NTV torque in transition regimes between quasilinear and non-linear limit. Results including non-linear attenuation were obtained for the circular tokamak as in the quasilinear case. The modifications include the non-linear attenuation factor $\Theta(D)$ inside the integrals for the diffusion coefficients and the calculation of D from plasma parameters. $\Theta(D)$ has been pre-tabulated from a numerical calculation for the solution of the dimensionless kinetic equation (2.45) described in section 2.6. Plasma parameters and perturbation amplitudes were chosen representative for a medium sized tokamak (deuterium plasma, density $n \approx 2\cdot 10^{13}\ \mathrm{cm}^{-1}$, ion temperature $T_\mathrm{i} \approx 1.5$ keV) with RMPs. The figures show results for computations with a perturbed magnetic field module $B = B_0\cdot(1+\varepsilon_\mathrm{M}\cos(m\theta+n\varphi))$ by a single harmonic in Boozer angles (θ,φ) with $m=0$ and $n=3$, evaluated at a flux surface of aspect ratio $A=10$.

In Fig. 4.1 the non-ambipolar radial diffusion coefficient D_{11} normalized by the plateau coefficient $D_p = \pi q v_T^3/(16R\bar{\omega}_{c\alpha}^2)$ and the squared relative magnetic perturbation amplitude ε_M^2 is plotted over the Mach number $M_t = \Omega_{tE}R/v_T$, which

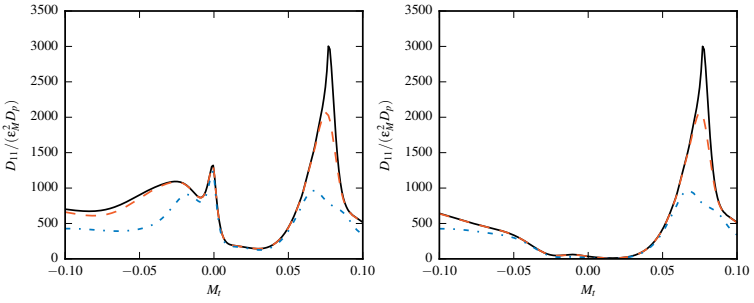

Figure 5.8: Normalized transport coefficient D_{11} depending on Mach number M_t at quasilinear limit (solid black) and for finite relative perturbation amplitudes $\varepsilon_{\mathrm{M}} = 10^{-3}$ (dashed) and 10^{-2} (dash-dotted). Left: All resonances including superbanana resonance ($m_2 = 0$) with peak near $M_t = 0$. Right: Results omitting superbanana resonance ($m_2 \neq 0$) with peak at $M_t = 0.07$.

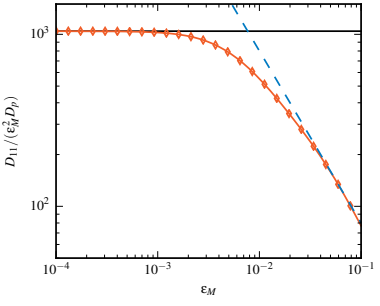

Figure 5.9: Normalized D_{11} ($\diamond$) over perturbation strength at $M_t = -0.036$ (superbanana resonance). Quasilinear (solid black line), non-linear limit (dashed).

is proportional to the radial electric field E_r. Here, v_T is the thermal velocity and R the major radius. To demonstrate the importance of non-linear attenuation for drift-orbit resonance regimes, the superbanana resonance $m_2 = 0$, which is dominating around the electric zero with $M_t = 0$, has been excluded in the right plot. Non-linear effects are clearly visible at $\varepsilon_{\mathrm{M}} = 10^{-3} - 10^{-2}$ and are more pronounced at higher perturbation amplitudes and higher absolute Mach number values.

Fig. 5.9 shows the transition between quasilinear (superbanana plateau) and non-linear (superbanana) resonant transport regimes at $M_t = -0.036$, where most contributions are caused by the superbanana resonance. Similar to the attenuation parameter, the normalized diffusion coefficient reaches the quasilinear limit at small

$\varepsilon_{\mathrm{M}} < 10^{-3}$ and a non-linear behaviour at large $\varepsilon_{\mathrm{M}} > 10^{-3}$. As visible in Fig. 5.8 at $M_t \approx 0.07$, for drift-orbit resonances the non-linear onset is reached already at smaller perturbation amplitudes in this case.

Considering the present results for perturbation amplitudes from RMPs of a few tenths of a percent, analysis of non-linear attenuation is necessary in order not to overestimate toroidal torque in resonant transport regimes. At the chosen parameters for a typical medium sized tokamak, the overall attenuation can be in the order of tens of percents, depending on Mach number and perturbation strength. The central assumption made is the sufficient distance of resonances in phase-space. While this is fulfiled per definition for the superbanana resonance, further investigations are necessary to validate the assumption for bounce-transit and drift resonances.

5.3 Treatment of finite orbit width

The extension to orbits of finite width is possible within the Hamiltonian approach firstly for computation of canonical actions, angles and frequencies, secondly for canonical (bounce) averages of the magnetic perturbation, and thirdly for conservation laws involving integration over canonical angles used to compute particle transport and torque. For equilibrium fields of characteristic length scale much larger than the orbit width the first modification would lead to relatively small changes while requiring pre-computation and interpolation of frequencies in two instead of one dimension in phase-space, since scaling laws cannot be used anymore. The latter two modifications can however be done without a substantial degradation of computational efficiency and lead to more accurate results for perturbations with significant radial variations on the scale of the orbit width. Here, we are going to introduce the required new concepts to treat orbits of finite width within this approximation. While the present approach is in principle also applicable at any point of the transition between quasilinear and non-linear limit in Eq. (4.101), special care needs to be taken with regard to the radial width of super-orbits, which can be larger than the usual orbits width. This is why we are going to focus on the quasilinear limit here. Analytical treatments with emphasis on stochastic motion of orbits of finite width have been published by Eriksson and Helander (1993) and Kolesnichenko et al. (1998). Recently, an approach to treat neoclassical toroidal viscous torque taking effects from finite orbit width into account has been published by Shaing and Sabbagh (2016). More details and results in the present Hamiltonian approach can be found in (Albert et al., 2017).

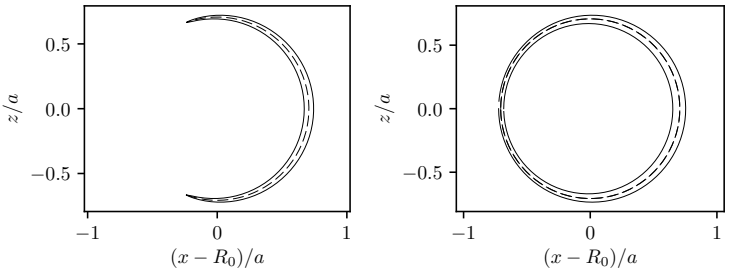

Figure 5.10: Example for poloidal projection of thermal deuteron orbits in a representative tokamak with circular flux surfaces and typical parameters of ASDEX Upgrade. Dashed lines show the banana tip radius r_φ from Eq. (3.30) and solid lines the actual orbits (left: trapped, right: passing). In the right figure the co-passing orbit lies entirely outside r_φ and the counter-passing orbit inside.

Full orbits and bounce averages

An example for orbits of finite width computed for a tokamak with circular flux surfaces and parameters similar to ASDEX Upgrade shots at reactor-relevant collisionality is shown in Figure 5.10. For those orbits covering roughly one tenth of the radial range it is evident that finite orbit width effects can play a role, especially with respect to the small radial length scale of perturbations near resonant surfaces.

Let us consider the harmonics in canonical angles $\boldsymbol{\theta}$ of a quantity a given as a function of straight field line flux coordinates $\boldsymbol{x} = (r, \vartheta, \varphi)$ in the guiding-centre approximation inside an axisymmetric magnetic field,

$$a_{\boldsymbol{m}} = \frac{1}{2\pi} \int \mathrm{d}\theta^2 \, a_{0n}(\vartheta) e^{i(n\Delta\varphi(\theta^2, \boldsymbol{J}) - m_2\theta^2)}. \tag{5.4}$$

For equilibrium fields with sufficiently small radial gradients as defined above, and with a small enough correction to the angles ϑ, φ from Eq. (3.16) we use the same expression as in Eq. (3.116) with

$$a_{\boldsymbol{m}} = \left\langle a_{0n}(r(\vartheta), \vartheta) e^{inq\vartheta_{\mathrm{orb}} - i(m_2 + nq\delta_{\mathrm{tp}})\omega_b \tau} \right\rangle_b . \tag{5.5}$$

In contrast to the case of thin orbits, changes of the quantity a_{0n} on the radial scale similar to the orbit width are taken into account here by evaluation of $r(\vartheta)$ during integration along the orbit. This is particularly relevant to the evaluation of a Hamiltonian perturbation $H_{\boldsymbol{m}}$ for radially small-scale magnetic perturbations. During the bounce integral the initial point ϑ_0 where $\tau = 0$ should be correctly specified for $\vartheta_{\mathrm{orb}} = \vartheta(\tau) - \vartheta(0)$.

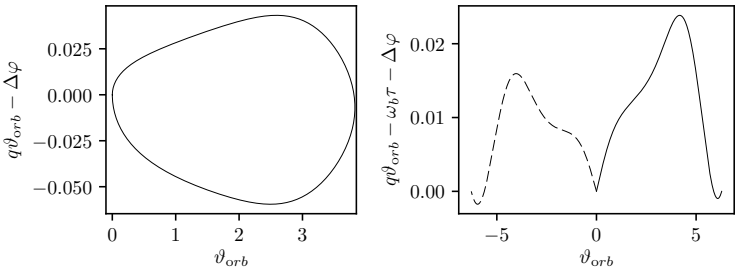

Figure 5.11: Examples of differences of the approximate and exact $\Delta\varphi$ to toroidal canonical angle over ϑ_{orb} for parameters as in Figure 5.10 (left: trapped, right: passing). In the right plot the solid line shows the co-passing and the dashed line the counter-passing orbit. Here the evaluation of $q(\vartheta_{\mathrm{orb}} - \omega_b\delta_{\mathrm{tp}}\tau)$ is performed for the zero-order orbit at r_φ and the exact $\Delta\varphi$ is evaluated for the full orbit.

To illustrate the error that is introduced in the phase of the exponent in Eq. (5.5), Figure (5.11) shows the approximate deviation of the approximation $\Delta\varphi \approx q(\vartheta_{\mathrm{orb}} - \omega_b\delta_{\mathrm{tp}}\tau)$ from the exact quantity $\Delta\varphi = \varphi - \theta^3 = \varphi - \Omega^3\tau$. We can see that for typical toroidal mode-numbers $n = 2$ or $n = 3$ used for RMPs this error is sufficiently small to justify the use of Eq. (5.5) here. Problems with this approximation can potentially arise very close to the trapped-passing boundary and for high toroidal mode-numbers n. In such cases the exact expression for $\Delta\varphi$ should be used instead in Eq. (5.4).

Volume averaged conservation laws

Starting from a flux surface averaged conservation law, instead of setting $r_c(\boldsymbol{\theta}, \boldsymbol{J}) \approx r_\varphi(p_\varphi)$ in expressions of the form of Eq. (4.24), we perform integrals along the full orbit including radial drift away from the flux surface of $r = r_\varphi$. Physically this means that one orbit contributes to sources on all flux surfaces that it passes during its bounce or transit period. To resolve the term $\delta(r_c(\boldsymbol{\theta}, \boldsymbol{J}) - r)$ inside the flux surface average, we introduce another average over a finite radial region between flux surfaces at radius r_a and r_b,

$$\langle A \rangle_{ab} \equiv \frac{1}{\Delta r_{ab}} \int_{r_a}^{r_b} \mathrm{d}r \, \langle A \rangle \tag{5.6}$$

$$= \frac{1}{\Delta r_{ab}} \int_{r_a}^{r_b} \mathrm{d}r \, \frac{1}{S(r)} \int \mathrm{d}^3\theta \int \mathrm{d}^3 J \, \delta(r_c(\boldsymbol{\theta}, \boldsymbol{J}) - r) a(\boldsymbol{r}_c(\boldsymbol{\theta}, \boldsymbol{J})) \, f(t, \boldsymbol{\theta}, \boldsymbol{J}). \tag{5.7}$$

Here the integral describing volumetric contributions between r_a and r_b is normalised by the radial distance $\Delta r_{ab} = r_b - r_a$. This makes expressions directly comparable to their radially local counterparts in the limiting case of zero orbit width

together with $\Delta r_{ab} \to 0$, where all contributions come from a single flux surface with $r = r_a = r_b = r_\varphi$. In particular, for the toroidal torque density given in Eq. (4.69), we have

$$\langle T_\varphi \rangle_{ab} = -\frac{1}{\Delta r_{ab}} \sum_{\boldsymbol{m}} n \int_{r_a}^{r_b} \mathrm{d}r \, \frac{1}{S(r)} \int \mathrm{d}^3\theta \int \mathrm{d}^3 J \, \delta(r_c(\boldsymbol{\theta}, \boldsymbol{J}) - r) \, Q_{\boldsymbol{m}}(\boldsymbol{J}). \tag{5.8}$$

An exact computation with flux surface area S from Eq. (4.17) is possible, but a further simplification can be made if Δr_{ab} is smaller than the characteristic length scale of the equilibrium field. Since we will choose it to be of similar or smaller order than the orbit width $\Delta r_c^{\max} \lesssim 2 \cdot \max |r_c - r_\varphi|$ at thermal velocity, this condition is well fulfiled within the approximation defined earlier and we set $S(r) \approx S((r_a + r_b)/2) \equiv S_{ab}$. A next order approximation would be a correction due to the geometric scaling $S \propto r^2$ from Eq. 4.17, which is not considered here. Consequently, the constant term $1/S_{ab}$ can be extracted as a common factor in Eq. (5.7). Keeping the angular dependency only for the canonical bounce phase θ^2 relevant for guiding-centre motion in the unperturbed axisymmetric field and changing one integration variable from $J_3 = p_\varphi$ to r_φ with first derivative $p'_\varphi(r_\varphi)$ from Eq. (3.31) yields

$$\begin{aligned} \langle T_\varphi \rangle_{ab} = &- \frac{(2\pi)^2}{S_{ab} \Delta r_{ab}} \sum_{\boldsymbol{m}} n \int \mathrm{d}J_\perp \int \mathrm{d}J_\vartheta \\ &\int \mathrm{d}\theta^2 \int_{r_a}^{r_b} \mathrm{d}r \int \mathrm{d}r_\varphi \left| p'_\varphi(r_\varphi) \right| \, \delta(r_c(\theta^2, \boldsymbol{J}) - r) \, Q_{\boldsymbol{m}}(\boldsymbol{J}). \end{aligned} \tag{5.9}$$

The integral over r is resolved via the general relation

$$\int \mathrm{d}\theta^2 \int_{r_a}^{r_b} \mathrm{d}r \int \mathrm{d}r_\varphi \delta(r_c(\theta^2, r_\varphi) - r) g(r_\varphi) = (\theta_b^2 - \theta_a^2) \int \mathrm{d}r_\varphi \begin{cases} g(r_\varphi) & \text{if } r_c \in (r_a, r_b) \\ 0 & \text{otherwise} \end{cases} \tag{5.10}$$

Here we have formally omitted the notation of dependencies on $J_\perp$ and J_ϑ. Regarding the canonical bounce phase θ^2, no explicit dependency remains from Eq. (5.9), making integration trivial. We notice that the term

$$(\theta_b^2 - \theta_a^2) = 2\pi \frac{\Delta \tau_{ab}}{\tau_b} \tag{5.11}$$

measures the fraction of the bounce time τ_b of the full orbit spent between radius r_a and r_b. The evaluation of integrals over r_φ is possible to second-order accuracy via the midpoint rule

$$\int \mathrm{d}r_\varphi g(r_\varphi) \approx \sum_i \Delta r_\varphi^i \, g^i, \tag{5.12}$$

with $g^i = g((r_\varphi^i + r_\varphi^{i-1})/2)$ evaluated at the midpoint of each interval $(r_\varphi^{i-1},\, r_\varphi^i)$. Though not strictly necessary, we choose an equidistant grid with N_r steps, which we use also to define a set of intervals $(r_a,\, r_b)$ for the evaluation of locally volume-averaged torque densities.[1] This simplifies expressions such as Eq. (5.9) by the cancellation of $\Delta r_{ab} = \Delta r_\varphi^i = \Delta r$. In addition, for the special case $\Delta r > \Delta r_c^{\max}$ it leads to orbits that are respectively contained in single intervals $(r_a,\, r_b)$ with r_φ centred in-between and $\Delta\tau_{ab} = \tau_b$, which represents a natural connection to the limiting case of thin orbits. To sum up, the volume-averaged quasilinear toroidal torque density between two sufficiently close flux surfaces a and b of Eq. (5.9) can be represented by

$$\langle T_\varphi \rangle_{ab} = -\frac{(2\pi)^3}{S_{ab}} \sum_{i=1}^{N_r} \frac{\Delta\tau_{ab}}{\tau_b} \left|p_\varphi'^i\right| \sum_{\boldsymbol{m}} n \int \mathrm{d}J_\perp \int \mathrm{d}J_\vartheta\, Q_{\boldsymbol{m}}^i. \tag{5.13}$$

The result is the analogue to Eq. (4.70) for orbit widths that are comparable to the radial perturbation scale. Because of the assumption of sufficiently large-scale equilibrium field it is still possible to formally define radially local transport coefficients as defined in section 4.8 for computations. However, due to the radially non-local nature of the toroidal momentum source in Eq. (5.13), the direct presentation of $\langle T_\varphi \rangle_{ab}$ appears more suited for a straightforward physical interpretation.

5.4 Summary and Outlook

Within this text, a unified description of low-collisional quasilinear and non-linear resonant transport regimes leading to neoclassical viscous torque in tokamak plasmas with non-axisymmetric magnetic perturbations has been developed. The method takes into account the full device geometry and follows from Hamiltonian perturbation theory in action-angle coordinates in combination with kinetic theory. This allows for a physically justifiable transition between quasilinear and non-linear regimes.

The general form of the method has been described independently from the specific problem. Here, the transition of a dimensionless perturbation of the distribution function between quasilinear and non-linear limit has been illustrated. From this general result, a non-linear attenuation factor for the actual problem of toroidal torque has been derived. This factor can be tabulated as a function of a parameter depending on collisionality and perturbation amplitude from a numerical solution of the general form of the dimensionless perturbed kinetic equation.

To allow the application of the method, exact expressions for action-angle variables in a tokamak have been constructed based on the guiding-centre Lagrangian in

[1] Actual computations are performed on an equidistant grid in ψ_{tor} rather than r_{eff} from Eq. (4.16).

straight field line magnetic flux coordinates. For efficient numerical computation of canonical (bounce and drift) frequencies, a first-order expansion in orbit width is employed later. In this formalism, a magnetic shear term, that is absent in the standard local neoclassical ansatz, appears naturally.

The obtained expressions for canonical frequencies and transport coefficients have been validated against existing works analytically and numerically and have been shown to match in the common range of applicability. Based on the Hamiltonian approach, the code NEO-RT has been developed and applied on a model tokamak and ASDEX Upgrade with resonant magnetic perturbations. The features included in the Hamiltonian approach, namely full geometry, magnetic drift, magnetic shear, and non-linear attenuation have been demonstrated to be relevant in those cases. The close match with results from the quasilinear version of the code NEO-2 possessing a full (energy- and momentum-conserving) collision operator verify the theoretical result of the negligible role of momentum conservation in the collision model for resonant transport regimes at sub-sonic toroidal rotation.

A major limitation for the applicability of the method to compute non-linear attenuation are well-separated resonances in phase-space. Close to the zero-crossing of the radial electric field with main contributions from the superbanana resonance, this is the case. Otherwise, for drift-orbit resonances, this can be safely assumed in analogy to the pendulum Hamiltonian as long as the dominant resonances are far from the trapped-passing boundary. If this is not the case, further analysis of the Chirikov criterion on the width and distance of resonances is necessary.

Besides the possible consideration of the effect of finite orbit width on canonical frequencies and angles, further analysis of the radial width of super-orbits is required when approaching the non-linear limit. The used concepts permit also an extension to consider effects from a non-negligible Larmor radius compared to characteristic length scales of the perturbation. In the latter case, the largeness of the gyrofrequency would allow for simplifications while spatial finite-Larmor-radius effects could be fully taken into account. Also, the extension to faster toroidal rotation is possible, where the radial electric field has a non-negligible influence on the parallel motion of the full orbit. Those are possible points to be treated in the future to better judge the range of applicability of the Hamiltonian approach and to balance accuracy against computation time.

Appendix A

Construction of magnetic flux coordinates

Magnetic flux coordinates D'haeseleer et al. (1991) where field lines become straight in coordinate space are required for the formulation of the described methodology formulated on curved magnetic geometries. In this appendix the general form of flux coordinates and their most important properties will be outlined.

A.1 Clebsch Form

The zero-divergence condition for magnetic fields is implicitly given by writing the field in Clebsch form,

$$\boldsymbol{B} = \nabla r \times \nabla \nu. \tag{A.1}$$

Here, r is an arbitrary radial coordinate with $\boldsymbol{B} = \text{const.}$ and $\nu(r, \varphi, \vartheta)$ can be written as a function of r and two angle coordinates φ and ϑ.
The divergence of the magnetic field is then given by

$$\nabla \cdot \boldsymbol{B} = \nabla \cdot (\nabla r \times \nabla \nu) = \underbrace{(\nabla \cdot (\nabla r))}_{=0} \times \nabla \nu + \nabla r \times \underbrace{(\nabla \cdot (\nabla \nu))}_{=0} = 0.$$

Contravariant coordinates are given by first derivatives of the function ν,

$$\boldsymbol{B} = \frac{1}{\sqrt{g}} \varepsilon^{ijk} \left(\partial_i r \partial_j \nu\right) \boldsymbol{e}_k \tag{A.2}$$

$$B^r = 0 \tag{A.3}$$

$$B^\varphi = \frac{1}{\sqrt{g}} \partial_\vartheta \nu \tag{A.4}$$

$$B^\vartheta = -\frac{1}{\sqrt{g}} \partial_\varphi \nu. \tag{A.5}$$

The periodicity condition

$$\boldsymbol{B}(r_0, \varphi, \vartheta) = \boldsymbol{B}(r_0, \varphi + 2\pi, \vartheta) = \boldsymbol{B}(r_0, \varphi, \vartheta + 2\pi) \tag{A.6}$$

can be fulfiled if ν is a sum of linear terms in the angle variables and a periodic function $\tilde{\nu}$,

$$\nu(r, \varphi, \vartheta) = a(r)\varphi + b(r)\vartheta + \tilde{\nu}(r, \varphi, \vartheta) \tag{A.7}$$

For a linear function in φ and ϑ,

$$\nu(r, \varphi, \vartheta) = c(r) + a(r)\varphi + b(r)\vartheta,$$

the gradient is given by

$$\nabla\nu = (c'(r) + a'(r)\varphi + b'(r)\vartheta)\nabla r + a(r)\nabla\varphi + b(r)\nabla\vartheta.$$

The magnetic field (A.1) is still periodic, since

$$\begin{aligned}\nabla r \times \nabla\nu &= (c'(r) + a'(r)\varphi + b'(r)\vartheta)(\underbrace{\nabla r \times \nabla r}_{=0}) + a(r)\nabla r \times \nabla\varphi + b(r)\nabla r \times \nabla\vartheta \\ &= a(r)\nabla r \times \nabla\varphi + b(r)\nabla r \times \nabla\vartheta.\end{aligned}$$

Adding higher terms to ν, e.g. φ^2 results in a non-periodic field in the angle variables,

$$\nabla r \times \nabla(d(r)\varphi^2) = (d'(r)\varphi^2)(\nabla r \times \nabla r) + d(r)\frac{\varphi}{2}\nabla\varphi.$$

A.2 Magnetic flux

Introducing toroidal and poloidal fluxes by integration over toroidal and poloidal surfaces,

$$\psi_{\mathrm{tor}}(r) = \frac{1}{2\pi}\int_{S_{\mathrm{tor}}} \boldsymbol{B}\cdot\mathrm{d}\boldsymbol{S} = \frac{1}{(2\pi)^2}\int_V \boldsymbol{B}\cdot\nabla\varphi\,\mathrm{d}V, \tag{A.8}$$

$$\psi_{\mathrm{pol}}(r) = \frac{1}{2\pi}\int_{S_{\mathrm{pol}}} \boldsymbol{B}\cdot\mathrm{d}\boldsymbol{S} = \frac{1}{(2\pi)^2}\int_V \boldsymbol{B}\cdot\nabla\vartheta\,\mathrm{d}V. \tag{A.9}$$

The equivalence of these volume and surface integrals may be illustrated for a toroidal surface: We cut the torus at a given toroidal surface with $\varphi = 0$ and evaluate the integral

$$\oint_{\mathrm{torus}} \varphi\boldsymbol{B}\cdot\mathrm{d}\boldsymbol{S} = \int_V \nabla(\varphi\boldsymbol{B})\,\mathrm{d}V = \int_V \boldsymbol{B}\cdot\nabla\varphi\,\mathrm{d}V \tag{A.10}$$

along a closed toroidal surface, ending at the cut with $\varphi = 2\pi$ and use Stokes' theorem and $\nabla \cdot \boldsymbol{B} = 0$. The left side can be split into

$$-\int_{\varphi=0} \varphi \boldsymbol{B} \cdot \mathrm{d}\boldsymbol{S} + \int_{S_{\mathrm{torus}}} \varphi \boldsymbol{B} \cdot \mathrm{d}\boldsymbol{S} + \int_{\varphi=2\pi} \varphi \boldsymbol{B} \cdot \mathrm{d}\boldsymbol{S}.$$

The first term vanishes because of $\varphi = 0$, the second term because of the field lines of $\boldsymbol{B}$ going along the toroidal surface. The remaining term

$$\int_{\varphi=2\pi} \varphi \boldsymbol{B} \cdot \mathrm{d}\boldsymbol{S} = 2\pi \int_{S_{\mathrm{tor}}} \boldsymbol{B} \cdot \mathrm{d}\boldsymbol{S}$$

for the toroidal surface S_{tor} at $\varphi = 2\pi$ can thus be expressed by the volume integral (A.10).

The fluxes (A.8) and (A.9) correspond to the functions $a(r)$ and $b(r)$: The first derivative of the toroidal flux with respect to r is

$$\begin{aligned}
\psi'_{\mathrm{tor}}(r) = \frac{\mathrm{d}\psi_{\mathrm{tor}}}{\mathrm{d}r} &= \frac{1}{(2\pi)^2} \frac{\mathrm{d}}{\mathrm{d}r} \int_0^r \mathrm{d}r' \int_0^{2\pi} \mathrm{d}\varphi \int_0^{2\pi} \mathrm{d}\vartheta \sqrt{g} \boldsymbol{B} \cdot \nabla \varphi \\
&= \frac{1}{(2\pi)^2} \int_0^{2\pi} \mathrm{d}\varphi \int_0^{2\pi} \mathrm{d}\vartheta \sqrt{g} \boldsymbol{B} \cdot \nabla \varphi \\
&= \frac{1}{(2\pi)^2} \int_0^{2\pi} \mathrm{d}\varphi \int_0^{2\pi} \mathrm{d}\vartheta \sqrt{g} B^{\varphi} \\
&= \frac{1}{(2\pi)^2} \int_0^{2\pi} \mathrm{d}\varphi \int_0^{2\pi} \mathrm{d}\vartheta \partial_{\vartheta} \nu \\
&= \frac{1}{(2\pi)^2} \int_0^{2\pi} \mathrm{d}\varphi \int_0^{2\pi} \mathrm{d}\vartheta \left(b(r) + \partial_{\vartheta} \tilde{\nu}(r, \varphi, \vartheta) \right).
\end{aligned}$$

Since the integral over the second term vanishes, we can identify

$$\psi'_{\mathrm{tor}}(r) = b(r).$$

Similarly, it can be shown that

$$\psi'_{\mathrm{pol}} = -a(r)$$

and finally, 120 can be written as

$$\nu(r, \varphi, \vartheta) = \psi'_{\mathrm{tor}}(r)\vartheta - \psi'_{\mathrm{pol}}(r)\varphi + \tilde{\nu}(r, \varphi, \vartheta). \tag{A.11}$$

A.3 Transformation to flux coordinates

If $\tilde{\nu}$ vanishes, the coordinates (r, φ, ϑ) are called flux coordinates and the magnetic field can be written in the simple form

$$\begin{aligned}\boldsymbol{B} &= \nabla\varphi \times \nabla\psi_{\mathrm{pol}}(r) + \nabla\psi_{\mathrm{tor}}(r) \times \nabla\vartheta \\ &= -\psi'_{\mathrm{pol}}(r)\nabla r \times \nabla\varphi + \psi'_{\mathrm{tor}}(r)\nabla r \times \nabla\vartheta \\ &= \nabla r \times \nabla(\psi'_{\mathrm{tor}}(r)\vartheta - \psi'_{\mathrm{pol}}(r)\varphi). \\ &= \frac{\psi'_{\mathrm{pol}}(r)}{\sqrt{g}}\boldsymbol{E}_\vartheta + \frac{\psi'_{\mathrm{tor}}(r)}{\sqrt{g}}\boldsymbol{E}_\varphi. \end{aligned} \tag{A.12}$$

In flux coordinates, magnetic field lines are straight lines due to

$$B^\varphi = qB^\vartheta, \tag{A.13}$$

where q is known as the the safety factor, given by the ratio

$$q = \frac{\psi'_{\mathrm{tor}}(r)}{\psi'_{\mathrm{pol}}(r)}. \tag{A.14}$$

A corresponding vector potential is given by

$$\boldsymbol{A}(r) = \psi_{\mathrm{tor}}(r)\nabla\vartheta - \psi_{\mathrm{pol}}(r)\nabla\varphi. \tag{A.15}$$

Although it would be straightforward to use a vector potential

$$\boldsymbol{A} = -\nu(r)\nabla r,$$

this form has the problem of non-uniqueness with respect to the angular coordinates.

Transformation from non-flux coordinates to flux coordinates is possible by a change of one of the two angle coordinates that cancel out the periodic part in (A.11), either

$$\vartheta = \vartheta_0 + \frac{\tilde{\nu}(\rho, \varphi, \vartheta)}{\psi'_{\mathrm{tor}}(r)} \tag{A.16}$$

or

$$\varphi = \varphi_0 - \frac{\tilde{\nu}(\rho, \varphi, \vartheta)}{\psi'_{\mathrm{pol}}(r)}. \tag{A.17}$$

Appendix B

Analytical comparison to existing results

Results for quasilinear diffusion in the superbanana plateau regime have been published by Shaing et al. (2009b) for the large-aspect-ratio approximation with circular flux surfaces and in Shaing (2015) for arbitrary tokamak geometries. The resonant plateau regime by bounce-transit and drift resonances has been analysed in Shaing et al. (2009a) for the large-aspect-ratio limit with circular flux surfaces. In those works, Hamada coordinates are used with the normalized enclosed volume $r = \hat{V} = V/4\pi^2$ as the radial variable, metric determinant $\sqrt{g_H} = 1$ and contravariant components of the magnetic field constant on a flux surface with $B^\vartheta = \psi'_{\mathrm{pol}}$, $B^\varphi = \psi'_{\mathrm{tor}}$. This leads to a specific form of a number of formulas, including the bounce average 3.90 omitting the sign σ with

$$\tau_b = \oint \frac{\mathrm{d}\vartheta}{v_\parallel h^\vartheta} = \oint \mathrm{d}\vartheta \frac{B}{v_\parallel \psi'_{\mathrm{pol}}}\,, \tag{B.1}$$

$$\langle a \rangle_b = \oint \mathrm{d}\vartheta \frac{a}{v_\parallel h^\vartheta} = \oint \mathrm{d}\vartheta \frac{B}{v_\parallel \psi'_{\mathrm{pol}}} a\,. \tag{B.2}$$

B.1 Toroidal drift frequencies

First, we compare the present toroidal drift frequencies to the ones given by Shaing (2015). Formula (10) of this reference contains the bounce averaged toroidal drift frequency as defined in (3.102), which, in our notation, is written as

$$\Omega_{tE} = \frac{c\Phi'}{\psi'_{\mathrm{pol}}}, \tag{B.3}$$

$$\langle \Omega_{tB} \rangle_b = -\frac{1}{\psi'_{\mathrm{pol}}} \left\langle \frac{J_\perp \omega_c + m v_\parallel^2}{m\omega_c} \frac{\partial B}{\partial r} - \frac{v_\parallel^2}{\omega_c} \frac{1}{B} \frac{\partial (B^2)}{\partial r} + \frac{v_\parallel^2}{\omega_c} \frac{\psi''_{\mathrm{pol}}}{\psi'_{\mathrm{pol}}} B \right\rangle_b . \tag{B.4}$$

The pressure P has been set to zero here, since we consider orbits directly in the actual equilibrium where finite β effects are implicitly included. Shaing defines the magnetic moment μ without mass, which leads to the additional factor when changing to the notation using the perpendicular invariant $J_1 = J_\perp$. In addition, the signs are swapped due to the definition of the toroidal angle φ_0 in the opposite direction. Using $B^2 = B^\vartheta \left(B_\vartheta + qB_\varphi\right)$ we can write

$$\begin{aligned}\psi''_{\mathrm{pol}} &= \frac{\mathrm{d}B^\vartheta}{\mathrm{d}r} = \frac{\mathrm{d}}{\mathrm{d}r}\left(\frac{B^2}{B_\vartheta + qB_\varphi}\right) \\ &= -\frac{B^2}{\left(B_\vartheta + qB_\varphi\right)^2}\frac{\partial}{\partial r}\left(B_\vartheta + qB_\varphi\right) + \frac{1}{B_\vartheta + qB_\varphi}\frac{\partial(B^2)}{\partial r} \\ &= -\frac{1}{B_\vartheta + qB_\varphi}\left(B^\vartheta \frac{\partial}{\partial r}\left(B_\vartheta + qB_\varphi\right) + \frac{\partial(B^2)}{\partial r}\right). \end{aligned} \tag{B.5}$$

Also,

$$\begin{aligned}\frac{\psi''_{\mathrm{pol}}}{\psi'_{\mathrm{pol}}}B &= \frac{B}{B^\vartheta\left(B_\vartheta + qB_\varphi\right)}\left(-B^\vartheta\frac{\partial}{\partial r}\left(B_\vartheta + qB_\varphi\right) + \frac{\partial(B^2)}{\partial r}\right) \\ &= \frac{1}{B}\left(-B^\vartheta\frac{\partial}{\partial r}\left(B_\vartheta + qB_\varphi\right) + \frac{\partial(B^2)}{\partial r}\right). \end{aligned} \tag{B.6}$$

The last term cancels out with the middle term in Eq. (B.4), so we obtain

$$\langle\Omega_{tB}\rangle_b = \frac{1}{\psi'_{\mathrm{pol}}}\left\langle -\frac{J_\perp\omega_c + mv_\parallel^2}{m\omega_c}\frac{\partial B}{\partial r} + \frac{v_\parallel^2}{\omega_c}h^\vartheta\left(\frac{\partial B_\vartheta}{\partial r} - q\frac{\partial B_\varphi}{\partial r} - \frac{\mathrm{d}q}{\mathrm{d}r}B_\varphi\right)\right\rangle_b \tag{B.7}$$

which is identical to the bounce-averaged magnetic drift frequency in Eq. (3.105). In particular, the radial derivative of the safety factor (magnetic shear) is present as it appears in the second derivative in the poloidal flux ψ''_{pol} in Eq. (B.4).

B.2 Bounce integrals in the large-aspect-ratio limit

For a circular concentric flux surface, the unperturbed magnetic field modulus is written as

$$B = B_a(1 - \varepsilon\cos\vartheta)\,, \tag{B.8}$$

with magnetic field modulus B_a on axis and aspect ratio ε relating flux surface minor radius to the device major radius. With $\kappa = k^2$ from Shaing et al. (2009a), bounce integrals are given by

$$\int\frac{\mathrm{d}\vartheta}{v_\parallel h^\vartheta}a(\vartheta) = \sqrt{\frac{m_\alpha}{4\mu B_a\varepsilon}}\frac{1}{\psi'_{\mathrm{pol}}}\int\mathrm{d}\vartheta\,\frac{B_a(1-\varepsilon\cos\vartheta)}{\sqrt{\kappa - \sin^2\frac{\vartheta}{2}}}a(\vartheta)\,. \tag{B.9}$$

In the large aspect ratio limit the ε term is neglected and the bounce time in Eq. (B.1) for trapped particles becomes

$$\begin{aligned}\tau_b &= \sqrt{\frac{m_\alpha}{4\mu B_a \varepsilon}} \frac{B_a}{\psi'_{\mathrm{pol}}} \oint \frac{\mathrm{d}\vartheta}{\sqrt{\kappa - \sin^2 \frac{\vartheta}{2}}} \\ &= \sqrt{\frac{m_\alpha}{\mu B_a \varepsilon}} \frac{B_a}{\psi'_{\mathrm{pol}}} 4K(\kappa)\,. \end{aligned} \tag{B.10}$$

Here the integral is performed over the full orbit, so twice between the turning points defined by

$$\sin^2 \frac{\vartheta^\pm}{2} = \kappa \tag{B.11}$$

$$\Rightarrow \vartheta^\pm = \pm 2 \arcsin \sqrt{\kappa}\,. \tag{B.12}$$

($0 < \kappa < 1$ for trapped particles). In the notation of Shaing, a bounce integral is performed just once between ϑ^+ and ϑ^-. Finally we obtain an expression for bounce averaging in the large aspect ratio as

$$\langle a \rangle_b = \frac{1}{4K(\kappa)} \int_{\vartheta^-}^{\vartheta^+} \frac{\mathrm{d}\vartheta\, a(\vartheta)}{\sqrt{\kappa - \sin^2 \frac{\vartheta}{2}}}\,. \tag{B.13}$$

This means that we have to replace $K(\kappa)$ in the formulas of Shaing et al. (2009a) by

$$K(\kappa) = \frac{\tau_b}{4} \sqrt{\frac{\mu B_a \varepsilon}{m_\alpha}} \frac{\psi'_{\mathrm{pol}}}{B_a} \tag{B.14}$$

to translate to the notation of the present work.

The bounce integration for passing particles is formally identical to trapped particles but performed over the full range in ϑ where $v_\parallel$ doesn't change sign ($\kappa > 1$) .

Using the same approximation as in Eq. (B.10), the bounce (transit) time for passing particles is

$$\begin{aligned}\tau_b = \frac{4K(\kappa^{-1})}{\kappa} &\sqrt{\frac{m_\alpha}{4\mu B_a \varepsilon}} \frac{B_a}{\psi'_{\mathrm{pol}}} \\ &\sqrt{\frac{m_\alpha}{\mu B_a \varepsilon}} \frac{B_a}{\psi'_{\mathrm{pol}}} \frac{2K(\kappa^{-1})}{\sqrt{\kappa}}\,. \end{aligned} \tag{B.15}$$

in the large-aspect-ratio limit. Due to the mathematical equivalence of the guiding-centre motion in the large-aspect-ratio limit with circular, concentric flux surfaces to the particle in a cosine potential (pendulum), those bounce times represent an exact analogy to the ones in section 1.3, differing only by a normalisation factor.

For integrations we use the transformations

$$x = u^2, \tag{B.16}$$

$$\mathrm{d}x = 2u\,\mathrm{d}u, \tag{B.17}$$

$$v_\parallel^2 = 4\frac{\mu B_a \varepsilon}{m_\alpha}\left(\kappa - \sin^2\frac{\vartheta}{2}\right) = (1-\eta B_0)u^2 v_T^2, \tag{B.18}$$

$$\kappa = \frac{H_0 - e_\alpha\Phi - \mu B_a(1-\varepsilon)}{2\mu B_a \varepsilon} \tag{B.19}$$

with

$$\mu = \frac{mu^2}{2}v_t^2\eta = \frac{mx}{2}v_t^2\eta. \tag{B.20}$$

We get

$$\kappa = \frac{1-\eta B_a(1-\varepsilon)}{2\eta B_a\varepsilon} \tag{B.21}$$

$$= \frac{1/\eta - B_a(1-\varepsilon)}{2B_a\varepsilon}. \tag{B.22}$$

The derivative is

$$\frac{\mathrm{d}\kappa}{\mathrm{d}\eta} = -\frac{1}{2\eta^2 B_a\varepsilon}. \tag{B.23}$$

From this section it is clear that we can use expressions (8) and (33) of Shaing et al. (2009a) as the equivalent to the poloidal canonical angle of Eq. (3.76) here. Using the variable transformation for integrals in velocity space allows us to translate from viscous coefficients μ_{ij} in the reference to our expressions for transport coefficients D_{ij} of Eq. (4.84), what will be done in the following section.

B.3 Eulerian approach to drift-orbit resonances

Shaing et al. (2009a) constructs the Eulerian approach for drift-orbit resonances neglecting magnetic drifts. We write the drift-kinetic equation with mass flow as in Shaing and Spong (1990); Shaing (1990) referring to Hazeltine and Ware (1978) as

$$(\boldsymbol{v}_\parallel + \boldsymbol{v}_d + \boldsymbol{V})\cdot\nabla f + \dot{w}\frac{\partial f}{\partial w} = C(f), \tag{B.24}$$

where the velocity space coordinates are $w = v^2/2$ and $\mu = v_\perp^2/(2B)$. The parallel velocity is given by $\boldsymbol{v}_\parallel = v_\parallel \boldsymbol{b} = \sqrt{(1/2-\mu B)w}\boldsymbol{b}$. (In the review paper Shaing et al.

(2015) this is Eq. (6.4.1) where the $\dot{w}$ is a typo in the partial derivative denominator). The drift velocity is Hazeltine and Ware (1978)

$$\begin{aligned}\boldsymbol{v}_d = &\frac{\mathbf{F}\times\boldsymbol{b}}{\omega_{c\alpha}} + \frac{\mu B\boldsymbol{b}}{m_\alpha\omega_{c\alpha}}\left(\frac{J_\parallel}{B}\right) + \frac{\boldsymbol{b}}{\omega_{c\alpha}}\times \\ &\Big(\mu\nabla B + (\boldsymbol{v}_\parallel\cdot\nabla)\boldsymbol{V} + (\boldsymbol{V}\cdot\nabla)\boldsymbol{v}_\parallel + v_\parallel^2(\boldsymbol{b}\cdot\nabla)\boldsymbol{b}\Big)\end{aligned} \tag{B.25}$$

with the normalised external force $\mathbf{F}$ as the third term in the momentum equation in addition to Lorentz force and fluid inertia $m_\alpha D\boldsymbol{V}/Dt$ given by

$$\mathbf{F} = \frac{e_\alpha}{m_\alpha}(\mathbf{E} + \frac{1}{c}\boldsymbol{V}\times\boldsymbol{B}) - \frac{\partial\boldsymbol{V}}{\partial t} - \boldsymbol{V}\cdot\nabla\boldsymbol{V}. \tag{B.26}$$

$\mathbf{F}$ consists of the pressure gradient and collisional forces $\mathbf{R}$ with

$$\mathbf{F} = \frac{\nabla p_\alpha}{n_\alpha m_\alpha} + \frac{\mathbf{R}}{n_\alpha m_\alpha}. \tag{B.27}$$

The change in time of the normalised kinetic energy w up to first order in gyroradius is

$$\begin{aligned}\dot{w} = &\mathbf{F}\cdot\boldsymbol{v}_\parallel - \mu B\nabla\cdot\boldsymbol{V} - (v_\parallel^2 - \mu B)(\boldsymbol{b}\cdot(\boldsymbol{b}\cdot\nabla)\boldsymbol{V}) \\ &+ \boldsymbol{v}_d\cdot\mathbf{F} - (\mu B/\omega_{c\alpha})\boldsymbol{b}\cdot\nabla\times\mathbf{F}.\end{aligned} \tag{B.28}$$

The total distribution function is written as

$$f = f_M\left(1 - (2v_\parallel/v_{T\alpha}^2)(1 - \frac{4}{5}\frac{w}{v_{T\alpha}^2})\frac{q_\parallel}{p_\alpha}\right) + g \tag{B.29}$$

with parallel heat flow $q_\parallel$, thermal velocity $v_{T\alpha} = \sqrt{2T_\alpha/m_\alpha}$ and pressure $p_\alpha = n_\alpha T_\alpha$. For the Maxwellian

$$f_M = \frac{n_\alpha}{(\pi v_{t\alpha})^3}\exp(-2w/v_{t\alpha}^2) \tag{B.30}$$

we have the derivatives

$$\nabla f_M = 0, \tag{B.31}$$

$$\frac{\partial f_M}{\partial w} = -\frac{2}{v_{T\alpha}^2}f_M, \tag{B.32}$$

$$\begin{aligned}\nabla f = &f_M\left(1 - (2v_\parallel/v_{t\alpha}^2)(1 - \frac{4}{5}\frac{w}{v_{T\alpha}^2})\nabla\left(\frac{q_\parallel}{p_\alpha}\right)\right) + \nabla g \\ \frac{\partial f}{\partial w} = &-\frac{2}{v_{T\alpha}^2}f_M + \frac{\partial g}{\partial w} \\ &+ (2v_\parallel/v_{t\alpha}^2)(1 - \frac{4}{5}\frac{w}{v_{T\alpha}^2})\frac{q_\parallel}{p_\alpha}f_M \\ &- \frac{4}{5}(2v_\parallel/v_{t\alpha}^2)\frac{q_\parallel}{p_\alpha v_{t\alpha}^2}f_M + \frac{2}{v_t^2}\frac{\partial v_\parallel}{\partial w}(1 - \frac{4}{5}\frac{w}{v_{t\alpha}^2})f_M \\ &+ (2v_\parallel/v_{T\alpha}^2)(1 - \frac{4}{5}\frac{w}{v_{T\alpha}^2})\frac{\partial}{\partial w}\left(\frac{q_\parallel}{p_\alpha}\right)f_M.\end{aligned} \tag{B.33}$$

Of course, for the Maxwellian $C(f_M) = 0$. For now, we ignore the terms related to the heat flux and write

$$(\boldsymbol{v}_\parallel + \boldsymbol{v}_d + \boldsymbol{V}) \cdot \nabla g + \dot{w}\frac{\partial g}{\partial w} - C(g) = -\frac{2}{v_{t\alpha}^2} f_M \cdot (\mathbf{F} \cdot \boldsymbol{v}_\parallel - \mu B \nabla \cdot \boldsymbol{V} - (v_\parallel^2 - \mu B)(\boldsymbol{b} \cdot (\boldsymbol{b} \cdot \nabla)\boldsymbol{V}) + \boldsymbol{v}_d \cdot \mathbf{F} - (\mu B/\omega_{c\alpha})\boldsymbol{b} \cdot \nabla \times \mathbf{F}) - C(f_M). \quad \text{(B.34)}$$

$C(f_M)$ is not zero for finite $\boldsymbol{V}$. The first term arising from in $\dot{w}\frac{\partial f_M}{\partial w}$ is

$$-\frac{2v_\parallel}{v_{T\alpha}^2}\frac{\boldsymbol{b} \cdot \mathbf{R}}{n_\alpha m_\alpha} f_M = -v_\parallel \frac{\boldsymbol{b} \cdot \mathbf{R}}{p_\alpha} f_M$$

and should cancel $C(f_M)$. The remaining assumptions are $\nabla p_\alpha \cdot \boldsymbol{b} = 0$, $\nabla p_\alpha \times \nabla T_\alpha = 0$, $\nabla \cdot \boldsymbol{V} = 0$, $\nabla \boldsymbol{q} = 0$ and neglecting viscous forces. The remaining term is $(v_\parallel^2 - \mu B)(\boldsymbol{b} \cdot (\boldsymbol{b} \cdot \nabla)\boldsymbol{V})$. We write

$$\begin{aligned} v_\parallel^2 - \mu B &= v_\parallel^2 - \frac{v^2 - v_\parallel^2}{2} \\ &= \frac{3}{2}v_\parallel^2 - \frac{1}{2}v^2 \\ &= -v^2\left(\frac{1}{2} - \frac{3}{2}\frac{v_\parallel^2}{v^2}\right). \end{aligned} \quad \text{(B.35)}$$

Finally

$$(\boldsymbol{v}_\parallel + \boldsymbol{v}_d + \boldsymbol{V}) \cdot \nabla g + \dot{w}\frac{\partial g}{\partial w} - C(g) = \frac{2v^2}{v_{T\alpha}^2}\left(\frac{1}{2} - \frac{3}{2}\frac{v_\parallel^2}{v^2}\right)(\boldsymbol{b} \cdot (\boldsymbol{b} \cdot \nabla)\boldsymbol{V}) f_M. \quad \text{(B.36)}$$

We note that for $\nabla \cdot \boldsymbol{V} = 0$ and $\nabla \cdot \boldsymbol{B} = 0$

$$\boldsymbol{b} \cdot (\boldsymbol{b} \cdot \nabla)\boldsymbol{V} = \frac{1}{B}\boldsymbol{V} \cdot \nabla B. \quad \text{(B.37)}$$

Including heat fluxes, the final expression is

$$(\boldsymbol{v}_\parallel + \boldsymbol{v}_d + \boldsymbol{V}) \cdot \nabla g + \dot{w}\frac{\partial g}{\partial w} - C(g) = \frac{2v^2}{v_{T\alpha}^2}\left(\frac{1}{2} - \frac{3}{2}\frac{v_\parallel^2}{v^2}\right)\left(\frac{\boldsymbol{V} \cdot \nabla B}{B} - (2v_\parallel/v_{T\alpha}^2)(1 - \frac{4}{5}\frac{w}{v_{T\alpha}^2})\frac{\boldsymbol{q} \cdot \nabla B}{B p_\alpha}\right) f_M. \quad \text{(B.38)}$$

In Shaing et al. (2009a), Eq. (3), the flow velocity is split into parallel and perpendicular part from $\mathbf{E} \times \boldsymbol{B}$ drift and $\boldsymbol{v}_d \cdot \nabla g$ is neglected, with

$$(\boldsymbol{v}_\parallel + \boldsymbol{v}_d + \boldsymbol{V}) \cdot \nabla g \approx ((v_\parallel + V_\parallel)\boldsymbol{b} + \boldsymbol{V}_E) \cdot \nabla g. \quad \text{(B.39)}$$

Derivations by Shaing are done in Hamada coordinates. We translate the normalised volume coordinate $\hat{V} = V/4\pi^2$ (used by Shaing to get $\sqrt{g_H} = 1$ and called V there) to the normalised flux s as the radial coordinate with

$$\psi'(V) = \psi'_{\rm tor}(s)\frac{ds}{d\hat{V}} = q(s)\psi'_{\rm pol}(s)\frac{ds}{d\hat{V}}, \tag{B.40}$$

$$\chi'(V) = \psi'_{\rm pol}(s)\frac{ds}{d\hat{V}}. \tag{B.41}$$

Primes on ψ and χ are defined w.r.t. V, otherwise to s. In Kasilov et al. (2014) velocity components are listed as

$$\begin{aligned} V^\vartheta &= \frac{ckB_\varphi}{e_\alpha\sqrt{g}\,\langle B^2\rangle}\frac{\partial T_\alpha}{\partial s} \\ &= \frac{ckB_\varphi T_\alpha}{e_\alpha\sqrt{g}\,\langle B^2\rangle}A_2, \end{aligned} \tag{B.42}$$

$$\begin{aligned} V^\varphi &= \frac{c}{\sqrt{g}B^\vartheta}\left(-\frac{\partial\Phi}{\partial s} - \frac{1}{e_\alpha n_\alpha}\frac{\partial p_\alpha}{\partial s}\right) + qV^\vartheta \\ &= -\frac{c}{\sqrt{g}B^\vartheta}\frac{T_\alpha}{e_\alpha}\left(\frac{e_\alpha}{T_\alpha}\frac{\partial\Phi}{\partial s} + \frac{1}{n_\alpha}\frac{\partial n_\alpha}{\partial s} + \frac{1}{T_\alpha}\frac{\partial T_\alpha}{\partial s}\right) + qV^\vartheta \\ &= -\frac{c}{\psi'_{\rm pol}}\frac{T_\alpha}{e_\alpha}\left(A_1 + \frac{5}{2}A_2\right)/\left\langle|\nabla s|\right\rangle + q\frac{ckB_\varphi T_\alpha}{e_\alpha\sqrt{g}\,\langle B^2\rangle}A_2/\left\langle|\nabla s|\right\rangle. \end{aligned} \tag{B.43}$$

Here, thermodynamic forces are defined as

$$A_1/\left\langle|\nabla s|\right\rangle = \frac{1}{n_\alpha}\frac{\partial n_\alpha}{\partial s} + \frac{e_\alpha}{T_\alpha}\frac{\partial\Phi}{\partial s} - \frac{3}{2}\frac{1}{T_\alpha}\frac{\partial T_\alpha}{\partial s} = \frac{1}{p_\alpha}\frac{\partial p_\alpha}{\partial s} + \frac{e_\alpha}{T_\alpha}\frac{\partial\Phi}{\partial s} - \frac{5}{2}\frac{1}{T_\alpha}\frac{\partial T_\alpha}{\partial s}, \tag{B.44}$$

$$A_2/\left\langle|\nabla s|\right\rangle = \frac{1}{T_\alpha}\frac{\partial T_\alpha}{\partial s}. \tag{B.45}$$

Notice that

$$\frac{1}{p_\alpha}\frac{\partial p_\alpha}{\partial s} = \frac{1}{n_\alpha T_\alpha}\frac{\partial}{\partial s}(n_\alpha T_\alpha) = \frac{1}{n_\alpha}\frac{\partial n_\alpha}{\partial s} + \frac{1}{T_\alpha}\frac{\partial T_\alpha}{\partial s}. \tag{B.46}$$

The validity of (B.42) and (B.43) arises from the divergence-free plasma flow velocity $\mathbf{V}$ which is given by Shaing et al. (2010)

$$\boldsymbol{V} = V_\parallel\boldsymbol{h} + \boldsymbol{V}_\perp, \tag{B.47}$$

$$\boldsymbol{V}_\perp = c\frac{\boldsymbol{b}\times\nabla\Phi}{B^2} + c\frac{\boldsymbol{b}\times\nabla p_\alpha}{Ne_\alpha B^2}. \tag{B.48}$$

Its components are related to the gradients and thus to thermodynamic forces with

$$-\frac{e_\alpha}{cT_\alpha}\left(\chi'(\hat{V})V^\varphi - \psi'(\hat{V})V^\vartheta\right) = \frac{1}{p_\alpha}\frac{\partial p_\alpha}{\partial\hat{V}} + \frac{e_\alpha}{T_\alpha}\frac{\partial\Phi}{\partial\hat{V}}, \tag{B.49}$$

so in our notation

$$\begin{aligned}\frac{e_\alpha}{cT_\alpha}\left(\psi'_{\rm pol}(s)V^\varphi-\psi'_{\rm tor}(s)V^\vartheta\right)&=\frac{1}{p_\alpha}\frac{\partial p_\alpha}{\partial s}+\frac{e_\alpha}{T_\alpha}\frac{\partial\Phi}{\partial s}\\&=\frac{1}{n_\alpha T_\alpha}\frac{\partial}{\partial s}(nT_\alpha)+\frac{e_\alpha}{T_\alpha}\frac{\partial\Phi}{\partial s}\\&=\frac{1}{n_\alpha}\frac{\partial n_\alpha}{\partial s}+\frac{1}{T_\alpha}\frac{\partial T_\alpha}{\partial s}+\frac{e_\alpha}{T_\alpha}\frac{\partial\Phi}{\partial s}.\end{aligned}\tag{B.50}$$

we obtain

$$\frac{e_\alpha}{cT_\alpha}\psi'_{\rm pol}\left(qV^\vartheta-V^\varphi\right)\langle|\nabla s|\rangle=A_1+\frac{5}{2}A_2,\tag{B.51}$$

which is in accordance with the above results. Shaing et al. (2009a) define coefficients μ for the neoclassical toroidal plasma viscosity by

$$\langle\boldsymbol{b}_t\cdot\nabla\cdot\boldsymbol{\pi}\rangle=\mu_{p1}\boldsymbol{V}\cdot\nabla\vartheta+\mu_{t1}\boldsymbol{V}\cdot\nabla\varphi+\frac{2}{5}\mu_{p2}\frac{\boldsymbol{q}\cdot\nabla\vartheta}{p_\alpha}+\frac{2}{5}\mu_{t2}\frac{\boldsymbol{q}\cdot\nabla\varphi}{p_\alpha}.\tag{B.52}$$

The task is, to relate μ coefficients to D_{11} and D_{12}. We use the flux-force relation Shaing et al. (2009b)

$$\Gamma=\frac{c}{e_\alpha\chi'\psi'}\langle\boldsymbol{b}_t\cdot\nabla\cdot\boldsymbol{\pi}\rangle\tag{B.53}$$

and neglect the smaller last two terms containing heat fluxes in (B.52) to write

$$\frac{c}{e_\alpha q\psi'^2_{\rm pol}}\left(\mu_{p1}V^\vartheta+\mu_{t1}V^\varphi\right)\left(\frac{d\hat{V}}{ds}\right)^2=-n_\alpha(D_{11}A_1+D_{12}A_2).\tag{B.54}$$

$$=\frac{c}{e_\alpha q\chi'^2}\left(\mu_{p1}V^\vartheta+\mu_{t1}V^\varphi\right)\tag{B.55}$$

We insert expressions (B.42) and (B.43) to obtain

$$\begin{aligned}D_{11}A_1+D_{12}A_2=\left(\frac{d\hat{V}}{ds}\right)^2\frac{1}{\langle|\nabla s|\rangle}\Bigg[&-\mu_{p1}\frac{1}{q\psi'^2_{\rm pol}}\frac{c^2kB_\varphi T_\alpha}{n_\alpha e_\alpha^2\sqrt{g}\,\langle B^2\rangle}A_2\\&+\mu_{t1}\frac{c^2}{q\psi'^3_{\rm pol}}\frac{T_\alpha}{n_\alpha e_\alpha^2}\left(A_1+\frac{5}{2}A_2\right)-\mu_{t1}\frac{1}{\psi'^2_{\rm pol}}\frac{c^2kB_\varphi T_\alpha}{n_\alpha e_\alpha^2\sqrt{g}\,\langle B^2\rangle}A_2\Bigg].\end{aligned}\tag{B.56}$$

So for the coefficients we have

$$D_{11} = \left(\frac{d\hat{V}}{ds}\right)^2 \frac{1}{\langle|\nabla s|\rangle} \frac{c^2 T_\alpha}{n_\alpha e_\alpha^2 q \psi'^3_{\rm pol}} \mu_{t1} \equiv A\mu_{t1}, \tag{B.57}$$

$$D_{12} = \left(\frac{d\hat{V}}{ds}\right)^2 \frac{1}{\langle|\nabla s|\rangle} \left[-\frac{1}{q\psi'^2_{\rm pol}} \frac{c^2 k B_\varphi T_\alpha}{n_\alpha e_\alpha^2 \sqrt{g}\,\langle B^2\rangle} \mu_{p1} + \left(\frac{5}{2} \frac{c^2 T_\alpha}{n_\alpha e_\alpha^2 q \psi'^3_{\rm pol}} - \frac{1}{\psi'^2_{\rm pol}} \frac{c^2 k B_\varphi T_\alpha}{n_\alpha e_\alpha^2 \sqrt{g}\,\langle B^2\rangle} \right) \mu_{t1} \right] \tag{B.58}$$

$$\equiv C\mu_{p1} + \left(\frac{5}{2}A - qC\right)\mu_{t1} \tag{B.59}$$

$$= C\mu_{p1} + \left(\frac{5}{2} - q\frac{C}{A}\right) D_{11} \tag{B.60}$$

with

$$A = \left(\frac{d\hat{V}}{ds}\right)^2 \frac{1}{\langle|\nabla s|\rangle} \frac{c^2 T_\alpha}{n_\alpha e_\alpha^2 q \psi'^3_{\rm pol}}, \tag{B.61}$$

$$C = -\left(\frac{d\hat{V}}{ds}\right)^2 \frac{1}{\langle|\nabla s|\rangle} \frac{1}{q\psi'^2_{\rm pol}} \frac{c^2 k B_\varphi T_\alpha}{n_\alpha e_\alpha^2 \sqrt{g}\,\langle B^2\rangle}. \tag{B.62}$$

In the following section, we will explicitly compare Eq. (4.84) to Eq. (27) of Shaing et al. (2009b).

B.4 Transport coefficients for bounce-drift resonances

Using the large-aspect ratio expressions for bounce resonances, we can transform transport coefficients from the quasilinear Hamiltonian formalism to

$$D_{1k} = \frac{\pi^{3/2} n^2 c^2 v_T}{e_\alpha^2 \langle|\nabla s|\rangle^2 \psi'_{\rm pol}(s)} \frac{ds}{dV} \int_0^\infty du \tag{B.63}$$

$$u^3 e^{-u^2} \sum_{m_2} \sum_{\rm res} \left(\tau_b |H_{\mathbf{m}}|^2 \left| m_2 \frac{\partial \omega_b}{\partial \eta} + n \frac{\partial \Omega^3}{\partial \eta} \right|^{-1} \right)_{\eta=\eta_{\rm res}} w_k$$

$$= \frac{1}{4\sqrt{\pi}} \frac{n^2 c^2 v_T B_a}{e_\alpha^2 \langle|\nabla s|\rangle^2 \psi'^2_{\rm pol}} \int_0^\infty du$$

$$\sqrt{\frac{m_\alpha}{\mu B_a \varepsilon}} u^3 e^{-u^2} \sum_{m_2} \sum_{\rm res} \left(4K(\kappa) |H_{\mathbf{m}}|^2 \left| m_2 \frac{\partial \omega_b}{\partial \eta} + n \frac{\partial \Omega^3}{\partial \eta} \right|^{-1} \right)_{\eta=\eta_{\rm res}} w_k$$

$$= \frac{1}{2\sqrt{\pi}} \frac{n^2 c^2 v_T B_a}{e_\alpha^2 \langle|\nabla s|\rangle^2 \chi'^2} \left(\frac{ds}{d\hat{V}}\right)^2 \int_0^\infty dx$$

$$\sqrt{\frac{m_\alpha}{\mu B_a \varepsilon}} x e^{-x} \sum_{m_2} \sum_{\rm res} \left(K(\kappa) |H_{\mathbf{m}}|^2 \left| m_2 \frac{\partial \omega_b}{\partial \eta} + n \frac{\partial \Omega^3}{\partial \eta} \right|^{-1} \right)_{\eta=\eta_{\rm res}} w_k.$$

The derivative in the resonance condition is

$$\begin{aligned}\frac{\partial}{\partial\eta}\left(n\Omega_{tE}+m_2\omega_b\right) &= \frac{\partial\kappa}{\partial\eta}\frac{\partial}{\partial\kappa}\left(-n\frac{c}{\psi'_{\rm pol}}\frac{\partial\Phi}{\partial s}+m_2\frac{\pi}{2K(\kappa)}\sqrt{\frac{\mu B_a\varepsilon}{m_\alpha}}\frac{\psi'_{\rm pol}}{B_a}\frac{ds}{d\hat{V}}\right) \qquad \text{(B.64)}\\ &= -\frac{1}{2\eta^2 B_a\varepsilon}\frac{\partial}{\partial\kappa}\left(-n\frac{c}{\chi'}\frac{\partial\Phi}{\partial\hat{V}}+m_2\frac{\pi}{2K(\kappa)}\sqrt{\frac{\mu B_a\varepsilon}{m_\alpha}}\frac{\chi'}{B_a}\right)\\ &= \frac{m_2}{2\eta^2 B_a\varepsilon}\frac{\partial}{\partial\kappa}\left[\sqrt{\frac{\mu B_a\varepsilon}{m_\alpha}}\frac{\chi'}{B_a}\left(\frac{n}{m_2}\frac{c}{\chi'}\sqrt{\frac{m_\alpha}{\mu B_a\varepsilon}}\frac{B_a}{\chi'}\frac{\partial\Phi}{\partial\hat{V}}-\frac{\pi}{2K(\kappa)}\right)\right]\\ &\approx \frac{m_2 v_t\chi'}{2\varepsilon}\sqrt{\frac{x\varepsilon}{2}}\frac{\partial}{\partial\kappa}\left[\frac{n}{m_2}\frac{\sqrt{2}B_a}{\sqrt{x\varepsilon}\chi'}\frac{c}{\chi'}\frac{\partial\Phi}{\partial\hat{V}}-\frac{\pi}{2K(\kappa)}\right]=\frac{m_2 v_t\chi'}{2\varepsilon}\sqrt{\frac{x\varepsilon}{2}}\frac{\partial G_{nm_2}}{\partial\kappa}\end{aligned}$$

where we assumed for trapped particles in the large aspect ratio limit that

$$\mu B_a \approx \frac{m_\alpha x}{2}v_t^2 \qquad \text{(B.65)}$$

$$\Rightarrow \eta B_a \approx 1 \qquad \text{(B.66)}$$

$$\Rightarrow \sqrt{\frac{\mu B_a\varepsilon}{m_\alpha}} \approx \sqrt{\frac{x\varepsilon}{2}}v_t \qquad \text{(B.67)}$$

$$\Rightarrow \tau_b \approx 4K(\kappa)\sqrt{\frac{2}{x\varepsilon}}\frac{B_a}{v_t\chi'}. \qquad \text{(B.68)}$$

We can write D_{1k} as

$$\begin{aligned}D_{1k} &= \frac{1}{2\sqrt{\pi}}\frac{n^2c^2B_a}{e_\alpha^2\left\langle|\nabla s|\right\rangle^2\chi'^2}\left(\frac{ds}{d\hat{V}}\right)^2\int_0^\infty dx\\ &\sqrt{\frac{2}{x\varepsilon}}xe^{-x}\sum_{m_2}\sum_{\rm res}\left(K(\kappa)|H_{\mathbf{m}}|^2\left|\frac{m_2v_t\chi'}{2\varepsilon}\sqrt{\frac{x\varepsilon}{2}}\frac{\partial G_{nm_2}}{\partial\kappa}\right|^{-1}\right)_{\eta=\eta_{\rm res}}w_k\\ &= \sqrt{\pi}\frac{n^2c^2B_a}{e_\alpha^2\left\langle|\nabla s|\right\rangle^2\chi'^2v_t}\left(\frac{ds}{d\hat{V}}\right)^2\int_0^\infty dx\\ &e^{-x}\sum_{m_2}\sum_{\rm res}\left(\frac{K(\kappa)}{\pi/2}|H_{\mathbf{m}}|^2\left|m_2\chi'\frac{\partial G_{nm_2}}{\partial\kappa}\right|^{-1}\right)_{\eta=\eta_{\rm res}}w_k \qquad \text{(B.69)}\end{aligned}$$

The perturbation defined by Shaing is

$$\frac{1}{B}\frac{\partial B}{\partial\theta^3}=\sum_{n,m_2}in\frac{B_n}{B}=\sum_{n,m_2}b_{nm_2}e^{i(m_2\theta^2+n\theta^3)}, \qquad \text{(B.70)}$$

$$\begin{aligned}\frac{\tilde{B}}{B_0} &= \frac{\tilde{B}}{B_a+\varepsilon\cos\vartheta}=\frac{\tilde{B}}{B_a}-\frac{\tilde{B}\cos\vartheta}{2{B_a}^2}\varepsilon+\mathcal{O}(\varepsilon^2)\\ &= \frac{\tilde{B}}{B_a}+\mathcal{O}(\varepsilon\tilde{B}/B_a)+\mathcal{O}(\varepsilon^2)\approx\frac{\tilde{B}}{B_a}. \qquad \text{(B.71)}\end{aligned}$$

We compare this to the Hamiltonian perturbation

$$\tilde{H} = \left(m_\alpha v_\parallel^2(\vartheta) + \frac{e_\alpha}{m_\alpha c} J_\perp B_0(\vartheta) \right) \frac{\tilde{B}}{B_0} \tag{B.72}$$

$$\approx \frac{m_\alpha x v_t^2}{2} \frac{\tilde{B}}{B_a} \tag{B.73}$$

$$\Rightarrow H_{m_2 n} = \frac{m_\alpha x v_t^2}{2} \frac{b_{nm_2}}{in} \tag{B.74}$$

Note, that one has to be careful with the sign convention because Shaing defines

$$\tilde{B} = -\varepsilon_{mn} \exp(m\vartheta - n\zeta), \tag{B.75}$$

$$\zeta_0 = q\vartheta - \zeta, \tag{B.76}$$

$$\omega_E = +\frac{c\Phi'}{\chi'}. \tag{B.77}$$

If one uses $\zeta = -\varphi$ we get the usual expansion and canonical angle (to the lowest order in Larmor radius) with

$$\tilde{B} = -\varepsilon_{mn} \exp(m\vartheta + n\varphi), \tag{B.78}$$

$$\theta^3 \equiv \zeta_0 = q\vartheta + \varphi. \tag{B.79}$$

The minus sign for the perturbation does not cause any troubles, because we include it in $\tilde{B}$. Inserting this in the transport coefficient expression yields

$$D_{1k} = \frac{\sqrt{\pi}}{4} \frac{m_\alpha^2 |n| c^2 B_a v_t^3}{e_\alpha^2 \langle |\nabla s| \rangle^2 \chi'^2} \left(\frac{ds}{d\hat{V}} \right)^2 \int_0^\infty dx$$
$$x^2 e^{-x} \sum_{m_2} \sum_{\text{res}} \left(\frac{K(\kappa)}{\pi/2} |b_{nm_2}|^2 \left| m_2 \chi' \frac{\partial G_{nm_2}}{\partial \kappa} \right|^{-1} \right)_{\eta=\eta_{\text{res}}} w_k. \tag{B.80}$$

For μ_{t1} we obtain

$$\mu_{t1} = n_\alpha m_\alpha v_t \frac{\sqrt{\pi}}{2} B_a \frac{\psi'}{|\chi'|} \frac{1}{\langle |\nabla s| \rangle} \frac{\partial s}{\partial \hat{V}} \int_0^\infty dx$$
$$x^2 e^{-x} \sum_{m_2} \frac{|n|}{|m_2|} \sum_{\text{res}} \left(\frac{K(\kappa)}{\pi/2} |b_{nm_2}|^2 \left| \frac{\partial G_{nm_2}}{\partial \kappa} \right|^{-1} \right)_{\eta=\eta_{\text{res}}}. \tag{B.81}$$

There is a difference in the definition of fluxes by Shaing as he uses a total flux Γ_{Shaing} with normalisation to the Volume $\hat{V} = 4\pi$ rather than our flux density Γ_{us} as in Eq. (4.83). The relation is

$$\Gamma_{\text{Shaing}} = \hat{S} \Gamma_{\text{us}} \tag{B.82}$$

Shaing uses

$$\Gamma_{\text{Shaing}} = \mathbf{\Gamma} \cdot \nabla \hat{V} \tag{B.83}$$

whereas we take

$$\Gamma_{\rm us} = \mathbf{\Gamma} \cdot \nabla r \tag{B.84}$$

with the effective radius r defined by

$$\nabla V = S \nabla r \tag{B.85}$$

or

$$\nabla \hat{V} = \hat{S} \nabla r \tag{B.86}$$

If we take s as the radial variable, we get

$$\Gamma_{\rm Shaing} = \frac{\partial \hat{V}}{\partial s}\frac{\partial r}{\partial s}\Gamma_{\rm us} = \frac{\partial \hat{V}}{\partial s}\frac{1}{\langle |\nabla s| \rangle}\Gamma_{\rm us}.$$

Thus, the results are matching. In the large aspect ratio limit, we have

$$V \approx 4\pi^2 R_0 r, \tag{B.87}$$

$$\hat{S} = \frac{d\hat{V}}{dr} \approx R_0 = \frac{r}{\varepsilon}. \tag{B.88}$$

For the effective radius r we use the translation

$$\langle |\nabla s| \rangle = \frac{ds}{dr} = \frac{ds}{d\hat{V}}\frac{d\hat{V}}{dr} \approx R_0 \frac{ds}{d\hat{V}}. \tag{B.89}$$

To sum up, we have proven the consistency of viscous coefficient μ_{t1} for trapped particles in Eq. (27) Shaing et al. (2009b) with our expression for transport coefficients of Eq. (4.84).

B.5 Expressions for the transit-drift resonance

In the same matter as in the previous sections, terms for transport coefficients can be compared for the transit-drift resonance of passing particles. As we will see, the article of Shaing et al. (2009a) contains an inconsistency with regard to Fourier integrals, which will become clear below.

The bounce integration for passing orbits is formally similar to trapped orbits but performed over the full range in ϑ where $v_\parallel$ doesn't change sign ($\kappa > 1$). We start from the resonance condition

$$\frac{\partial}{\partial \eta}\left(n\Omega_{tE} + (m_2 + nq)\,\omega_b\right) =$$

$$\frac{1}{2\eta^2\kappa^2 B_a\varepsilon}\frac{\partial}{\partial(1/\kappa)}\left(-n\frac{c}{\chi'}\frac{\partial\Phi}{\partial\hat{V}}+2\left(m_2+nq\right)\sqrt{\frac{\mu B_a\varepsilon}{m_\alpha}}\frac{\chi'}{B_a}\frac{\pi\sqrt{\kappa}}{2K(1/\sqrt{\kappa})}\right)$$
$$=-\frac{1}{2\eta^2\kappa^2 B_a\varepsilon}\frac{\partial}{\partial(1/\kappa)}\left(n\frac{c}{\chi'}\frac{\partial\Phi}{\partial\hat{V}}-2\left(m_2+nq\right)\sqrt{\frac{\varepsilon x v_t^2/2}{2\varepsilon\kappa+(\varepsilon-1)}}\frac{\chi'}{B_a}\frac{\pi\sqrt{\kappa}}{2K(1/\kappa)}\right)$$
$$=\frac{m_2\sqrt{x}v_t}{2\eta^2\kappa^2 B_a\varepsilon}\frac{\chi'}{B_a}\frac{\partial}{\partial(1/\kappa)}\left(\frac{n}{m_2}\frac{c}{\sqrt{x}v_t\chi'}\frac{B_a}{\chi'}\frac{\partial\Phi}{\partial\hat{V}}-\left(1+\frac{n}{m_2}q\right)\sqrt{\frac{2\varepsilon\kappa}{2\varepsilon\kappa+(\varepsilon-1)}}\frac{\pi}{2K(1/\kappa)}\right) \tag{B.90}$$

Our term with nq is not present in Shaing's paper in (45). The reason for this lies in his Fourier expansion of a non-periodic function.

For circulating particles in (35) and (39) one should obtain

$$\sigma(l-nq)\omega_t+n\omega_E \tag{B.91}$$

instead of

$$\sigma l\omega_t+n\omega_E \tag{B.92}$$

in the perturbed solution g_{nl}. The reason for that is the following:

To have the correct periodicity for the orbit of circulating particles, it must be possible to express the angle ξ defined in Eq. (33) as a function of θ by

$$\xi(\theta)=\theta+\alpha(\theta), \tag{B.93}$$

where $\alpha(\theta)$ is a periodic function. This is indeed the case for

$$\alpha(\theta)=\frac{\pi}{K(1/\kappa)}F(\theta/2,1/\kappa)-\theta \tag{B.94}$$

with elliptic integrals for $1/\kappa<1$. Since $\xi(\theta)$ is invertible we can write the inverse transformation

$$\theta(\xi)=\xi+\beta(\xi), \tag{B.95}$$

where $\alpha(\theta)=-\beta(\xi(\theta))$. $\beta(\xi)$ is periodic in ξ but $\theta(\xi)$ is not.

The issue appears in the Fourier expansion in (37) and (38). Consider a function

$$g(\theta,\zeta_0)=\sum_{m,n}g_{mn}e^{i((m-nq)\theta+n\zeta_0)},$$
$$g(\xi,\zeta_0)=\sum_{m,n}g_{mn}e^{i((m-nq)(\xi+\beta(\xi))+n\zeta_0)}$$
$$=\sum_{m,n}g_{mn}e^{i(m\xi+n\zeta_0)}e^{i(m-nq)\beta(\xi)}e^{-inq\xi}.$$

Since $\beta(\xi)$ is periodic, all terms are periodic in ξ except for the last one, $e^{-inq\xi}$. Since the whole function is not periodic in ξ it is not possible to write it as a Fourier series

$$\sum_{n,l} g_{nl} e^{i(l\xi + n\zeta_0)}.$$

Instead, the non-periodic term has to be separated, leading to

$$g(\xi, \zeta_0) = \sum_{n,l} g_{nl} e^{i(l\xi+n\zeta_0)} e^{-inq\xi} = \sum_{n,l} g_{nl} e^{i((l-nq)\xi+n\zeta_0)} \tag{B.96}$$

with Fourier coefficients

$$g_{nl} = \sum_m \int d\xi \, g_{mn} e^{i(m\xi+n\zeta_0+(m-nq)\beta(\xi)-l\xi-n\xi_0)} \tag{B.97}$$

$$= \sum_m \int d\xi \, g_{mn} e^{i((m-nq)\theta(\xi)-(l-nq)\xi)}. \tag{B.98}$$

We write

$$v_\parallel \frac{\partial g}{\partial \theta} = v_\parallel \frac{\partial \xi}{\partial \theta} \frac{\partial g}{\partial \xi} = \sigma \omega_t \sum_{n,l} i(l - nq) g_{nl} e^{i((l-nq)\xi+n\zeta_0)}. \tag{B.99}$$

For trapped particles, the situation is different, since the motion in θ is limited by the turning points. In this case, $\theta(\eta)$ is a periodic function in η and we can write

$$g(\theta, \zeta_0) = \sum_{m,n} g_{mn} e^{i((m-nq)\theta+n\zeta_0)},$$
$$g(\eta, \zeta_0) = \sum_{m,n} g_{mn} e^{i((m-nq)\theta(\eta)+n\zeta_0)},$$

which is a periodic function in η, so

$$g(\eta, \zeta_0) = \sum_{n,l} g_{nl} e^{i(l\xi+n\zeta_0)} \tag{B.100}$$

with coefficients calculated as described in the appendix of the article by Shaing et al. (2009a). We have thus shown that in order to match the expressions for Fourier series in canonical angles given in Eq. (3.116) here, an additional factor $e^{-inq\xi}$ could be added in expressions (34), resulting in a matching Fourier series of Eq. (37) and (38) for passing orbits.

Useful formulas

Magnetic flux coordinates:

$$\frac{1}{m\sqrt{g}\omega_c h^\vartheta} = \frac{c}{e\psi'_{\mathrm{pol}}} \tag{B.101}$$

Velocities and actions:

$$v_\parallel = \sigma v\sqrt{1-\eta B} \tag{B.102}$$
$$v_\perp = v\sqrt{\eta B} \tag{B.103}$$
$$J_\perp = mc\mu/e = mv_\perp^2/(2\omega_c) = \frac{mv^2}{2}\frac{mc}{e}\eta \tag{B.104}$$
$$J_\perp\omega_c = \mu B = \frac{mv_\perp^2}{2} = \frac{mv^2}{2}\eta B \tag{B.105}$$

$$\left|\frac{\partial(J_\perp, J_\vartheta)}{\partial(v,\eta)}\right| = \frac{m^3v^3c\tau_b}{2\pi e} \tag{B.106}$$

Large-aspect ratio limit

$$B \approx \frac{B_0}{1+\varepsilon\cos\vartheta} \tag{B.107}$$
$$\frac{B(\pi)}{B(0)} \approx \frac{1+\varepsilon}{1-\varepsilon} \tag{B.108}$$
$$\frac{B(\pi)}{B(0)} - \varepsilon\frac{B(\pi)}{B(0)} = 1+\varepsilon \tag{B.109}$$
$$\varepsilon \approx \frac{\frac{B(\pi)}{B(0)}-1}{\frac{B(\pi)}{B(0)}+1} \tag{B.110}$$

Plateau diffusion coefficient:

$$D_p = \frac{\pi q v_{\mathrm{th}}\rho_L^2}{16R_0} \tag{B.111}$$

Ripple plateau diffusion coefficient:

$$D_{rp} = \frac{\sqrt{\pi} m_\varphi q^2 A^2 v_{\mathrm{th}} \rho_L^2}{4R} \varepsilon_M^2 \tag{B.112}$$

List of Figures

1.1 Pendulum orbits in phase-space, energy dependence of bounce frequency 22
1.2 Contours of actions and angles for the pendulum 23
1.3 Perturbation spectrum and non-linear bounce frequency for the pendulum 29
1.4 Pendulum orbits and energy dependence on perturbation amplitude . . 31

2.1 Airy functions and Scorer functions 42
2.2 Action-dependent part of quasilinear dimensionless distribution function 43
2.3 Contours of quasilinear dimensionless distribution function 43
2.4 Contours of non-linear dimensionless distribution function 47
2.5 Numerical solution of dimensionless distribution function at $\bar{\theta} = 0; \pi$ . . 48
2.6 Contours of numerical solution for dimensionless distribution function . 50

4.1 Attenuation factor depending on resonant diffusivity D 100

5.1 Superbanana plateau for RMPs, analytical validation, resonance 103
5.2 RMP: transport coefficients over Mach number, comparison NEO-2 . . . 104
5.3 RMP: contributions to integral for transport coefficients. 105
5.4 Ripple: transport coefficients over Mach number, comparison NEO-2 . . 106
5.5 RMP: influence of magnetic drift and shear on transport 106
5.6 AUG #30835: NTV torque from different models 109
5.7 AUG #30835: NTV torque from models with magnetic shear 110
5.8 Transport coefficient D_{11} at different non-linearities 111
5.9 Transport coefficient D_{11} dependency on perturbation amplitude 111
5.10 Illustration of finite orbit width (poloidal projection) 113
5.11 Illustration of finite orbit width (error in approximation of $\Delta\varphi$) 114

Bibliography

SS Abdullaev and KH Finken. Hamiltonian guiding center equations in a toroidal system. *Phys. Plasmas*, 9(10):4193–4204, 2002.

CG Albert. *Hamiltonian Theory of Resonant Transport Regimes in Tokamak Plasmas with Non-Axisymmetric Magnetic Perturbations*. PhD thesis, TU Graz, Institute of Theoretical and Computational Physics, Petersgasse 16, 7 2017.

CG Albert and SV Kasilov. NEO-RT: Code for computing tokamak NTV torque in resonant transport regimes. `https://github.com/itpplasma/NEO-RT`, 2017. accessed 09/4/2020.

CG Albert, MF Heyn, G Kapper, SV Kasilov, W Kernbichler, and AF Martitsch. Evaluation of toroidal torque by non-resonant magnetic perturbations in tokamaks for resonant transport regimes using a Hamiltonian approach. *Phys. Plasmas*, 23(8):082515, 2016a.

CG Albert, MF Heyn, G Kapper, SV Kasilov, W Kernbichler, and AF Martitsch. Hamiltonian approach for evaluation of toroidal torque from finite amplitude non-axisymmetric perturbations of a tokamak magnetic field in resonant transport regimes. In *43rd EPS Conference on Plasma Physics*, page P1.051, 2016b.

CG Albert, MF Heyn, SV Kasilov, W Kernbichler, AF Martitsch, and AM Runov. Kinetic modeling of 3D equilibria in a tokamak. In *J. Phys. Conf. Series*, volume 775, page 012001. IOP Publishing, 2016c.

CG Albert, MF Heyn, SV Kasilov, W Kernbichler, and AF Martitsch. Finite orbit width effects on resonant transport regimes of neoclassical toroidal viscous torque within the Hamiltonian approach. In *44th EPS Conference on Plasma Physics*, page P1.182, 2017.

VI Arnold. *Mathematical methods of classical mechanics*, volume 60. Springer, 1989.

LA Artsimovich. Tokamak devices. *Nuclear Fusion*, 12(2):215, 1972.

A Bécoulet, DJ Gambier, and A Samain. Hamiltonian theory of the ion cyclotron minority heating dynamics in tokamak plasmas. *Physics of Fluids B: Plasma Physics*, 3(1):137–150, 1991.

AH Boozer. Enhanced transport in tokamaks due to toroidal ripple. *Phys. Fluids*, 23(11): 2283–2290, 1980.

AH Boozer. Physics of magnetically confined plasmas. *Rev. Mod. Phys.*, 76(4):1071, 2005.

AH Boozer. Perturbation to the magnetic field strength. *Phys. Plasmas*, 13(4):044501, 2006.

AJ Brizard. Jacobi zeta function and action-angle coordinates for the pendulum. *Commun. Nonlin. Sci. Numer. Simul.*, 18(3):511–518, 2013.

BV Chirikov. Resonance processes in magnetic traps. *J. Nuclear Energy C*, 1(4):253, 1960.

BV Chirikov. A universal instability of many-dimensional oscillator systems. *Phys. Rep.*, 52 (5):263–379, 1979.

WD D'haeseleer, WNG Hitchon, JD Callen, and JL Shohet. *Flux coordinates and magnetic field structure*. Springer Series in Computational Physics. Springer Berlin Heidelberg, 1991.

YN Dnestrovskii and DP Kostomarov. *Numerical simulation of plasmas*. Springer, 2012.

IG Eriksson and P Helander. Finite orbit width effects on stochastic ripple diffusion. *Nuclear fusion*, 33(5):767, 1993.

LG Eriksson and P Helander. Monte Carlo operators for orbit-averaged Fokker–Planck equations. *Phys. Plasmas*, 1(2):308–314, 1994.

TE Evans, RA Moyer, PR Thomas, JG Watkins, TH Osborne, JA Boedo, EJ Doyle, ME Fenstermacher, KH Finken, RJ Groebner, et al. Suppression of large edge-localized modes in high-confinement DIII-D plasmas with a stochastic magnetic boundary. *Phys. Rev. Lett.*, 92(23):235003, 2004.

A Gil, J Segura, and NM Temme. *Numerical methods for special functions*. SIAM, 2007.

H Goldstein. *Classical mechanics*. Addison-Wesley, 2nd ed. edition, 1980.

IS Gradshtein and IM Ryzhik. Table of integrals, series, and products. 1965.

RD Hazeltine and AA Ware. The drift kinetic equation for toroidal plasmas with large mass velocities. *Plasma Physics*, 20(7):673, 1978.

RD Hazeltine, SM Mahajan, and DA Hitchcock. Quasi-linear diffusion and radial transport in tokamaks. *Phys. Fluids*, 24(6):1164–1179, 1981.

P Helander and DJ Sigmar. *Collisional transport in magnetized plasmas*, volume 4. Cambridge University Press, 2005.

MF Heyn, IB Ivanov, SV Kasilov, W Kernbichler, I Joseph, A Moyer, and AM Runov. Kinetic estimate of the shielding of resonant magnetic field perturbations by the plasma in DIII-D. *Nuclear Fusion*, 48:024005, 2008.

FL Hinton and RD Hazeltine. Theory of plasma transport in toroidal confinement systems. *Rev. Mod. Phys.*, 48(2):239, 1976.

SP Hirshman. The ambipolarity paradox in toroidal diffusion, revisited. *Nuclear Fusion*, 18 (7):917, 1978.

SP Hirshman and DJ Sigmar. Neoclassical transport of impurities in tokamak plasmas. *Nuclear Fusion*, 21(9):1079, 1981.

K Ida and JC Rice. Rotation and momentum transport in tokamaks and helical systems. *Nuclear Fusion*, 54(4):045001, 2014.

SV Kasilov, AI Pyatak, and KN Stepanov. Nonlocal theory of cyclotron and cerenkov absorption in nonuniformly magnetized plasma. *Rev. Plasma Physics*, 20:61, 1997.

SV Kasilov, W Kernbichler, AF Martitsch, H Maassberg, and MF Heyn. Evaluation of the toroidal torque driven by external non-resonant non-axisymmetric magnetic field perturbations in a tokamak. *Phys. Plasmas*, 21(9):092506, 2014.

AN Kaufman. Quasilinear diffusion of an axisymmetric toroidal plasma. *Phys. Fluids*, 15(6): 1063–1069, 1972.

M Keilhacker, A Gibson, C Gormezano, PJ Lomas, PR Thomas, ML Watkins, P Andrew, B Balet, D Borba, CD Challis, et al. High fusion performance from deuterium-tritium plasmas in jet. *Nuclear Fusion*, 39(2):209, 1999.

W Kernbichler, SV Kasilov, G Kapper, AF Martitsch, VV Nemov, C Albert, and MF Heyn. Solution of drift kinetic equation in stellarators and tokamaks with broken symmetry using the code NEO-2. *Plasma Phys. Contr. Fusion*, 58(10):104001, 2016.

Ya I Kolesnichenko, VV Lutsenko, RB White, and Yu V Yakovenko. Theory of resonance influence of sawtooth crashes on ions with large orbit width. *Phys. Plasmas*, 5(8):2963–2976, 1998.

Ya I Kolesnichenko, RB White, and Yu V Yakovenko. Precession of toroidally passing particles in tokamaks and spherical tori. *Phys. Plasmas*, 10(5):1449–1457, 2003.

HA Kramers. Brownian motion in a field of force and the diffusion model of chemical reactions. *Physica*, 7(4):284–304, 1940.

LD Landau and EM Lifshitz. *Course of theoretical physics: Mechanics*. Pergamon Press, 1960.

M Landreman, HM Smith, A Mollén, and P Helander. Comparison of particle trajectories and collision operators for collisional transport in nonaxisymmetric plasmas. *Phys. Plasmas*, 21(4):042503, 2014.

JD Lawson. Some criteria for a power producing thermonuclear reactor. *Proc. Phys. Society. Section B*, 70(1):6, 1957.

M Li, BN Breizman, and L Zheng. Canonical straight field line magnetic flux coordinates for tokamaks. *J. Comp. Phys.*, 326:334–341, 2016.

AJ Lichtenberg and MA Lieberman. *Regular and Chaotic Dynamics*. Springer, 1983.

RG Littlejohn. Variational principles of guiding centre motion. *J. Plasma Phys.*, 29:111–125, 2 1983.

A Loarte, G Saibene, R Sartori, D Campbell, M Becoulet, L Horton, T Eich, A Herrmann, G Matthews, N Asakura, et al. Characteristics of type i ELM energy and particle losses in existing devices and their extrapolation to ITER. *Plasma Phys. Contr. Fusion*, 45(9):1549, 2003.

SM Mahajan, RD Hazeltine, and DA Hitchcock. Quasilinear momentum and energy transport. *Phys. Fluids*, 26(3):700–704, 1983.

AF Martitsch, SV Kasilov, W Kernbichler, G Kapper, CG Albert, MF Heyn, HM Smith, E Strumberger, S Fietz, W Suttrop, et al. Effect of 3d magnetic perturbations on the plasma rotation in asdex upgrade. *Plasma Phys. Contr. Fusion*, 58(7):074007, 2016.

JD Meiss and RD Hazeltine. Canonical coordinates for guiding center particles. *Phys. Fluids B*, 2(11):2563–2567, 1990.

VV Nemov, SV Kasilov, W Kernbichler, and MF Heyn. Evaluation of $1/\nu$ neoclassical transport in stellarators. *Phys. Plasmas*, 6(12):4622–4632, 1999.

DR Nicholson. *Introduction to plasma theory*. Cambridge Univ Press, 1983.

J Nuckolls and L Wood. Laser compression of matter to super-high densities: thermonuclear (ctr) applications. *Nature*, 239:139, 1972.

J Ongena, R Koch, R Wolf, and H Zohm. Magnetic-confinement fusion. *Nature Physics*, 12 (5):398–410, 2016.

MV Osipenko and RV Shurygin. Quasilinear hydrodynamics of trapped and flight particles during the alfven hf heating. *Fiz. Plazmy*, 15(11):1353–1367, 1989.

MV Osipenko and RV Shurygin. Radial transport of circulating and trapped ions during icr heating in a tokamak. *Fiz. Plazmy*, 16(12):1425–1436, 1990.

JK Park, AH Boozer, and JE Menard. Nonambipolar transport by trapped particles in tokamaks. *Phys. Rev. Lett.*, 102:065002, Feb 2009.

Yu A Romanov and GF Filippov. Interaction of fast electron beams with longitudinal plasma waves. *Sov. Phys. JETP*, 13:87–92, 1961.

S Satake, JK Park, H Sugama, and R Kanno. Neoclassical toroidal viscosity calculations in tokamaks using a δf Monte Carlo simulation and their verifications. *Phys. Rev. Letters*, 107(5):055001, 2011.

KC Shaing. Plasma flows and radial electric field in nonaxisymmetric toroidal plasmas. *Phys. Fluids*, 29(7):2231–2234, 1986.

KC Shaing. Poloidal and parallel plasma viscosities in tokamak geometry. *Phys. Fluids B*, 2 (11):2847–2849, 1990.

KC Shaing. Superbanana and superbanana plateau transport in finite aspect ratio tokamaks with broken symmetry. *J. Plasma Phys.*, 81:905810203, 4 2015.

KC Shaing and JD Callen. Neoclassical flows and transport in nonaxisymmetric toroidal plasmas. *Phys. Fluids*, 26(11):3315–3326, 1983.

KC Shaing and SA Sabbagh. Neoclassical toroidal plasma viscosity with effects of finite banana width for finite aspect ratio tokamaks. *Physics of Plasmas*, 23(7):072511, 2016.

KC Shaing and DA Spong. Extending the collisional fluid equations into the long mean-free-path regime in toroidal plasmas. i. plasma viscosity. *Phys. Fluids B*, 2(6):1190–1194, 1990.

KC Shaing, MS Chu, and SA Sabbagh. Eulerian approach to bounce-transit and drift resonance and neoclassical toroidal plasma viscosity in tokamaks. *Plasma Phys. Contr. Fusion*, 51(7):075015, 2009a.

KC Shaing, SA Sabbagh, and MS Chu. Neoclassical toroidal plasma viscosity in the superbanana plateau regime for tokamaks. *Plasma Phys. Contr. Fusion*, 51(3):035009, 2009b.

KC Shaing, SA Sabbagh, and MS Chu. An approximate analytic expression for neoclassical toroidal plasma viscosity in tokamaks. *Nuclear Fusion*, 50(2):025022, 2010.

KC Shaing, K Ida, and SA Sabbagh. Neoclassical plasma viscosity and transport processes in non-axisymmetric tori. *Nuclear Fusion*, 55(12):125001, 2015.

H Smith. private communication.

L Spitzer. The stellarator concept. *Phys. Fluids*, 1(4):253–264, 1958.

Y Sun, Y Liang, KC Shaing, HR Koslowski, C Wiegmann, and T Zhang. Neoclassical toroidal plasma viscosity torque in collisionless regimes in tokamaks. *Phys. Rev. Letters*, 105(14): 145002, 2010.

JB Taylor. Equilibrium and stability of plasma in arbitrary mirror fields. *Phys. Fluids*, 7(6): 767–773, 1964.

AV Timofeev and MD Tokman. Quasi-linear equation for electron cyclotron resonance interaction with monochromatic radiation in magnetic traps. *Plasma Phys. Rep.*, 20(4): 336–340, 1994.

GE Uhlenbeck and LS Ornstein. On the theory of the Brownian motion. *Phys. Rev.*, 36(5): 823, 1930.

NG Van Kampen. *Stochastic processes in physics and chemistry*. AIP, 1983.

AA Vedenov, EP Velikhov, and RZ Sagdeev. Nonlinear oscillations of rarified plasma. *Nuclear Fusion*, 1(2):82, 1961.

F Wagner, G Fussmann, T Grave, M Keilhacker, M Kornherr, K Lackner, K McCormick, ER Müller, A Stäbler, G Becker, et al. Development of an edge transport barrier at the h-mode transition of ASDEX. *Physical Review Letters*, 53(15):1453, 1984.

J Wesson. *Tokamaks*, volume 149. Oxford University Press, 2011.

RB White. Canonical Hamiltonian guiding center variables. *Phys. Fluids B*, 2(4):845–847, 1990.

RB White and MS Chance. Hamiltonian guiding center drift orbit calculation for plasmas of arbitrary cross section. *Phys. Fluids*, 27(10):2455–2467, 1984.

RB White, AH Boozer, and R Hay. Drift Hamiltonian in magnetic coordinates. *Phys. Fluids*, 25(3):575–576, 1982.

VE Zakharov and VI Karpman. On the nonlinear theory of the damping of plasma waves. *Sov. Phys. JETP*, 16:351, 1963.

H Zohm. Edge localized modes (ELMs). *Plasma Phys. Contr. Fusion*, 38(2):105, 1996.

Monographic Series TU Graz

Computation in Engineering and Science

Vol. 1 Steffen Alvermann
Effective Viscoelastic Behavior of Cellular Auxetic Materials
2008
ISBN 978-3-902465-92-4

Vol. 2 Sendy Fransiscus Tantono
The Mechanical Behaviour of a Soilbag under Vertical Compression
2008
ISBN 978-3-902465-97-9

Vol. 3 Thomas Rüberg
Non-conforming FEM/BEM Coupling in Time Domain
2008
ISBN 978-3-902465-98-6

Vol. 4 Dimitrios E. Kiousis
Biomechanical and Computational Modeling of Atherosclerotic Arteries
2008
ISBN 978-3-85125-023-7

Vol. 5 Lars Kielhorn
A Time-Domain Symmetric Galerkin BEM for Viscoelastodynamics
2009
ISBN 978-3-85125-042-8

Vol. 6 Gerhard Unger
Analysis of Boundary Element Methods for Laplacian Eigenvalue Problems
2009
ISBN 978-3-85125-081-7

Monographic Series TU Graz

Computation in Engineering and Science

Vol. 7 Gerhard Sommer

Mechanical Properties of Healthy and Diseased Human Arteries
2010
ISBN 978-3-85125-111-1

Vol. 8 Mathias Nenning

Infinite Elements for Elasto- and Poroelastodynamics
2010
ISBN 978-3-85125-130-2

Vol. 9 Thanh Xuan Phan

Boundary Element Methods for Boundary Control Problems
2011
ISBN 978-3-85125-149-4

Vol. 10 Loris Nagler

Simulation of Sound Transmission through Poroelastic Plate-like Structures
2011
ISBN 978-3-85125-153-1

Vol. 11 Markus Windisch

Boundary Element Tearing and Interconnecting Methods for Acoustic and Electromagnetic Scattering
2011
ISBN 978-3-85125-152-4

Vol. 12 Christian Walchshofer

Analysis of the Dynamics at the Base of a Lifted Strongly Buoyant Jet Flame Using Direct Numerical Simulation
2011
ISBN 978-3-85125-185-2

Monographic Series TU Graz

Computation in Engineering and Science

Vol. 13 Matthias Messner

Fast Boundary Element Methods in Acoustics
2012
ISBN 978-3-85125-202-6

Vol. 14 Peter Urthaler

Analysis of Boundary Element Methods for Wave Propagation in Porous Media
2012
ISBN 978-3-85125-216-3

Vol. 15 Peng Li

Boundary Element Method for Wave Propagation in Partially Saturated Poroelastic Continua
2012
ISBN 978-3-85125-236-1

Vol. 16 Andreas Jörg Schriefl

Quantification of Collagen Fiber Morphologies in Human Arterial Walls
2013
ISBN 978-3-85125-238-5

Vol. 17 Thomas S. E. Eriksson

Cardiovascular Mechanics
2013
ISBN 978-3-85125-277-4

Vol. 18 Jianhua Tong

Biomechanics of Abdominal Aortic Aneurysms
2013
ISBN 978-3-85125-279-8

Monographic Series TU Graz

Computation in Engineering and Science

Vol. 19 Jonathan Rohleder

Titchmarsh–Weyl Theory and Inverse Problems for Elliptic Differential Operators
2013
ISBN 978-3-85125-283-5

Vol. 20 Martin Neumüller

Space-Time Methods
2013
ISBN 978-3-85125-290-3

Vol. 21 Michael J. Unterberger

Microstructurally-Motivated Constitutive Modeling of Cross-Linked Filamentous Actin Networks
2013
ISBN 978-3-85125-303-0

Vol. 22 Vladimir Lotoreichik

Singular Values and Trace Formulae for Resolvent Power Differences of Self-Adjoint Elliptic Operators
2013
ISBN 978-3-85125-304-7

Vol. 23 Michael Meßner

A Fast Multipole Galerkin Boundary Element Method for the Transient Heat Equation
2014
ISBN 978-3-85125-350-4

Vol. 24 Lorenz Johannes John

Optimal Boundary Control in Energy Spaces
2014
ISBN 978-3-85125-373-3

Monographic Series TU Graz

Computation in Engineering and Science

Vol. 25 Hannah Weisbecker

Softening and Damage Behavior of Human Arteries
2014
ISBN 978-3-85125-370-2

Vol. 26 Bernhard Kager

Efficient Convolution Quadrature based Boundary Element Formulation for Time-Domain Elastodynamics
2015
ISBN 978-3-85125-382-5

Vol. 27 Christoph M. Augustin

Classical and All-floating FETI Methods with Applications to Biomechanical Models
2015
ISBN 978-3-85125-418-1

Vol. 28 Elias Karabelas

Space-Time Discontinuous Galerkin Methods for Cardiac Electromechanics
2016
ISBN 978-3-85125-461-7

Vol. 29 Thomas Traub

A Kernel Interpolation Based Fast Multipole Method for Elastodynamic Problems
2016
ISBN 978-3-85125-465-5

Vol. 30 Matthias Gsell

Mortar Domain Decomposition Methods for Quasilinear Problems and Applications
2017
ISBN 978-3-85125-522-5

Monographic Series TU Graz

Computation in Engineering and Science

Vol. 31 Christian Kühn

Schrödinger operators and singular infinite rank perturbations
2017
ISBN 978-3-85125-551-5

Vol. 32 Michael H. Gfrerer

Vibro-Acoustic Simulation of Poroelastic Shell Structures
2018
ISBN 978-3-85125-573-7

Vol. 33 Markus Holzmann

Spectral Analysis of Transmission and Boundary Value Problems for Dirac Operators
2018
ISBN 978-3-85125-642-0

Vol. 34 Osman Gültekin

Computational Inelasticity of Fibrous Biological Tissues with a Focus on Viscoelasticity, Damage and Rupture
2019
ISBN 978-3-85125-655-0

Vol. 35 Justyna Anna Niestrawska

Experimental and Computational Analyses of Pathological Soft Tissues – Towards a Better Understanding of the Pathogenesis of AAA
2019
ISBN 978-3-85125-678-9

Monographic Series TU Graz

Computation in Engineering and Science

Vol. 36 Marco Zank

Inf-Sup Stable Space-Time Methods for Time-Dependent Partial Differential Equations
2020
ISBN 978-3-85125-721-2

Vol. 37 Christoph Irrenfried

Convective turbulent near wall heat transfer at high Prandtl numbers
2020
ISBN 978-3-85125-724-3

Vol. 38 Christopher Albert

Hamiltonian Theory of Resonant Transport Regimes in Tokamaks with Perturbed Axisymmetry
2020
ISBN 978-3-85125-746-5